

~~CONFIDENTIAL~~ ~~Shirkey~~

# High Performance N2O4/AMINE Elements "BLOWAPART"

NASA CR.  
160273

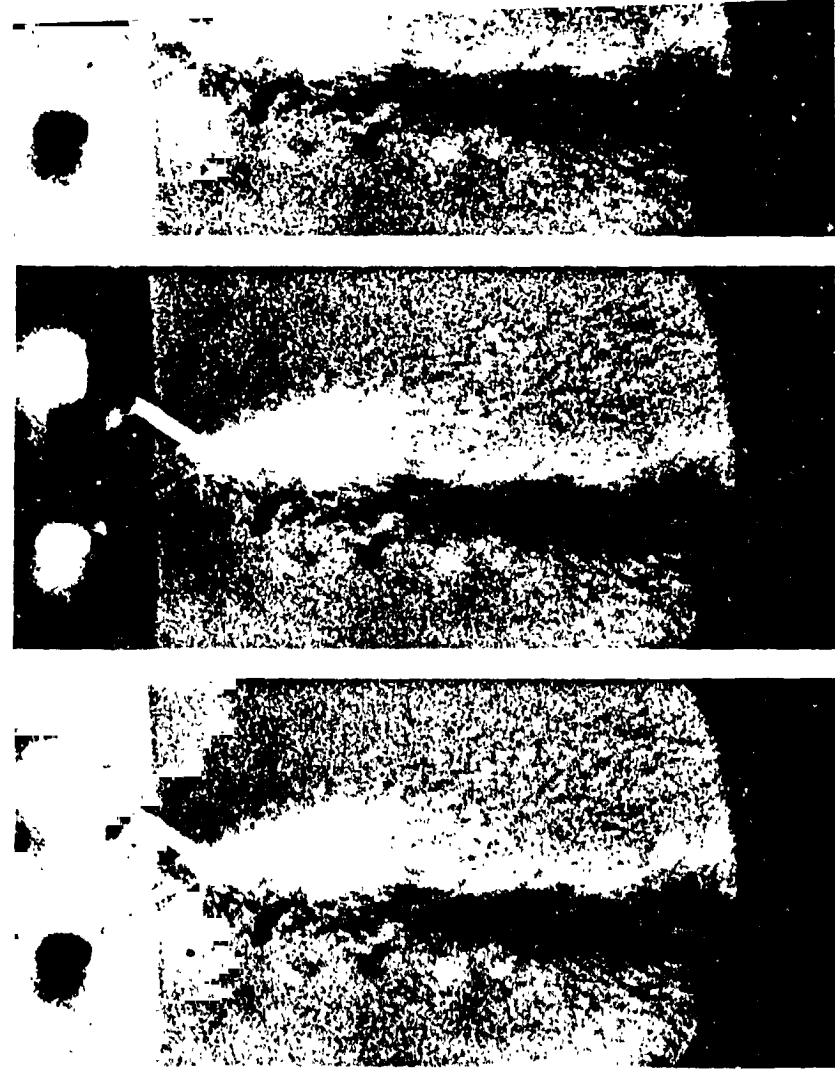
Final Report

March 1979  
N79-27324

L (NASA-CR-160273) HIGH PERFORMANCE  
N2O4/AMINE ELEMENTS BLOWAPART Final Report  
(Aerojet Liquid Rocket Co.) 171 p  
HC A08/MF A01

CSSL 201

G3/28 Unclass  
29209



ORIGINAL PAGE IS  
OF POOR QUALITY

Contract NAS 9-14186

Prepared By:

B. R. Lawver

**NASA** JOHNSON  
SPACE  
CENTER

ORIGINAL CONTAINS  
COLOR ILLUSTRATIONS

AEROJET  
LIQUID ROCKET  
COMPANY 

HIGH PERFORMANCE  
N<sub>2</sub>O<sub>4</sub>/AMINE ELEMENTS - "BLOWAPART"

Contract NAS 9-14186  
Final Report 14186-DRL-5

March 1979

Prepared by:  
B. R. Lawver

Prepared for:  
NASA-Johnson Space Center  
Houston, Texas

## FOREWORD

This final report describes analytical and experimental work conducted to identify the mechanisms governing Reactive Stream Separation (RSS) and to develop techniques for predicting its occurrence. RSS is a combustion induced phenomenon that results in striation of hypergolic propellant oxidizer and fuel sprays fans. This reduced intra-element mixing (compared to the well-mixed distribution developed in a non-reacting cold flow case) can influence thrust chamber performance, heat transfer, and stability. The activity was performed by Aerojet Liquid Rocket Company on Contract NAS 9-14186, under the direction of Merlyn Lausten, NASA/JSC Project Manager. Aerojet personnel included L. B. Bassham, Program Manager, D. L. Kors, Project Manager and B. R. Lawver, Project Engineer. J. W. Salmon also served as ALRC Program Manager, commencing in January of 1978. The following individuals also contributed significantly to the success of the program:

Paul Lloyd	Test Engineering
Arnold Keller	Test Engineering
Duane Robertson	Test Instrumentation
Cliff Thompson	Combustor Design
Lee Lang	Combustor Design
Gene Hron	Fabrication
Judy Schneider	Data Analysis
Dick Walker	Data Analysis.

ORIGINAL PAGE IS  
OF POOR QUALITY

## TABLE OF CONTENTS

	<u>Page</u>
I. Summary	1
II. Introduction	4
III. Technical Approach	7
IV. Results and Conclusions	13
V. Application of Results and Recommendations	17
VI. Technical Discussion	21
A. Experimental Hardware & Test Setup	21
B. Photographic Equipment and Techniques	40
C. Test Results	45
D. RSS Model Development	80
References	93
Appendix A Injector Element Design Criteria	
Appendix B Summary of Injectors, Test Conditions, and Test Results	

## LIST OF TABLES

<u>Table No.</u>		<u>Page</u>
I	Summary of Injector Elements and Test Conditions	5
II	High Frequency Response Instrumentation	37
III	Low Frequency Response Instrumentation	38
IV	Injector Element Cold Flow Data Summary	52

## LIST OF FIGURES

<u>Figure No.</u>		<u>Page</u>
1	RSS Model Development Approach	8
2	Blowpart Technology Program Approach	9
3	RSS Model Development Chronology	10
4	Vaporization Model Correlates RSS for Coherent Stream Impingement Injector Elements	14
5	Vaporization Model Correlates RSS for Self-Atomizing Injector Elements	15
6	Photographic Test Chamber	22
7	Injector Element Orifice Configurations	24
8	Rounded Inlet Unlike Doublet Injector	25
9	F-O-F Triplet Injector	28
10	XDT and Splash Plate Platelet Injectors	29
11	Sharp-edged Inlet Unlike Doublet Injector	31
12	Space Shuttle/RCS Unlike Doublet Injector	32
13	Space Shuttle/OMS TLOL Platelet Injector	33
14	Hot Fire Test Setup	34
15	Propellant Flow System Schematic	35
16	Instrumentation Schematic	39
17	High Intensity Lamps Overpower Flame Light Emission	41
18	Photographic Equipment Setup	43
19	Pressure Drop Characteristics of the Rounded Inlet Unlike Doublet Elements	46
20	Pressure Drop Characteristics of the Triplet Elements	47
21	Pressure Drop Characteristics of the XDT and Splash Plate Platelet Elements	48
22	Pressure Drop Characteristics of the Sharp Edged Unlike Doublet Elements	49
23	Pressure Drop Characteristics of the Space Shuttle/RCS Unlike Doublet Elements	50
24	Pressure Drop Characteristics of the Space Shuttle/OMS Platelet TLOL Element	51

## LIST OF FIGURES (cont.)

<u>Figure No.</u>		<u>Page</u>
25	Impingement Offset Causes Fan Rotation with the Space Shuttle/RCS Unlike Doublet	55
26	Space Shuttle/RCS Unlike Doublet Non-Reactive Impingement	56
27	Rounded Inlet Unlike Doublet Non-Reactive Impingement	58
28	High Speed Photography Defines Four Modes of Reactive Stream Impingement	59
29	A-50 Fuel Behaves Like MMH Fuel	63
30	$N_2H_4$ Fuel Exhibits the Same RSS Limits as MMH Fuel	64
31	Increasing Fuel Velocity Promotes RSS	66
32	Increasing Chamber Pressure Promotes RSS	67
33	Increasing Fuel Temperature Promotes RSS	69
34	Reactive Stream Impingement with the Small F-O-F Triplet Element	70
35	Reactive Stream Impingement with the Large F-O-F Triplet Element	71
36	Reactive Stream Impingement with the Small Sharp Edged Unlike Doublet	72
37	Reactive Stream Impingement with the Large Sharp Edged Unlike Doublet	73
38	Reactive Stream Impingement with the Space Shuttle/OMS Unlike Doublet No. 7	74
39	Reactive Stream Impingement with the XDT Platelet Element No. 10	76
40	Reactive Stream Impingement with the Splash-Plate Element No. 11	77
41	Reactive Stream Impingement with the Space Shuttle/OMS TL0L Platelet Element No. 9	78
42	Reactive Stream Impingement with the Space Shuttle/OMS TL0L Platelet Element Using $N_2H_4$ Fuel	79
43	Task I RSS Data Correlations	81
44	High Pressure Monopropellant Decomposition RSS Model	83

LIST OF FIGURES (cont.)

<u>Figure No.</u>		<u>Page</u>
45	Weber Number Model	85
46	Vapor Phase Reaction Model	86
47	Fuel Weber Number and MRVP RSS Correlation	87
48	Fuel Vaporization Controlled RSS Model	89



## ABSTRACT

An experimental and analytical program was conducted to develop an understanding of the mechanisms controlling hypergolic propellant reactive stream separation (RSS). RSS is a combustion induced phenomenon that results in striation of hypergolic propellant oxidizer and fuel sprays fans. This reduced intra-element mixing (compared to the well-mixed distribution developed in a non-reacting cold flow case) can influence thrust chamber performance, heat transfer, and stability. The program end product was development of design criteria for coping with RSS to allow the design of high performing, stable injectors. RSS mechanisms were identified using high speed color photography to observe reactive stream mixing of single element injectors tested with  $N_2O_4$ /MMH,  $N_2O_4$ /A-50, and  $N_2O_4$ / $N_2H_4$  propellants. Three hundred and fifty six tests were run over a chamber pressure range of 60-1000 psia, a fuel temperature range of 55°F-300°F, and a fuel velocity range of 30-200 ft/sec. This wide parametric characterization included modeling of the Space Shuttle Orbital Maneuvering System (OMS) and Reaction Control System (RCS) engine injectors.

Tests were conducted using five different conventionally machined unlike doublet elements and two triplet elements. Also, three platelet elements were tested. Platelet injectors are fabricated by bonding together a stack of thin metal sheets which have etched flow passages. A simulation of the Space Shuttle/RCS engine injector element was included in the unlike doublets and a simulation of the Space Shuttle/OMS engine platelet like-on-like doublet injector element was included in the platelet injectors.

The single element firings were conducted in a specially constructed chamber fitted with quartz windows for photographically viewing the impingement spray field. Analysis of the film identified the occurrence of reactive stream separation as evidenced by non-uniform spray fields.

ABSTRACT (cont.)

Distinct regions of mixing and separation were identified and correlated for each of the injectors tested. Color photographs of the combustion phenomena are included. Finally, a working model was developed that correlates RSS as a function of a fuel vaporization rate control parameter.

The most important design criteria derived from this work states that: "the element should be designed to avoid transition between mixed and separated modes within the engine operational envelope".

## I. SUMMARY

The objective of this program was to develop an understanding of the mechanisms controlling hypergolic propellant reactive stream separation (RSS). RSS is a combustion induced phenomenon that results in striation of hypergolic propellant oxidizer and fuel sprays fans. This reduced intra-element mixing (compared to the well-mixed distribution developed in a non-reacting cold flow case) can influence thrust chamber performance, heat transfer, and stability. The program end product was development of design criteria for coping with RSS to allow the design of high performing stable injectors. This objective was accomplished through high speed color photography and analysis of single element injector tests using  $N_2O_4/MMH$ ,  $N_2O_4/A-50$ , and  $N_2O_4/N_2H_4$  propellants. Three hundred and fifty six tests were run over a chamber pressure range of 60-1000 psia, a fuel temperature range of 55°F-300°F, and a fuel velocity range of 30-200 ft/sec. This wide parametric characterization included modeling of the Space Shuttle Orbital Maneuvering System (OMS) and Reaction Control System (RCS) engine injectors.

Tests were conducted using five different conventionally machined unlike doublet injectors and two triplet elements. Also, three platelet injectors elements were tested. Platelet injectors are fabricated by bonding together a stack of thin metal sheets which have etched flow passages. A simulation of the Space Shuttle/RCS injector was included in the unlike doublets and a simulation of the Space Shuttle/OMS engine platelet like-on-like doublet injector (T-LOL) was included in the platelet injectors.

The hot firings were conducted in a specially constructed chamber fitted with quartz windows for photographically viewing the impingement spray field. Analysis of the film identified the occurrence of reactive stream separation as evidenced by non-uniform spray fields. Four modes of impingement were identified from the film; Penetration, Mixing, Mix/Separate and Separation. Penetration occurs at low injection velocity (less than 50 ft/sec), low fuel temperatures (below 70°F) and low chamber pressure (less than 100 psia) and

## I, Summary (cont.)

is evidenced by "shoot-through" of the fuel and oxidizer. Penetration has been reported in earlier cold flow work and was also observed on this program using propellant simulants as well as reactive streams. Penetration is a consequence of the non-reactive momentum exchange mixing process. Mixing is observed at moderate injection velocities (50-100 ft/sec), moderate fuel temperatures (70-90°F) and moderate chamber pressures (100-200 psia). It is evidenced by a highly uniform spray field which looks similar to a non-reactive spray field. Mix/Separate occurs at the onset of RSS. It is evidenced by a slightly non-uniform spray field. Separation is observed at higher injection velocities (greater than 100 ft/sec), higher fuel temperature (greater than 90°F), and higher chamber pressures (greater than 200 psia). It is evidenced by highly non-uniform spray fields in which distinct regions of unmixed fuel and oxidizer exist.

Distinct regions of mixing and separation were identified and correlated for each of the injectors tested. It was found that regimes of RSS with the coherent stream types of injector (i.e., the unlike doublets and triplets) are all correlated by the equation;

$$P_c = 4.4 \times 10^8 (\text{REF})^{-1.5} \quad \text{Equation (1)}$$

where:

REF = Fuel Orifice Reynolds Number.

Mixing occurs at chamber pressures less than that specified by Equation (1) and separation occurs at greater chamber pressures. Regimes of RSS with the self-atomizing platelet types of injectors (i.e., the etched flow passages create mechanical jet atomization for a single element) are correlated by:

## I, Summary (cont.)

$$P_c = 1272 (\text{REF})^{-0.24} (\text{XDT \& Splash Plate}) \quad \text{Equation (2a)}$$

$$P_c = 839 (\text{REF})^{-0.24} (\text{TL0L}). \quad \text{Equation (2b)}$$

Again mixing occurs at chamber pressures below this value and separation occurs at pressures greater than this. The fuel Reynold's number (REF) successfully correlated RSS because fuel vaporization was identified as the combustion rate limiting mechanism for the propellant combinations tested.

Injector design criteria were developed and are included as Appendix A of this report. The most important design criteria derived from this work states that, "transitions from regimes of mixing to separation and vice-versa should be avoided within the engine operational envelope". If an element can not be made to operate entirely within the mixing regime then it is better to redesign the element such that it operates entirely within the separation regime. The reason for this design approach is to create relatively constant combustion response to allow optimum design of injector/chamber performance, heat transfer, and stability characteristics. Coherent jet RSS was shown to be a strong function of the operating chamber pressure. The self-atomizing elements tend to operate predominately in the separated mode for most practical applications and are relatively insensitive to chamber pressure change. They are therefore ideal for engines which must operate over wide  $P_c$ -MR ranges.

Testing with the Space Shuttle/RCS unlike doublet identified non-reactive off-momentum effects that can also modify spray mixing uniformity with unlike doublets. These results show that elements that are insensitive to momentum changes such as the triplet or pentad are preferable to unlike doublets for engines that must operate over a wide mixture ratio range.

## II. INTRODUCTION

The objective of this program was to develop an understanding of the mechanisms controlling hypergolic propellant reactive stream separation (RSS). The program end product was development of design criteria for coping with RSS to allow the design of high performing stable injectors.

Hypergolic earth-storeable  $N_2O_4$ /Amine propellants have been historically used for a wide range of liquid propulsion system applications. They are used on the first, second and third stages of the Titan II and Titan III launch vehicle. Also, they have been the near exclusive choice for reaction control and orbital maneuvering systems with low to moderate  $\Delta V$  requirements (e.g., Apollo and Space Shuttle). These propellants are highly reactive and can experience reactive stream separation (RSS) (i.e., blowapart) which can inhibit intra-element mixing hence reducing the overall spray mixture ratio and mass distribution. Modifications of the spray uniformity can result in altered combustion efficiency, gas-side heat transfer coefficient, and stability. It is imperative that the RSS phenomena be understood so that the designer of today's high efficiency engines can cope with its effects.

Several studies (References 1-17) have been conducted over the past decade in an effort to understand the RSS phenomena, identify operational limits of RSS, and develop design criteria for its avoidance. Several RSS models were postulated but none were able to account for all of the experimental data. Also conflicting data were reported due to problems of definition and problems of experimental limitation.

This study was undertaken to; clarify some of the previous studies; to provide a consistent set of data for the identification of mechanisms responsible for RSS and; to map RSS regimes for a wide range of injector elements including Space Shuttle applications. The injector elements and the range of parameters tested are summarized in Table I. A more detailed data summary is included in Appendix B.

TABLE I

## SUMMARY OF INJECTOR ELEMENTS AND TEST CONDITIONS

<u>Fuel</u>	<u>Injector* Elements</u>	<u>P<sub>c</sub> (psia)</u>	<u>V<sub>f</sub> (ft/sec)</u>	<u>T<sub>f</sub> (°F)</u>	<u>MR</u>
H <sub>2</sub>	1,2,3,4,5 6,7,8,9,10,11	40-1000	30-220	50-300	1.4-3.2
A-50	1	90-1000	50-160	60-85	1.6-1.7
H <sub>2</sub>	1,4,5,8	60-400	30-175	60-90	1.4-2.0
<u>*Injector Element Code</u>					
1.	Rounded Inlet Unlike Doublet, D <sub>f</sub> = 0.020 Long Impingement (.160 in.)	5.	Small Sharp Edged Unlike Doublet, D <sub>f</sub> = 0.020	9.	Space Shuttle/OMS TL0L Platelet Injector, D <sub>f</sub> = 0.028
2.	Rounded Inlet Unlike Doublet, D <sub>f</sub> = 0.020 Short Impingement (.040 in.)	6.	Large Sharp Edged Unlike Doublet, D <sub>f</sub> = 0.030	10.	XDT Platelet, D <sub>f</sub> = 0.021
3.	Small F-0-F Triplet D <sub>f</sub> = 0.020	7.	Space Shuttle/RCS Unlike Doublet, D <sub>f</sub> = 0.023	11.	Splashplate Platelet, D <sub>f</sub> = 0.021
4.	Large F-0-F Triplet D <sub>f</sub> = 0.023	8.	Space Shuttle/RCS Unlike Doublet, Offset Impingement, D <sub>f</sub> = 0.023		

## II, Introduction (cont.)

Fuel vaporization rate controlled combustion was identified as the RSS governing mechanism and was used to develop an RSS model. RSS operating limits were defined for all of the injector elements listed in Table I.

Injector design criteria were developed and are included as Appendix A of this report. The primary element design criteria states that the elements should be designed to avoid transitions between mixed and separated modes within the engine operating Pc-MR range. The element design criteria provides the necessary data required to meet this goal.

The technology developed on this program has been used to aid the development of the Space Shuttle Orbital Manuevering System (SS/OMS) engine, the development of an advanced injector during the Improved Transtage Injector Program (ITIP), and to characterize the Space Shuttle Reaction Control System (SS/RCS) engine injector element. The study results are also applicable to future systems, particularly those utilizing earth storable hypergolic propellants.



### III. TECHNICAL APPROACH

The objective of this program was to develop an understanding of the mechanisms controlling hypergolic propellant RSS. Design criteria for coping with RSS to allow the design of high performing stable injectors would be developed with that understanding. The approach taken was to clarify some of the previous studies to provide a consistent set of data for the identification of mechanisms responsible for RSS, and to map RSS regimes for a wide range of injector elements that included Space Shuttle engine applications. Clarification of the previous studies was accomplished through an evaluation of the data and RSS models found in the literature. These results were used to initiate an iterative model development/test program as shown in Figure 1.

The program was incrementally funded as indicated in Figure 2. Spreading the funding over a four year period has proven to be a cost effective way to develop this technology. Sufficient time was available to thoroughly assess the data, apply the results to engine development problems, and get feedback for program direction, as illustrated in Figure 1. This work was especially instrumental in the successful development of the Space Shuttle/OMS engine platelet injector.

The inter-relationship of each task toward development of the program final vaporization controlled RSS model is shown in Figure 3. The Task I objectives were to; critique all existing models relating to RSS, review and summarize all associated RSS data, and formulate updated RSS model based on existing data. The results of this work are documented in Reference 18.

The Task II objective was to prepare a detailed program plan, i.e., to formulate a detailed method of approach to be taken for model testing and verification in subsequent tasks. This work is documented in Reference 19.

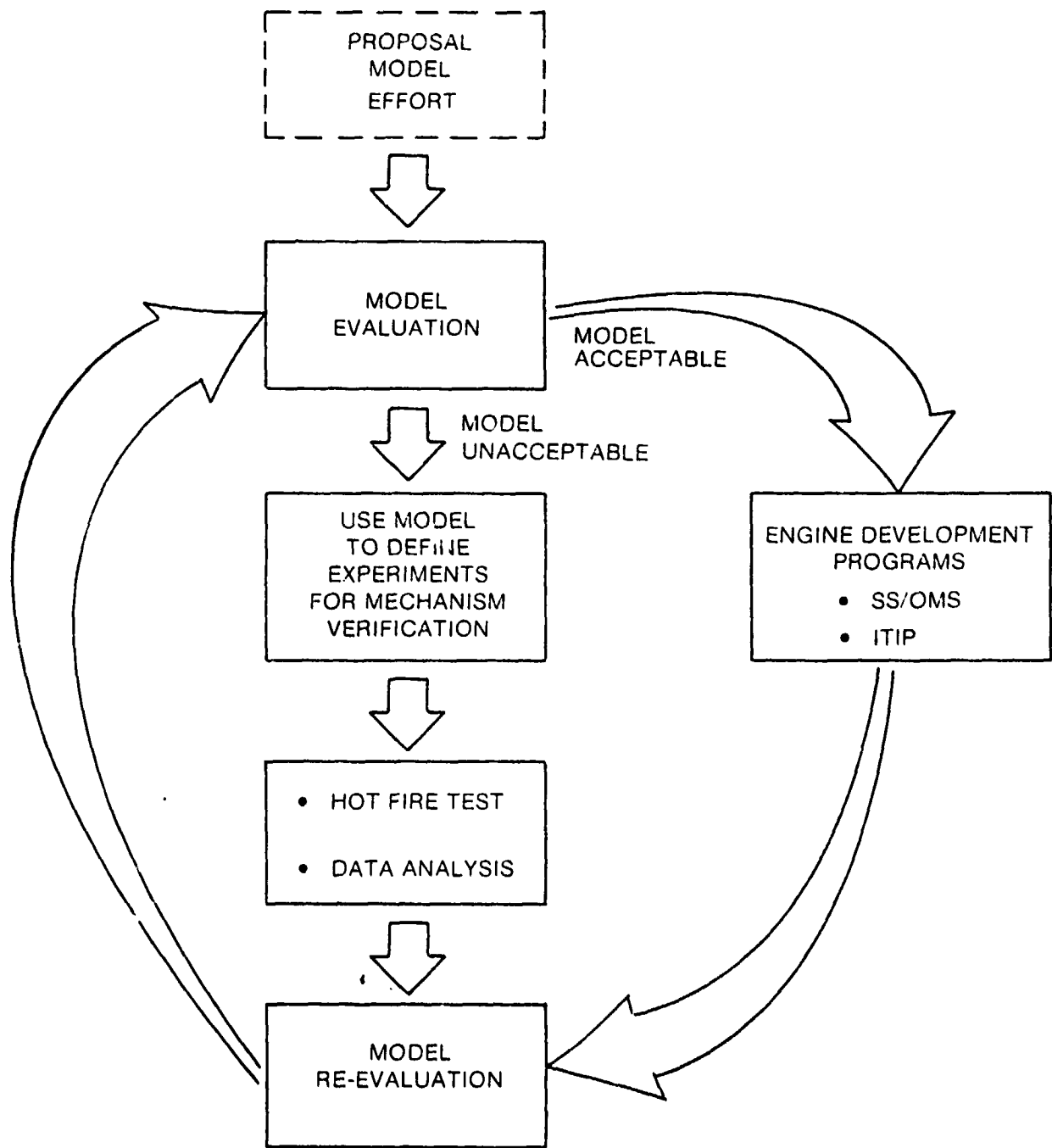


Figure 1. RSS Model Development Approach

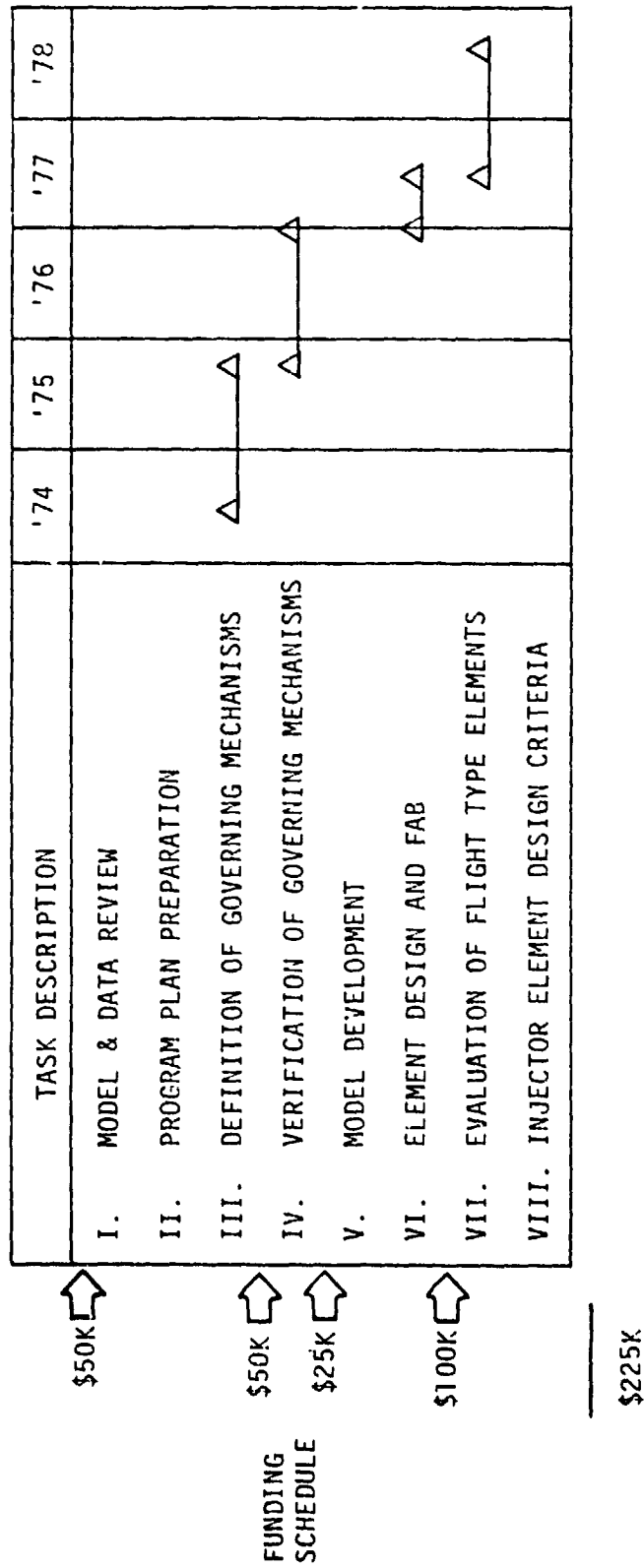


Figure 2. Blowpart Technology Program Approach

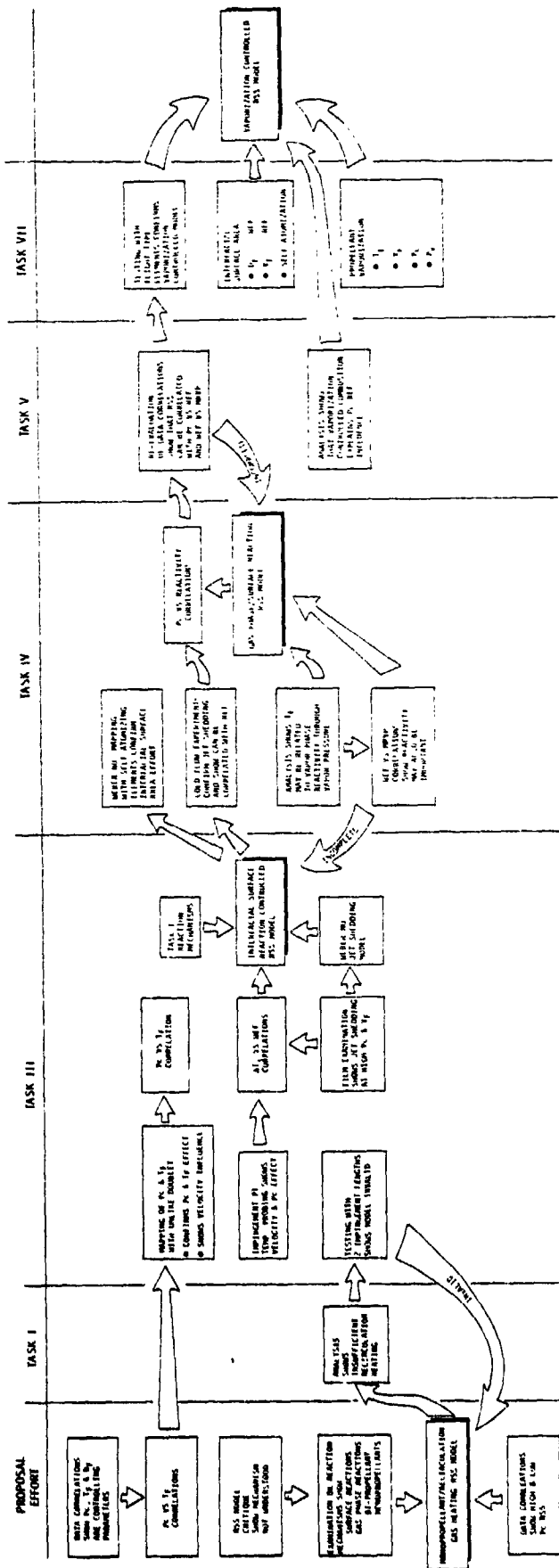


Figure 3. RSS Model Development Chronology

ORIGINAL PAGE IS  
OF POOR QUALITY

### III, Technical Approach (cont.)

The Task III objectives were to define the mechanisms governing RSS, establish limits for RSS and to define appropriate models. The work included; design, fabrication and testing of two single element unlike doublet injectors, incorporation of high speed photographic techniques for visual propellant stream characterization, and correlation of RSS with various independent test variables. The results of the Task III work are documented in Reference 20.

The Task IV objectives were to; establish operating limits for RSS for other injector types, and verify mechanisms governing RSS and the appropriate physical models resulting from the Task III work. The Task IV effort included the design, fabrication and testing of triplet and self-atomizing platelet injectors. The term "self-atomizing" as used here means that a single propellant provides the atomization, either by self impingement or by impingement with a surface. This work is documented in Reference 21.

The objective of Task V was to review all available reactive stream separation data and develop a more comprehensive RSS model. This model effort was directed toward definition of mixed and separated zones which can be related to injector element design and operating parameters. The output of this task was used to select operating conditions to be tested in Task VII, the final model verification tests.

The objective of Task VI was to design and fabricate two flight type injectors. A sharp-edged unlike doublet and the Space Shuttle/RCS unlike doublet element were selected. Each of the injectors incorporated independently manifolded elements so that two different single element designs were built within each of the injector bodies. In addition, a previously designed and fabricated platelet like doublet element (TL0L), which dupli-

### III, Technical Approach (cont.)

cates the SS/OMS engine core element design was made available for Task VII testing. The results of Task V and VI are documented in Reference 22.

The Task VII objectives were to define regimes of RSS for the flight type injector elements fabricated in Task VI. Testing included the sharp-edged unlike doublet, the Space Shuttle/RCS unlike doublet, the Space Shuttle/OMS platelet TLOL, and the rounded inlet unlike doublet. Both MMH and  $N_2H_4$  fuels were tested. The results of this work are included herein.

The Task VIII objective was to prepare an element design criteria for coping with the effects of RSS. The design criteria are included as Appendix A.

#### IV. RESULTS AND CONCLUSIONS

##### A. RESULTS

Regimes of RSS were identified for the following coherent jet and self-atomizing impingement type injector elements using high speed color photography;

Coherent Jet Elements	{	◦ Unlike Doublet
		◦ Rounded Inlet Long L/D (L/D = 12)
		◦ Sharp Edged Short L/D (L/D = 5)
		◦ Space Shuttle/RCS (L/D = 10)
		◦ Fuel-Oxidizer-Fuel Triplet
Self-Atomizing Elements	{	◦ X-Doublet Platelet
		◦ Splash Plate Platelet
		◦ Space Shuttle/OMS Like-on-Like Doublet Platelet

Vaporization controlled combustion has been identified as the mechanism controlling RSS with both coherent and self-atomizing injector elements. Data correlations for coherent jet elements made on the basis of a vaporization controlled RSS model show that regimes of RSS are correlated with chamber pressure and the fuel orifice Reynolds Number as shown in Figure 4. The fuel orifice Reynolds Number correlates RSS because fuel vaporization is combustion rate controlling for the  $N_2O_4$ /Amine fuels propellant combinations. The Reynolds number includes the design parameters that have a first order influence on vaporizing rate. The chamber pressure exhibits the strongest influence on RSS, increasing chamber pressure promotes RSS. Orifice diameter, injection velocity and propellant temperature effects are correlated with the fuel orifice Reynolds Number. Increasing anyone of these promotes RSS. Self-atomizing elements experience RSS at lower pressure and show less of a Reynolds Number dependence than the coherent jets as shown in Figure 5.

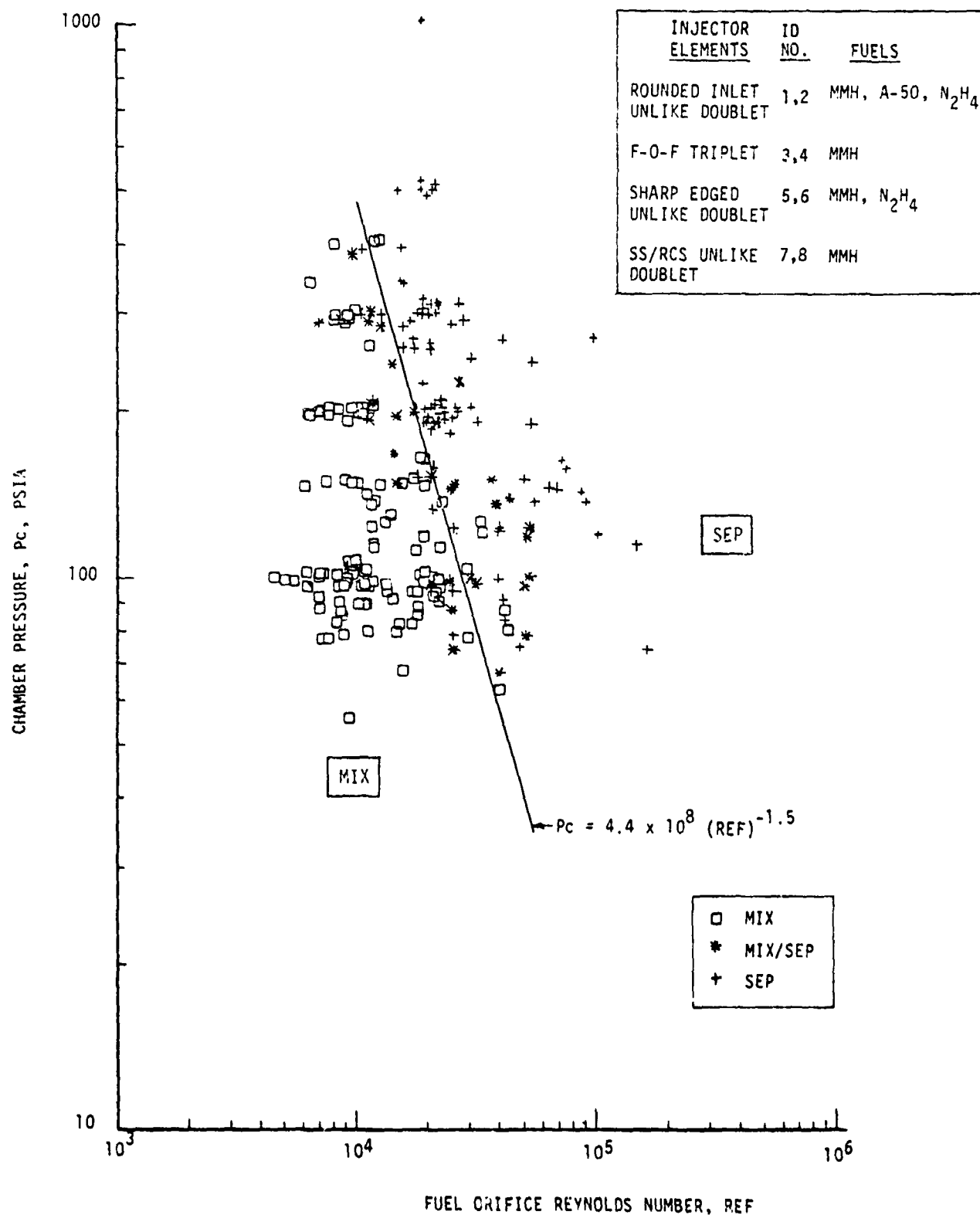
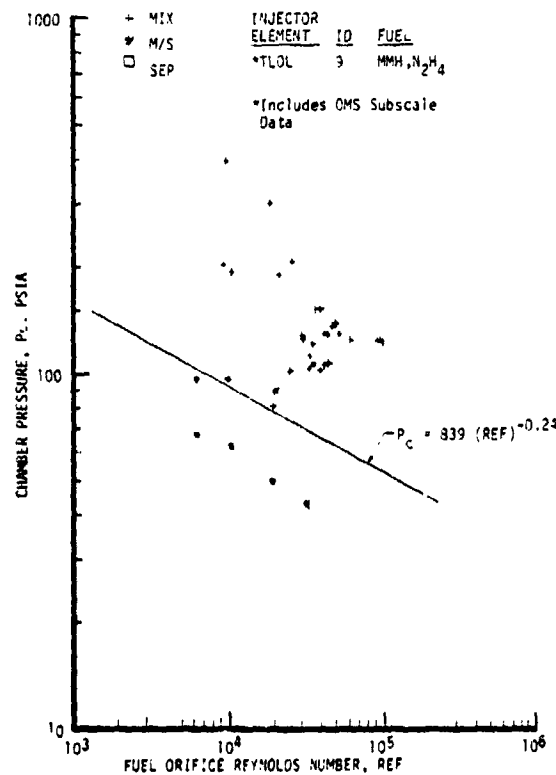
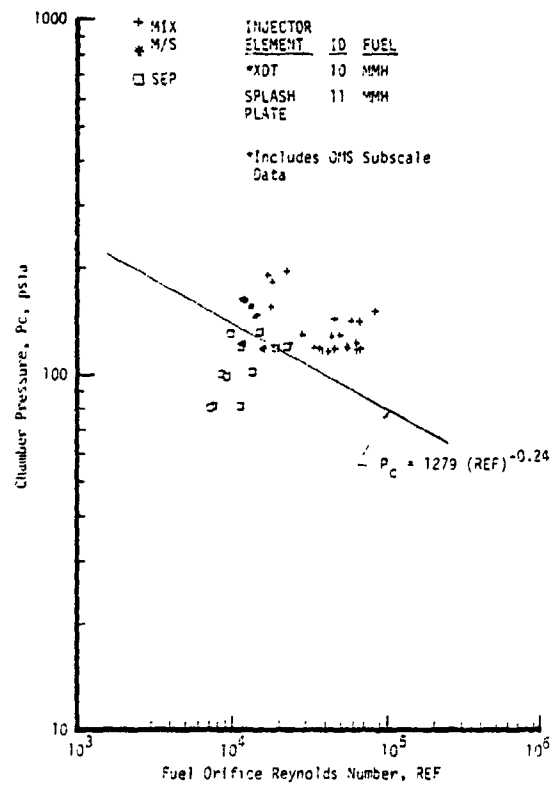


Figure 4. Vaporization Model Correlates RSS for Coherent Stream Impingement Injector Elements





ORIGINAL PAGE IS  
OF POOR QUALITY

Figure 5. Vaporization Model Correlates RSS for Self-Atomizing Injector Elements

#### IV, Results and Conclusions (cont )

##### B. CONCLUSIONS

The following conclusions are drawn from this work.

1. The single element hot fire investigation technique has provided an effective, low-cost approach for understanding the earth-storable hypergolic propellant combustion process.
2. Photographic coverage of single element combustion has been verified as a valuable process understanding technique.
3. RSS is a consequence of vaporization controlled combustion at the impingement interface.
4. RSS regimes are defined by the chamber pressure and fuel orifice Reynolds Number for a wide range of injector elements.
5. Operation in RSS transition regimes should be avoided if the spray mass and mixture ratio distributions are to be controlled.
6. RSS technology has benefited storable engine development.
7. Non-hypergolic impingement may experience RSS since vaporization is the controlling mechanism.

## V. APPLICATION OF RESULTS AND RECOMMENDATIONS

### A. APPLICATION OF RESULTS

The application of the results of this program can be grouped under three headings; 1) development of RSS design criteria and high speed color photography techniques for hypergolic propellants, 2) application of these techniques on current hypergolic propellant technology and development programs, and 3) application of these techniques to advanced systems utilizing other propellant combinations.

#### 1. Hypergolic Propellant RSS Models and Techniques

The primary result of this program is the development of design criteria for coping with RSS experienced with hypergolic  $N_2O_4$ /Amine propellants. These design criteria provide guidelines for the design of high performing stable injectors. Criteria for both coherent stream and atomized spray impingement type of injector elements are included. (See Appendix A).

A secondary but important result of this program is the development of high speed color photography techniques for observing single element injector combustion. RSS design criteria could not have been developed without these techniques. The high speed color photography is applicable to both single and multiple element injector combustion tests.

#### 2. Application to Current Programs

These photographic techniques were used on the Acoustic Cavity Technology for High Performance Injector Program (Ref. 23), Contract NAS 9-14232, to observe cavity/injector pattern interactions. The understanding gained has aided the development of stability prediction models at the Aerojet Liquid Rocket Company.

## V, A Application of Results (cont.)

The technology and techniques developed on this program were used on the Space Shuttle/OMS engine injector development program (Ref. 24) to solve an injector related "resurge" stability problem. A high frequency "resurge" instability persisted despite numerous design modifications. Analysis of OMS and OME technology test results indicated that "resurge" instability involved chamber acoustics, injector hydraulics, and the combustion process. The first order stability influencing parameters were found to be the injector element design, the injector ring manifold and orifice hydraulics and the chamber acoustic cavity configuration.

ALRC combustor stability models were used to evaluate injector designs to predict differences in their stability characteristics. Their predicted stability behavior were then compared to the experimentally known behavior to identify the probable mechanisms and appropriate design parameters which might account for the stability differences. The following parameters were identified as stabilizing influences and consequently selected for element design criteria:

- ° Element hydraulic inertance
- ° Unlike impingement height
- ° Atomization
- ° Element and pattern mixing rate
- ° Energy Release Efficiency (ERE) vs chamber length profile.

Understanding of these combustion parameters was accomplished through the use of uni-element and multi-element subscale injectors. Uni-element injector cold flow tests were conducted to characterize the element and spray hydraulics to determine the spray fan geometry, the unlike impingement height, the relative atomization distribution, and the element pressure drop. The more promising uni-element designs were hot fire tested in

## V, A, Application of Results (cont.)

the photographic chamber designed and fabricated on this program to compare element spray combustion rates and sensitivity. Hot fire characterization was achieved through:

1. Analysis of high speed movies using techniques developed on this contract to identify the influence of design parameters and operating conditions on relative spray mixing and "blowpart".
2. Measurement of  $C^*$  performance used to quantify spray mixing influences.
3. Perturbation of the element sprays with a shock tube to measure their high frequency combustion pressure response.

The fundamental understanding of the combustion process gained from the subscale tests was used to synthesize three fullscale platelet injector patterns for dynamic combustion stability demonstration. No evidence of "resurge" instability was encountered on any of the three full scale platelet injectors. Furthermore, all delivered acceptable performance and demonstrated that it is not necessary to sacrifice performance to improve stability characteristics. Good chamber compatibility was also achieved.

The transverse like-on-like (TLOL) platelet injector element was selected for the OMS engine as a result of the subscale program. The spray mass and mixture ratio distributions produced by this element were found to be insensitive to engine operating point which permits greater predictability of performance, compatibility and stability. The TLOL platelet element OMS injector pattern design has in fact demonstrated good performance, excellent combustion stability and excellent chamber compatibility. The OMS engine is the first manned engine to be flight qualified to the rigid CPIA 247 stability specification.

## V, A, Application of Results (cont.)

The Space Shuttle/RCS engine injector element was photographically characterized over its full chamber pressure/mixture ratio operating range. This element was observed to be extremely sensitive to operating condition not only from an RSS standpoint but also from a stream momentum balance standpoint. These photos have aided understanding of the SS/RCS engine performance and compatibility.

### 3. Application to Future Systems

The photographic techniques developed on this program can be used to establish an understanding of combustion phenomena associated with any fuels and injectors. The fuel vaporization rate controlled RSS model developed during the program is currently being extended to hydrocarbon fuels on the Photographic Combustion Characterization of LOX/Hydrocarbon Type Propellants Program, Contract NAS 9-15724. This investigation will also utilize single element photography to gain understanding of combustion processes.

## B. RECOMMENDATIONS

The following recommendations are made on the basis of the program results.

1. The RSS criteria should be incorporated into the JANNAF standardized performance computer programs to warn the designer of operation within RSS regimes.

2. The photographic techniques should be used to define combustion mechanisms with fuels for prospective new engines.

## VI. TECHNICAL DISCUSSION

### A. EXPERIMENTAL HARDWARE AND TEST SETUP

#### 1. Test Apparatus

The test apparatus consists of a test chamber equipped with transparent viewing ports and removable injectors and nozzles as shown in Figure 6. The test chamber and an unlike doublet injector were designed and fabricated during the Task III effort. Two triplet and two platelet injector elements were designed and fabricated during the Task IV effort. Two sharp-edged unlike doublet elements and two Space Shuttle/RCS unlike doublet elements were designed and fabricated during Task V and VI.

##### a. Test Chamber

The test chamber was machined from a 4-inch square x 6-inch long block of 304 CRES. The combustion chamber section is 4 inches (10.16 cm) long, to which a 2 in. (5.08 cm) L\* spacer is bolted to increase the combustion zone length to 6 inches (15.2 cm). The block was bored to provide a 2.75 inch (6.99 cm) diameter combustion chamber. Four circular quartz windows were provided to facilitate photography and to allow flexibility in photographic lighting of the combustion process. The windows are 1/2 inch (1.27 cm) thick to provide a safety margin for 1000 psia ( $6.89 \times 10^5 \text{ N/m}^2$ ) operation. The flat quartz windows are sandwiched between durabula gaskets for cushioning against ignition shocks and uneven loading. A silicon "O" ring provides sealing on the window periphery. Quartz windows are used to provide good propellant compatibility and well defined optical properties.

The chamber was designed to provide an inert gas ( $\text{GN}_2$ ) film purge to prevent obscuring the view by propellant spray impingement

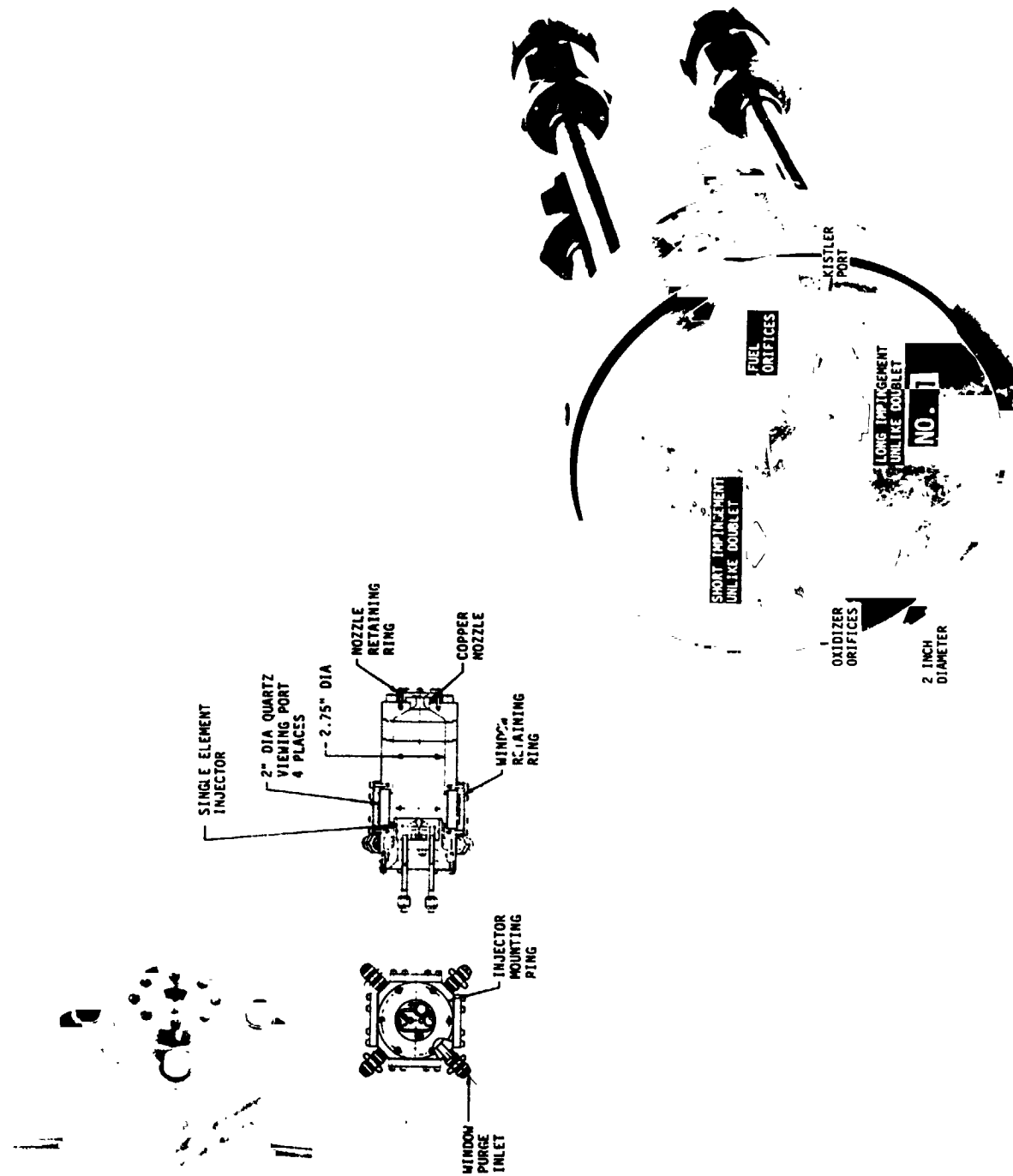


Figure 6. Photographic Test Chamber and Single Element Injector

ORIGINAL PAGE IS  
OF POOR QUALITY



## VI, A, Experimental Hardware and Test Setup (cont.)

on the windows. The gas purge flow is injected through four inlets into an annular manifold. The gas is directed from the manifold through an annular gap and made to flow around the periphery of the chamber wall. The gas passages were sized such that the  $\text{GN}_2$  is injected into the chamber at 50 ft/sec (15.2 m/sec) at 300 psia ( $2.07 \times 10^6 \text{ N/m}^2$ ) chamber pressure to minimize mixing with the propellant spray and combustion gas. Task II testing showed that the cold  $\text{GN}_2$  purge gas causes poor spray field visibility due to the density gradient created between it and the hot combustion gas. A significant improvement in visibility was made during Task IV by eliminating the purge gas entirely. All subsequent tests were run without purge gas.

Provisions was made for mounting both high and low frequency response pressure transducers and thermocouples. The nozzles consist of removable copper inserts drilled to provide the desired operating pressures.

### b. Injectors

Four different unlike doublet injectors, two triplet injectors, and three platelet injectors were tested during the program. The detailed orifice configurations for each of these injectors are shown in Figure 7. All but the SS/OMS platelet injector were designed and fabricated on this program. The SS/OMS injector was obtained from the OMS subscale injector development program (Reference 24).

#### (1) Task III Injector

The injector bodies were made in a cylindrical "piston" shape as shown in Figure 8 to fit into the chamber purge ring located at the forward end of the chamber. The injector is held in the

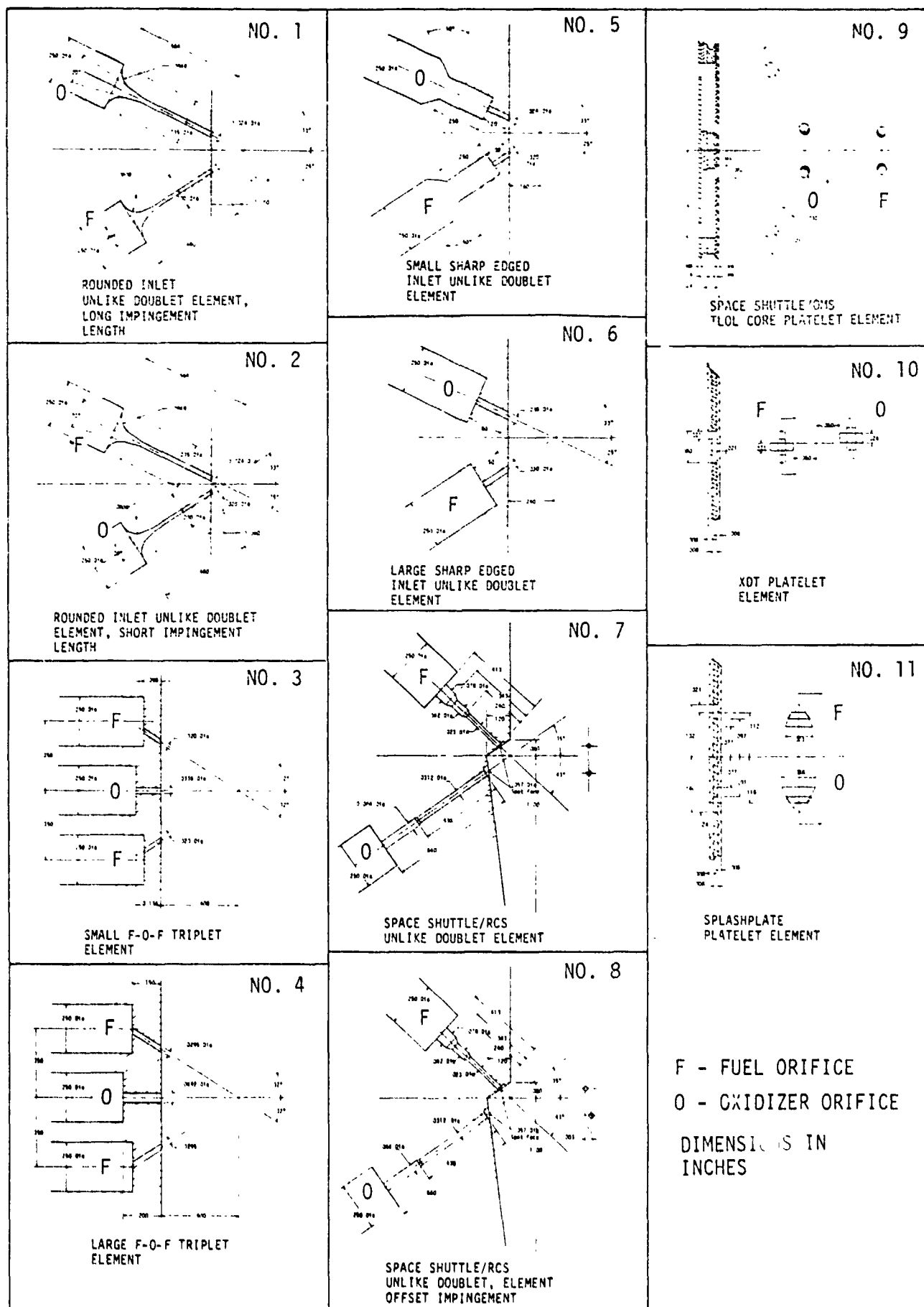
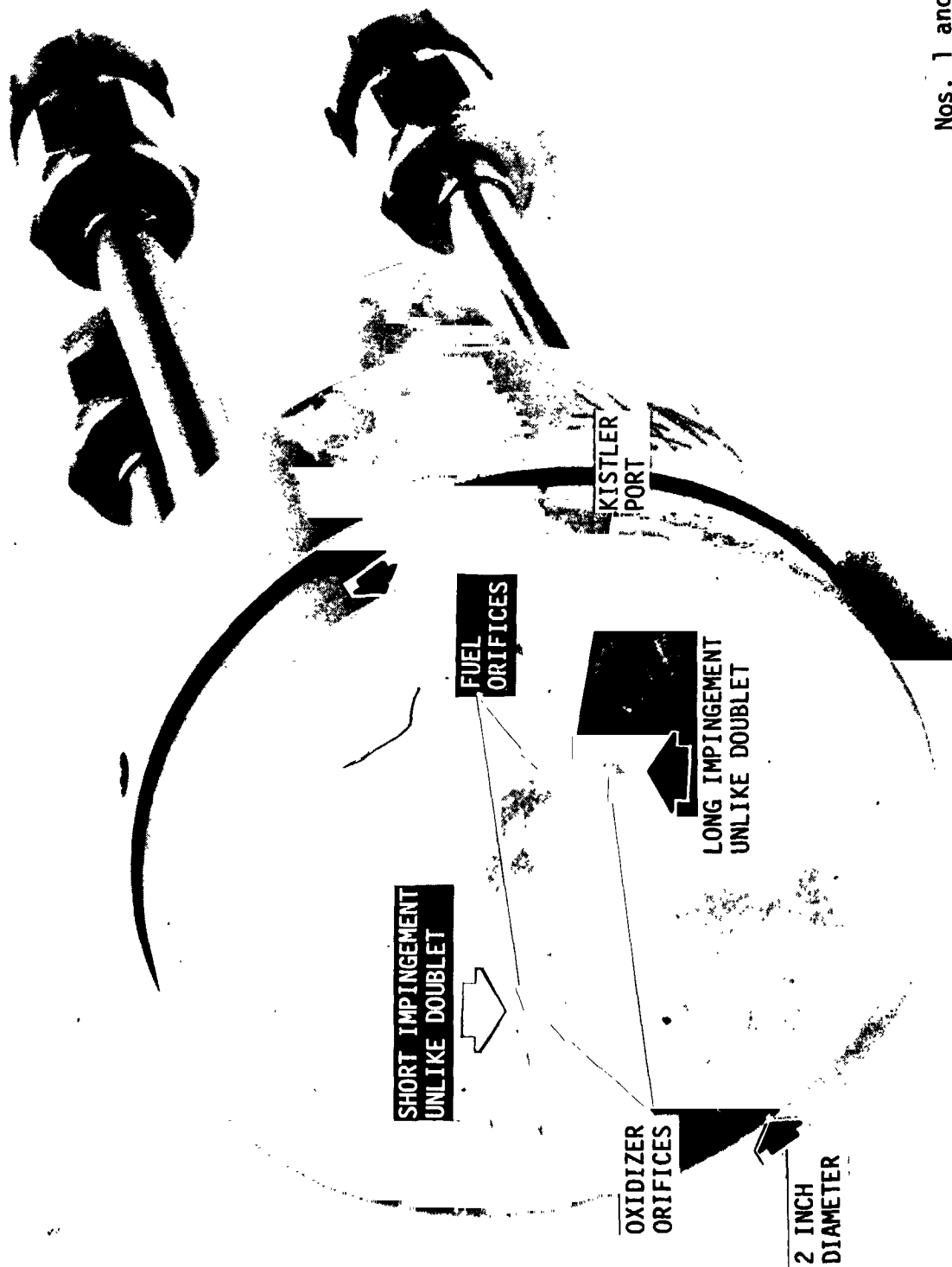


Figure 7. Injector Element Orifice Configurations



Nos. 1 and 2

Figure 8. Rounded Inlet Unlike Doublet Injector

ORIGINAL PAGE IS  
OF POOR QUALITY

## VI, A, Experimental Hardware and Test Setup (cont.)

purge ring by allen head screws. A silicon rubber O-ring seals the injector to the purge ring.

The injector consists of a main body with brazed-on inlet tubes. The injectors were made of 304 CRES to permit braze assembly and provide dimensionally stable orifices. Two injector patterns were incorporated in one body as shown in Figure 6 to reduce fabrication costs. The Task III rounded inlet unlike doublet element design parameters are included in Figure 5. The orifice L/D's were made long (24/1) with rounded inlets to provide controlled hydraulics.

The injector orifices were flow tested prior to the Task III hot fire testing to measure Kw's and to verify impingement accuracy. The flow data are discussed in Section VI.C.1. Subsequent cold flow tests were run during Task IV to characterize the rounded inlet orifice hydraulics. Results of these tests are also discussed in Section VI.C.1.

A high frequency response Kistler pressure transducer mounting port was provided in the long impingement doublet as shown in Figure 6 to measure impingement point disturbances. This port was also used to install a high response thermocouple for measuring the impingement point temperature rise.

### (2) Task IV Injectors

The F-O-F triplet element and the self-atomizing platelet element were selected for test evaluation during Task IV. Two different triplet injectors were designed to evaluate the influence of orifice diameter on RSS. The large triplet element has 0.030 inch (.076 cm) diameter fuel orifices and the small one has 0.020 (.05 cm) inch dia.

## VI, A, Experimental Hardware and Test Setup (cont.)

fuel orifices as shown in Figure 9. The orifice design details are shown in the schematic of Figure 7. Both elements were EDM machined into the same injector body to reduce fabrication costs. Separate propellant inlets were provided.

The orifices were designed with short L/D's and sharp edged inlets to simulate typical rocket injector orifice hydraulics. The results of a cold flow evaluation of the triplet injectors are discussed in Section VI.C.1.

The X-doublet and the splashplate self atomizing platelet elements shown in Figure 10 were selected for test evaluation. Both elements were photoetched into the same platelet stack to minimize cost. The platelet stack was bolted to an injector body provided with a single set of propellant inlets. Manifolding of the desired element was accomplished by rotation of the platelet stack. "O" rings were used to seal the platelet stack propellant passages to the injector body.

The X-doublet element consists of a parallel self-atomizing fuel and a parallel self-atomized oxidizer stream placed in close proximity to one another such that mixing occurs by parallel stream momentum exchange. Self-atomization is accomplished by self-impingement within the platelet stack as shown in Figures 10 and 13. The resultant atomized stream is ejected perpendicularly from the platelet stack. The splash plate element consists of one self-atomized fuel stream impinging on one self-atomized oxidizer stream. The self-atomization is produced by impinging the propellant stream against a splash plate as shown in Figure 10.

### (3) Task VI Injector

The sharp-edged inlet unlike doublet, the Space Shuttle/RCS unlike doublet, and the Space Shuttle/OMS platelet



Nos. 3 and 4

Figure 9. F-0-F Triplet Injector

ORIGINAL PAGE IS  
OF POOR QUALITY

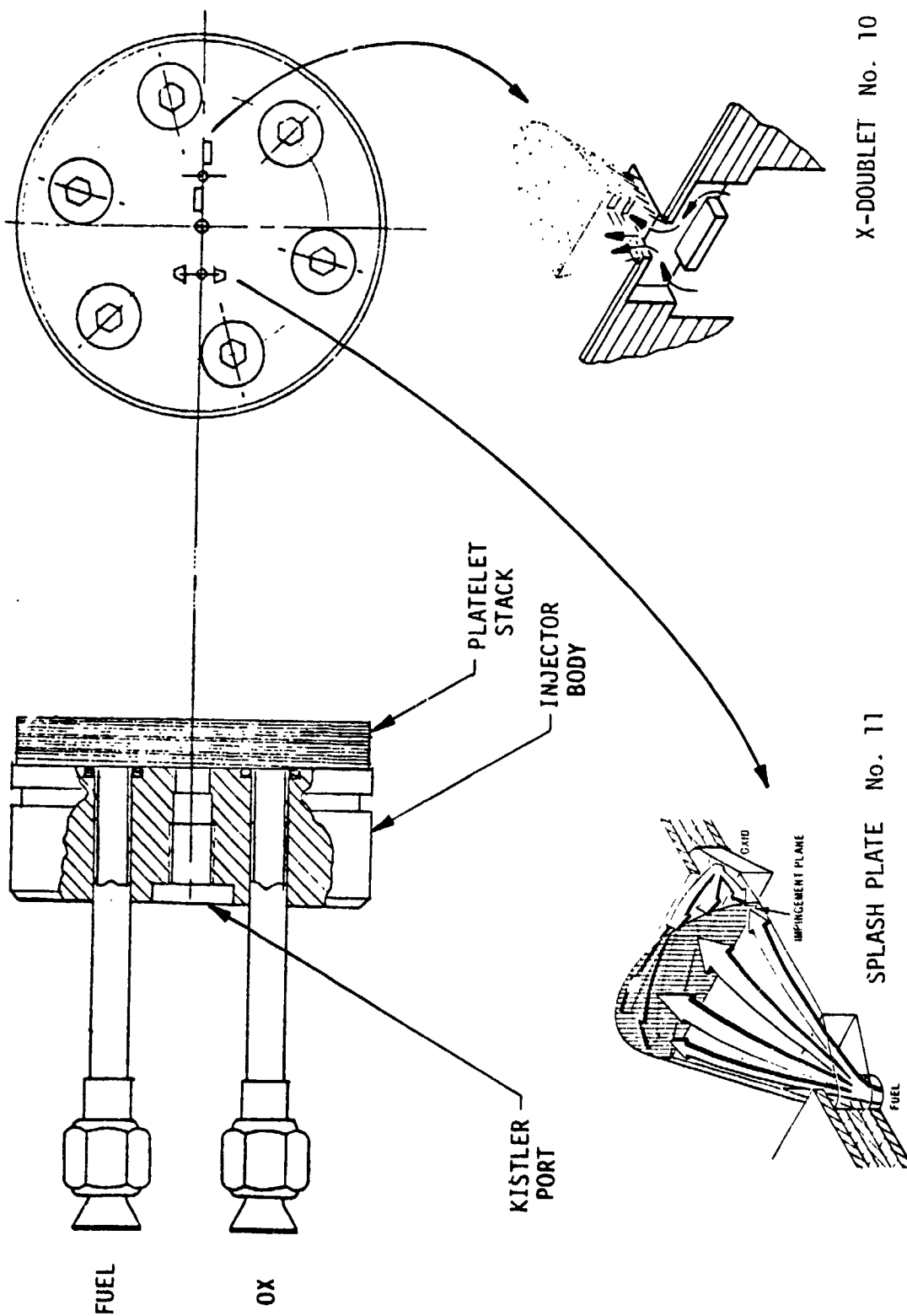


Figure 10. XDT and Splash Plate Platelet Injectors

## VI, A, Experimental Hardware and Test Setup (cont.)

TLOL elements were selected in Task V for testing in Task VII. The sharp-edged inlet unlike doublet injectors are shown in Figure 11. The orifice configurations are shown in Figure 7. The L/D's were selected to be about 4/1 to represent a typical flight configuration. Two fuel orifice diameters were selected, a 0.020 in. diameter and a 0.030 in. diameter, to determine orifice diameter effects. Both elements were EDM'ed into the same injector body to save fabrication costs.

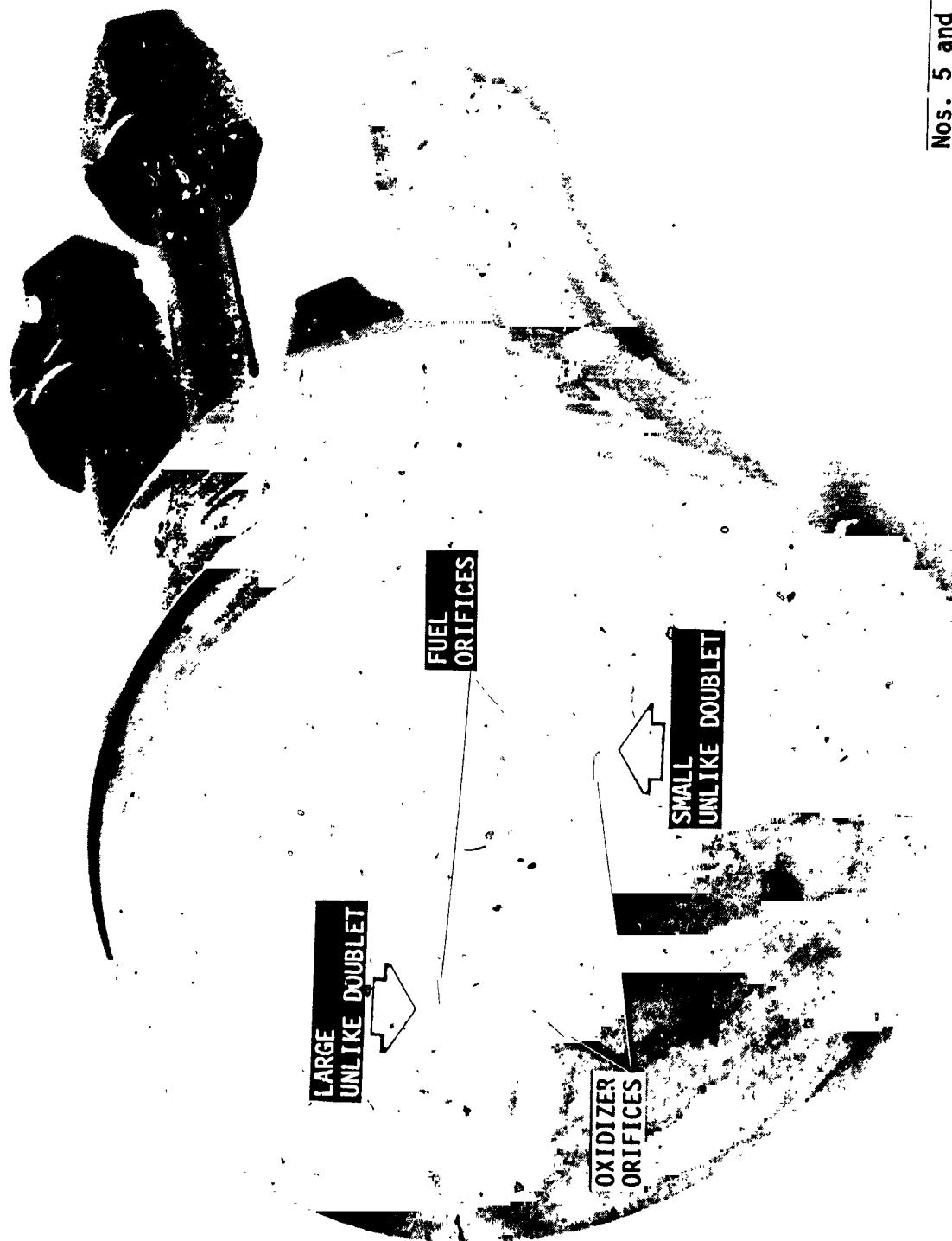
The Space Shuttle/RCS unlike doublet injector is shown in Figure 12. The detailed orifice configuration is shown in Figure 7. Two elements were designed and fabricated to test the effect of impingement mismatch. One element was made per the design with good centerline impingement. The second element was made with a 0.003 inch impingement mismatch. The results of cold flow of these elements are discussed in Section VI.C.1.

The Space Shuttle/OMS engine platelet Transverse Like On Like (TLOL) injector element is shown in Figure 13. The TLOL element is designed to simulate the spray mixing of a conventional like-on-like injector. The fuel and oxidizer streams are made to impinge on one another to form sprays which are subsequently impinged. The platelet stack contains two elements, the core element and the boundary element which differ only in unlike impingement height. The boundary element has a longer impingement height and lower fan cant angle than the core element. Only the core element was tested on this program.

### 2. Hot Fire Test Facility Setup

The test apparatus was setup in the ALRC Research Physics Laboratory Test Bay 2 as shown in Figure 14. A schematic of the propellant system used is shown in Figure 15. Propellant (MMH/A-50/N<sub>2</sub>H<sub>4</sub>/NTO) is stored in 50-gallon, 3000-psi run vessels. Gaseous nitrogen pressurization of these



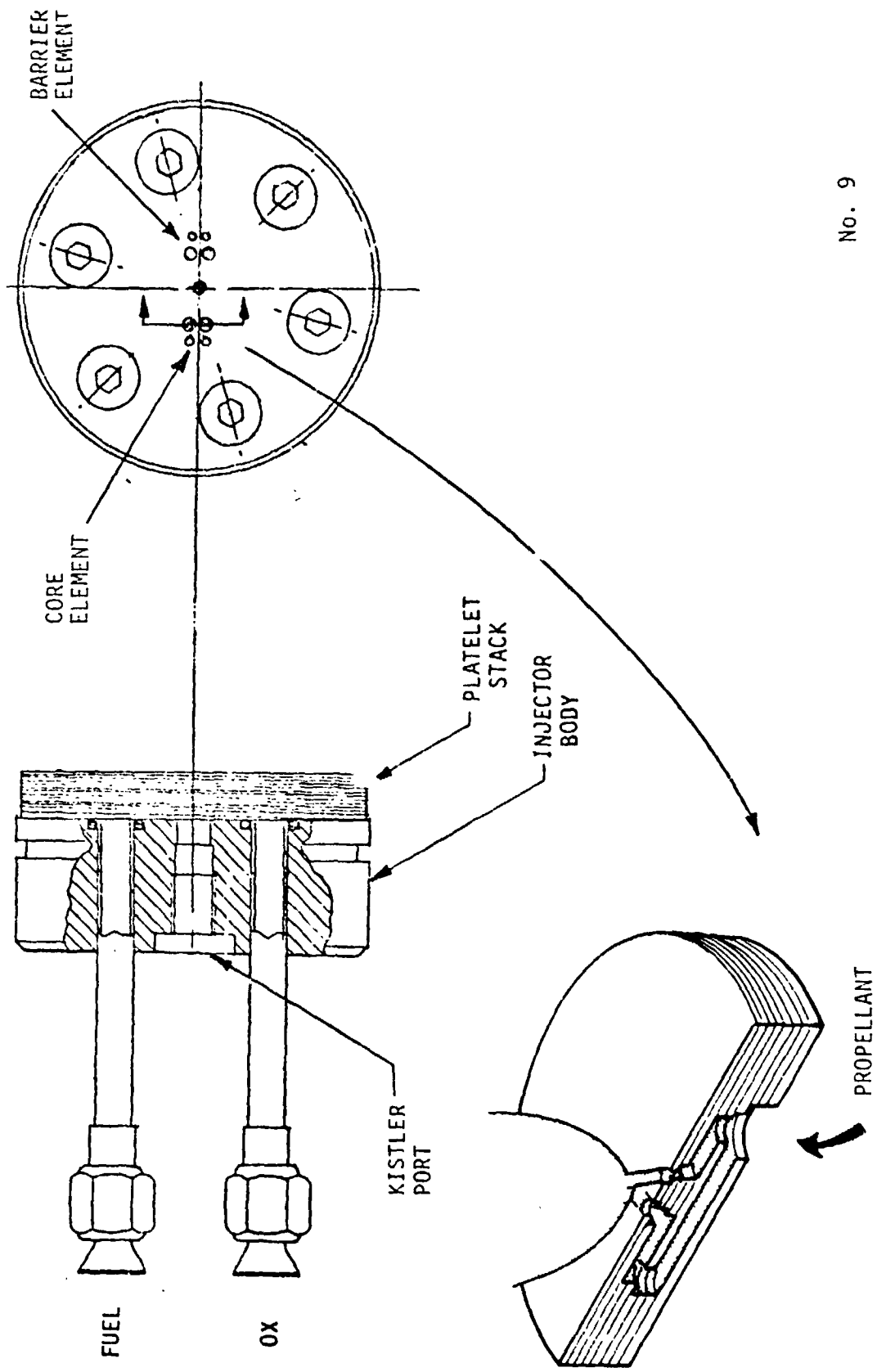


Nos. 5 and 6

Figure 11. Sharp-edged Inlet Unlike Doublet Injector



Figure 12. Space Shuttle/RCS Unlike Doublet Injector



No. 9

Figure 13. Space Shuttle/OMS TL0L Platelet Injector

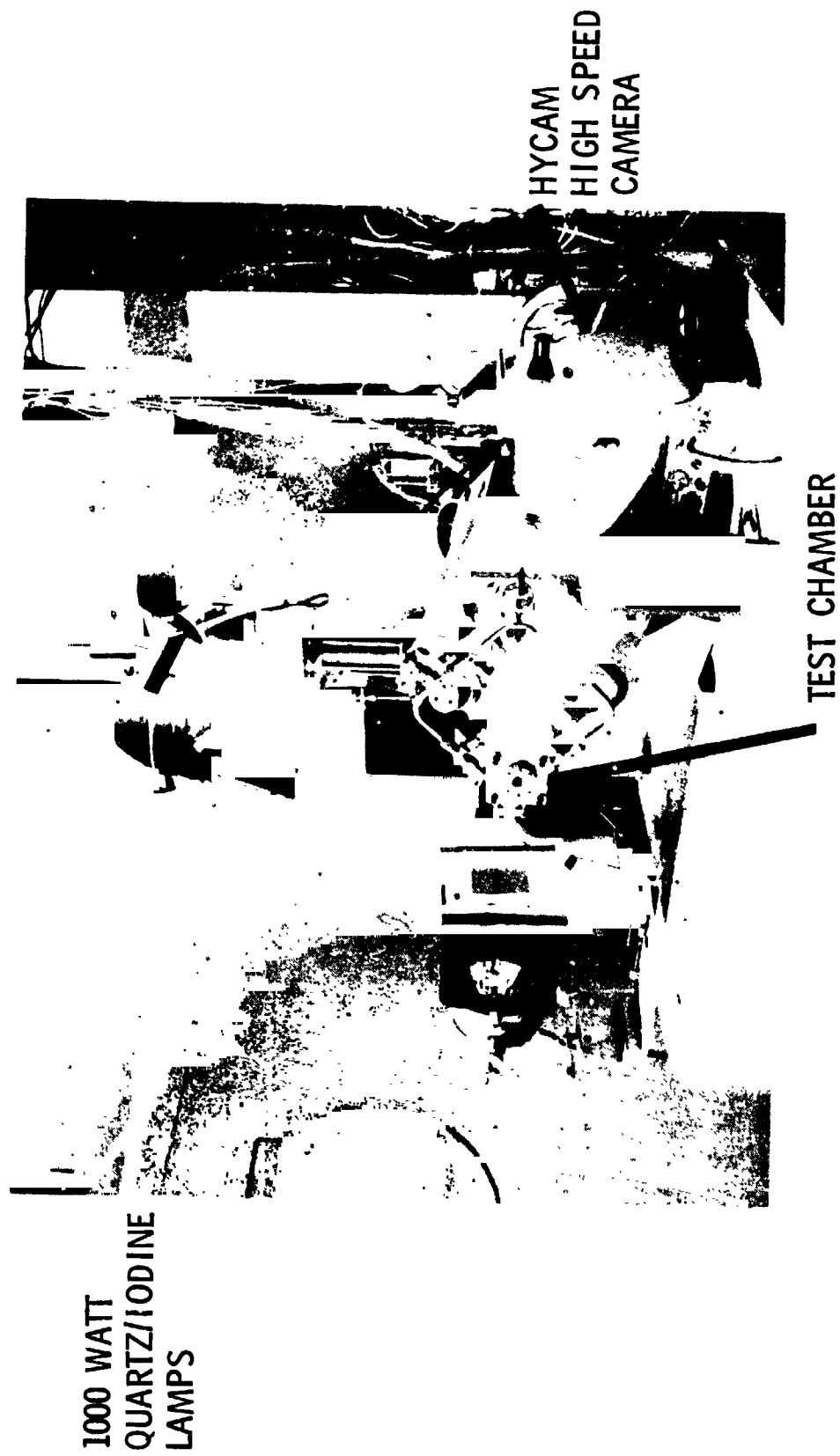


Figure 14. Hot Fire Test Setup

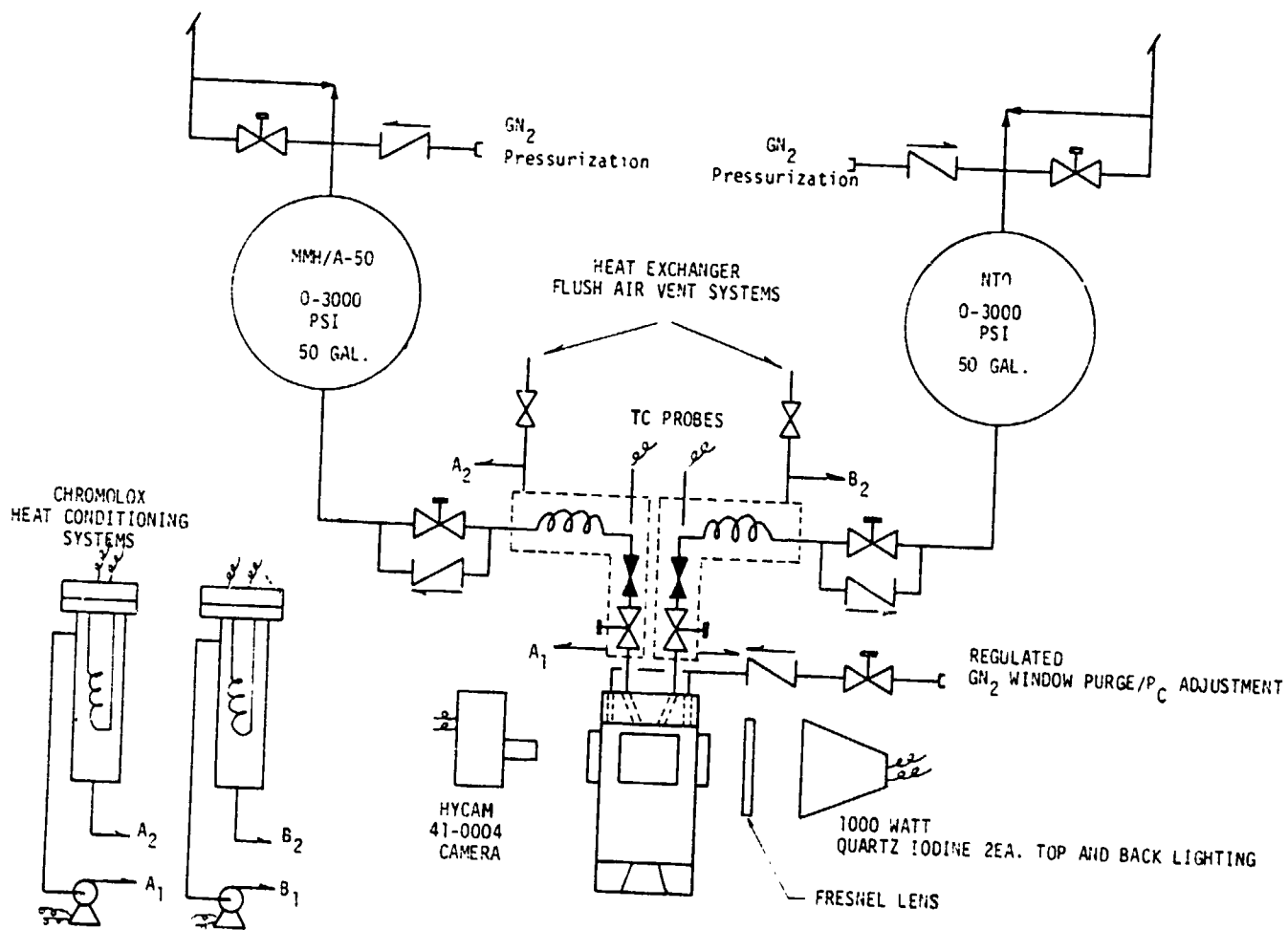


Figure 15. Propellant Flow System Schematic

## VI, A, Experimental Hardware and Test Setup (cont.)

systems was used to provide controlled run conditions over a wide range of injector and chamber pressures.

Propellant conditioning was provided by installing in-line heat exchangers immediately upstream of the thrust chamber valves. A hot water circulation type temperature conditioning system was used to provide independent conditioning of the ox and fuel to temperatures from ambient to 300°F.

A separately regulated  $\text{GN}_2$  supply was used to provide test chamber back pressure as well as provide window purge for the chamber viewports during the Task III testing. The window purge was eliminated early in the Task IV testing to improve photographic quality.

### 3. Cold Flow Test Setup

The cold flow tests were also conducted in the ALRC Research Physics Laboratory. Filtered, de-ionized water was used as the test fluid on most tests. Pressure measurements were made using Heise pressure gages and flow rate was measured using a time/volume technique, with run times of from 60 to 200 seconds. Strobe light photographs were taken of some of the injector flow tests to better evaluate propellant stream properties. Selected tests were also made with dyed water and freon as the test fluids to evaluate non-reactive stream impingement characteristics.

### 4. Hot Fire Instrumentation

The high frequency and low frequency instrumentation listed in Tables II and III were used in the locations shown in the schematic of Figure 16. Low frequency response test parameters were recorded

TABLE II  
HIGH FREQUENCY RESPONSE INSTRUMENTATION

<u>Test Parameter</u>	<u>Instrument</u>			<u>Range</u>	<u>Accuracy</u>
	<u>Symbol</u>	<u>Make</u>	<u>Model</u>		
Oxidizer Manifold Pressure	POJHF	Kistler	601	0-3000 psi (P-P)	$\pm 0.5\%$
Fuel Manifold Pressure	PFJHF	Kistler	601	0-3000 psi (P-P)	$\pm 0.5\%$
Chamber Pressure	PLHF	Kistler	601	0-3000 psi (P-P)	$\pm 0.5\%$
Injector Probe Temperature	TP1	C/A		0-1000 °F	$\pm 1\%$

TABLE III

LOW FREQUENCY RESPONSE INSTRUMENTATION

<u>Test Parameter</u>	<u>Symbol</u>	<u>Range</u>	<u>Units</u>	<u>Recorder</u>		
				<u>"O" Graph</u>	<u>Tape</u>	<u>Digital</u>
Oxid. Tank Pressure	POT	0-1500	Psia	X		
Fuel Tank Pressure	PFT	0-1500	Psia	X		
Oxid. Injector Pressure	POJ	0-1500	Psia	X		X
Fuel Injector Pressure	PFJ	0-1500	Psia	X		X
Chamber Pressure	PC	0-1000	Psia	X		X
Window Purge Pressure	PNZ	0-2000	Psia	X		X
Oxid. Flowrate	WO	0-0.1	Lb/sec	X		X
Fuel Flowrate	WF	0-0.1	Lb/sec	X		X
Oxid. Flowmeter Temp.	TOFM	0-500	°F	X		X
Fuel Flowmeter Temp.	TFFM	0-500	°F	X		X
Oxid. Injector Temp.	TOJ	0-500	°F	X		
Fuel Injector Temp.	TFJ	0-500	°F	X		
Oxid. Valve Voltage	VOV			X		
Fuel Valve Voltage	VFW			X		
Wind Purge Valve Voltage	VWPV			X		
Camera Voltage	VCAM			X	X	
Injector Purge Valve Voltage	VIPV			X		



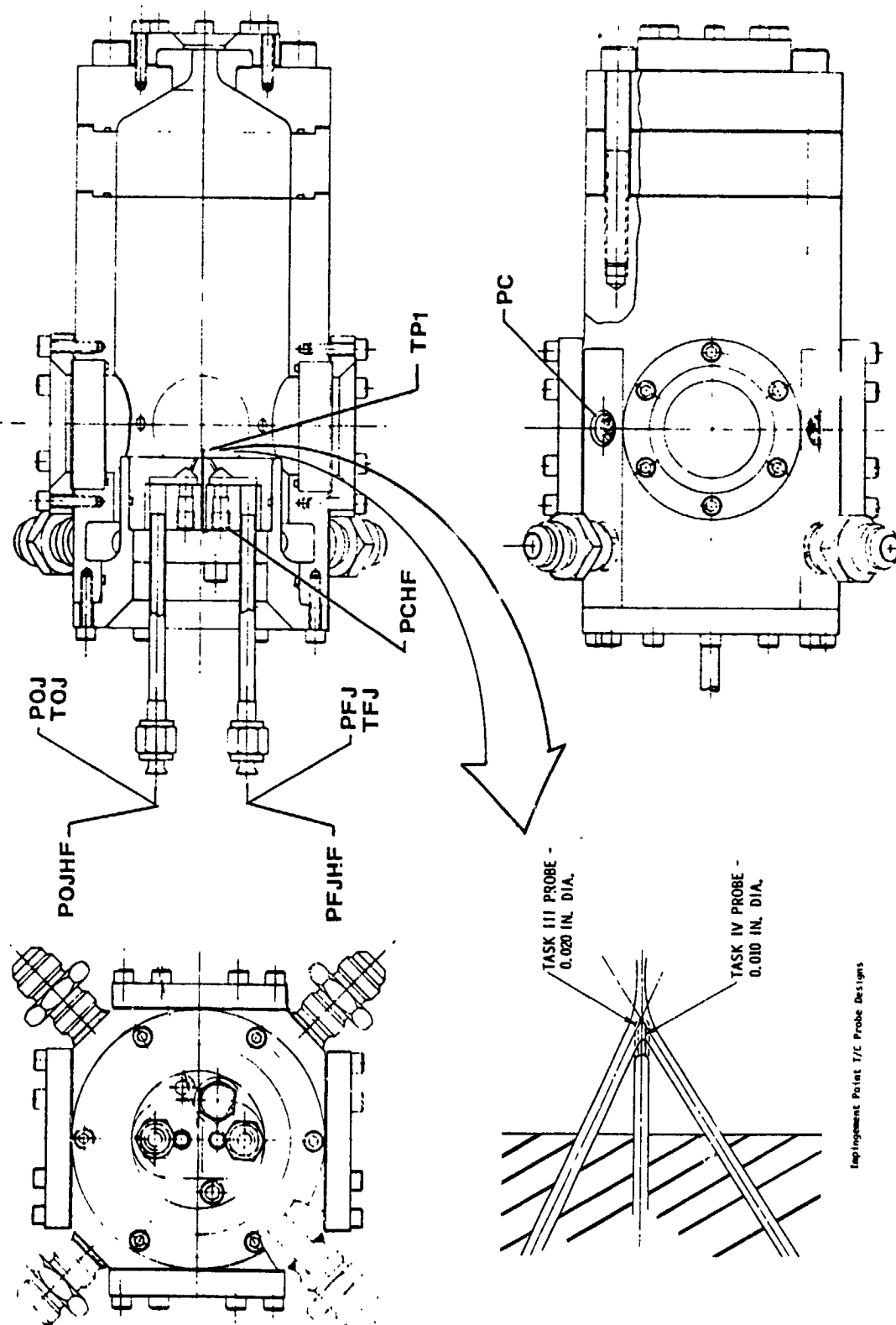


Figure 16. Instrumentation Schematic

ORIGINAL PAGE IS  
OF POOR QUALITY

## VI, A, Experimental Hardware and Test Setup (cont.)

on a Consolidated Electrodynamic Corporation's direct writing oscillograph. The high frequency response data were recorded on a Sangamo Model 3564 analog tape recorder.

The propellant flowrates were measured using the injector cold flow Kw's and the measured injection pressure drops. The pressure drops were electronically determined from the PoJ, PfJ and Pc transducers. Transducer loss and zero offsets were accounted for by pre-test calibration. The impingement point temperature was measured during Task III and IV testing using the probes shown in Figure 16.

The test operating point data were digitized and stored in an on-line HP 2100 A Computer/Real Time process controller for "quick look" test review.

### B. PHOTOGRAPHIC EQUIPMENT AND TECHNIQUE

The intent of photographic characterization of injector element combustion phenomena is to provide an understanding of the physico-chemical processes that are operative at engine operating conditions. This necessitates the ability to "look" through the flame to observe the liquid propellant streams and resultant sprays to determine relative spray mass and mixture ratio distributions by observing the liquid propellant colors.

It was found that the major problem associated with photographing combustion flow fields is that the combustion flame light emission is so intense that it masks the reflected light necessary to see the propellant streams as illustrated in Figure 17. The best technique found for overcoming the intense combustion light is to reduce the film exposure time such that the film in effect doesn't "see" the flame light and then to

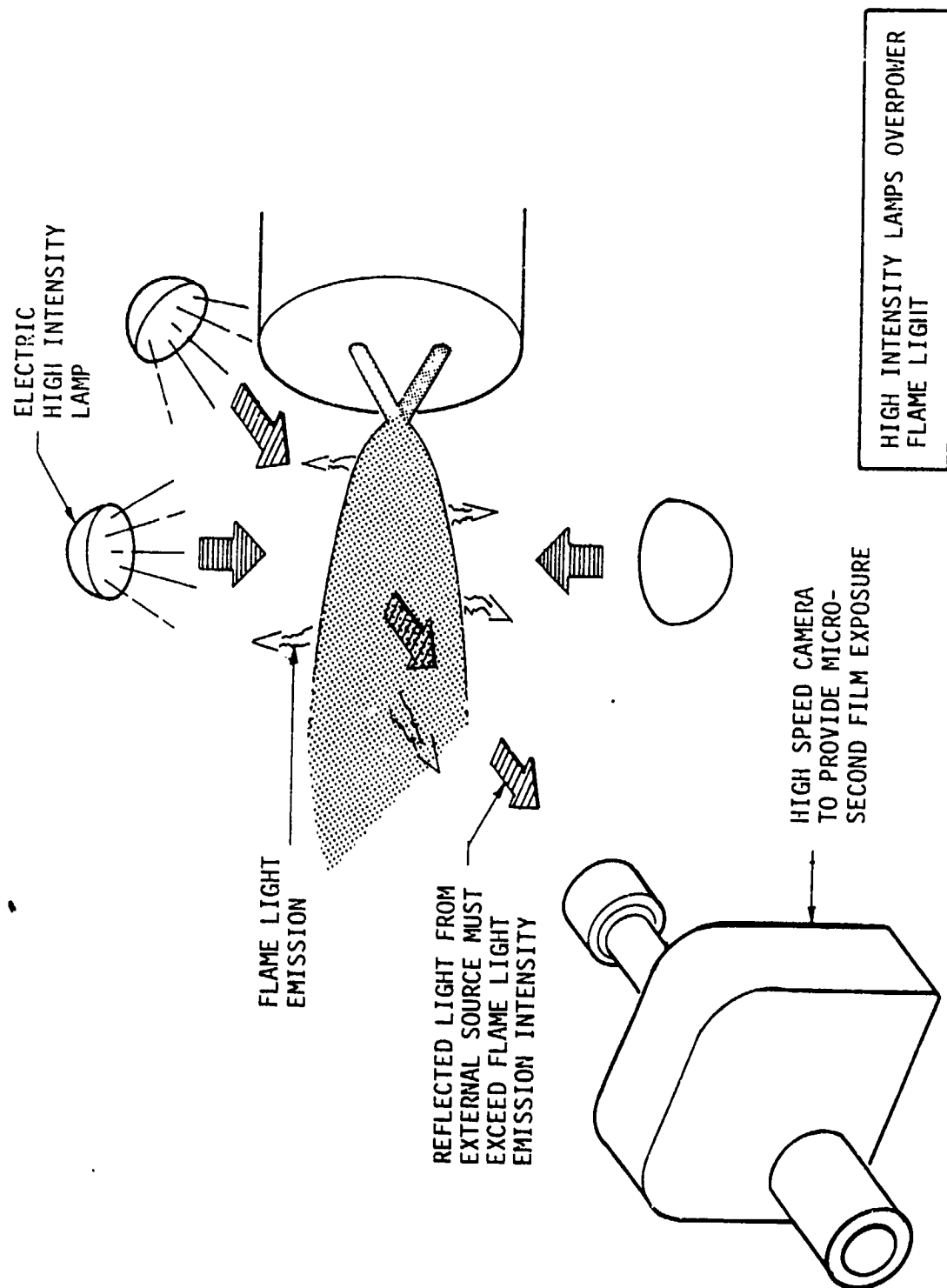


Figure 17. High Intensity Lamps Overpower Flame Light Emission

## VI, B, Photographic Equipment and Technique (cont.)

provide high intensity external lighting for viewing of the propellant streams. The external lighting must be provided from the back, top, bottom, and front to obtain a balance between reflected and absorbed light. It was found that use of back lighting alone will not provide the lighting balance required to properly interpret the film.

The photographic combustion characterization was accomplished using the equipment shown in Figure 18. The photographic equipment is centered around a Hycam model 41-0004 rotating prism high speed movie camera. This unique camera has the capability of varying the frame exposure time independent of the film frame rate through a replaceable rotating shutter. The shutter is mounted to the prism shaft and rotates at the same speed as the prism. The light exposure at a given frame rate is controlled by changing the shutter ratio of open time to close time. This is done with interchangeable shutters. The available shutter ratios are:

1/2.5, 1/10, 1/20, 1/50, and 1/100.

The light exposure time is determined by the product of the shutter ratio and the reciprocal of the frame rate:

$$\text{Exposure time} = \text{Shutter ratio} \times \frac{1}{\text{P.P.S. (Pictures per second)}}$$

Thus it is possible to obtain exposures of a few microseconds at relatively low frame rates. For example, most of the photos taken used a 25  $\mu\text{sec}$  exposure and a frame rate of only 800 fps. Some film were taken at frame rates as low as 400 fps. This capability permits four to five tests to be filmed on one 400 foot roll of film thus saving film costs.

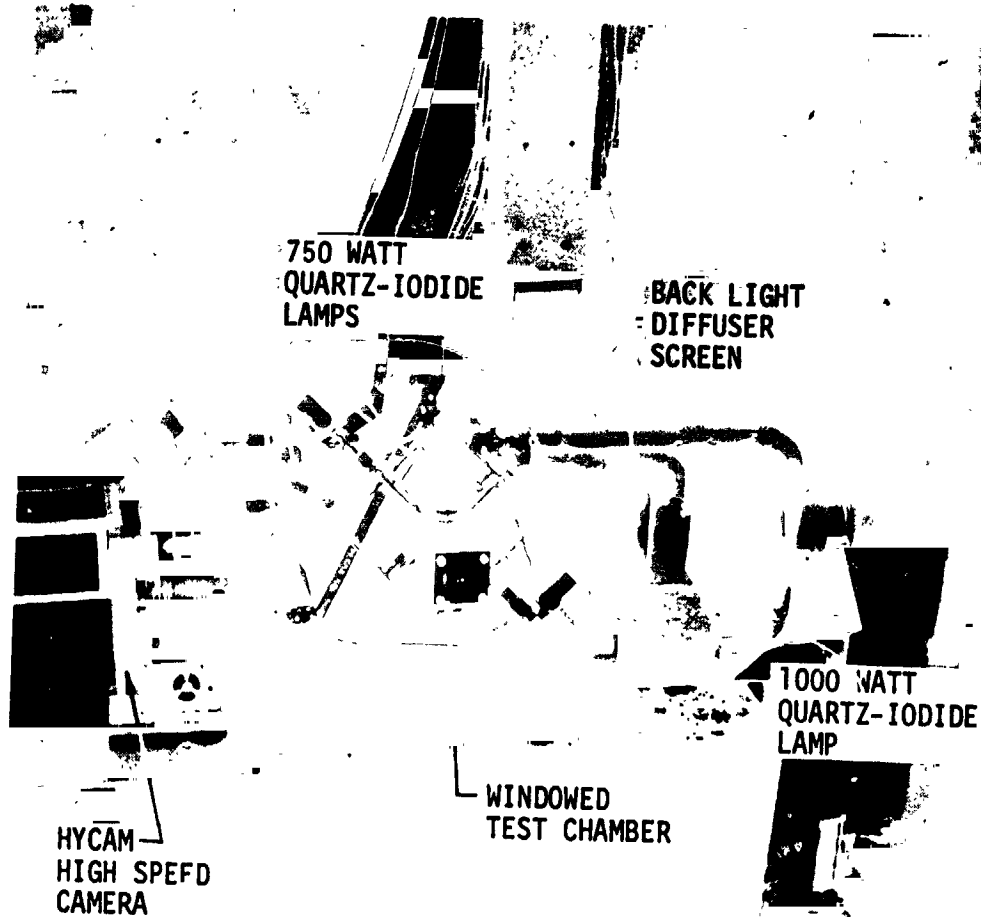


Figure 18. Photographic Equipment Setup

ORIGINAL PAGE IS  
OF POOR QUALITY

## VI, B, Photographic Equipment and Technique (cont.)

During Task III pictures were taken over a wide range of frame rates (8000 PPS to 400 PPS) and exposures (1.25  $\mu$ sec to 50  $\mu$ sec) to determine the best operating conditions. It was found that the best pictures were obtained at 400 pictures per second with the 1/100 shutter. A 35mm telephoto lense was used to provide magnification of the spray field. The lense aperature was varied from f/3.3 to f/5.6.

Lighting of the spray field was initially accomplished with the use of three 1000-watt quartz iodine lamps focused with Fresnel lenses as shown in Figure 12. One lamp was used to backlight the spray area with the second and third lamps used as top and front lighting to provide spray detail and definition. The lighting was improved during the Task IV testing by replacing the front and top lights with smaller 750 watt lamps and adding another lamp to light the bottom port as shown in Figure 17. The smaller lamps were placed within one inch of the top and bottom windows to minimize the illumination. The net effect was to improve the balance between the front lighting and the back lighting. Proper balance between the background, side and front lighting is essential to good quality photos.

The frame rate was increased to 800 PPS and the shutter opened to 1/50 during Task IV to further improve the photographic quality. Also during Task IV the  $\text{GN}_2$  purge which had been used during the Task III testing was eliminated which provided a significant improvement in film quality. The  $\text{GN}_2$  purge creates density gradients within the flow field which show up on the film. The effect is as though the field were being viewed through a film of turbulent water. The photos were acceptable at lower pressures (< 200 psia) where the density gradients were not severe but were unacceptable at higher pressures (> 200 psia). The density gradients were first eliminated by replacing the  $\text{GN}_2$  purge with a  $\text{GH}_e$  purge which had a density close to the combustion gas. However, no purge at all was found to be the best solution since that not only avoids the density gradient problem

## VI, B, Photographic Equipment and Technique (cont.)

but also permits the windows to heat up thus eliminating liquid condensation on the window.

Kodak Ektachrome Type EFB tungsten (3200°K) color film was used. Four hundred foot rolls of the No. 7242 film was selected to provide adequate viewing time. The film has an ASA 125 rating.

### C. TEST RESULTS

A total of 356 hot firings were conducted using the injector elements and fuels listed in Table I. Cold flow tests were also conducted to determine the injector element hydraulic resistances and to characterize non-reactive impingement phenomena.

#### 1. Cold Flow Test Results

##### a. Hydraulic Characteristics

Each of the injectors were cold flow tested to determine their hydraulic resistance and to verify impingement accuracy. The cold flow tests were conducted in the Research Physics Laboratory. Filtered, de-ionized water was used as the test fluid on most tests. Pressure measurements were made using Heiss pressure gages and flow rate was calculated using a time/volume technique, with run times of from 60 to 200 seconds. Strobe light photographs were taken of the elements to evaluate propellant stream properties.

The hydraulic resistances were determined for each of the elements from plots of flowrate versus pressure drop as shown in Figures 19 through 24. The resistance values are summarized in Table IV.

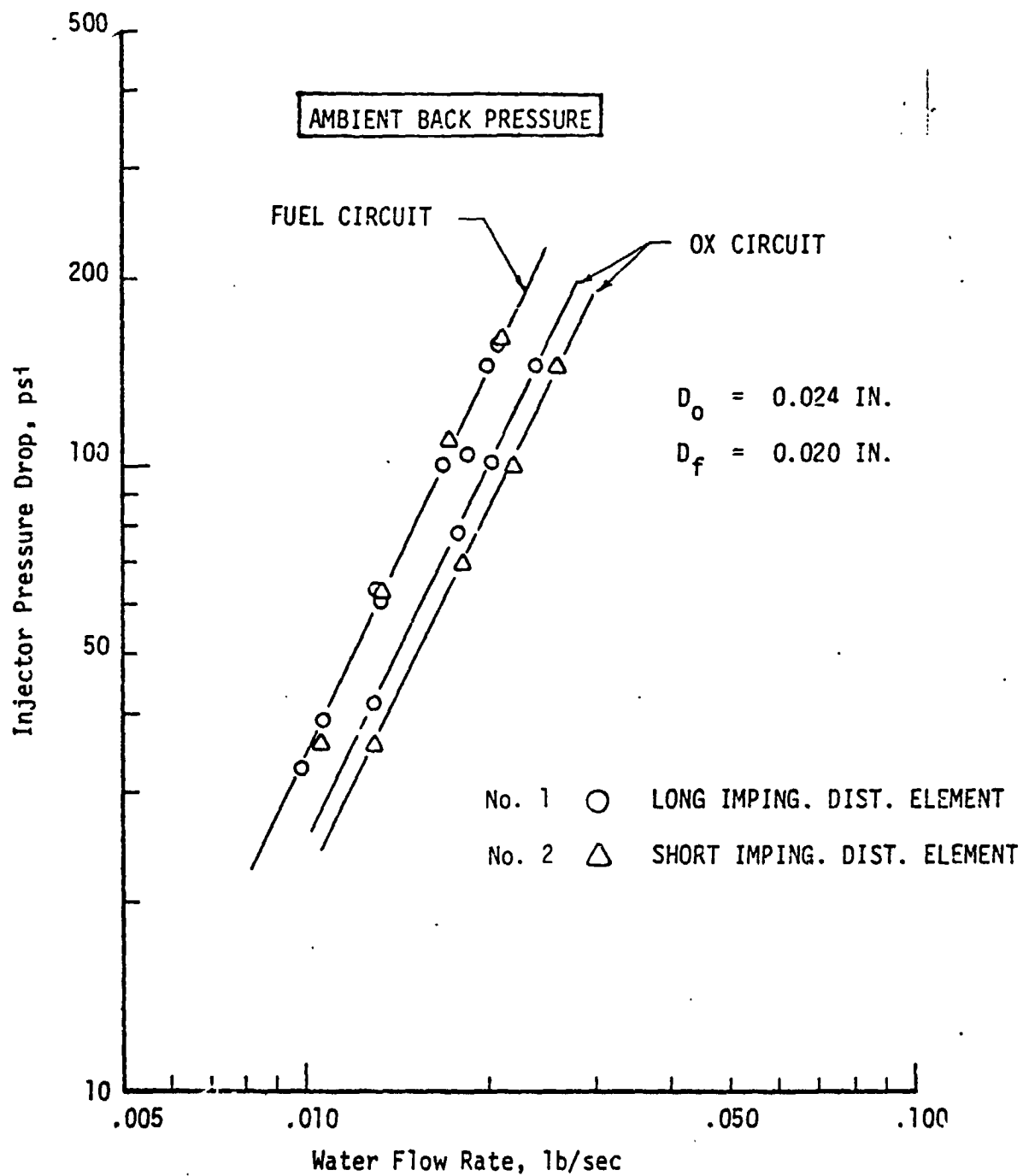


Figure 19. Pressure Drop Characteristics of the Rounded Inlet Unlike Doublet Elements



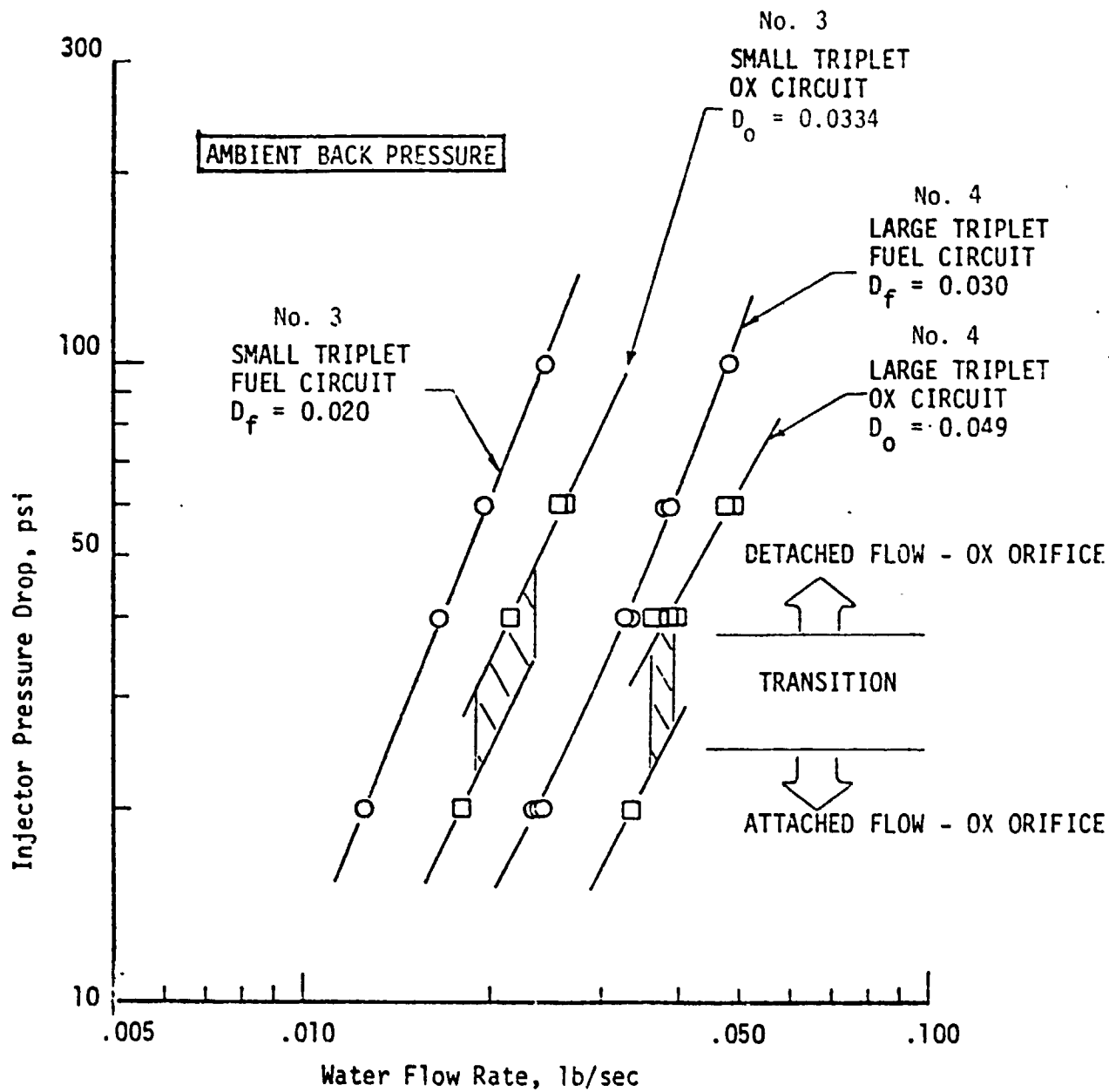


Figure 20. Pressure Drop Characteristics of the Triplet Elements

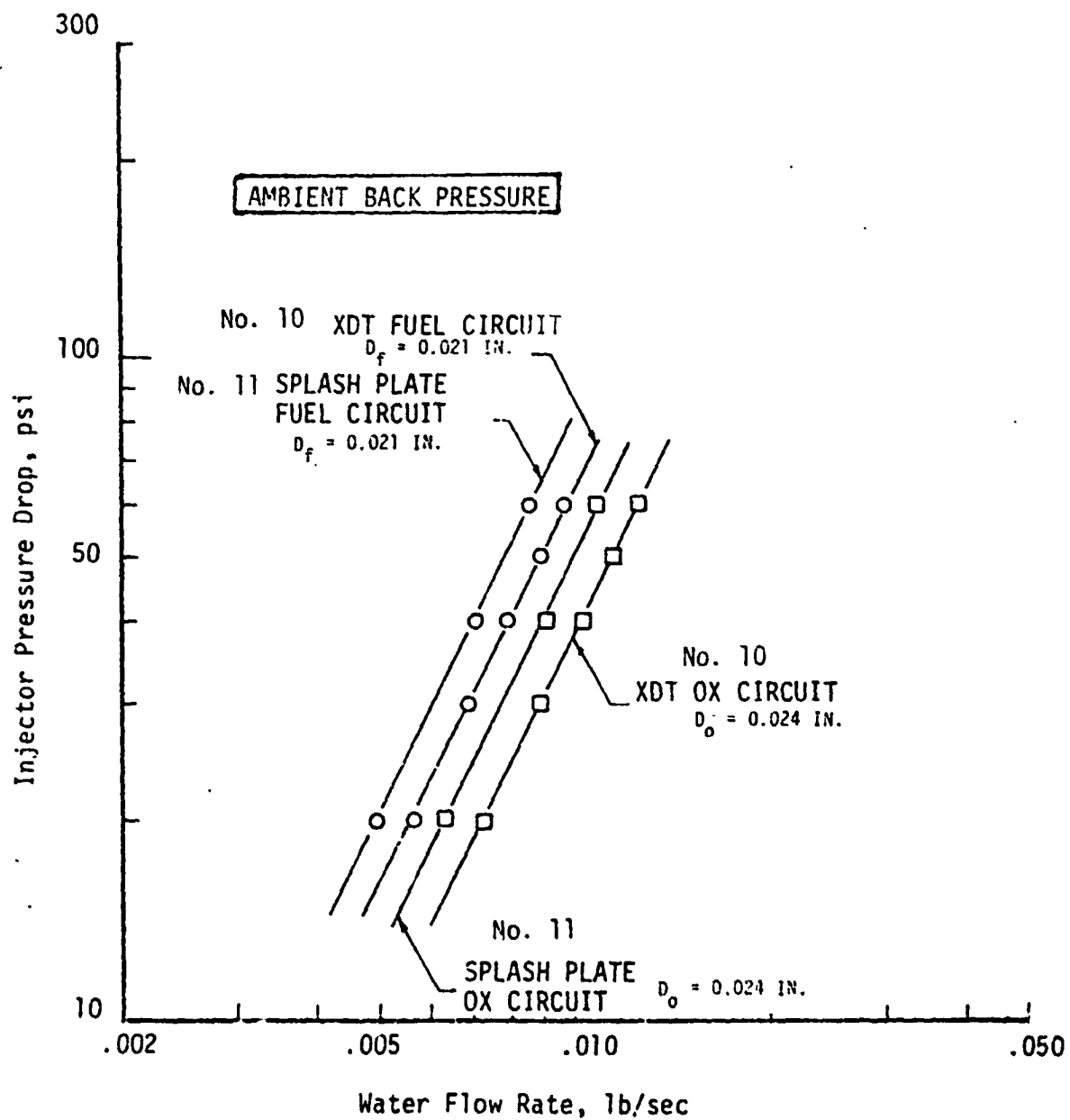


Figure 21. Pressure Drop Characteristics of the XDT and Splash Plate Platelet Elements

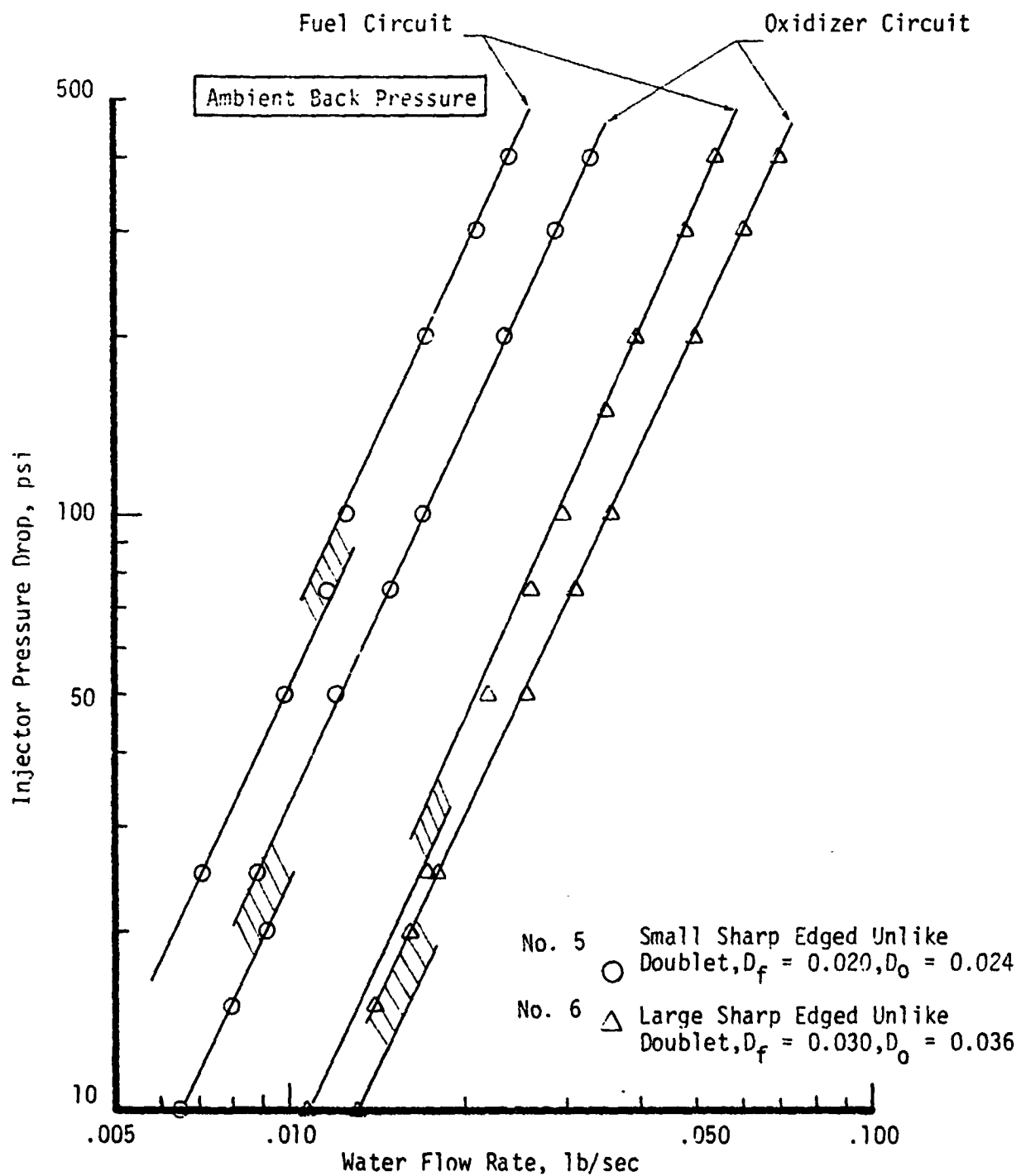


Figure 22. Pressure Drop Characteristics of the Sharp Edged Unlike Doublet Elements

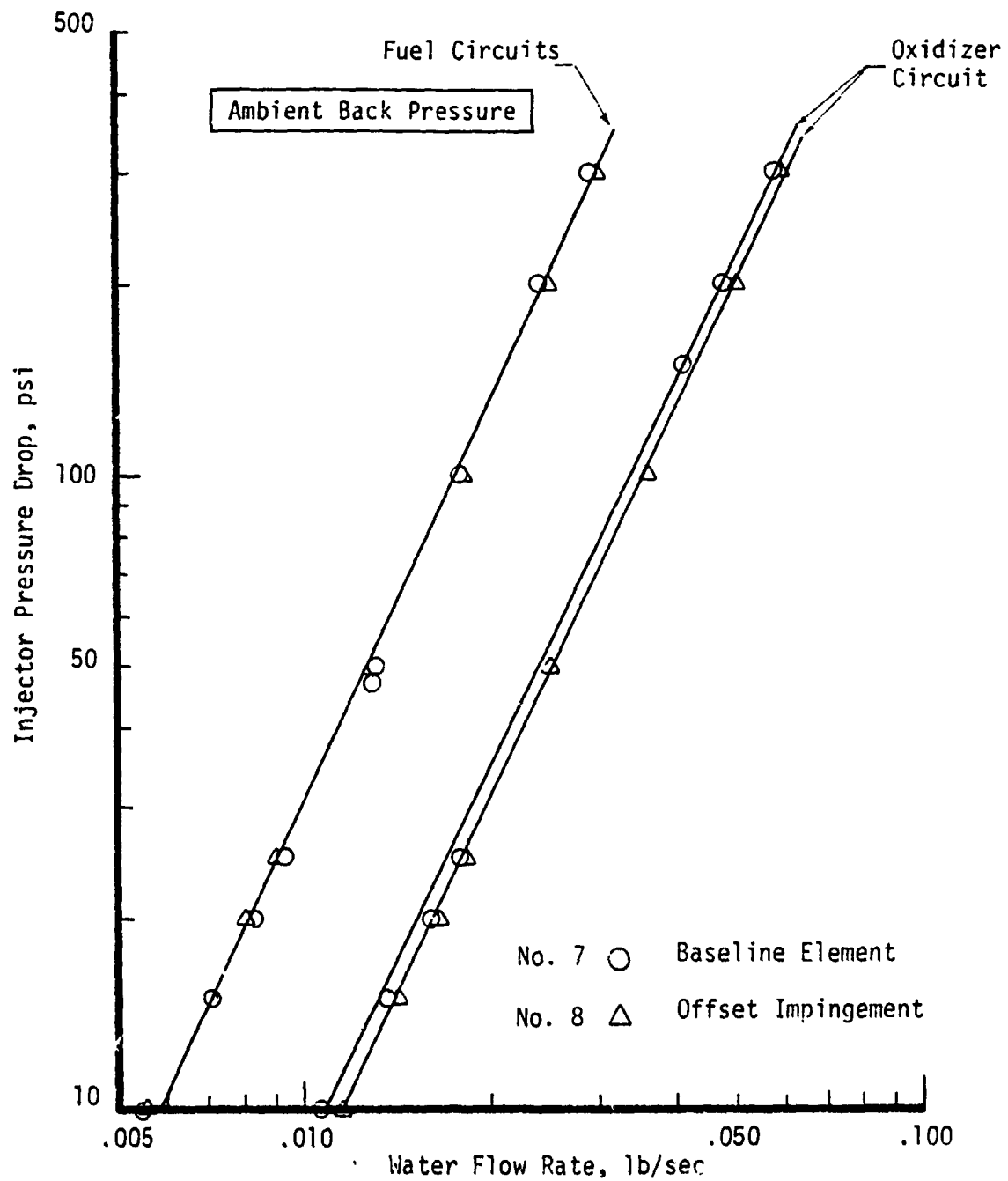


Figure 23. Pressure Drop Characteristics of the Space Shuttle/RCS Unlike Doublet Elements

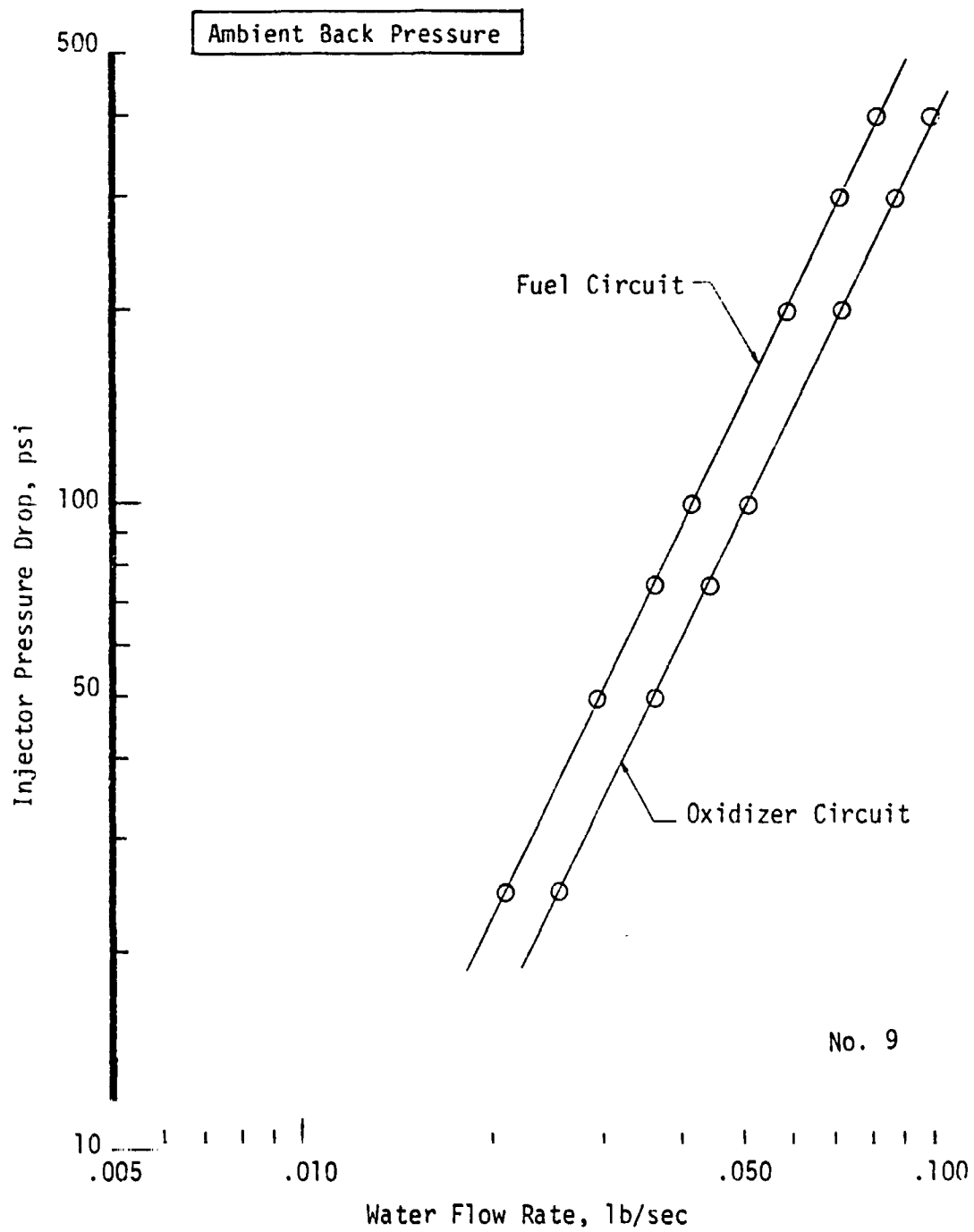


Figure 24. Pressure Drop Characteristics of the Space Shuttle/OMS Platelet TLQL Element

TABLE IV  
INJECTOR ELEMENT COLD FLOW DATA SUMMARY

Injector	Fuel Orifice		Oxidizer Orifice	
	<u>kW</u>	<u>C<sub>D</sub></u>	<u>kW</u>	<u>C<sub>D</sub></u>
Rounded Inlet Unlike Doublet, D <sub>f</sub> = 0.020 Nos. 1 and 2	0.00169	0.990	0.00215	0.900
Small F-O-F Triplet D <sub>f</sub> = 0.020 No. 3	0.00128	0.772	0.00402 0.00334	0.838 (Attached)* 0.696 (Detached)
Large F-O-F Triplet D <sub>f</sub> = 0.029 No. 4	0.00258	0.715	0.00754 0.00633	0.751 (Attached)* 0.631 (Detached)
XDT Platelet Element D <sub>f</sub> = 0.021 No. 10	0.00125	0.537	0.00162	0.534 (Detached)**
Splashplate Platelet Element D <sub>f</sub> = 0.021 No. 11	0.00110	0.602	0.00141	0.591 (Detached)**
Space Shuttle/RCS Unlike Doublet, D <sub>f</sub> = 0.023 No. 7	0.00181	0.824	0.00351	0.855
Space Shuttle/RCS Unlike Doublet, Offset Impingement, D <sub>f</sub> = 0.023 No. 8	0.00177	0.808	0.00363	0.883
Small Sharp Edged Unlike Doublet, D <sub>f</sub> = 0.020 No. 5	0.00129	0.780	0.00204 0.00168	0.856 (Attached)* 0.710 (Detached)
Large Sharp Edged Unlike Doublet, D <sub>f</sub> = 0.030 No. 6	0.00326 0.00295	0.889 0.790	0.00418 0.00355	0.780 (Attached)* 0.660 (Detached)
OMS Engine Platelet TL0L, D <sub>f</sub> = 0.028 Core No. 9	0.00409	0.630	0.00502	0.673 (Detached)**

\* Injector flowed attached during hot fire tests.  
\*\* Injector flowed detached during hot fire tests.

## VI, C, Test Results (cont.)

As noted in Table IV some of the orifices were found to flow in a detached mode at ambient back pressures. The platelet elements flow detached by design since their L/D's are less than one. This allows them to flow detached also at hot fire conditions and avoids hydraulic flip.

Some of the triplet and sharp edged unlike doublets flowed detached due to the low ambient backpressure and short orifice L/D ( $\approx 4$ ). These orifices were found to flow attached at the hot fire test conditions (i.e., high back pressure). The rounded inlet unlike doublet and the Space Shuttle/RCS element always flowed attached due to the contoured inlets and long L/D's (24/1 and 12/1).

The stream quality of the rounded inlet unlike doublet and the triplet elements are discussed in detail in the interim Report (Ref. 21). The results showed that the rounded inlet unlike doublet flow remains laminar until the Reynolds Number based on the orifice length reaches about 300,000 as predicted by the flow model of Reference 25. The triplet short L/D orifices produce turbulent flow over the whole flow range. It was also found that droplet shedding from the stream surface begins at a Weber Number of 3.0 for the triplet streams as compared to 12.0 for the rounded inlet streams. The more turbulent triplet streams were expected to exhibit RSS more readily than the more coherent rounded inlet unlike doublet streams. However, the final data correlations do not show a significant difference in RSS characteristics between the two injectors.

## VI, C, Test Results (cont.)

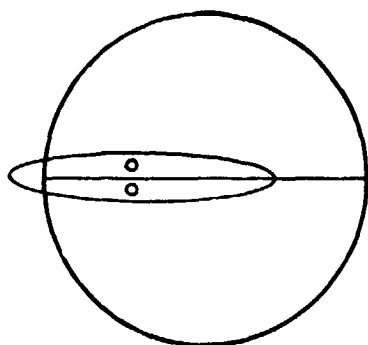
### b. Non-Reactive Impingement of the Unlike Doublet

The Space Shuttle/RCS unlike doublet injector elements were cold flowed to observe the influence of the intentional 0.003 in. impingement offset. As shown in Figure 25 the 0.003 in offset causes the fan to rotate about 20-30°. The mis-impingement was intended to promote secondary mixing of adjacent propellant spray fans. The mis-impingement appears to promote RSS since the hot firing movies show large amounts of unmixed oxidizer within the chamber. The rotation of the fan caused so much unmixed oxidizer to spray on the viewing window that a clear definition could not be made. It is concluded that misimpingement should be avoided since the resultant spray mixing is impaired.

Spray nonuniformity due to fuel and oxidizer diameter mismatch was another cold flow phenomenon observed with the Space Shuttle/RCS unlike doublet elements. Figure 26 shows stroboscopic still photos of the SS/RCS element cold flow. The large diameter mismatch ( $D_f = 0.023$  and  $D_o = 0.0312$ ) produces a "banana" shaped spray distribution which results in two poorly mixed, poorly atomized, oxidizer rich lobes. These oxidizer rich zones are apparent in the hot fire movies.

The effect of off-nominal momentum ratio on the spray distributions is also illustrated in Figure 26. Operation at the fuel rich off-momentum condition is shown in the second photo. The low oxidizer momentum and diameter mismatch cause the oxidizer stream to "umbrella" around the fuel stream resulting in poor mixing. The hot fire results show that these effects coupled with RSS can result in poor performance, stability, and compatibility. The oxidizer rich off-momentum condition produces good mixing due to the splash plate effect of the step in the injector face. The hot fire results confirm the improved mixing at the oxidizer rich condition. It is suspected that if the



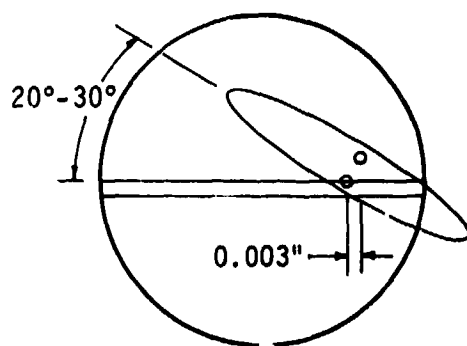


END VIEW

SIDE VIEW

a. NORMAL IMPINGEMENT

$\Delta P_{ox}$	= 21 PSIG
$\Delta P_f$	= 32 PSIG

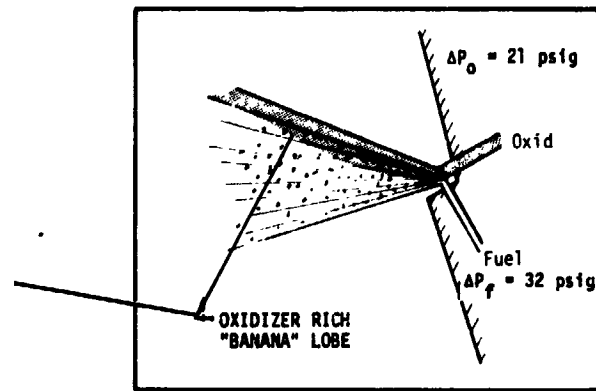


END VIEW

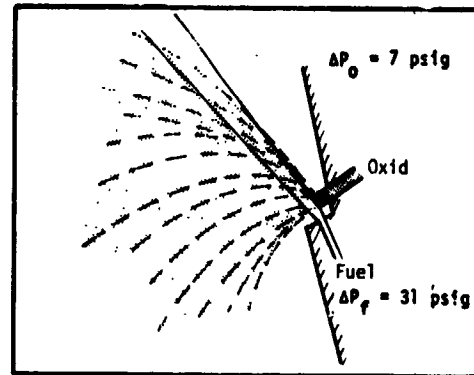
SIDE VIEW

b. OFFSET IMPINGEMENT

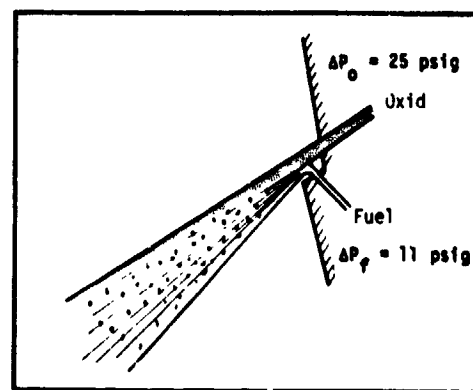
Figure 25. Impingement Offset Causes Fan Rotation  
With the Space Shuttle/RCS Unlike Doublet



a. Orifice Diameter Mismatch Produces Non-Uniform Spray



b. Fuel Rich Momentum Condition Causes Oxidizer Stream to "Umbrella" Around Fuel Stream



c. Oxidizer Rich Momentum Condition Produces Good Mixing

Figure 26. Space Shuttle/RCS Unlike Doublet Non-Reactive Impingement

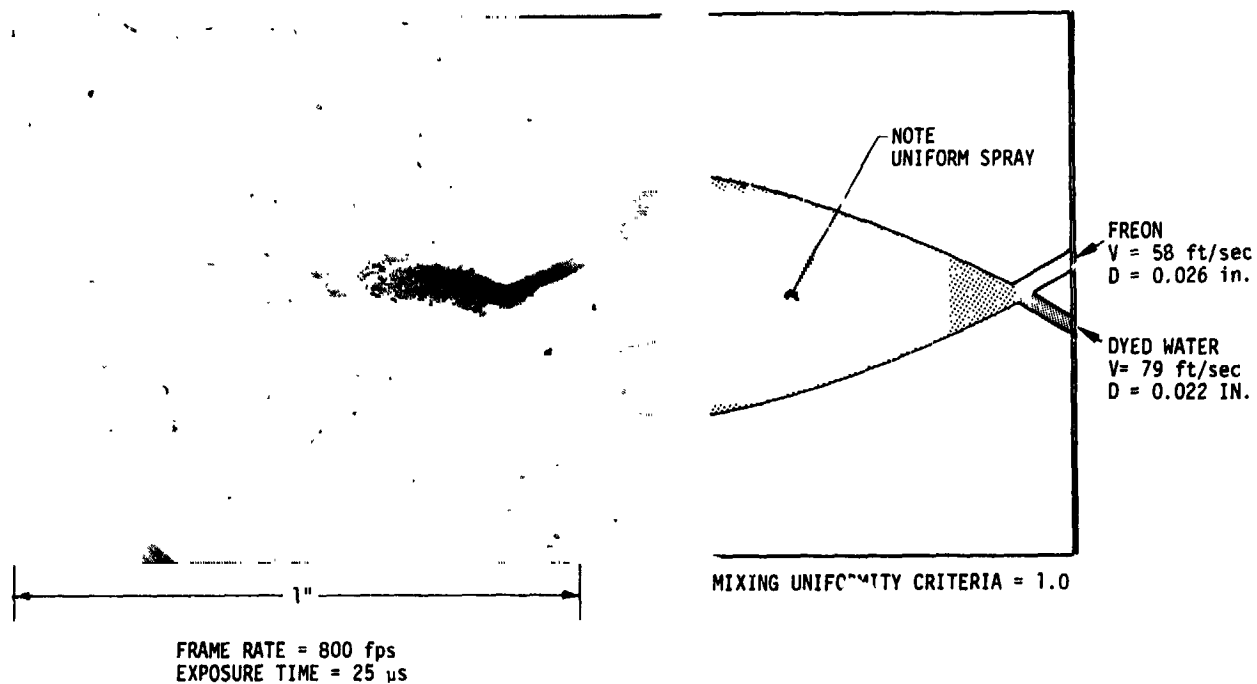
## VI. C, Test Results (cont.)

fuel free stream length were as great as that of the oxidizer stream than equally poor mixing would occur.

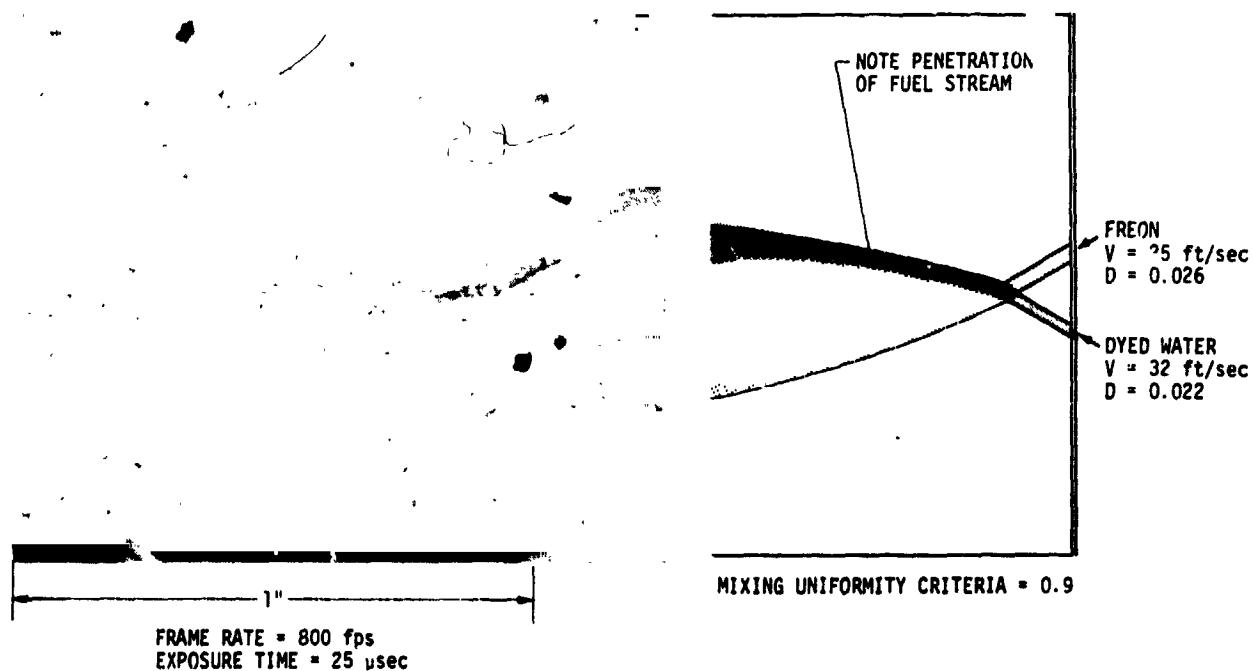
A selected number of cold flow tests were run with the rounded inlet unlike doublets to film the non-reactive impingement process to serve as a baseline in interpreting the hot fire movies. The non-reactive stream impingement is shown in the photograph of Figure 27. This photograph is an enlargement of a 16mm high speed movie film. The propellant simulants are dyed water (the blue stream) for fuel and freon (the clear stream) for oxidizer. The momentum ratio condition is for best mixing according to the Rupe criteria. (Ref 30). The spray uniformity attained at the optimum stream momentum ratio condition is clearly evident. The propellant "shoot-through" (i.e., penetration) phenomena reported by Rupe is also observed with lower stream momentum as shown in Figure 27. The "mixing" and "penetration" impingement modes are observed in hot firing and look a great deal like these cold flow photos, except for the propellant color differences.

### 2. Hot Fire Test Results

The hot fire tests were conducted in three separate groups during Task III, Task IV and Task VII. The test results are included in Appendix B. Appendix B includes a description of the injector element, the chamber pressure, the injection velocities and temperatures, the mixture ratio and the mode of operation. Included are various correlation parameters. The operation mode is specified as "mix", "separate" (SEP), "mix/separate" (M/S), "mix/penetrate" (M/P), or "undefined". These modes were identified from the high speed movies as illustrated in Figure 28 which shows an example of each of the modes. These photos are blowups of 16 mm movie film.



a. Rupe's Mixing Uniformity Criteria Define for Uniform Spary Non-reactive Impingement



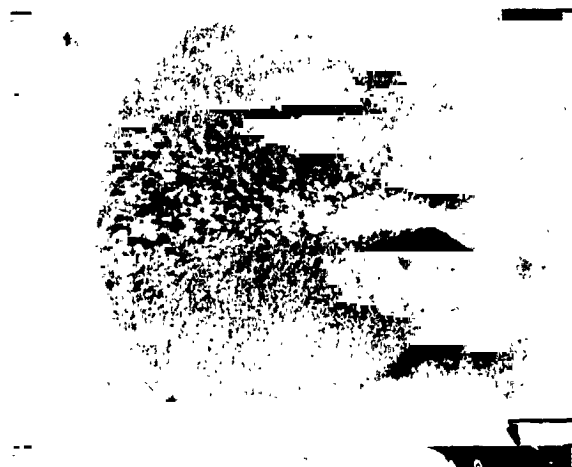
b. Low Stream Momentum Produces Penetration Phenomena for Non-reactive Impingement

Figure 27. Rounded Inlet Unlike Doublet Non-Reactive Impingement



#### PENETRATE

$P_c = 78 \text{ psia}$   
 $V_f = 49 \text{ ft/sec}$   
 $T_f = 75^\circ\text{F}$   
 $REF = 0.832 \times 10^4$



#### MIX

$P_c = 124 \text{ psia}$   
 $V_f = 73 \text{ ft/sec}$   
 $T_f = 82^\circ\text{F}$   
 $REF = 1.32 \times 10^4$



ROUNDED INLET UNLIKE  
 DOUBLET  $D_f = 0.020 \text{ in.}$   
 $D_o = 0.024 \text{ in.}$

#### MIX/SEPARATE

$P_c = 198 \text{ psia}$   
 $V_f = 114 \text{ ft/sec}$   
 $T_f = 76^\circ\text{F}$   
 $REF = 1.97 \times 10^4$



#### SEPARATE

$P_c = 144 \text{ psia}$   
 $V_f = 105 \text{ ft/sec}$   
 $T_f = 294^\circ\text{F}$   
 $REF = 7.72 \times 10^4$

Figure 28. High Speed Photography Defines Four Modes of Reactive Stream Impingement

## VI, C, Test Results (cont.)

The "Mix/Penetrated" model is characterized by a uniform spray field with some propellant penetration as evidenced by an oxidizer rich zone opposite the oxidizer stream in the downstream spray. "Penetration" occurs at low injection velocity (less than 50 ft/sec), low fuel temperatures (below 70°F), and low chamber pressure (less than 100 psia) and is evidenced by "shoot-through" of the fuel and oxidizer. Penetration has been reported in earlier cold flow work and was also observed on this program using propellant simulants as well as reactive streams. Penetration is a consequence of the none-reactive momentum exchange mixing process. "Mixing" is observed at moderate injection velocities, (50-100 ft/sec) moderate fuel temperatures, (70-90°F) and moderate chamber pressures (100-200 psia). It is evidenced by a highly uniform spray field which looks similar to a non-reactive spray field. "Mix/Separate" occurs at the onset of RSS. It is evidenced by a slightly non-uniform spray field. "Separation" is observed at higher injection (greater than 100 ft/sec), higher fuel temperature (greater than 90°F), and higher chamber pressures (greater than 200 psia). It is evidenced by highly non-uniform spray fields in which distinct regions of unmixed fuel and oxidizer exist. The "Undefined" designation was assigned to tests where: (1) movie film were not taken, (2) the injector was improperly rotated in relation to the camera, (3) or the film could not be interpreted due to poor visibility. The only film that exhibited poor visibility were those taken of the SS/RCS unlike doublet with the offset impingement where oxidizer spray on the window obscured the view. The first few tests within the SS/RCS injector were run with the injector rotated 90° such that the broad side of the fan was viewed. Operating modes could not be identified for these tests.

A total of fifty-one hot fire tests were run during the Task III testing. The chamber pressure was varied from 80 psia to 1000 psia. The fuel injection velocity was varied from 54 ft/sec to 148 ft/sec. The fuel temperature was run at ambient and 200°F to determine its effect on RSS. Twelve of the fifty-one tests were run with A-50 to determine fuel effects on RSS. Temperature probing of the impingement point was done

## VI, C, Test Results (cont.)

with a small diameter temperature probe to gain further insight into RSS mechanisms.

The results of the Task III testing showed that RSS depends on the chamber pressure, the fuel temperature, and the injection velocity. Increasing any one of these promotes RSS. Each of these effects were investigated further during the Task IV testing which included testing with the triplet injector and the XDT and splashplate platelet injectors. Additional A-50 testing was also included. One hundred thirty hot fire tests and 10 cold flow tests were run. The results of the cold flow tests are discussed in Section VI.C.1. The results of the Task IV testing confirmed the Task III results.

One hundred sixty four hot fire tests were run during Task VII. The tests included the sharp edged unlike doublet elements, the SS/RCS unlike doublet and the SS/OMS TLOL platelet element. Hydrazine fuel testing was also included with the rounded inlet unlike doublet, the sharp edged unlike doublets, and the SS/OMS TLOL platelet element.

The test results show that: (1) A-50 and  $N_2H_4$  fuel behave like MMH fuel in regards to RSS although combustion of the  $N_2H_4$  fuel is distinctly different as discussed below; (2) increasing the fuel velocity promotes RSS; (3) increasing chamber pressure promotes RSS; (4) increasing fuel temperature promotes RSS; and (5) self-atomizing/spray impingement elements promote RSS.

Correlations developed from this data show that RSS is controlled by a vaporization controlled interfacial reaction which is correlated by plotting chamber pressure ( $P_c$ ) versus fuel orifice Reynolds Number (REF). By plotting the A-50 and  $N_2H_4$  RSS data on these coordinates

## VI, C, Test Results (cont.)

it was found that both fuels exhibit the same RSS limit as MMH fuel as shown in Figures 29 and 30.

The combustion of the A-50 fuel is seen to be very similar to that of the MMH fuel by comparing Figure 26 to Figure 27. Whereas, the  $N_2H_4$  combustion is seen to be distinctly different by comparing Figure 30 to Figure 28. The MMH and A-50 combustion are characterized by a zone of yellow combustion at the impingement point followed by droplet vaporization in a blue spray field. The yellow color is due primarily to the  $NH_2$  radical emission caused by decomposition of the fuel. The blue color in the spray field is due to methyl radical emission as a result of bipropellant combustion of the fuel vapors. The  $N_2H_4$  combustion is characterized by both a yellow impingement zone and a yellow spray field. Again the yellow at the impingement zone due to a breaking down of some of the fuel resulting in  $NH_2$  radical emission. The yellow spray field is due to monopropellant combustion of the  $N_2H_4$  droplets which is characteristically yellow due to  $NH_2$  radical emission. The lack of blue emission is due to the absence of methyl radical in the  $N_2H_4$  fuel. Also note the larger quantities of unreacted  $NO_2$  vapors. The  $N_2H_4$  fuel burns primarily in a monopropellant mode leaving only the decomposition products to react with the  $NO_2$  whereas the methylated fuels burn primarily in a bipropellant mode with excess fuel vapor available for combustion with the  $NO_2$ .

A significant aspect of the  $N_2H_4$  combustion not visible in the photo of Figure 30 is the observation of the production of solid particles within the impingement zone. The solid particles are evidenced by bright red streaks emanating from the impingement zone. Also visible in some of the film is the production of reaction intermediates on the injector face due to fuel condensation and reaction with the  $NO_2$  vapor. The reaction is characteristic of the surface reactions reported



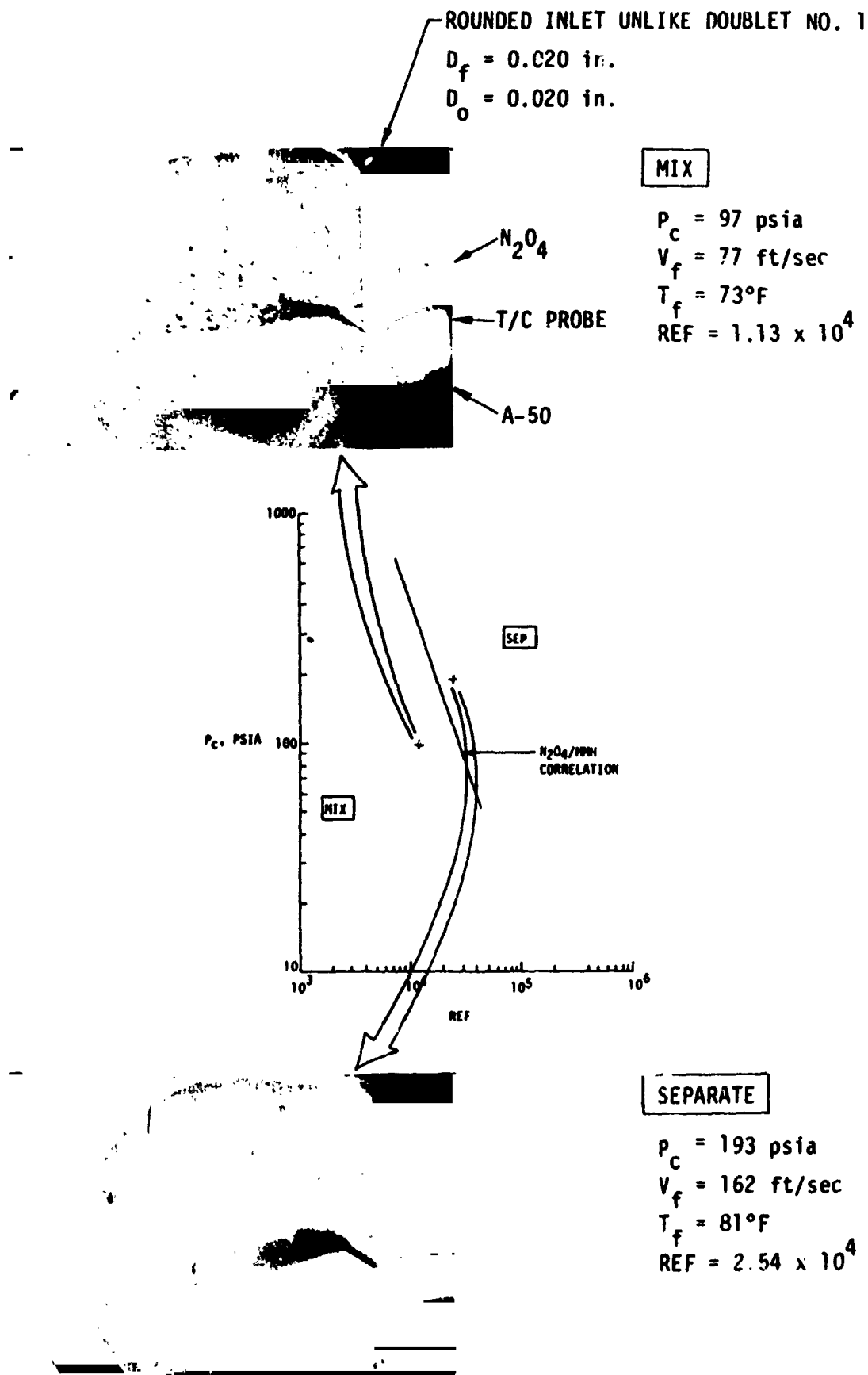


Figure 29. A-50 Fuel Behaves Like MMH Fuel

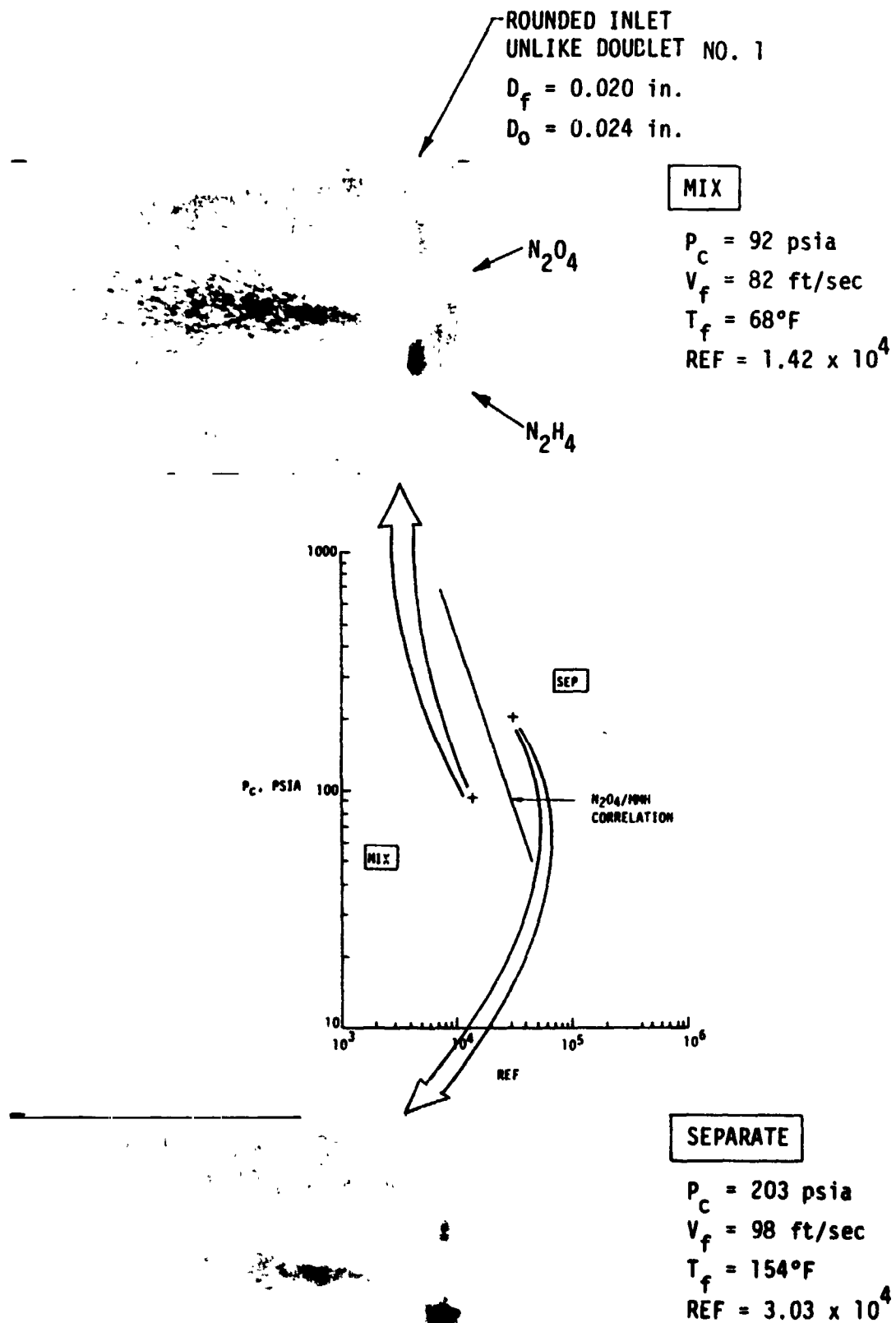


Figure 30.  $\text{N}_2\text{H}_4$  Fuel Exhibits the Same RSS Limits as MMH Fuel

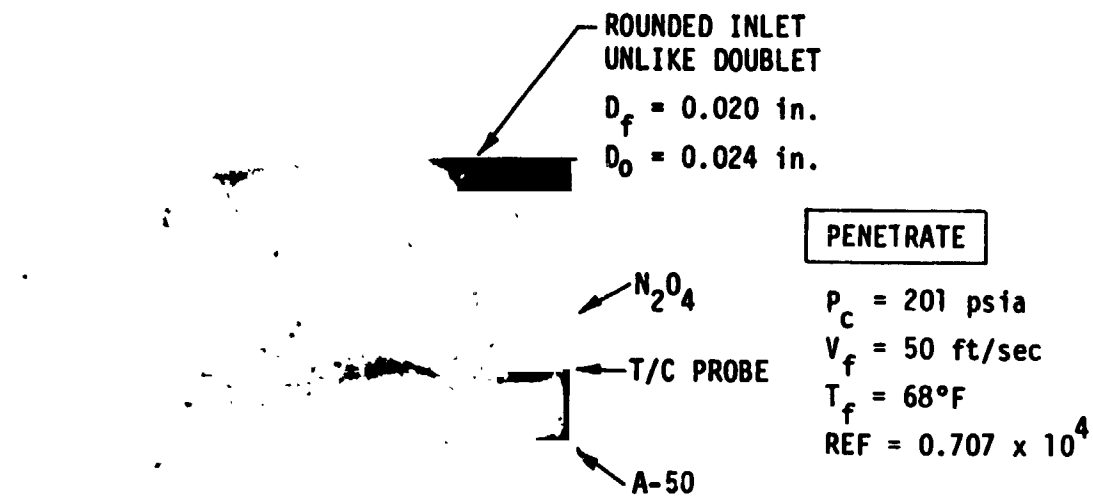
## VI, C, Test Results (cont.)

earlier by Zung (Ref. 26) and Lawver (Ref. 27). Observation of the production of reaction intermediates within the impingement zones of the  $N_2H_4$  fuel substantiates the "pop" mechanism proposed during Task I (Ref. 18) and explains the energetic nature of the  $N_2H_4$  fuel as compared to the MMH and A-50 fuels. It is concluded that two separate and distinct mechanisms control RSS and pops. "RSS" is controlled by vaporization limited combustion at the impingement interface whereas "pops" are caused by reaction intermediates formed at the impingement point by surface reactions which subsequently detonate in the spray field. The surface reactions occur with low vapor pressure fuel or under conditions of high heat loss such as with large streams ( $>0.060$  in. dia) and/or cold propellants. Design parameters that affect the reaction rates and resultant intermediate formation, and that would be used to model the "pop" phenomenon include temperature chamber pressure, jet diameter, and injection velocity.

The effect of increasing fuel velocity on RSS is illustrated in the photo of Figure 31. The tests were run at about 200 psia and ambient fuel temperatures using A-50 fuel. The effect of fuel velocity is clearly illustrated by the change in mode from penetration at 50 ft/sec to highly separated at 162 ft/sec. The fuel Reynolds Number increases from  $0.707 \times 10^4$  to  $2.54 \times 10^4$ .

Also shown in the photos is a thermocouple probe used to measure the impingement point temperature. The results of the temperature probing showed that the impingement point temperature increases with increasing chamber pressure and injection velocity which is consistent with a vaporization controlled mechanism.

The effect of increasing chamber pressure on RSS is illustrated in Figure 32. The upper photo was taken at a chamber pressure of 97 psia and a fuel velocity of 77 ft/sec with ambient temperature A-50 fuel and is characteristic of the "mix" operating mode. The lower photo was taken at a chamber pressure of 489 psia and a fuel velocity of 104 ft/sec with ambient temperature A-50 fuel. An equivalent test condition with



#### PENETRATE

$P_c = 201$  psia  
 $V_f = 50$  ft/sec  
 $T_f = 68^\circ F$   
 $REF = 0.707 \times 10^4$



#### MIX

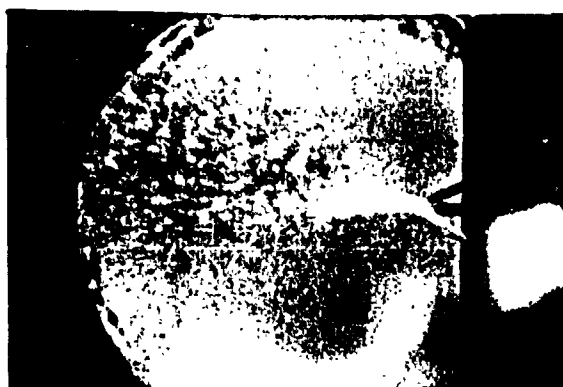
$P_c = 199$  psia  
 $V_f = 71$  ft/sec  
 $T_f = 69^\circ F$   
 $REF = 1.04 \times 10^4$



#### SEPARATE

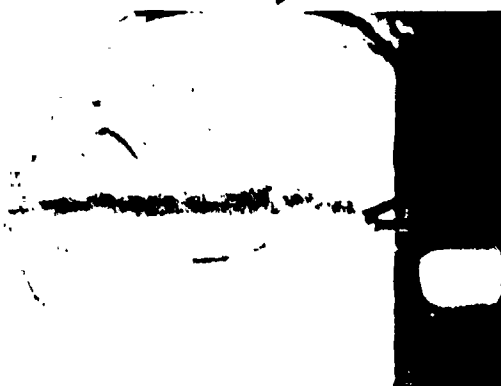
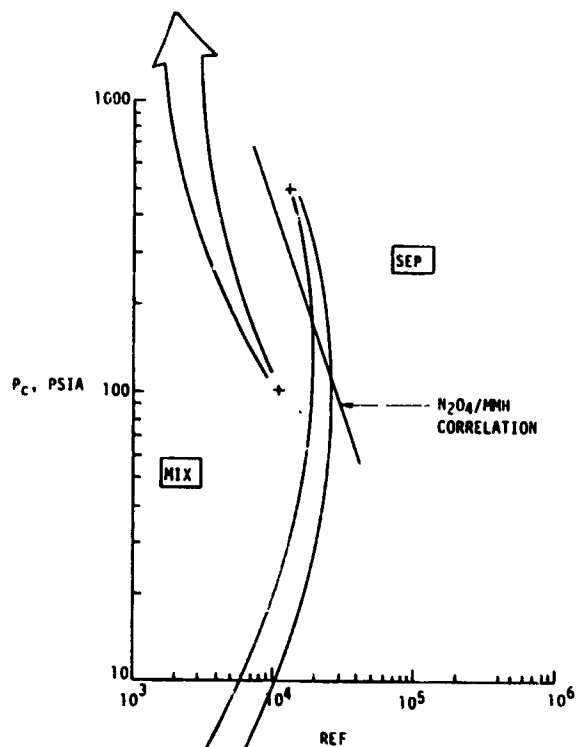
$P_c = 193$  psia  
 $V_f = 162$  ft/sec  
 $T_f = 81^\circ F$   
 $REF = 2.54 \times 10^4$

Figure 31. Increasing Fuel Velocity Promotes RSS



MIX

$P_c = 97$  psia  
 $V_f = 77$  ft/sec  
 $T_f = 73^\circ\text{F}$   
 $\text{REF} = 1.13 \times 10^4$



SEPARATE

$P_c = 489$  psia  
 $V_f = 104$  ft/sec  
 $T_f = 70^\circ\text{F}$   
 $\text{REF} = 1.50 \times 10^4$

Figure 32. Increasing Fuel Temperature Promotes RSS

## VI, C, Test Results (cont.)

the same fuel velocity as the lower chamber pressure was not available. However, the difference in REF ( $1.13 \times 10^4$  @  $P_c = 97$  and  $1.50 \times 10^4$  @  $P_c = 489$ ) between the two tests is not significant since an REF of  $1.50 \times 10^4$  is well within the "mix" regime at 97 psia. Therefore, the primary influence is that of chamber pressure which is seen to cause a high degree of separation at the 489 psia condition.

The effect of fuel temperature on RSS is illustrated in Figure 33 which shows separation induced by high fuel temperatures. The upper photo shows a mixing condition with ambient temperature MMH fuels at a chamber pressure of 147 psia and a velocity of 84 ft/sec. The lower picture shows separation with MMH fuel at a temperature of 294°F and a fuel velocity of 105 ft/sec at  $P_c = 144$  psia. The higher fuel velocity is not enough to induce RSS on its own, therefore the primary influence is due to a fuel temperature increase. As can be seen from Figures 31, 32, and 33, the primary factors controlling RSS are the chamber pressure and the fuel Reynolds Number. Therefore, increasing the fuel velocity, temperature or orifice diameter all tend toward increased RSS.

The RSS characteristics of all of the coherent stream elements (i.e., rounded inlet unlike doublet, triplet, sharp-edged unlike doublet, and RSS/RCS unlike doublet) were found to be smaller and are correlated with the same correlation equation. The similarity in behavior for the small and large triplets and sharp-edged unlike doublets is shown in Figures 34, 35, 36, and 37. The behavior of the SS/RCS unlike doublet is illustrated in Figure 38 which shows the element behavior over its whole  $P_c$ -MR operating range. The impingement mode and operating condition is indicated next to each photo.

The off-mixture ratio momentum effects on spray mixing are seen to be as strong as the RSS effects with the SS/RCS unlike doublet. It is clearly undesirable to operate at extreme off-MR conditions

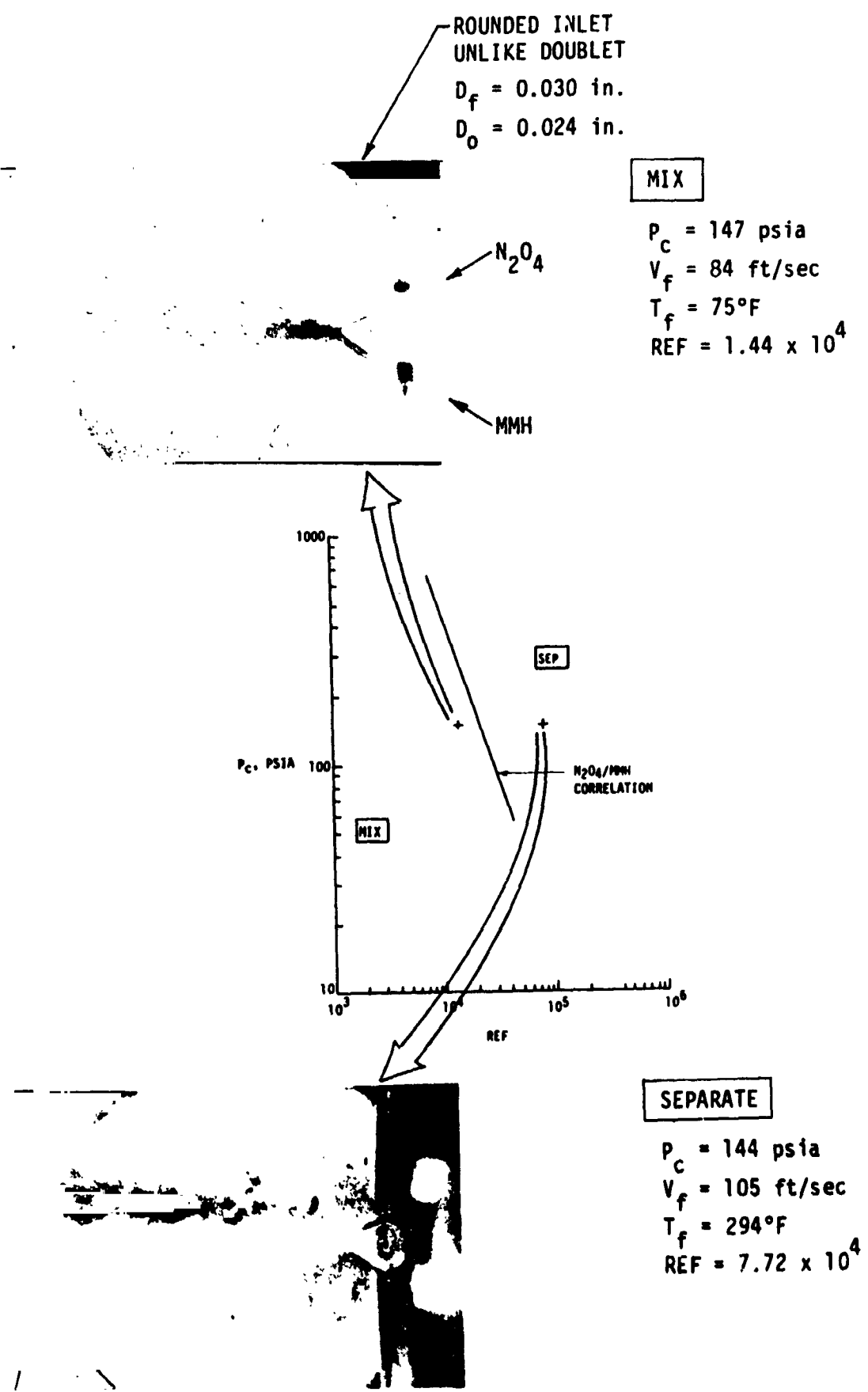


Figure 33. Increasing Fuel Temperature Promotes RSS

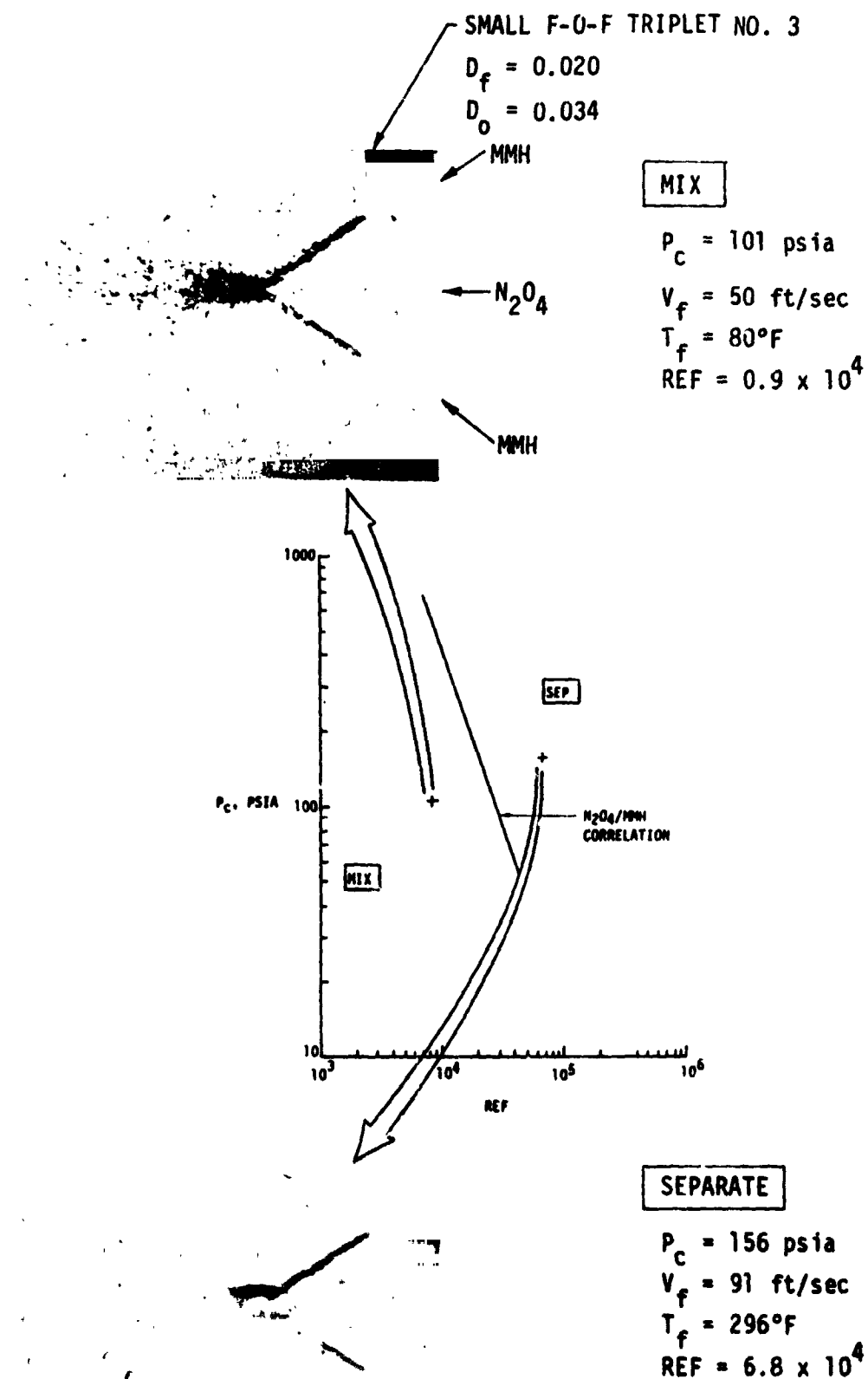


Figure 34. Reactive Stream Impingement with the Small F-O-F Triplet Element



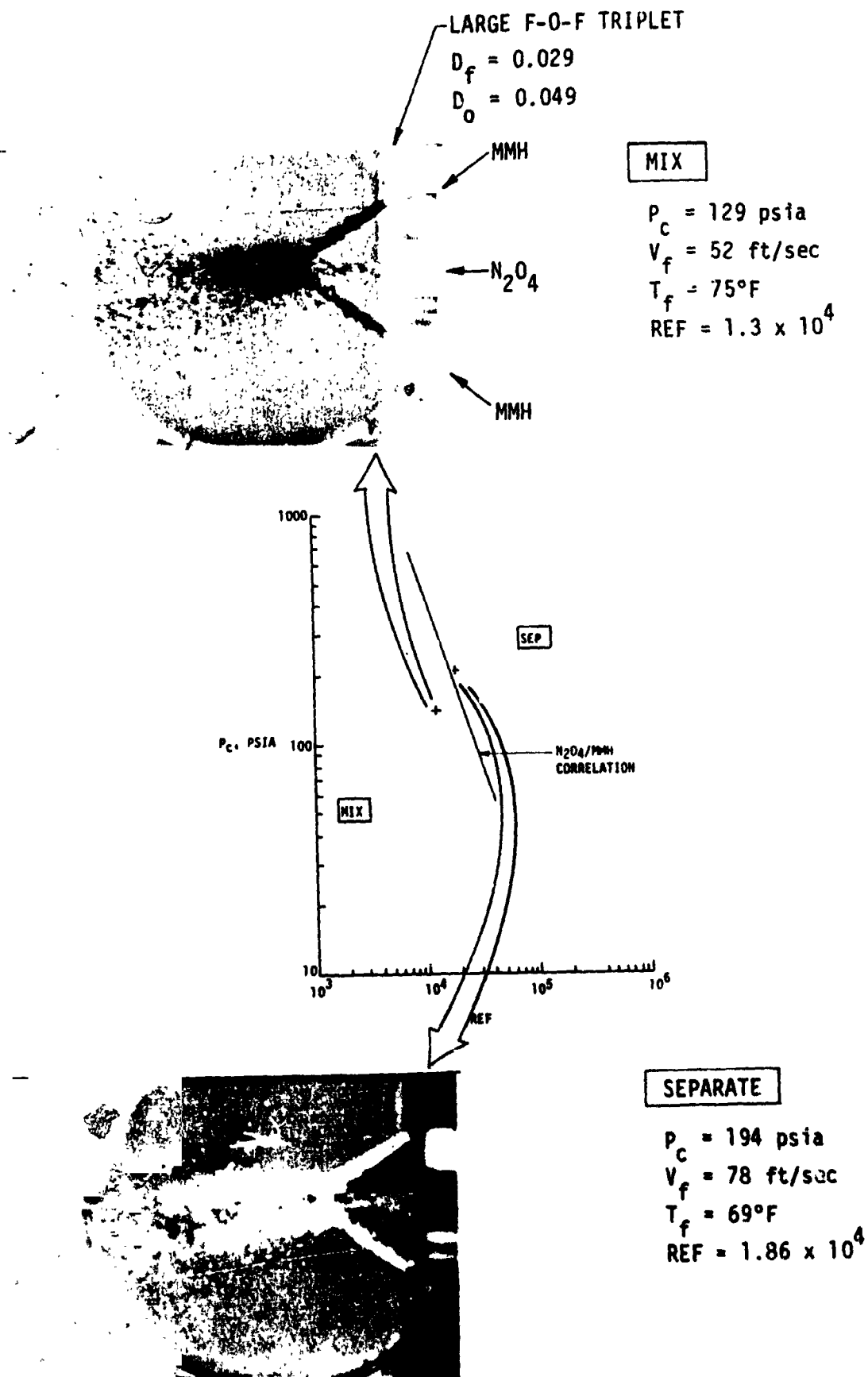


Figure 35. Reactive Stream Impingement with the Large F-O-F Triplet Element

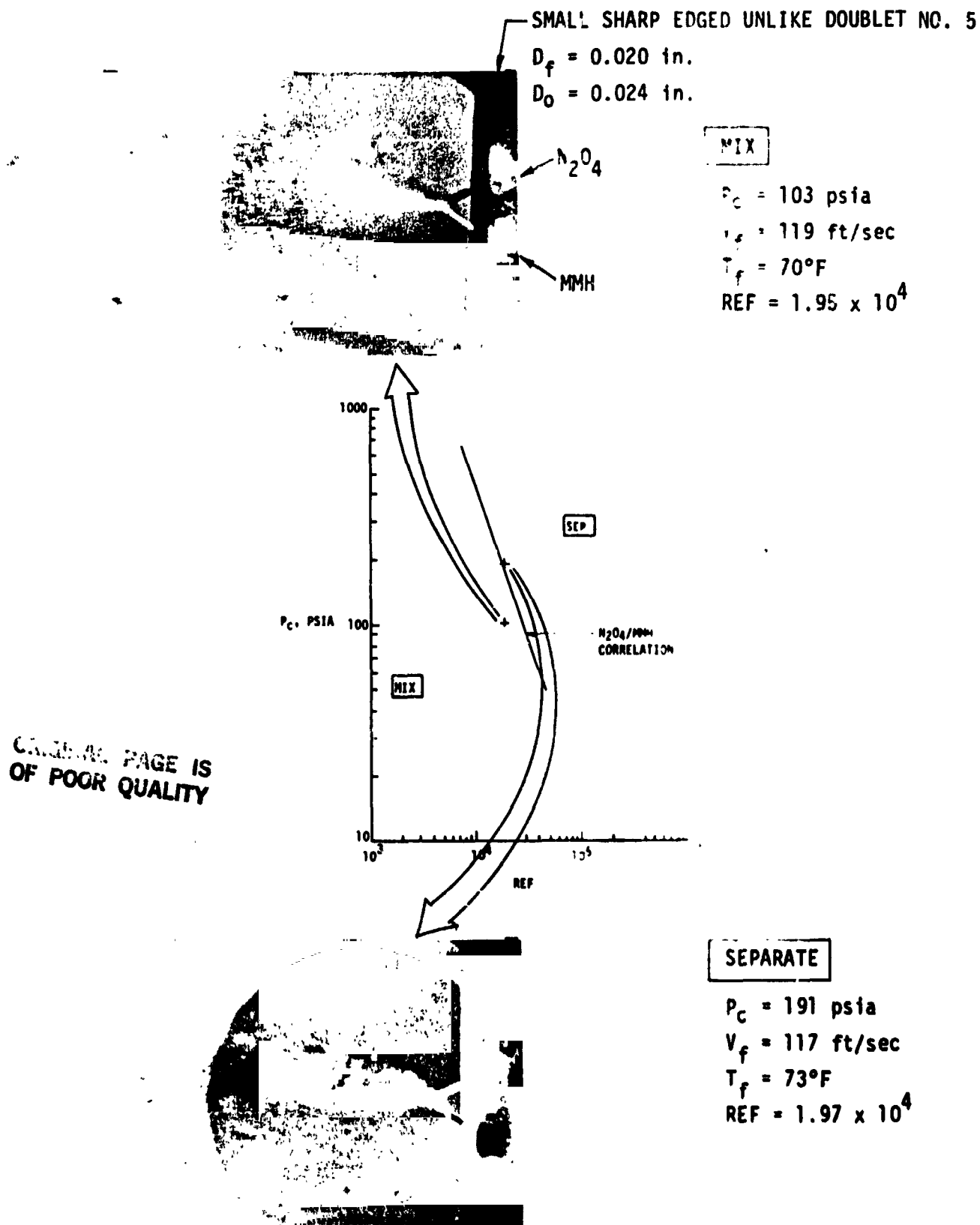
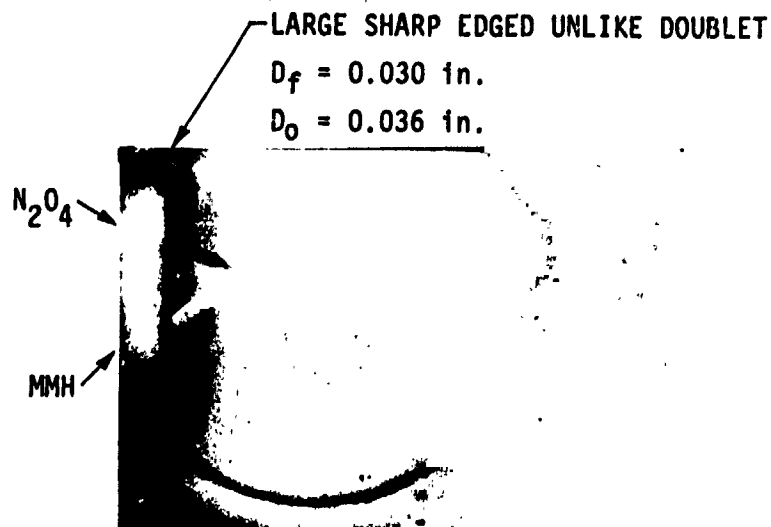


Figure 36. Reactive Stream Impingement with the Small Sharp Edged Unlike Doublet



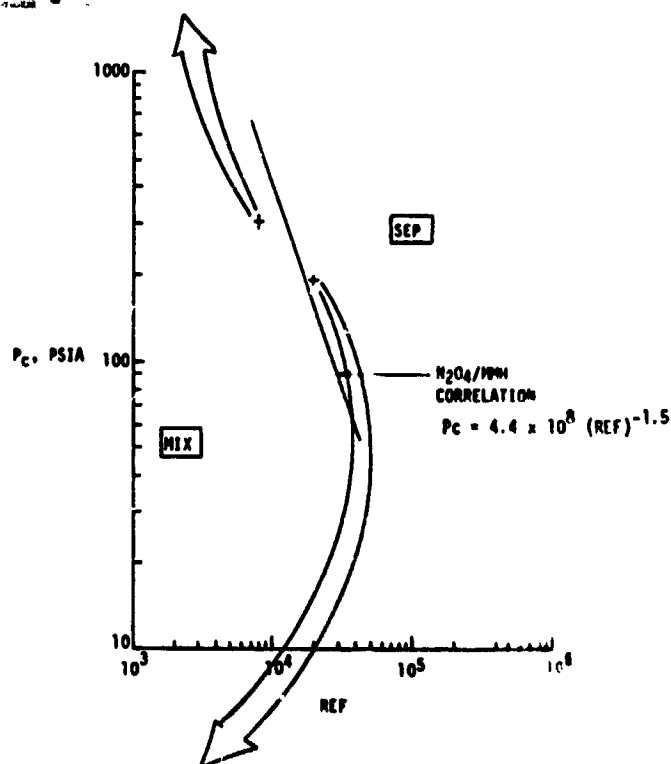
MIX

$P_c = 299$  psia

$V_f = 38$  ft/sec

$T_f = 69^\circ\text{F}$

REF =  $0.92 \times 10^4$



SEPARATE

$P_c = 195$  psia

$V_f = 76$  ft/sec

$T_f = 77^\circ\text{F}$

REF =  $1.99 \times 10^4$

Figure 37. Reactive Stream Impingement with the Large Sharp Edged Unlike Doublet

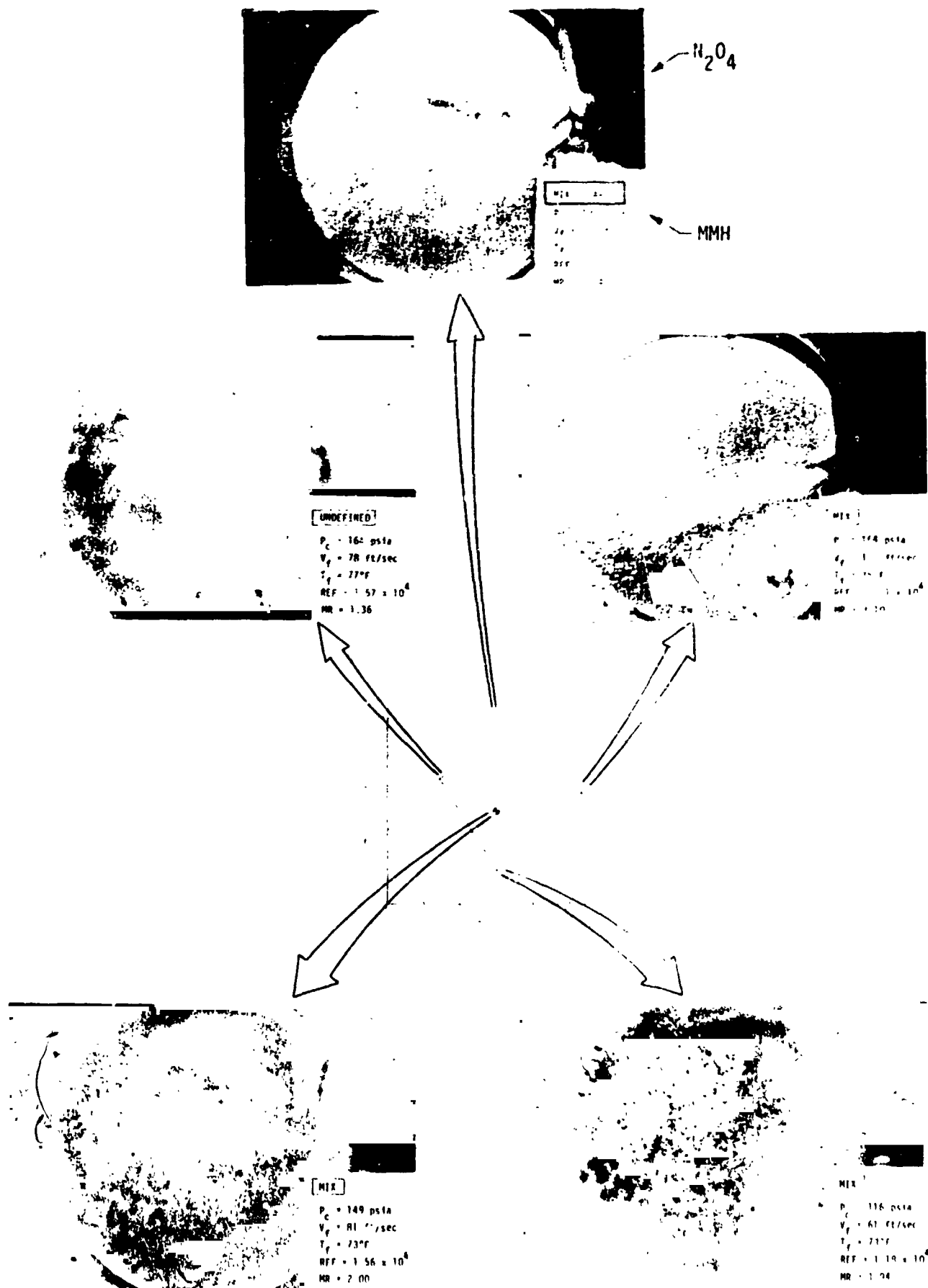


Figure 38. Reactive Stream Impingement with the Space Shuttle/OMS Unlike Doublet No. 7

## VI. C. Test Results (cont.)

with unlike doublet elements due to the strong effect on spray distributions. The triplet or pentad coherent elements or self-atomizing elements which are less sensitive to RSS and momentum effects would be better choices for injectors that must cover wide mixture ratio ranges.

The RSS Characteristics of the XDT, the splashplate and the SS/OMS TL0L self-atomizing elements were found to differ from the coherent stream elements in that RSS occurs at lower chamber pressures than for the coherent stream elements. The RSS characteristics of the XDT and the splashplate elements are illustrated in Figures 39 and 40. Increasing chamber pressure and fuel Reynolds Number (REF) promotes RSS. The chamber pressure is a much stronger effect than the fuel velocity (REF) as evidenced by the small slope of the correlation line. RSS sets in at such low chamber pressure levels (~100 psia) that these elements generally always operate in the separated mode.

The SS/OMS TL0L platelet element is an example of an element that operates in a separated mode over its entire operating range as illustrated in Figure 41. The operating conditions are indicated next to each photo. It is evident that this element is insensitive to engine operating mode. Although, it is always separated, the desired engine performance is attained by providing element overlap to take advantage of inter-element mixing. Excellent performance, compatibility and storability are provided by this element since the injector spray mass and mixture ratio distribution remain nearly constant over its whole operating range.

The SS/OMS TL0L element was found to operate much the same with  $N_2H_4$  fuel substituted for the MMH fuel as illustrated in Figure 42. The spray distributions are nearly identical over a wide chamber pressure range.

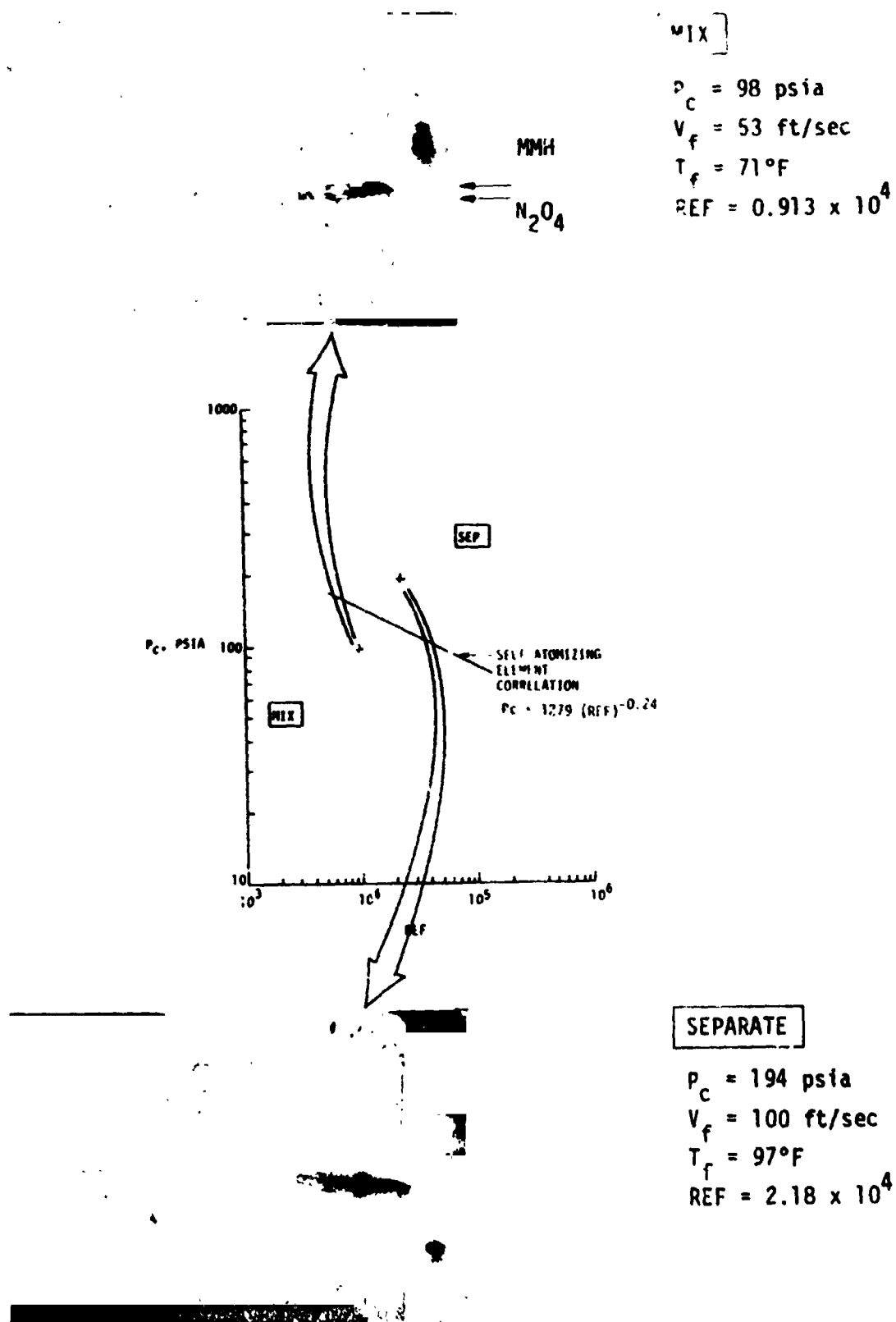


Figure 39. Reactive Stream Impingement with the XDT Platelet Element No. 10

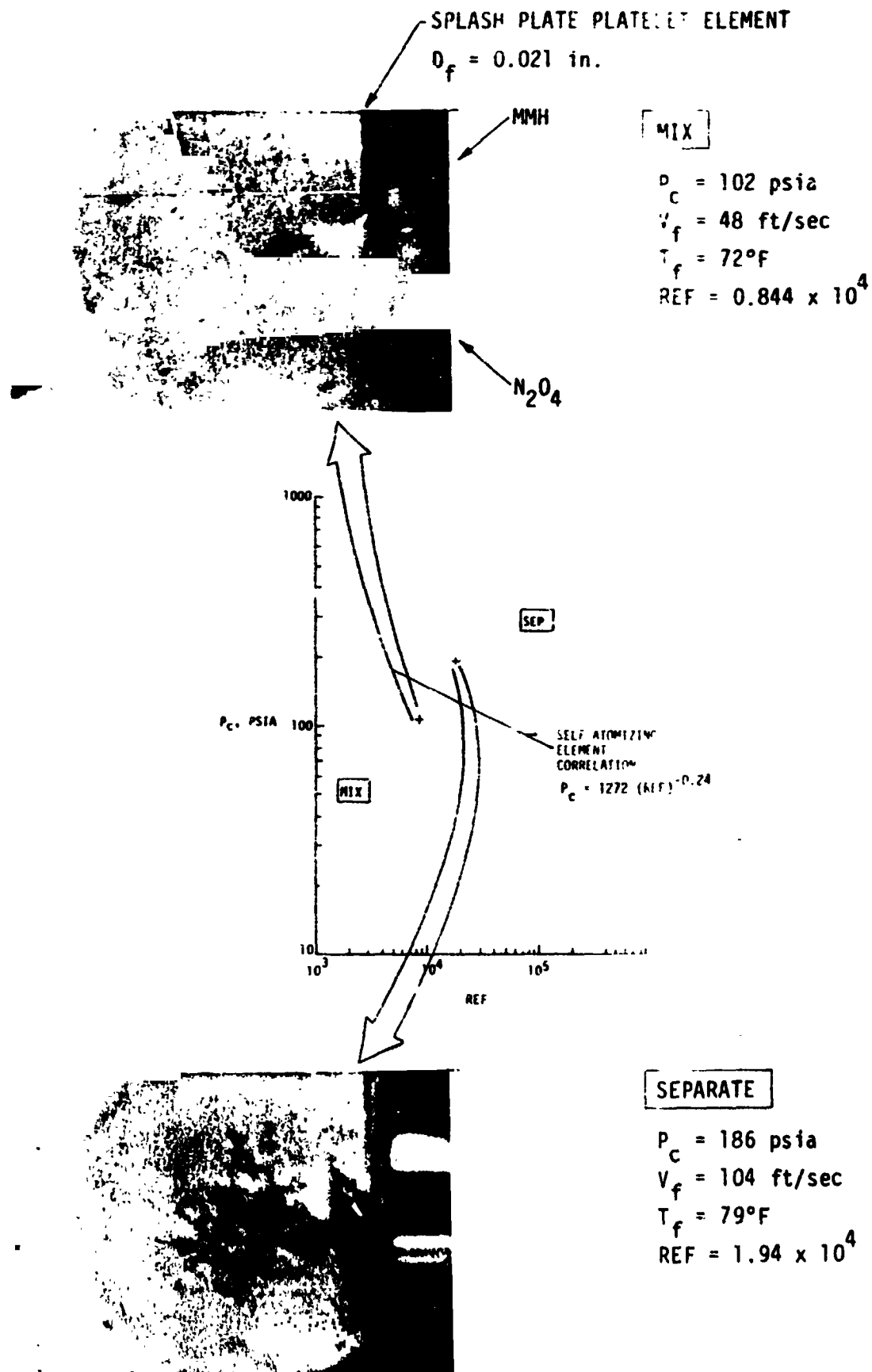


Figure 40. Reactive Stream Impingement with the Splash-Plate Element No. 11

MMH

$N_2O_4$

SEPARATE

$P_c = 140$  psia  
 $V_f = 73$  ft/sec  
 $T_f = 220^\circ F$   
 $REF = 4.91 \times 10^4$   
 $NR = 1.61$

SEPARATE

$P_c = 132$  psia  
 $V_f = 74$  ft/sec  
 $T_f = 226^\circ F$   
 $REF = 5.07 \times 10^4$   
 $NR = 1.47$

SEPARATE

$P_c = 131$  psia  
 $V_f = 64$  ft/sec  
 $T_f = 218^\circ F$   
 $REF = 4.16 \times 10^4$   
 $NR = 1.81$

SEPARATE

$P_c = 110$  psia  
 $V_f = 65$  ft/sec  
 $T_f = 226^\circ F$   
 $REF = 4.42 \times 10^4$   
 $NR = 1.46$

SEPARATE

$P_c = 113$  psia  
 $V_f = 56$  ft/sec  
 $T_f = 214^\circ F$   
 $REF = 3.53 \times 10^4$   
 $NR = 1.80$

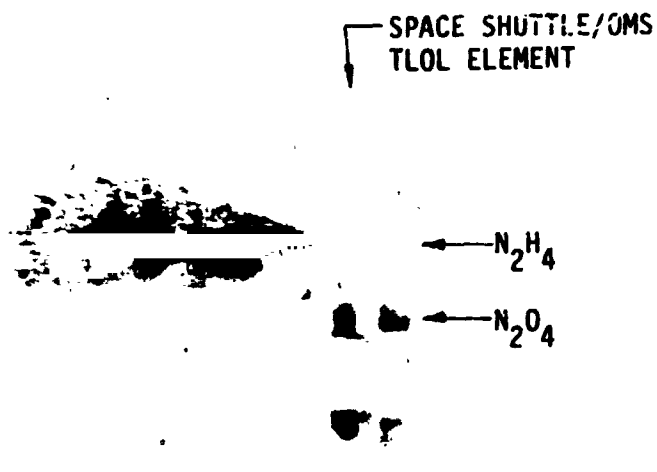
SEPARATE

$P_c = 103$  psia  
 $V_f = 54$  ft/sec  
 $T_f = 217^\circ F$   
 $REF = 3.52 \times 10^4$   
 $NR = 1.65$

ORIGINAL PAGE IS  
 OF POOR QUALITY

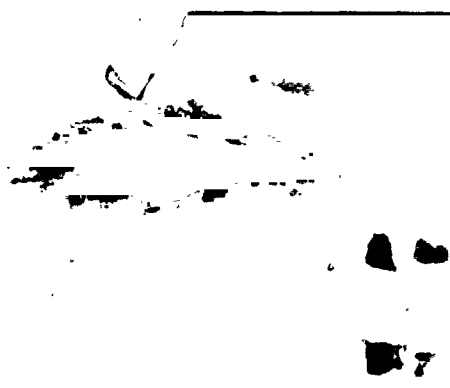
Figure 41. Reactive Stream Impingement with the Space Shuttle/  
 OMS TL0L Platelet Element No. 9





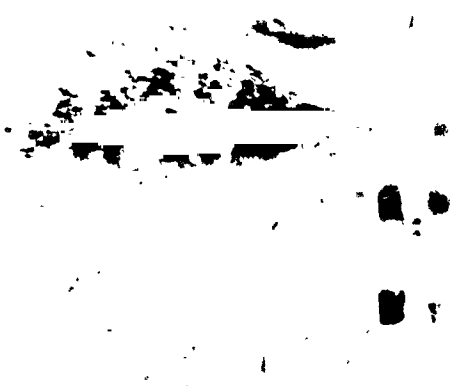
SEPARATE

$P_c = 110 \text{ psia}$   
 $V_f = 91 \text{ ft/sec}$   
 $T_f = 150^\circ\text{R}$   
 $\text{REF} = 3.5 \times 10^4$   
 $\text{MR} = 1.65$



SEPARATE

$P_c = 137 \text{ psia}$   
 $V_f = 119 \text{ ft/sec}$   
 $T_f = 152^\circ\text{F}$   
 $\text{REF} = 4.63 \times 10^4$   
 $\text{MR} = 1.62$



SEPARATE

$P_c = 206 \text{ psia}$   
 $V_f = 78 \text{ ft/sec}$   
 $T_f = 78^\circ\text{F}$   
 $\text{REF} = 1.86 \times 10^4$   
 $\text{MR} = 1.67$

Figure 42. Reactive Stream Impingement with the Space Shuttle/  
OMS TLOL Platelet Element Using  $\text{N}_2\text{H}_4$  Fuel

## VI, Technical Discussion (cont.)

### D. RSS MODEL DEVELOPMENT

The approach taken to develop an understanding of the RSS mechanisms which led to the vaporization controlled model is outlined in Figure 3. The process involved literature review, model evaluation, development of high speed color photography techniques, testing of single elements, and analytical modeling. Each of these efforts are discussed in a chronological development.

An evaluation of existing RSS models and development of RSS correlations was accomplished during the proposal effort and are reported in the Task I Data Dump (Ref. 18). The results showed that the existing models were inadequate and that the mechanisms controlling RSS were not understood. The data correlations, developed using the Zung (Ref. 17)  $N_2O_4/N_2H_4$  data, showed that the controlling design parameters were chamber pressure, fuel temperature and fuel orifice diameter as illustrated in Figure 43. The data defined a low pressure and a high pressure regime of RSS. The low pressure RSS is clearly due to flash vaporization of the  $N_2O_4$  when it is injected in a supersaturated condition. Low pressure RSS is of less significance to the engine designer than the high pressure RSS since it is generally not encountered at normal engine operating pressures.

The possible modes of hypergolic reactions were examined for possible RSS mechanisms since the cause of high pressure RSS was not obvious. Possible mechanisms were postulated for the various regimes on the basis of this examination. It was found that hypergolic reactions occur primarily in the gas phase. Liquid phase reactions are not possible (Ref. 14) due to extreme reactivity and immiscibility of these propellants. However, reactions do take place on the fuel surface under certain conditions (Refs. 26 and 27). These surface reactions lead to incomplete low enthalpy

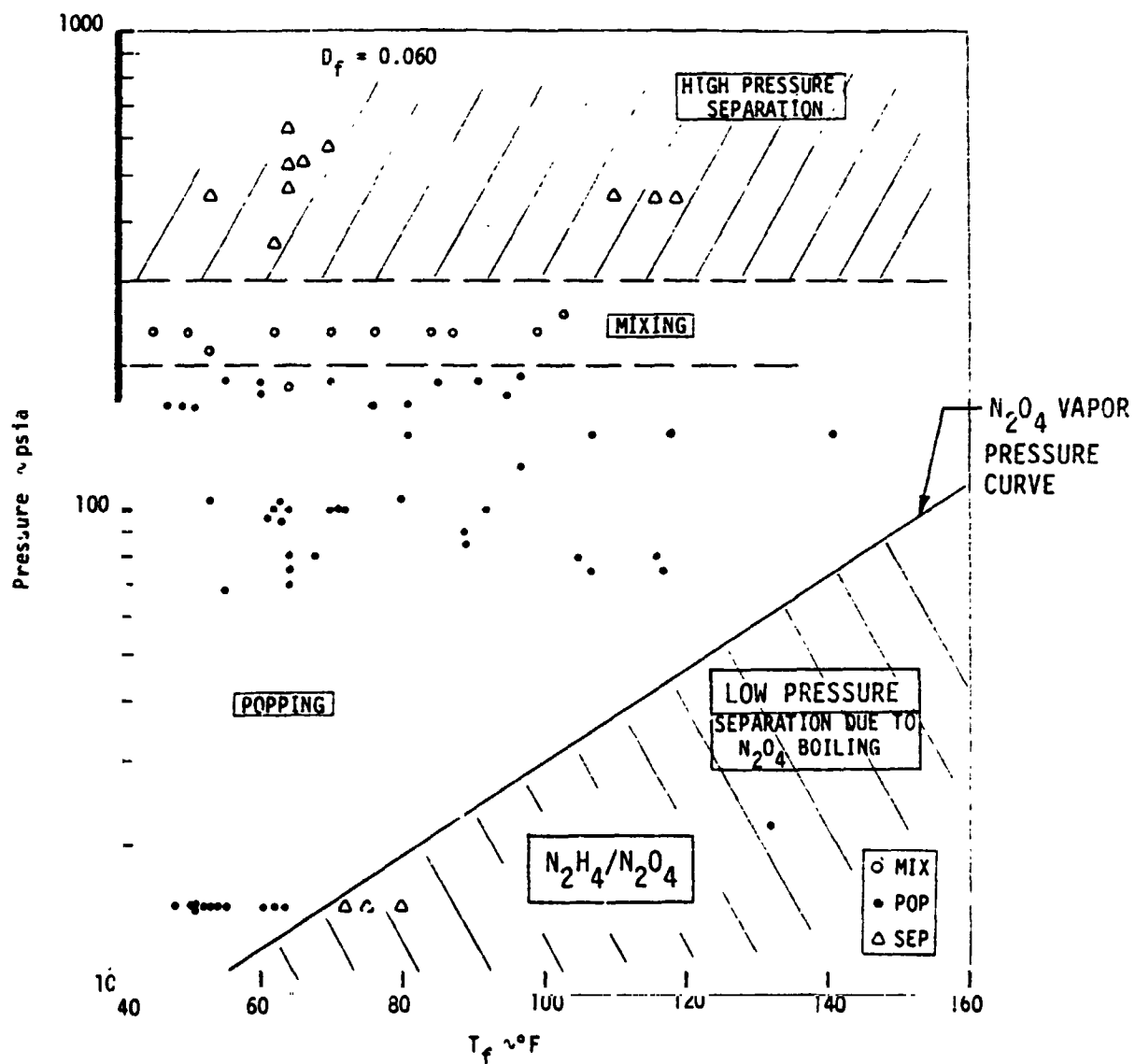


Figure 43. Task I RSS Data Correlations

#### VI, D, RSS Model Development (cont.)

combustion with the generation of solid reaction intermediates. The gas phase reactions can occur in both a bipropellant and a mono-propellant mode.

High pressure RSS was postulated to be a result of mono-propellant decomposition of the fuel ahead of impingement due to hot gas recirculation heating as shown in Figure 44. It was believed that the recirculation gas heats the fuel to the saturation temperature as shown in Figure 44, with RSS occurring when the saturation temperature exceeds the fuel vapor decomposition temperature ( $\sim 450^{\circ}\text{F}$ ). The monopropellant decomposition model predicted different chamber pressure limit for the Amine fuels depending on their vapor pressure as shown in Figure 44. However, the measured chamber pressure limits were subsequently found to be much lower and to depend on fuel velocity and temperature.

Analyses conducted during Task I indicated that significant heating of the bulk fuel stream does not occur although the surface film is rapidly heated to the saturation temperature. The two rounded inlet unlike injector elements shown in Figure 7 were designed to map RSS and to test the high pressure RSS model during Task III. One element was designed with a longer impingement length and, hence, more free stream heating than the other to test the recirculation gas heating effect on the monopropellant decomposition model.

The results of the Task III testing showed that the impingement length (i.e., recirculation gas heating) had no effect on RSS for the range of lengths tested. It was also found that the RSS limits did not agree with those predicted for MMH and A-50 fuels, therefore, it was concluded that the proposed model was not correct. These test results also showed that the transition from the mixed mode to the separated mode occurs

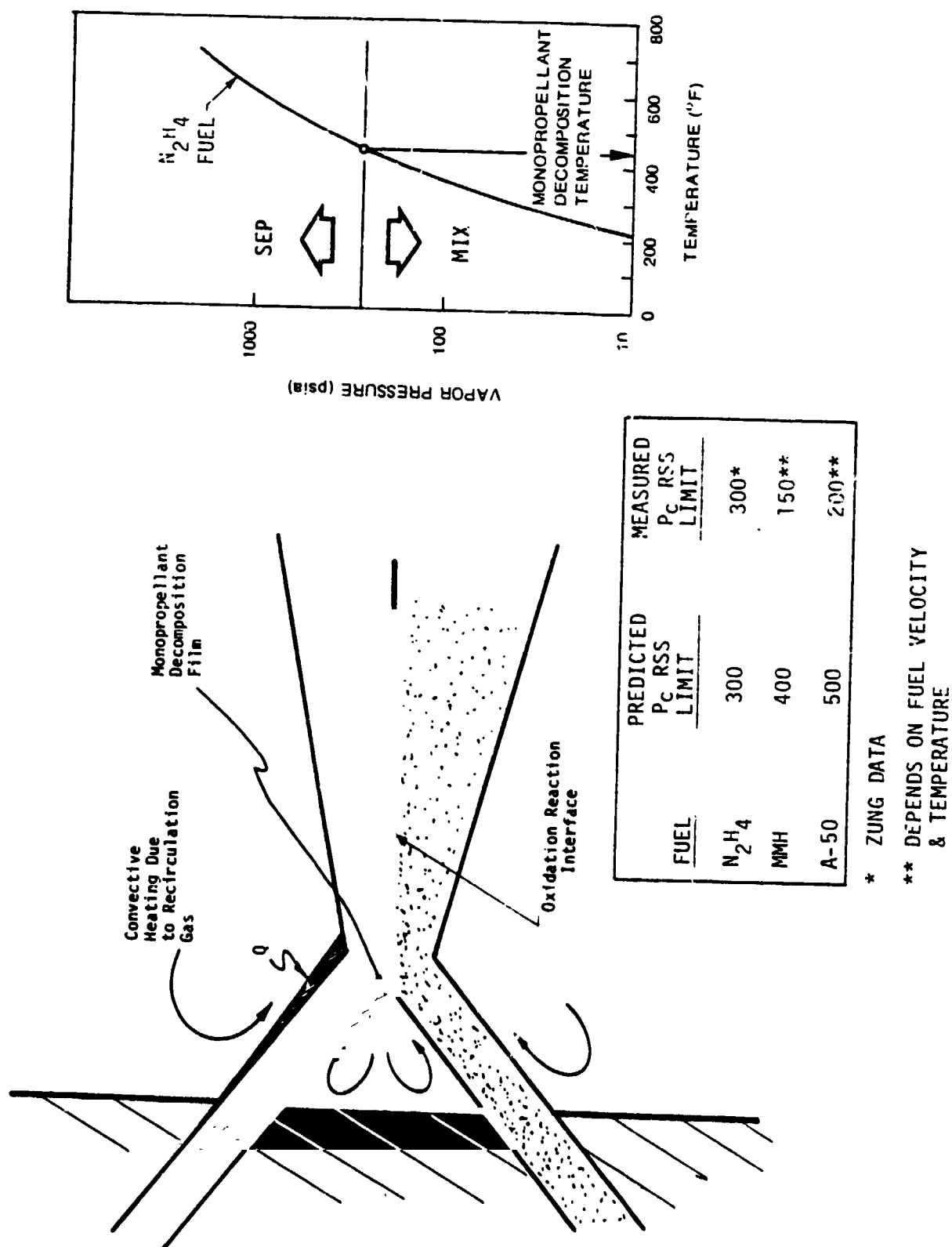


Figure 44. High Pressure Monopropellant Decomposition RSS Model

#### VI, D, RSS Model Development (cont.)

gradually with increasing chamber pressure rather than with an abrupt change as had been previously supposed. An injection velocity and fuel temperature effect on high pressure RSS was observed which was not indicated by the proposal and Task I data correlations.

Impingement point temperature probing with small diameter thermocouples and close examination of the movie film led to the development of a surface reaction controlled RSS model aimed at explaining the velocity effect. It was observed that aerodynamic shedding of liquid droplets from the fuel jet surface occurs when the fuel velocity exceeds a certain value identified by a critical Weber Number as shown in Figure 45. Because the impingement point temperature rise was found to increase with Weber Number (i.e., injection velocity and chamber pressure) it was postulated that RSS is controlled by a surface reaction. It was reasoned that increasing the Weber Number would increase the pre-impingement surface area due to droplet shedding and hence promote RSS.

The vapor phase reaction model shown in Figure 46 was derived in an attempt to explain the observed fuel temperature effect. It was postulated that the gas phase reactivity could be related to the vapor phase mixture ratio (MRVP). The MRVP decreases from extremely oxidizer rich values with ambient temperature fuel to near stoichiometric values when the fuel is heated. Hence, it was reasoned that increasing fuel temperature would increase reactivity and promote RSS. The rounded inlet unlike doublet data were correlated by plotting the fuel Weber Number versus the MRVP as shown in Figure 47. Although the correlation showed promise for the rounded inlet unlike doublet it was found to be unsatisfactory for some of the other elements. A more generally applicable correlation is provided by the chamber pressure and fuel Reynolds Number.

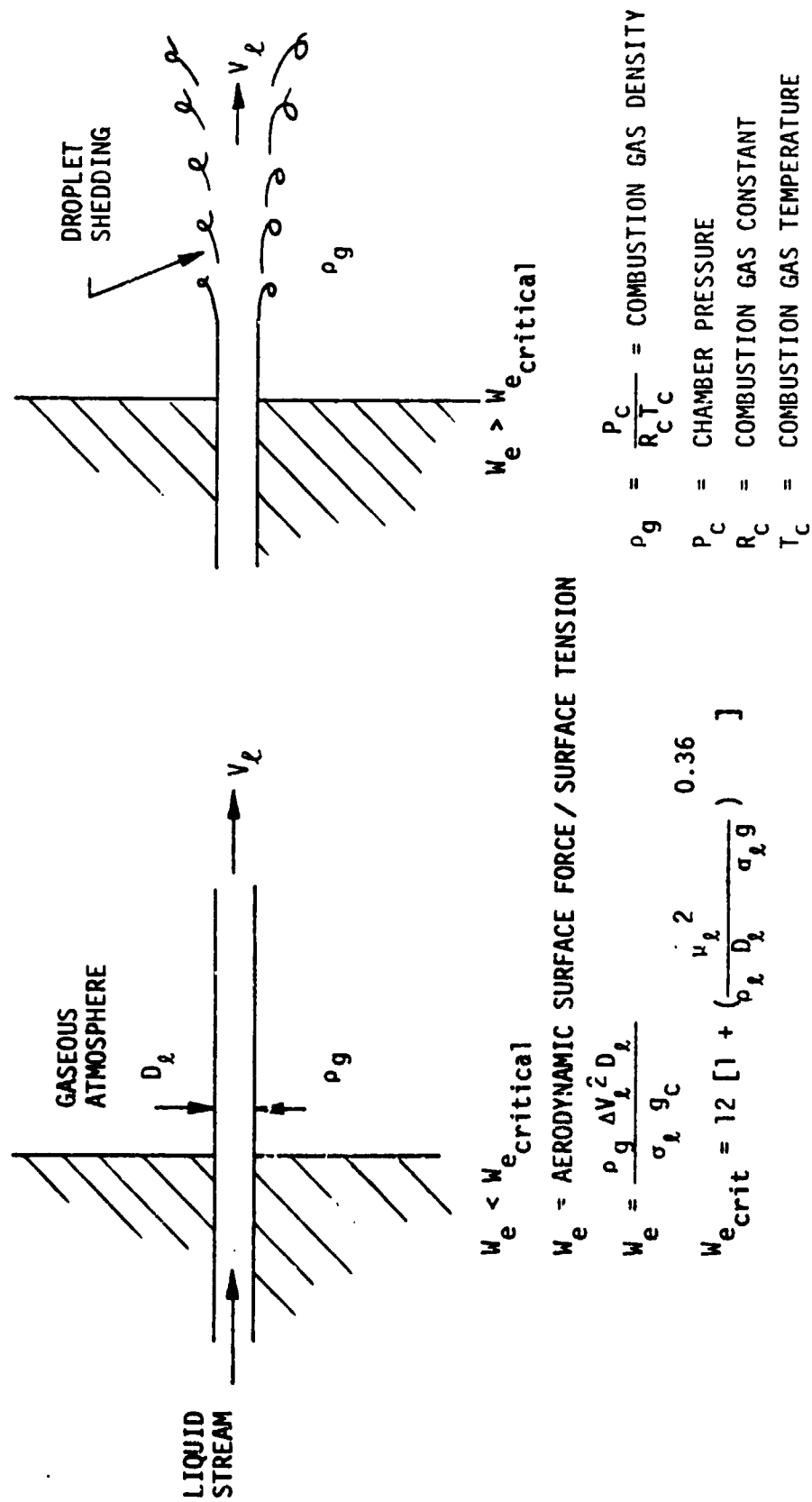
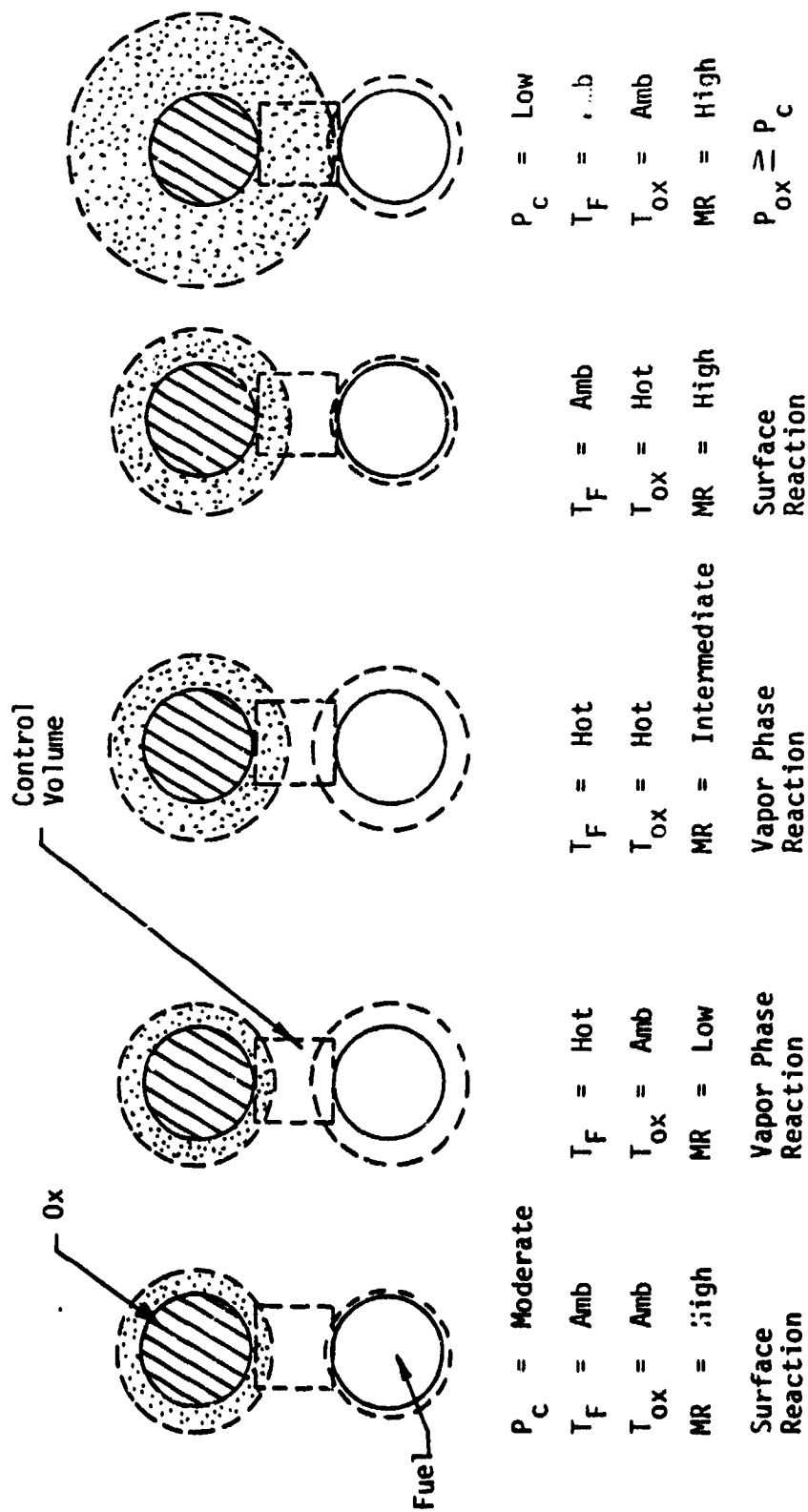


Figure 45. Weber Number Model



$$MR_{vp} = 2.0 \frac{p_{ox}}{p_f} \frac{T_f}{T_{ox}}$$

Figure 46. Vapor Phase Reaction Model



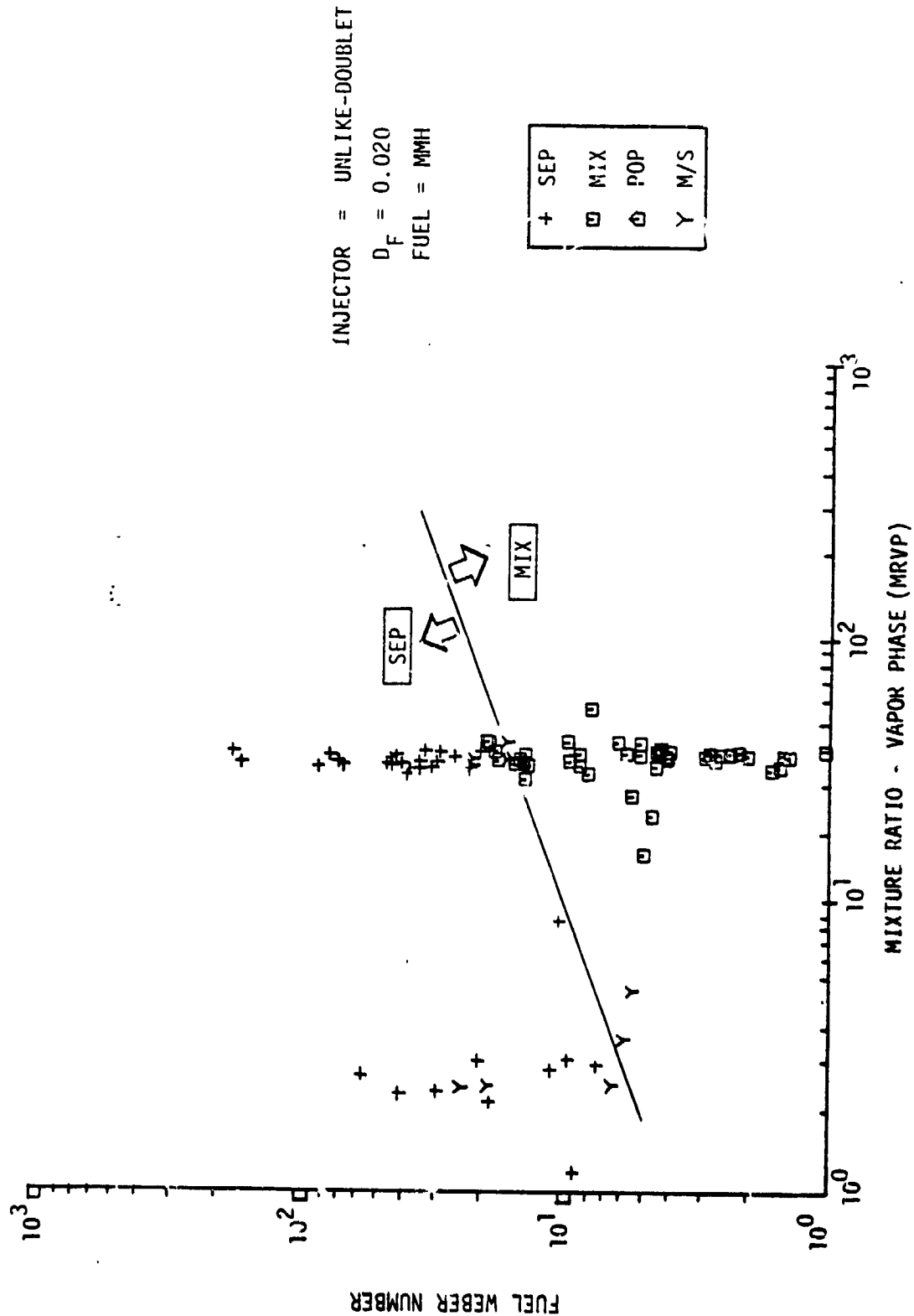


Figure 47. Fuel Weber Number and MRVP RSS Correlation

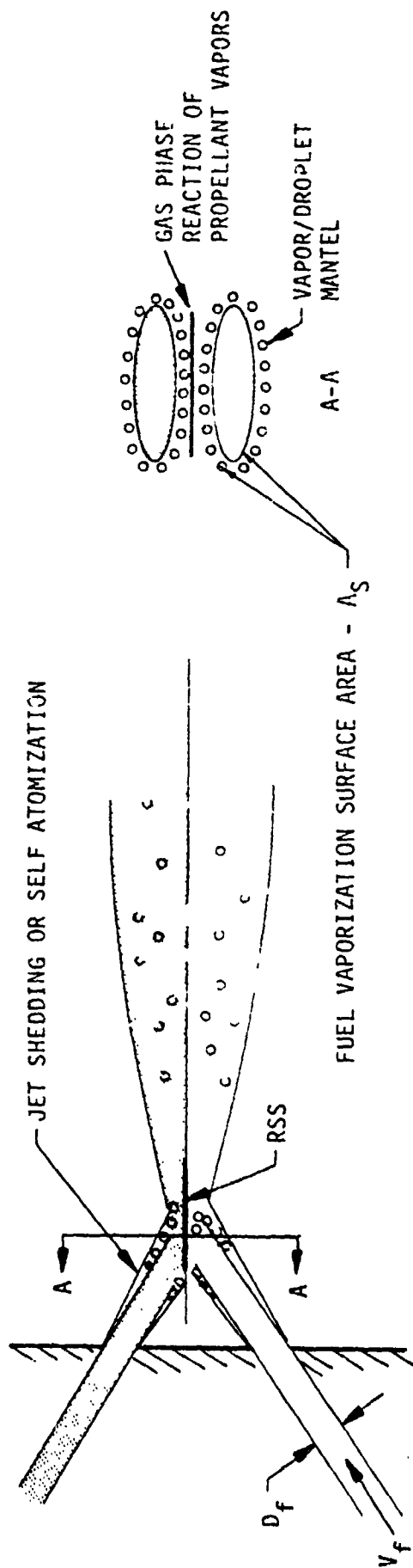
#### VI, D, RSS Model Development (cont.)

Task IV included testing of the small and large F-O-F triplet elements and the XDT and splash plate self-atomizing impingement type of injectors to test the influence of increased interfacial surface area on RSS. Hot firing confirmed that self-atomizing injector elements promote RSS due to increased interfacial surface area. Cold flow experiments were also made which showed that jet shedding with coherent streams could be correlated with Reynolds Number as well as with Weber Number. This led to development of the final data correlations during Task V. It was found that RSS could be correlated for both coherent stream injectors and self-atomizing injectors by plotting chamber pressure versus fuel Reynolds Number as shown in Figures 4 and 5. The vaporization controlled RSS model outlined in Figure 48 resulted from the Task V effort.

Testing during Task VII was done to, (1) verify the vaporization controlled RSS model using the sharp edged unlike doublet flight type injector elements and, (2) to characterize the Space Shuttle OMS engine and RCS engine injector elements over their respective operating ranges. The results show that RSS with flight type injectors correlate with the vaporization model using either MMH or  $N_2H_4$  fuel indicating the validity of the RSS model.

The strong RSS dependence on chamber pressure and fuel Reynolds Number can be related to a fuel vaporization rate controlled combustion mechanism by making the following assumptions:

1. The combustion gas generation rate prior to and at the impingement interface must exceed some minimum rate for RSS to occur.
2. Combustion gas generation occurs through gas phase reaction only.



#### VAPORIZATION RATE:

$$\dot{W}_V = A_S K_V P_{VS} = A_S K_V P_C$$

$$\dot{W}_V = \text{VAPORIZATION RATE}$$

$$A_S = \text{EVAPORATION SURFACE AREA}$$

$$K_V = \text{MASS TRANSFER COEFFICIENT}$$

$$P_{VS} = \text{FUEL VAPOR PRESSURE EVALUATED AT } T_{SAT}$$

$$P_C = \text{CHAMBER PRESSURE}$$

$$\text{MASS TRANSFER COEFFICIENT:}$$

$$Nu_m = D_S R T K_V / \omega = 2.0 + 0.6 Sc^{1/3} Re^{1/2}$$

$$D_S = \text{DROPLET DIAMETER}$$

$$R = \text{GAS CONSTANT}$$

$$T = \text{FILM TEMPERATURE}$$

$$\omega = \text{DIFFUSION COEFFICIENT}$$

#### ASSUMPTIONS:

- COMBUSTION GAS GENERATION RATE MUST EXCEED SOME MINIMUM RATE FOR RSS TO OCCUR
- COMBUSTION GAS GENERATION OCCURS THROUGH GAS PHASE REACTION ONLY
- COMBUSTION GAS GENERATION RATE IS LIMITED BY VAPORIZATION RATE FROM FUEL VAPORIZATION SURFACE AREA
- FUEL FILM IS HEATED TO SATURATION TEMPERATURE

$$\text{JET IMPINGEMENT: } P_C \propto Re^{-3/2}$$

$$A_S \propto Re$$

$$\text{SELF ATOMIZING IMPINGEMENT: } P_C \propto Re^{-1/2}$$

$$A_S \neq f(Re)$$

Figure 48. Fuel Vaporization Controlled RSS Model

## VI, D, RSS Model Development (cont.)

3. Combustion gas generation rate is limited by the fuel preimpingement vaporization rate since it is the more difficult propellant to vaporize.

The vaporization rate is related to the fuel vapor pressure and vaporization surface area through the mass transfer equation (Ref. 28):

$$\dot{W}_V = A_S K_V P_V \quad \text{Equation (3)}$$

where:

$$\begin{aligned} \dot{W}_V &= \text{evaporation rate} \\ A_S &= \text{fuel vaporization surface area} \\ K_V &= \text{mass transfer coefficient} \\ P_V &= \text{fuel vapor pressure} \end{aligned}$$

The fuel vaporization surface area includes all fuel vaporizing surfaces ahead of impingement. This includes the jet surface and droplet surfaces as shown in Figure 48.

From the movie film and the Task I analysis it is apparent that the surface of the fuel stream is rapidly heated to the saturation temperature such that the vapor pressure is essentially equal to the chamber pressure. Therefore,

$$\dot{W}_V = A_S K_V P_C \quad \text{Equation (4)}$$

where:

$$\begin{aligned} P_V &= P_C, \text{ at the saturation temperature} \\ P_C &= \text{chamber pressure} \end{aligned}$$

The mass transfer coefficient ( $K_V$ ) is related to the Nusselt Number for mass transfer:

$$Nu_m = \frac{D_S R T K_V}{\mu} \quad \text{Equation (5)}$$

## VI, D, RSS Model Development (cont.)

where:

- $D_s$  = droplet diameter
- $R$  = gas constant
- $T$  = average film temperature
- $D$  = diffusion coefficient

The evaporation constant can be related to the Reynolds Number through the Ranz and Marshall Nusselt number correlation for evaporation (Ref. 29):

$$Nu_m = 2.0 + 0.6 Sc^{1/3} Re^{1/2} \quad \text{Equation (6)}$$

where:

- $Sc$  = Schmidt Number
- $Re$  = Fuel Reynolds Number

The evaporation constant can be expressed in terms of the Reynolds Number by combining Equations (5) and (6). The critical fuel vaporization rate and, hence, chamber pressure at which RSS will occur then becomes a function primarily of the surface area for evaporation and the Reynolds Number;

$$\dot{W}_{v,Critical} \propto A_s f(Re^{1/2}) p_{c,Critical} \quad \text{Equation (7)}$$

$$p_{c,Critical} \propto A_s^{-1} Re^{-1/2} \quad \text{Equation (8)}$$

It is known that the pre-impingement surface area is velocity or Reynolds Number dependent for coherent streams such as those produced by drilled or EDM'd orifices with L/D's greater than about 4/1. Whereas, the pre-impingement surface area for self-atomizing injectors is only weakly

# VI, D, RSS Model Development (cont.)

dependent on the velocity or Reynolds number. Therefore, the critical chamber pressure for coherent streams is expected to be more dependent on Reynolds number than the self-atomizing injector elements:

$$\begin{array}{ll} \text{Rounded Inlet} & P_{c\text{Critical}} \propto \text{REF}^{-3/2} \\ \text{Unlike Doublets} & \end{array} \quad \text{Equation (9)}$$

where:

$$A_s \propto \text{REF}$$

$$\begin{array}{ll} \text{Self-Atomizing} & P_{c\text{Critical}} \propto \text{REF}^{-1/2} \\ \text{Elements} & \end{array} \quad \text{Equation (10)}$$

where:

$$A_s \neq f(\text{REF})$$

This model shows good agreement with the coherent stream experimental data in that the measured exponent on REF is equal to -3/2. The exponent on REF is found to be -0.24 rather than -0.5 for the self-atomizing elements. However, the agreement with the experimental data is sufficient to conclude that RSS is controlled primarily by fuel vaporization rate controlled combustion.

## REFERENCES

1. Lawver, B.R., "Rocket Engine Popping Phenomena", Aerojet-General Report No. TCER 9642:0095, March 1969.
2. Mills, T.R., Tkachenko, E.A., Lawver, B.R., and Breen, B.P., "Transients Influencing Rocket Engine Ignition and Popping", Dynamic Science Report No. NAS 7-467, January 1969.
3. Zung, L.B., "Hypergolic Impingement Mechanisms and Criteria for Jet Mixing or Separation", presented at the 6th ICRPG Liquid Propellant Combustion Instability Conference, 9-11 September 1969.
4. Nurick, W.H. and Cordill, J.D., "Reactive Stream Separation Photography", Final Report R-8490, Contract NAS 7-720, Rocketdyne, 1971.
5. Lee, A., and J. Houseman, "Popping Phenomena with  $N_2O_4/N_2H_4$  Injectors", presented at the Western States Section meeting of the Combustion Institute on Stable Combustion of Liquid Propellants, JPL, October 26-27 1970.
6. Elverum, G.W., Jr., and Staudhammer, P., "The Effect of Rapid Liquid-Phase Reactions on Injector Design and Combustion Rocket Motors", Progress Report 30-4. Jet Propulsion Laboratory, Pasadena, California, 25 August 1959.
7. Burrows, M.C., "Mixing Reaction of Hydrazine and Nitrogen Tetroxide at Elevated Pressure", AIAA Journal, Volume 5, No. 9, pp. 1700-1701, September 1967.
8. Weiss, R.R. and Klopotev, R.D., "Experimental Evaluation of the Titan III Transtage Engine Combustion Stability Characteristics", TR WO AFRPL TR-66-51, March 1966.
9. Evans, D.D., Stanford, H.B., and Riebling, R.W., "The Effect of Injector Element Scale on the Mixing and Combustion of Nitrogen Tetroxide-Hydrazine Propellant", Technical Report 32-1178, Jet Propulsion Laboratory, Pasadena, California, 1 November 1967.
10. Clayton, R., "Experimental Observations Relating the Inception of Liquid Rocket Engine Popping and Resonant Combustion of the Stagnation Dynamics of Injection Impingement", TR 32-1479, JPL, 15 December 1970.
11. Houseman, J., "Jet Separation and Optimum Mixing for an Unlike Doublet", presented at the 6th ICRPG Liquid Propellant Combustion Instability Conference, 9-11 September 1969.

#### REFERENCES (cont.)

12. Kushida, R., Houseman, J., "Criteria for Separation of Impinging Streams of Hypergolic Propellants", Technical Memorandum 33-395, Jet Propulsion Laboratory, Pasadena, California, July 1968.
13. Nadiz, E.W., and Breen, B.P., "Liquid Phase Kinetics for the Hypergolic Nitrogen Tetroxide Hydrazine System", presented at ICRPG 3rd Combustion Conference, October 1966.
14. Breen, B.P., Zung, L.B., and Lawver, B.R., "Injection and Combustion of Hypergolic Propellants", AFRPL-TR-69-48, Dynamic Science, a Division of Marshall Industries, Monrovia, California, April 1969.
15. Lawver, B.R. and Breen, B.P., "Hypergolic Stream Impingement Phenomena-Nitrogen Tetroxide/Hydrazine", NAS-CR-72444, Dynamic Science Division, Marshall Industries, Monrovia, Calif., October 1968.
16. Rodriguez, S.E. and Awworthy, A.E., "Liquid Phase Reactions of Hypergolic Propellants", Rocketdyne Final Report R-8374, Contract NAS-7-739, 1 December 1970.
17. Zung, L.B. and White, J.R., "Combustion Process of Impinging Hypergolic Propellants", NASA-CR-1704, Marshall Industries, Irvine, California, May 1971.
18. Lawver, B.P., "High Performance  $N_2O_4$ /Amine Elements - Blowapart", Task I Data Dump, Contract NAS 9-14186, Report 14186-DRL-3, Aerojet Liquid Rocket Company, 15 September 1974.
19. Lawver, B.R., "High Performance  $N_2O_4$ /Amine Elements", Work Plan, Contract NAS-9-14186, Report 14186-DRL-1, ALRC, 2 August 1974.
20. Lawver, B.R., "High Performance  $N_2O_4$ /Amine Elements - Blowapart", Task III Data Dump, Contract NAS-9-14186, Report 14186-DRL-3-1, ALRC, 15 November 1974.
21. Lawver, B.R., "High Performance  $N_2O_4$ /Amine Elements - Blowapart", Interim Report, Contract NAS-9-14186, Report 14186-3.1.1, ALRC, 13 May 1977.
22. Lawver, B.R., "High Performance  $N_2O_4$ /Amine Element-Blowapart", Task V and VI Data Dump, Contract NAS 9-14186, Report 14186-DRL-3-2, ALRC 25 October 1977.
23. "Acoustic Cavity Technology for High Performance Injectors", Final Report, Contract NAS-9-14232, Report 14232-3-1, ALRC, 1 October 1976.



#### REFERENCES (cont.)

24. Ito, J.I., "Development Test Report, OMS Injector Subscale Pattern Evaluation", Contract M4J7XMA-483030H, Report 6673:207, ALRC, March 1976.
25. Ito, J.I., "A General Model Describing Hydraulic Flip in Sharp Edge Orifices", 7th JANNAF Combustion Meeting, CPIA Publ. #204, Vol. 1, Feb. 1971.
26. Zung, L.B., Breen, B.P. and Kushida, R., "A Basic Study of Ignition of Hypergolic Liquid Propellants", Paper No. 68-43 Presented at Western States Section of the Combustion Institute, October 1968.
27. Lawver, B.R., "Some Observations on the Combustion of  $N_2H_4$  Droplets", AIAA Journal, Volume 4, No. 4, p. 659, April 1966.
28. Priem, R.S. and Heidmann, M.F., "Propellant Vaporization as a Design Criterion for Rocket Engine Combustion Chambers", NASA, Tec. Report. R-67, 1960.
29. Ranz, W.E. and Marshall, W.N., Jr., "Evaporation from Drops, Pt. I", Engineering Progress, Vol. 48, No. 3, March 1952, pp. 141-146.
30. Rupe, J.H., "A Correlation Between the Dynamic Properties of a Pair of Impinging Streams and the Uniformity of Mixture-Ratio Distribution in the Resulting Spray", JPL Progress Rept. No. 20-209, 1956.

APPENDIX A

HYPERGOLIC PROPELLANT  
INJECTOR ELEMENT DESIGN CRITERIA

Appendix A

HYPERGOLIC PROPELLANT  
INJECTOR ELEMENT DESIGN CRITERIA

Prepared by:

B. R. Lawver

March 1979

## Appendix A

### TABLE OF CONTENTS

	<u>Page</u>
I. Introduction	1
II. Liquid Rocket Combustion Process	2
III. Non-Reactive Stream Impingement Phenomena	7
IV. Reactive Stream Impingement Phenomena	27
V. Reactive Stream Impingement Data Correlations	38
VI. Reactive Stream Design Criteria	41
References	44

### LIST OF TABLES

<u>Table No.</u>		<u>Page</u>
I	Non-Reactive Spray Mixing Criteria for Hydraulically Stable Unlike Impinging Jets	14
II	Summary of Injector Elements and Test Conditions	30

## Appendix A

### LIST OF FIGURES

<u>Figure No.</u>		<u>Page</u>
1	Impingement Point Processes Impact Propellant Mixing	3
2	Space Shuttle/RCS Engine Injector	5
3	Space Shuttle/OMS Engine Injector	6
4	Rupe's Mixing Uniformity Criteria Defines Uniform Spray for Non-Reactive Impingement	8
5	Diameter Mismatch Produced "Banana" Shaped Mass and Mixture Ratio Distribution	10
6	Mixing Uniformity Criteria Defines Best Mixing Momentum Ratio	12
7	Momentum Ratio Imbalance Significantly Modifies Intra-element Mixing	15
8	Injector Stream Characteristics Depend on Orifice Configuration	17
9	Hydraulic Flip Modifies Pressure Drop and Stream Quality	18
10	Weber Number Model	21
11	Impingement Misalignment Causes Fan Rotation	23
12	Atomization Process Produces Periodic Ligament Shedding	25
13	Reactive Stream Impingement Inhibits Intra-Element Mixing	28
14	Reactive Stream Impingement with the F-O-F Triplet Element	31
15	Reactive Stream Impingement with the Sharp Edged Unlike Doublet	32
16	Reactive Stream Impingement with the Space Shuttle/OMS Unlike Doublet	33
17	Reactive Stream Impingement with the XDT Platelet Element	34
18	Reactive Stream Impingement with the Splashplate Element	35
19	Reactive Stream Impingement with the Space Shuttle/OMS TL0L Platelet Element	37
20	RSS Correlation for Coherent Stream Impingement Injector Elements	39
21	RSS Correlation for Atomized Spray Impingement Injector Elements	40

## Appendix A

### I. INTRODUCTION

The objective of this document is to present injector element design criteria that will aid an injector designer in understanding, avoiding, and coping with hypergolic propellants that result in Reactive Stream Separation (RSS) or reduced mixing of the oxidizer and fuel streams.

The liquid rocket engine combustion process is discussed at the outset to establish a frame of reference for the RSS design criteria. A discussion of non-reactive stream impingement phenomena is included to lay the ground work for understanding the influence of reactive stream phenomena on the impingement mixing process. This discussion is followed by a description of reactive stream phenomena illustrated with photographs. Data correlations are provided for coherent stream and atomized spray impingement injector element configurations which define regimes of reactive stream separation. Finally, reactive impingement design criteria are presented which enable the designer to predict regimes of RSS for his particular design and operating conditions.

The reactive impingement design criteria specified herein are applicable to the  $N_2O_4$  oxidizer and Amine fuels propellant combinations. The criteria are limited to elements with fuel orifice diameters of 0.030 inches or less. The following design and operating ranges are applicable:

Chamber Pressure	= 80 - 1000 psia
Fuel Velocity	= 25 - 200 ft/sec
Oxidizer Velocity	= 25 - 150 ft/sec
Fuel Temperature	= 50 - 300°F
Oxidizer Temperature	= 50 - 160°F

These criteria deal only with the optimization of the intra-element mixing processes. Other criteria required to achieve high performance, stability, and compatibility are not included.

## Appendix A

### II. LIQUID ROCKET COMBUSTION PROCESS

Liquid propellant rocket engine combustion represents a multi-faceted problem. It includes the following phenomenological processes as illustrated in Figure 1.

- ° Liquid stream injection
- ° Stream impingement and spray formation
- ° Propellant atomization
- ° Unlike propellant droplet mixing
- ° Droplet vaporization
- ° Vapor phase mixing
- ° Chemical reaction
- ° Combustion gas mixing
- ° Nozzle expansion

Engine performance is limited by the combustion and gas dynamic losses listed in Figure 1. The achievement of high performance requires that these performance losses be held to a minimum. It is generally recognized that the mixing loss associated with injector generated mixture ratio non-uniformities is the largest loss the injector designer has to deal with. The mass and mixture ratio uniformity which defines the mixing loss, is determined by the injector design and the impingement mixing process as illustrated in Figure 1. Therefore, the goal of any injector design is to produce uniform, stable, reproducible propellant mass and mixture ratio distributions. This goal is best achieved through an understanding of the physico-chemical mechanisms controlling the mixing process.

The injector promotes mixing through intra-element (within the element) and inter-element (element-to-element) mixing. Understanding the intra-element mixing process is key to injector design since pattern layout requires that the element distributions be known so that inter-element mixing can be optimized. Propellant distribution uniformity is

## Appendix A

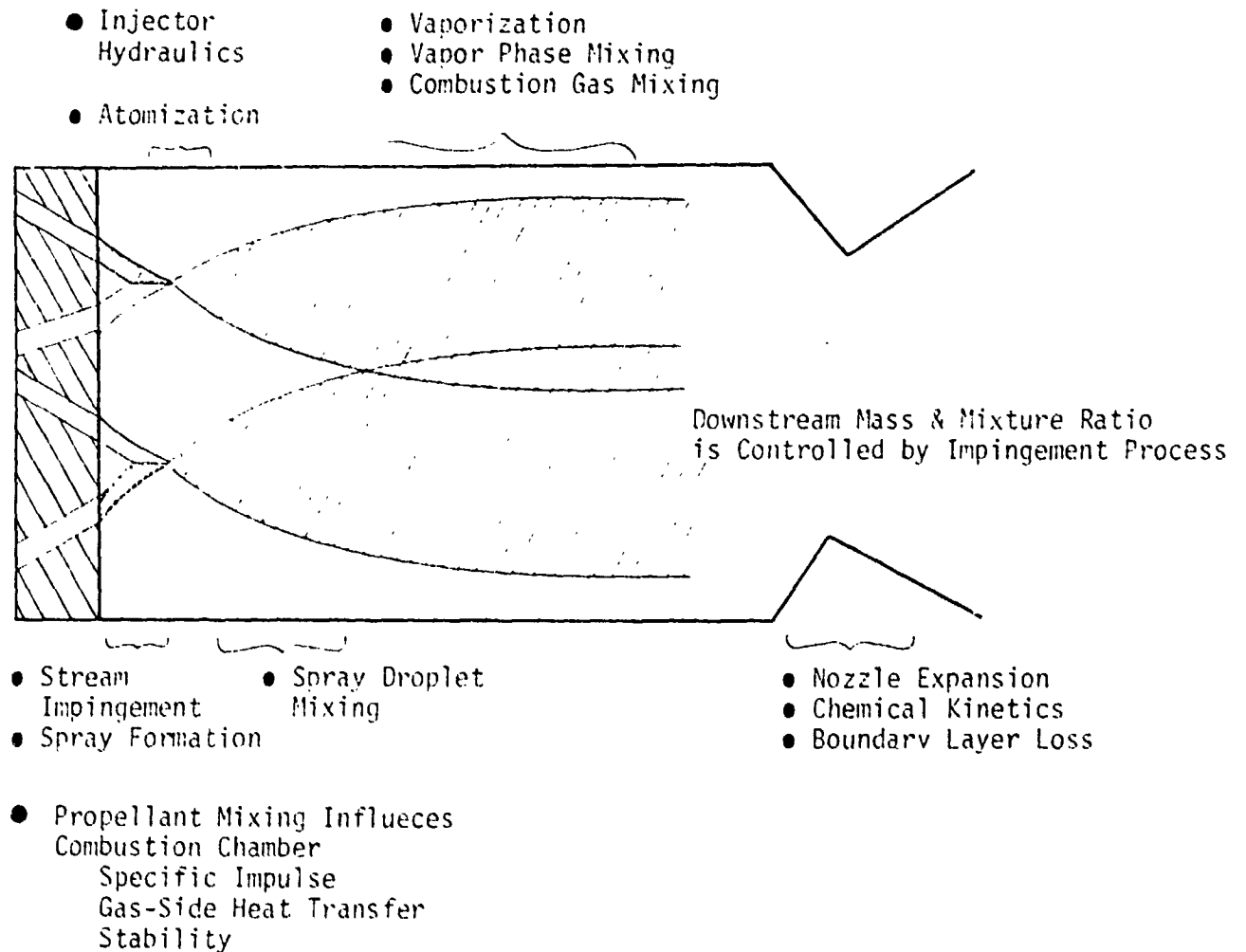


Figure 1. Impingement Point Processes Impact Propellant Mixing



## Appendix A

### II, Liquid Rocket Combustion Process (cont.)

achieved primarily through intra-element and inter-element liquid/droplet momentum exchange processes since downstream gas phase mixing is too slow to achieve the required mixing. Since impingement point spray mixing controls the spray mass and mixture ratio distributions, any injection or combustion process that inhibits or modifies the intra-element spray mixing process will impact performance, gas side heat transfer response and stability. Reactive Stream Separation (RSS) is a combustion related phenomena that exhibits this influence. However, there are also non-reactive related phenomena such as "hydraulic flip", momentum imbalance, and diameter mismatch that can impact the spray distributions which also need to be considered. Thus, high performance injector design criteria must include both reactive (hot fire) and non-reactive (cold flow) impingement phenomena effects upon the intra-element mixing process.

Intra-element mixing is generally achieved by momentum exchange through impingement of coherent streams or atomized sprays. Coherent streams are produced by drilled or electrical discharge machined (EDM) orifices. Atomized propellant sprays are produced by like impingement of coherent streams or by self-atomization using splash plates or platelet injector elements. Platelet injectors are fabricated by bonding together a stack of thin metal sheets which have etched flow passages. The Space Shuttle/RCS (SS/RCS) Engine injector shown in Figure 2 is an example of a coherent stream impingement injector element. Whereas the Space Shuttle/OMS (SS/OMS) Engine injector shown in Figure 3 is an example of the atomized spray impingement type of injector. Non-reactive and reactive impingement processes are discussed for both class of injectors.

# Appendix A

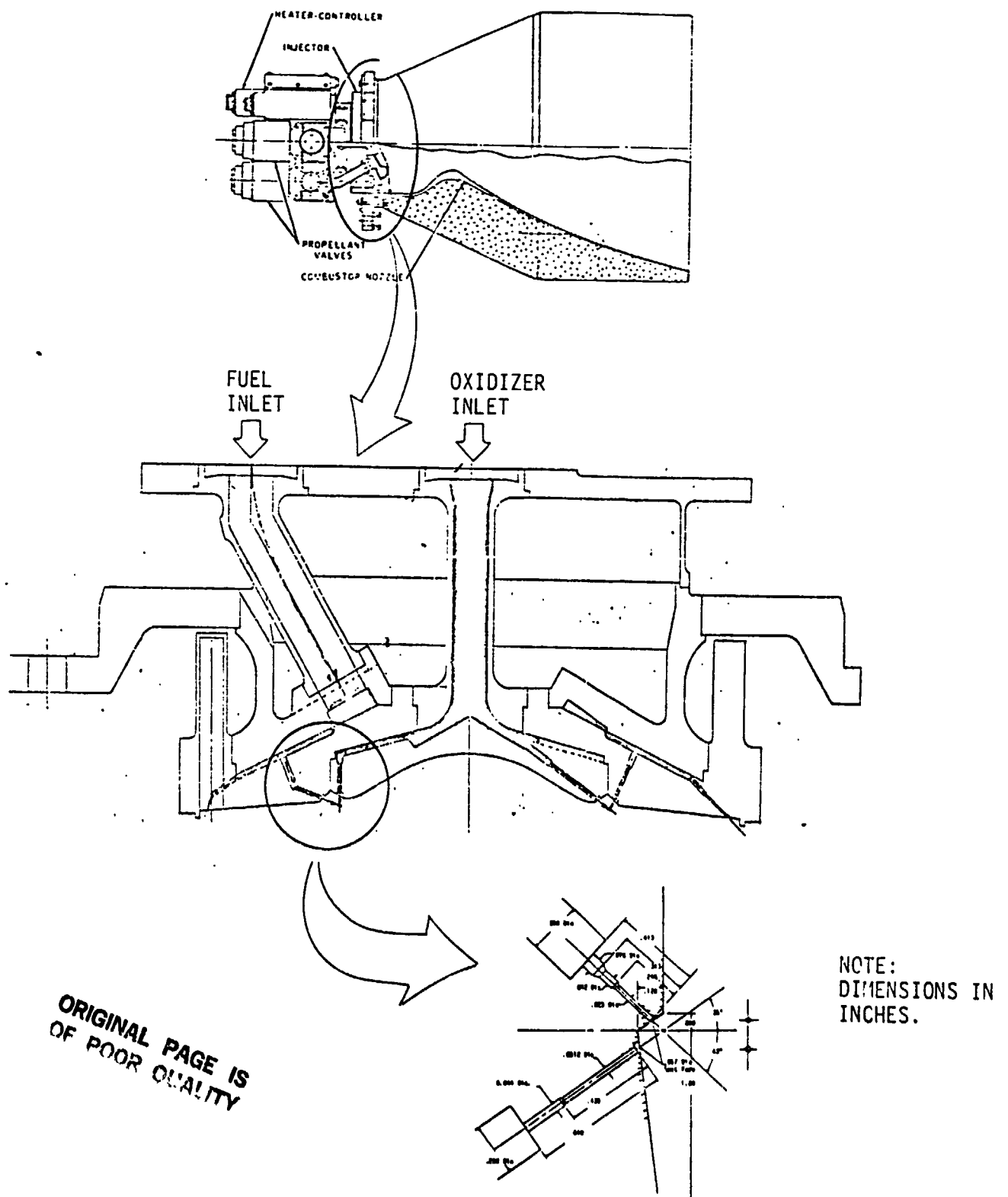


Figure 2. Space Shuttle/RCS Engine Injector

# Appendix A

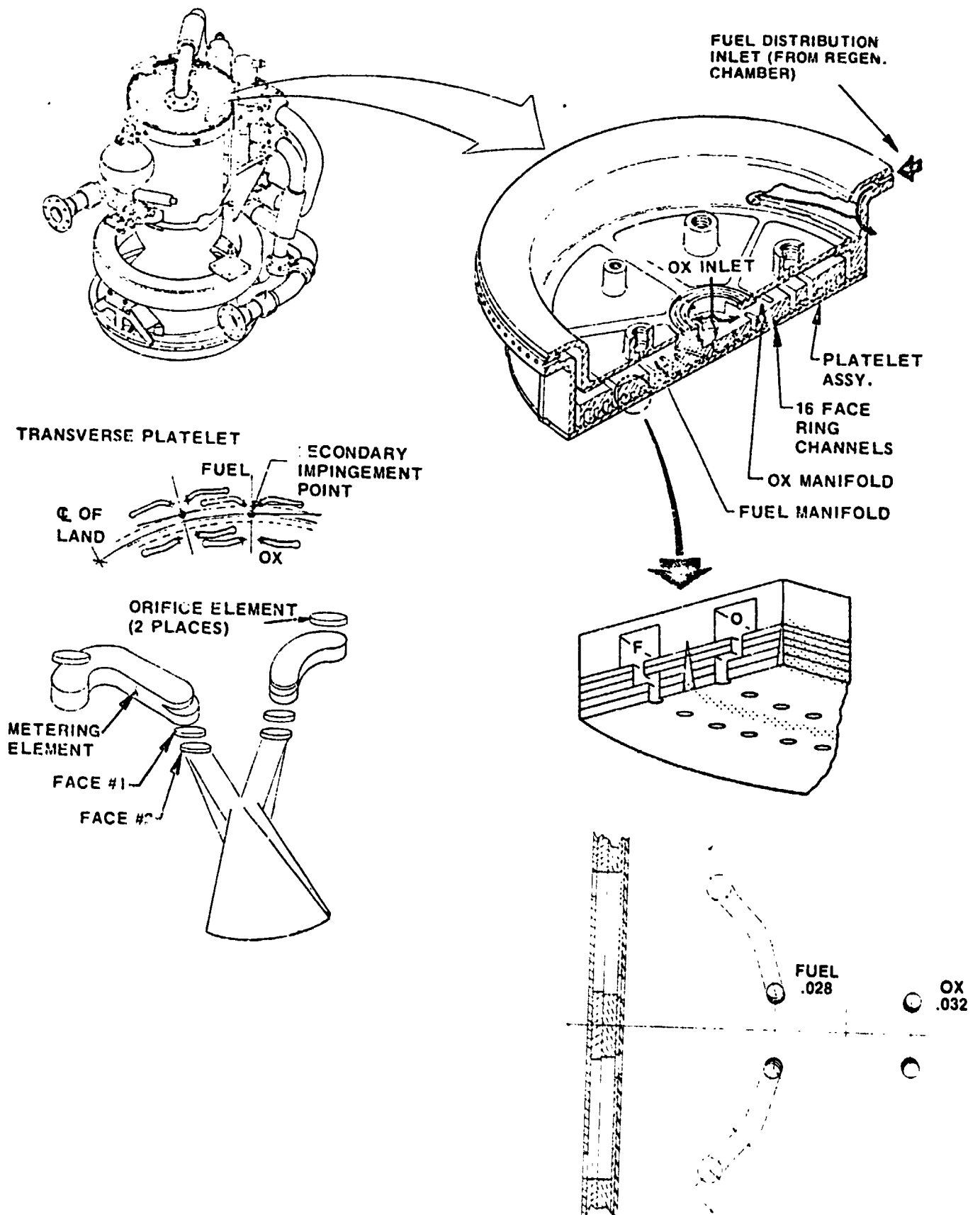


Figure 3. Space Shuttle/OMS Engine Injector

## Appendix A

### III. NON-REACTIVE STREAM IMPINGEMENT PHENOMENA

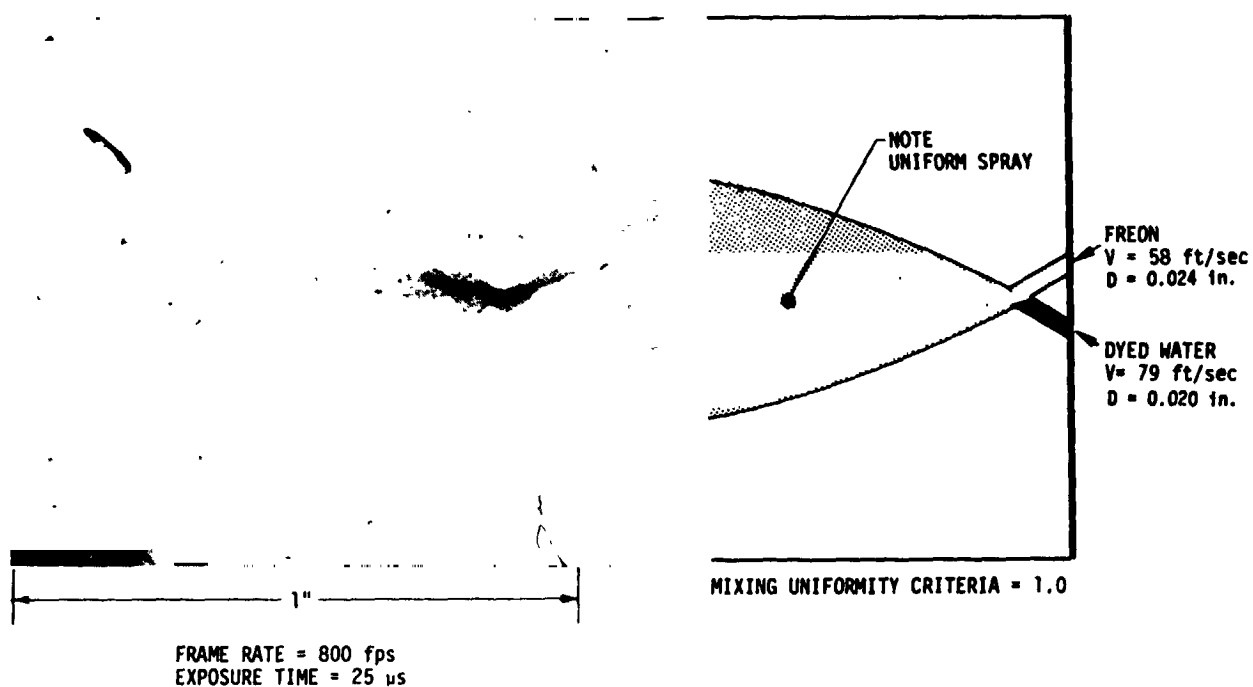
Non-reactive stream impingement phenomena which can effect spray distribution with coherent stream impingement include, "hydraulic flip", momentum imbalance, diameter mismatch and stream quality. The impingement phenomena observed with sprays depends on the method used to produce the sprays. For example, sprays produced by self-impingement of coherent jets are susceptible to the same processes as the coherent streams. Whereas, sprays produced by impingement with surfaces generally are not subject to "hydraulic flip" since these streams generally are made to flow detached. These non-reactive phenomena are discussed in detail for each class of injector below.

#### A. COHERENT STREAM IMPINGEMENT

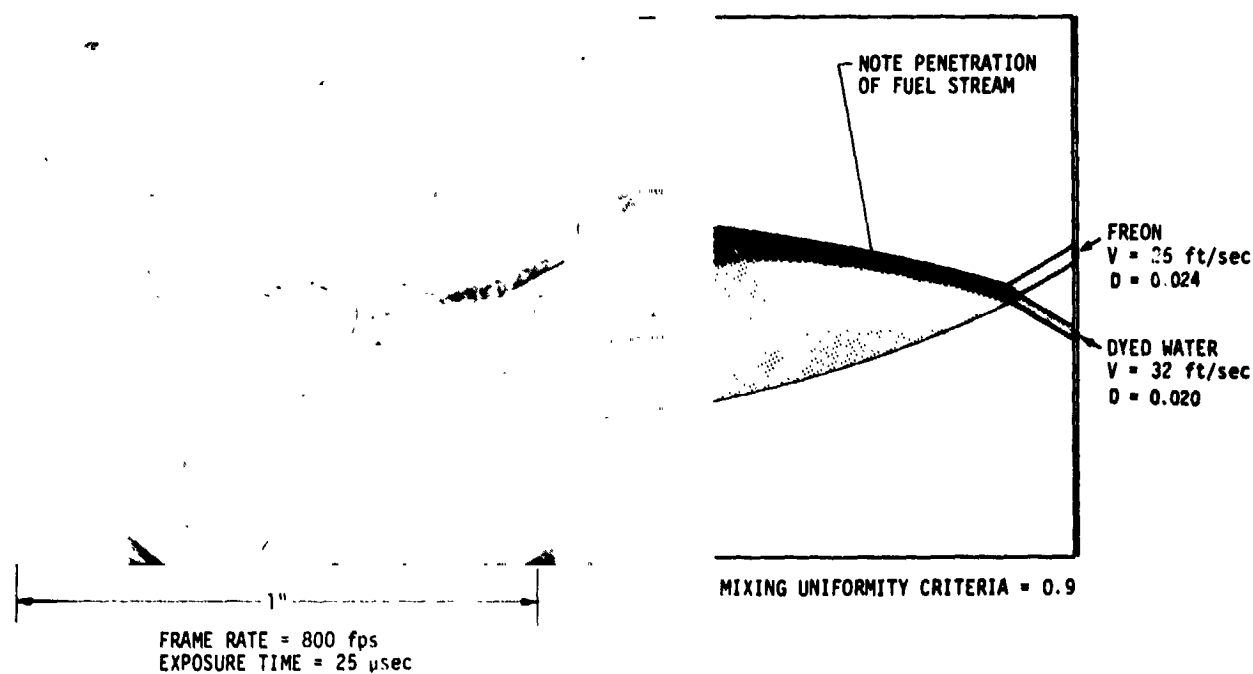
The preponderance of operational hypergolic propellant engines use coherent stream impingement to produce intra-element mixing. Rupe and his co-workers (Ref. 1, 2 and 3) were the first to recognize the importance of intra-element mixing upon injector performance. They expended considerable effort to develop empirical spray mass and mixture ratio distribution correlations based on cold flow data for engine design application. Rupe recognized early in these investigations that hydraulic stability is essential to efficient mixing. Rupe's work is the most definitive and widely used non-reactive injector design criteria.

The non-reactive coherent stream impingement mixing process is illustrated in the photographs of Figure 4. These photographs are enlargements of single frames taken from 16 mm high speed movie film. The injector is a rounded inlet unlike doublet used on the  $\text{H}_2\text{O}_4$ /Amine Fuels Program (NAS 9-14186). The propellant simulants are dyed water (the blue stream) for fuel and freon (the clear stream) for oxidizer. Rupe's mixing uniformity criteria is equal to 1.0 for optimum mixing. The spray uniformity

## Appendix A



- a. Rupe's Mixing Uniformity Criteria Defines Uniform Spray for Non-reactive Impingement



- b. Low Stream Momentum Produces Penetration Phenomena for Non-reactive Impingement

Figure 4. Rupe's Mixing Uniformity Criteria Defines Uniform Spray for Non-Reactive Impingement

## Appendix A

### III, A, Coherent Stream Impingement (cont.)

attained at the optimum stream momentum ratio condition, in the absence of combustion, is clearly evident in the upper photograph. The propellant "shoot-through" (i.e., penetration) phenomena reported by Rupe is also observed with lower stream momentums as shown in the lower photograph of Figure 4.

Non-reactive phenomena which can alter this spray uniformity are:

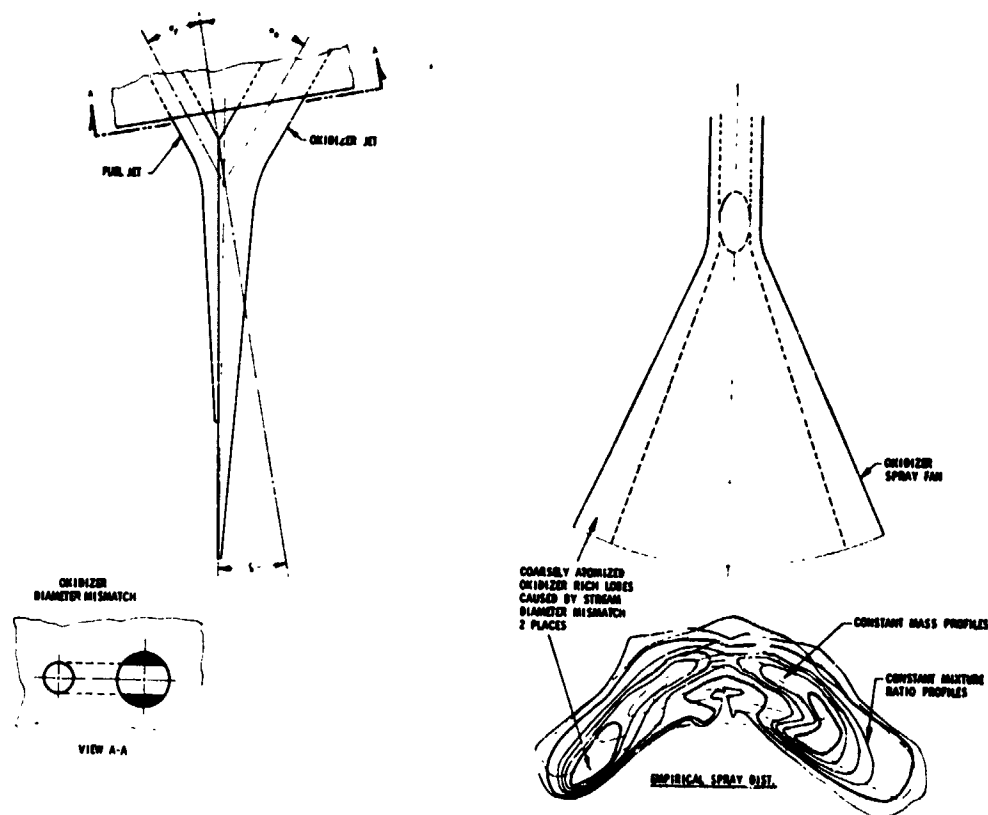
1. Fuel/Oxidizer Diameter Mismatch
2. Fuel/Oxidizer Momentum Imbalance
3. Stream Instability
4. Stream Quality
5. Impingement Misalignment

Each of these phenomena must be considered in designing coherent stream injectors.

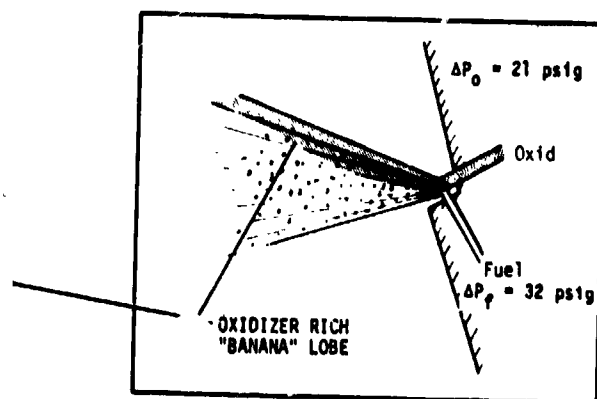
#### 1. Fuel/Oxidizer Diameter Mismatch

Rupe placed most of his emphasis upon investigating the unlike doublet element to characterize element mixing efficiencies. He found that equal fuel and oxidizer injection momentums and equal orifice diameters are required to maximize unlike doublet mixing efficiencies. However, the only commonly used propellant combination which satisfies both criteria is  $N_2O_4/N_2H_4$ . In most cases, the oxidizer injection momentum exceeds that of the fuel causing the oxidizer orifice diameter to be larger than that of the fuel. A slight diameter mismatch results in under penetration of the fuel jet into the higher momentum oxidizer stream causing reduced mixing efficiencies. Large diameter mismatches result in skewed spray distributions as illustrated in Figure 5.

## Appendix A



a. Measured Spray Distribution



b. Visual Evidence of Diameter Mismatch Effect

Figure 5. Diameter Mismatch Produced "Banana" Shaped Mass and Mixture Ratio Distribution

## Appendix A

### III, A, Coherent Stream Impingement (cont.)

Figure 5a displays the results of an experimentally measured spray distribution obtained with unequal diameter circular unlike doublet orifices using non-reactive propellant simulants. The large orifice diameter mismatch produces a "banana" shaped spray distribution which results in two poorly atomized, poorly mixed, oxidizer rich lobes emanating from the misimpingement cross section caused by the diameter mismatch. The diameter mismatch phenomena is further illustrated in Figure 5b. This stroboscopic still photo was taken of cold flow tests of a single element injector which simulates the Space Shuttle/RCS engine unlike doublet. The propellant simulants are water for fuel and oxidizer.

The problem of diameter mismatch can be alleviated either through the use of EDM'ed rectangular orifices (Ref. 4) or through the use of multiple orifice impingement elements such as the triplet or pentad. EDM'ed unlike doublets with rectangular cross section can be selected with equal element widths to eliminate jet diameter mismatch effects normally associated with circular orifice injectors. This non-circular orifice capability permits a greater degree of freedom in designing impinging coherent stream injectors. It is especially beneficial for those propellant combinations which normally operate at oxidizer to fuel mixture ratios, momentum ratios, and orifice area ratios between 1.0 to 2.0. This includes the important storable propellant combinations of  $N_2O_4/MMH$  and  $N_2O_4/A-50$  used on many current engines.

#### 2. Fuel/Oxidizer Momentum Imbalance

Rupe performed extensive studies to define the influence of stream momentum on the spray distribution uniformity. The results are shown in Figure 6 for several unlike doublet elements. The spray uniformity drops off as the momentum balance moves to either side of the optimum value.



# Appendix A

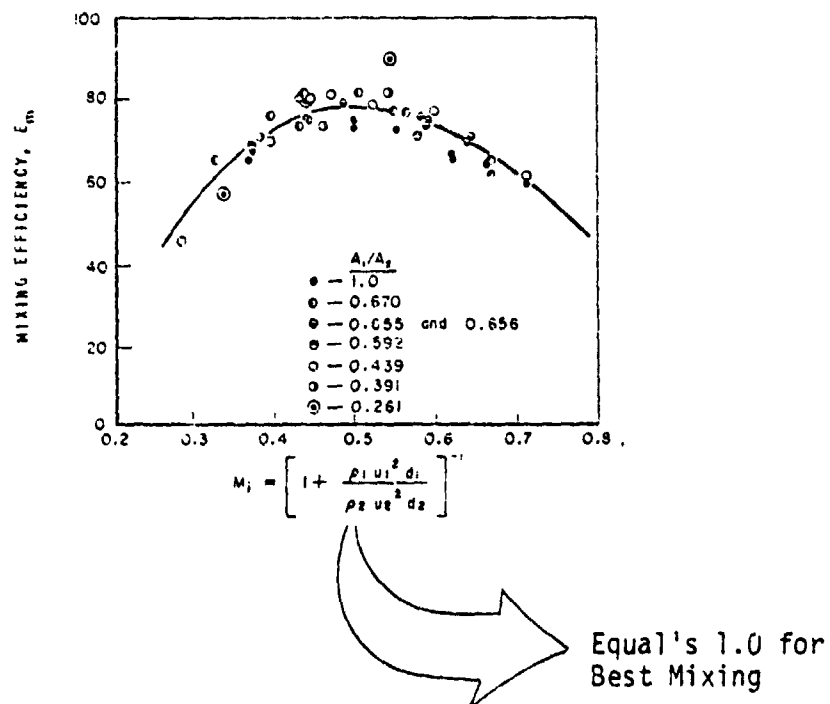


Figure 6. Mixing Uniformity Criteria Defines Best Mixing Momentum Ratio

## Appendix A

### III, A, Coherent Stream Impingement (cont.)

On the basis of these data, Rupe developed a spray mixing uniformity criteria for unlike impinging doublet propellant streams. The mixing uniformity criteria (Ref. 2) states that optimum spray mixing occurs when the product of the ratios of the velocity heads and stream diameters is equal to unity:

$$\rho_{ox} V_{ox}^2 D_{ox} / \rho_f V_f^2 D_f = 1.0 \quad \text{Equation (1)}$$

Similar mixing correlations were developed by Elverum and Morey (Ref. 3) for other types of impinging injector elements using Rupe's cold flow measurement techniques. These correlations are summarized in Table I for unlike jet impingement elements.

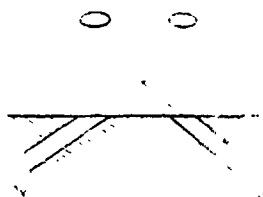
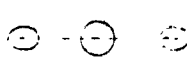
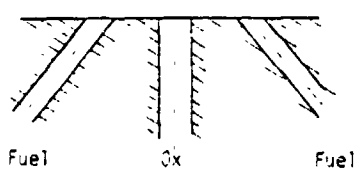
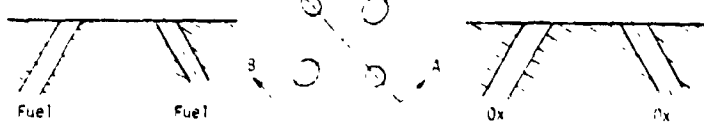
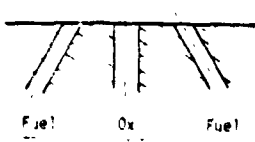
Operation at an oxidizer rich off-momentum conditions is illustrated in Figure 7 for the SS/RCS unlike doublet element. The resultant spray momentum angle is drastically changed in addition to modifying the intra-element mixing. Changes in spray momentum angle can seriously impact chamber gas-side heat transfer response and combustion stability. The sensitivity of spray momentum angle to momentum balance can be alleviated through the use of multiple impingement elements such as the triplet or pentad.

The fuel rich off-momentum condition is also illustrated in Figure 7 for the SS/RCS unlike doublet. The low oxidizer momentum and diameter mismatch cause the oxidizer stream to "umbrella" around the fuel stream resulting in poor mixing. These effects coupled with RSS can result in undesirable performance, stability, and compatibility variability over the engine operating range.

# Appendix A

## TABLE I

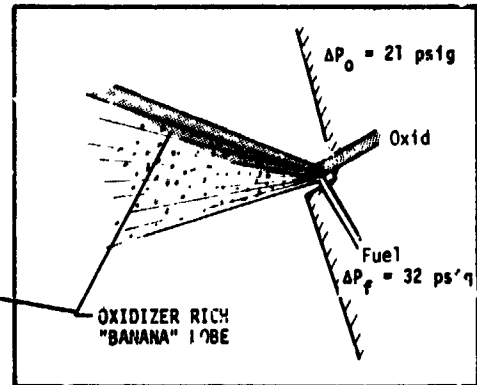
NON-REACTIVE SPRAY MIXING CRITERIA FOR HYDRAULICALLY  
STABLE UNLIKE IMPINGING JETS

ELEMENT NAME	DESIGN CHARACTERISTICS	MIXING OPTIMIZATION DESIGN CRITERION
Unlike Doublet (One-on-One)		$\left( \frac{\dot{W}_{ox}}{\dot{W}_f} \right) \times \left( \frac{V_{ox}}{V_f} \right) = \frac{D_{ox}}{D_f}$
Inline Triplet (Two-on-One)	 	$\left( \frac{\dot{W}_f}{\dot{W}_{ox}} \right)^2 \frac{P_{ox}}{P_f} \left( \frac{A_{ox}}{2 A_f} \right)^{1.75} = .66$ ( $2\theta_f = 60$ degrees) or $\frac{P_f V_f^2}{P_{ox} V_{ox}^2} \left( \frac{2 A_f}{A_{ox}} \right)^{0.25} = .42$ ( $2\theta_f = 90$ degrees)
Trans Quadlet (Two-on-Two)	 A-A B-B	Same as Unlike Doublet, or $\left( \frac{\dot{W}_{ox}}{\dot{W}_f} \right)^2 \frac{P_f}{P_{ox}} \left( \frac{D_f}{D_{ox}} \right)^3 = 1.0$
Pentad (Four-on-One)	 A-A	$\left( \frac{\dot{W}_f}{\dot{W}_{ox}} \right)^2 \frac{P_{ox}}{P_f} \left( \frac{A_{ox}}{4 A_f} \right)^{1.25} = 2.75$

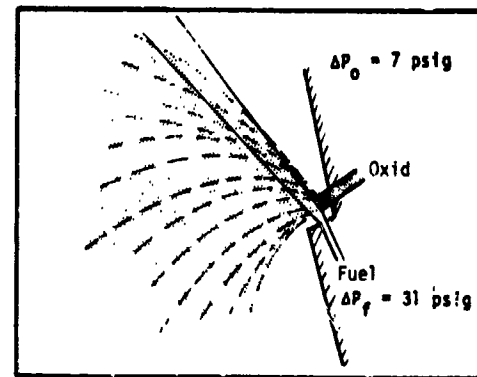
Correlations  
from Ref. (3)

$\dot{W}_f$  = Fuel Flowrate (lb/sec)  
 $\dot{W}_{ox}$  = Oxidizer Flowrate (lb/sec)  
 $\rho_f$  = Fuel Density (lb/ft<sup>3</sup>)  
 $\rho_{ox}$  = Oxidizer Density (lb/ft<sup>3</sup>)  
 $A_f$  = Fuel Orifice area (in.<sup>2</sup>)  
 $A_{ox}$  = Oxidizer Orifice Area (in.<sup>2</sup>)

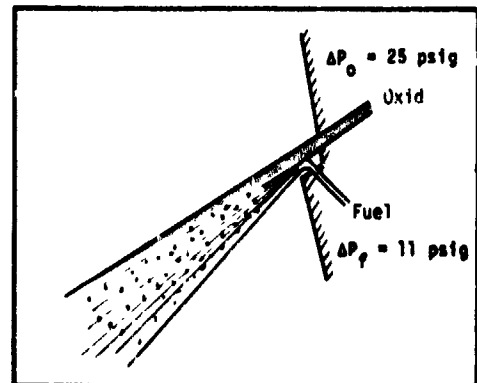
## Appendix A



a. Orifice Diameter Mismatch Produces Non-Uniform Spray



b. Fuel Rich Momentum Condition Causes Oxidizer Stream to "Umbrella" Around Fuel Stream



c. Oxidizer Rich Momentum Condition Produces Good Mixing

Figure 7. Momentum Ratio Imbalance Significantly Modifies Intra-element Mixing

## Appendix A

### III, A, Coherent Stream Impingement (cont.)

#### 3. Stream Stability

Rupe stresses the importance of stream stability throughout his work. Stream stability is controlled primarily by the orifice geometry. The orifice configurations that are most commonly used in rocket injectors are illustrated in Figure 8. The features of each are as follows: (a) represents the conventional sharp edged orifice, (b) is a rounded or contour approach orifice, (c) is a higher L/D, square-edged orifice, which produced a cylindrical jet as in (a) and (b), while (d) is that same orifice where the jet has reattached to the orifice wall, and (e) is the same as (d) but with a longer L/D.

For the sharp-edged orifice flow conditions of (a) and (c) the discharge coefficient  $C_d$  lies between 0.6 and 0.7. In (d), the flow reattaches to the wall allowing the orifice to flow "full". The result is agitated and divergent flow at the exit (bush or broomy flow), and the discharge coefficient rises to between 0.8 and 0.85. The bushy flow disappears as the orifice length is increased as in (e). A still higher  $C_d$  ( $\approx 0.97$ ) is achieved with (b) when the contour is not too abrupt and L/D is small (0.25 to 0.5). For the best designs  $C_d = 0.99$ , while with poor curvature and high manifold cross velocities the discharge coefficient may be as low as 0.90.

Early rocket injector designs were dominated by the configuration exemplified by (c) and (d) and hence are characterized by the flow properties just described. The transition between flow condition (c) and (d) is known as "hydraulic flip" and is sensitive to chamber pressure, orifice length/diameter ratio, orifice entrance configuration, and the fluid properties. The "hydraulic flip" is accompanied by a change in pressure drop as illustrated in Figure 9 and a change in stream quality from

## Appendix A

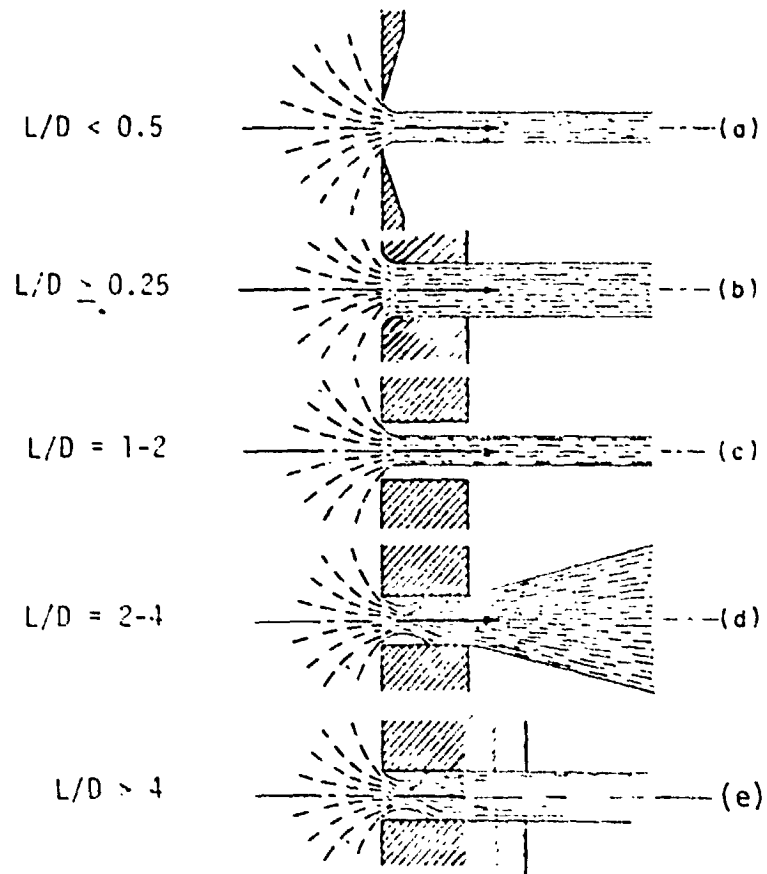


Figure 8. Injector Stream Characteristics Depend on Orifice Configuration

# Appendix A

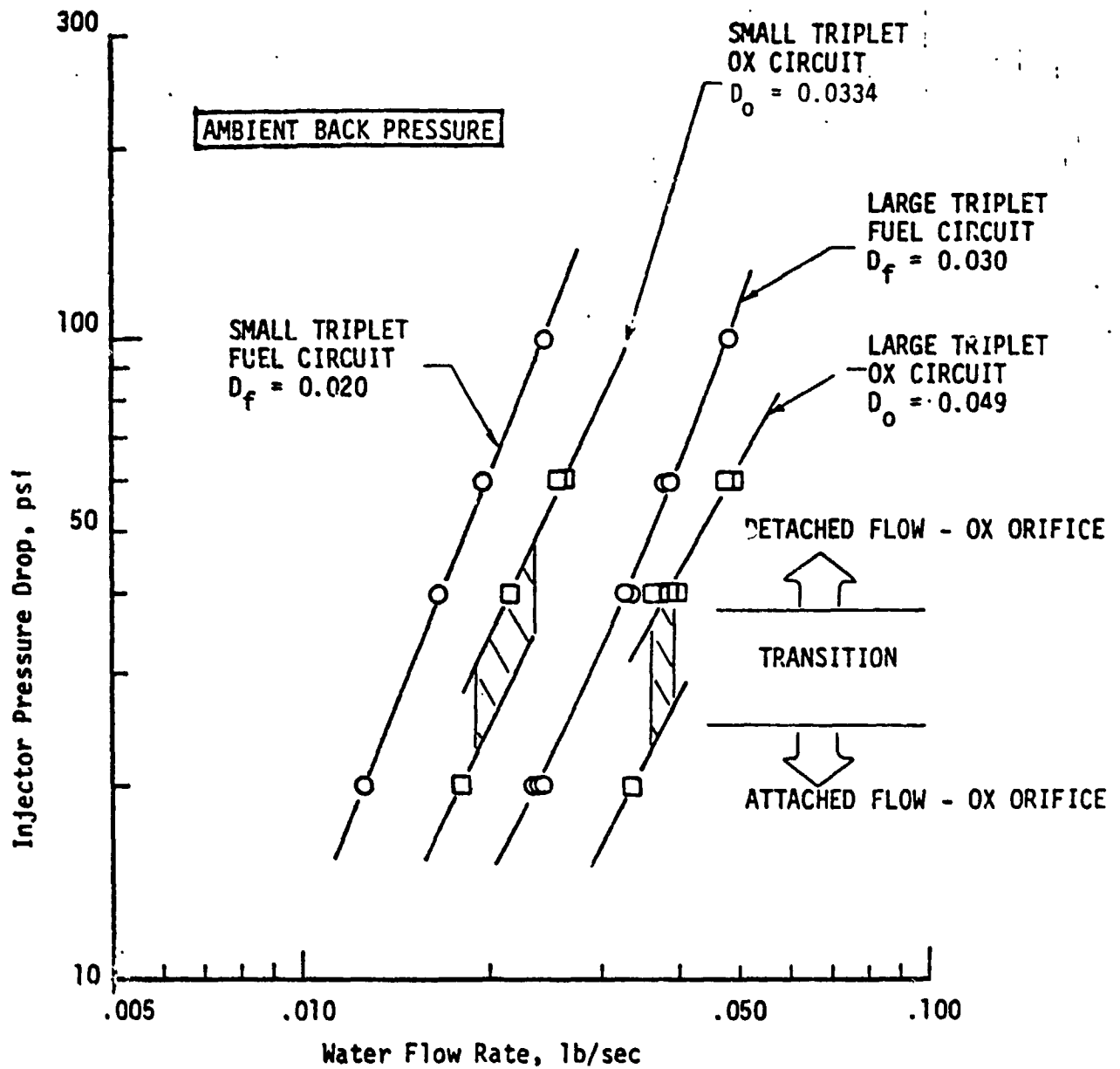


Figure 9. Hydraulic Flip Modifies Pressure Drop and Stream Quality

## Appendix A

### III, A, Coherent Stream Impingement (cont.)

coherent to bushy streams which impacts the spray mixing. Reference 5 describes the phenomenon of hydraulic flip in detail which occurs due to abrupt transitions between attached and detached flow in sharp edge orifices caused by either fluid cavitation or insufficient L/D. Stable, predictable orifice discharge coefficients free of hydraulic flip are necessary not only to obtain predictable orifice pressure drop and desired injection momentum ratios, but also to obtain maximum cold flow mixing efficiency.

Contoured inlet orifices provide the most stable and optimum injection mass distribution, however, the orifice inlets are frequently inaccessible for contouring and the designer has little or no choice other than to use sharp edge inlet orifices. Although orifice L/D ratios  $\geq 2:1$  usually flow attached for most applications, jet directional flow control is often poor. Combinations of high manifold cross velocity, low orifice static pressure drop and nonperpendicular orifice orientation to the manifold backside surface cause angular deviations between the injected stream and orifice axis unless the sharp edge orifice L/D  $\geq 4:1$ . Unless unlike jet impingement occurs right at the surface of the injector face, directional flow control is an important consideration for assuring desired impingement characteristics. Directional flow control becomes increasingly critical for coherent jets as the distance from the orifice exit to the unlike impingement point increases.

With the advent of EDM, most modern injector designs are exemplified by configuration (e) which generally provide stable well defined streams.



## Appendix A

### III, A, Coherent Stream Impingement (cont.)

#### 4. Stream Quality

A stream's quality is defined by its velocity profile and degree of pre-atomization. A high quality stream is one having a nearly uniform velocity profile and a coherent non-bushy appearance. Rupe's work (Refs. 1 and 2) shows that the intra-element mixing efficiency and reproducibility are highly dependent on stream quality. The stream velocity profile is determined primarily by the orifice configuration (Ref. 4) whereas bushiness or preatomization is influenced by both the orifice configuration and the fluid velocity.

The contoured inlet orifices and long L/D ( $\sim 100$ ) orifices such as those used by Rupe produce nearly flat velocity profiles and are required for maximum intra-element mixing efficiency. The velocity profile reflects the fraction of the fluid contained within the velocity boundary layer relative to the potential flow core. For contoured orifice inlets and/or long L/D orifices such as those used by Rupe, the mass in the boundary layer is very small and jet shedding is minimized. Likewise short L/D sharp edge orifices which flow detached from the vena contracta to the exit likewise have low mass in the velocity boundary layer and exhibit minimal shedding. A more detailed description of inlet contraction coefficient effects, Reynolds number and L/D effects upon exit velocity profile, static pressure recovery efficiency and element discharge coefficient is given in Reference 5.

The mechanism of droplet shedding from the jet surface prior to impingement is shown schematically in Figure 10. This pre-impingement shedding is caused by shear forces induced within the jet boundary layer. The onset of pre-impingement aerodynamic atomization is modeled through the Weber Number which is a function of the injection

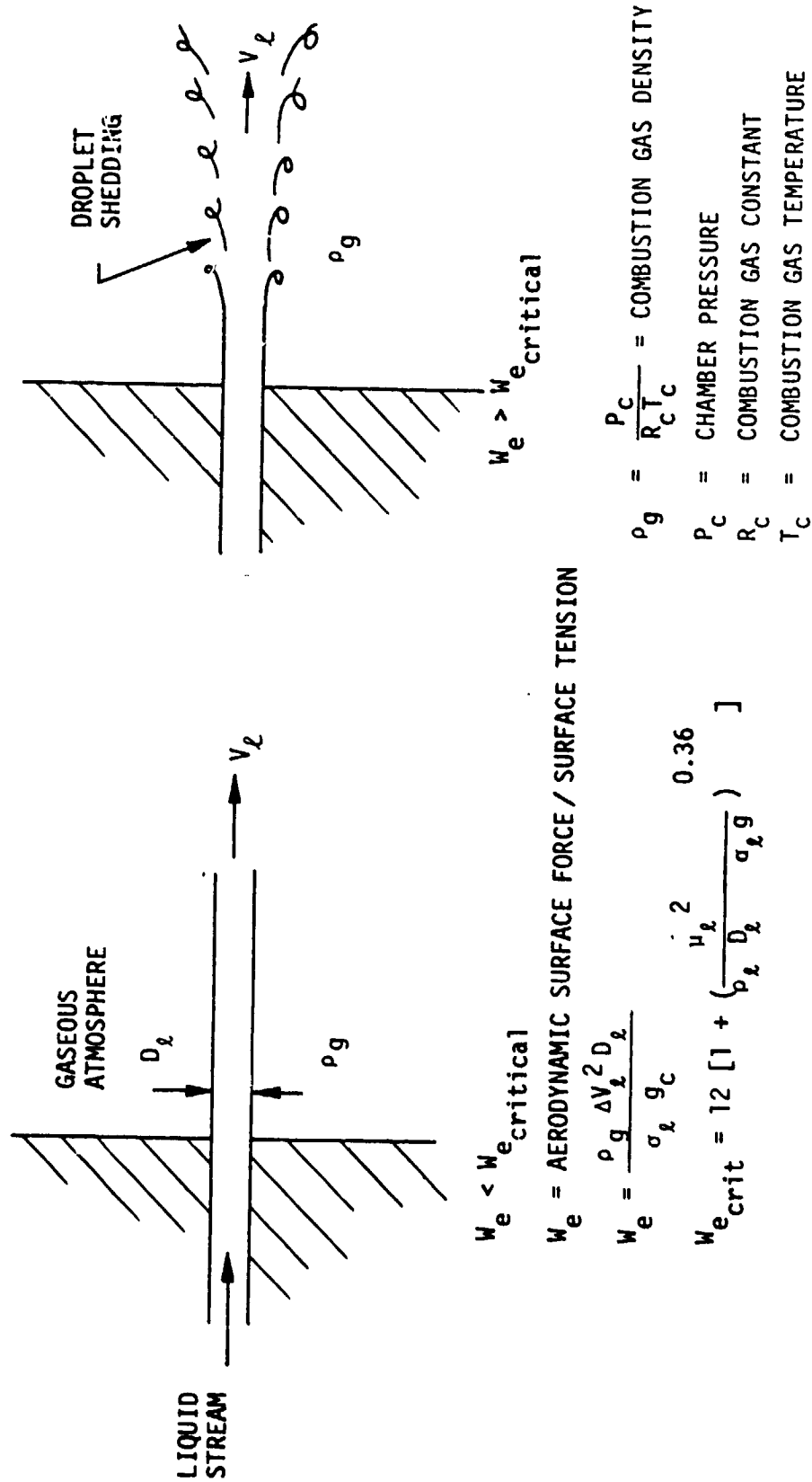


Figure 10. Weber Number Model

## Appendix A

### III, A, Coherent Stream Impingement (cont.)

velocity, chamber pressure, and fuel surface tension. The Weber Number is the ratio of aerodynamic shear forces to surface tension forces as defined in Equation (2):

$$WEF = [\rho_g V_f^2 D_f] / \sigma_f \quad \text{Equation (2)}$$

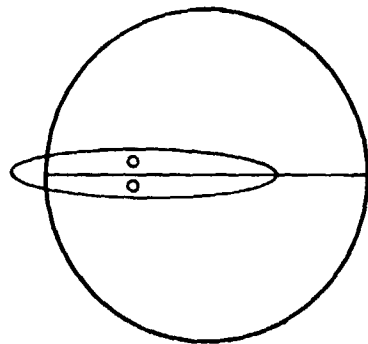
Thus the Weber Number (WEF) is a function of the propellant, through the surface tension ( $\sigma_f$ ), the chamber pressure through the gas density term ( $\rho_g$ ), and the injection process through the stream diameter ( $D_f$ ) and the injection velocity ( $V_f$ ).

A critical Weber Number exists above which the aerodynamic forces exceed the surface tension force resulting in stream shedding and atomization. Therefore, the interfacial surface area of streams operating above the critical Weber Number are greater than that of streams operating below the critical Weber Number. The increase in pre-impingement atomization promotes Reactive Stream Separation because RSS is vaporization controlled and vaporization rate increases as the stream surface area to volume ratio increases. This surface area increase will also affect the momentum exchange process.

#### 5. Impingement Misalignment

Impingement misalignment can cause gross changes in the intra-element mixing as reported by Rupe and co-workers. In addition to the changes in intra-element mixing, inter-element mixing is impacted due to rotation of the spray about the spray axis. An example of the impact of impingement misalignment on the resultant spray is illustrated in Figure 11. This is a stroboscopic photo of the resultant spray from a simulated JS/RCS unlike doublet which was intentionally misaligned by offsetting the orifices by 0.003 inches. The resultant fan rotation and spray nonuniformity are evident, indicating that impingement misalignment should be avoided.

# Appendix A

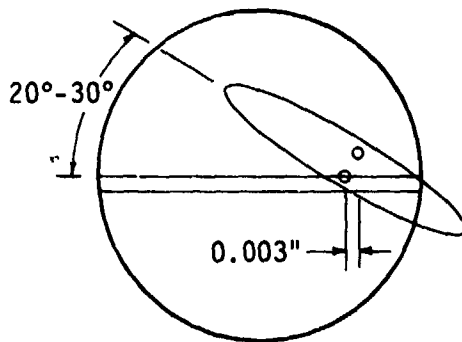


END VIEW

SIDE VIEW

## a. NORMAL IMPINGEMENT

$\Delta P_{ox}$	= 21 PSIG
$\Delta P_f$	= 32 PSIG



END VIEW

SIDE VIEW

## b. OFFSET IMPINGEMENT

Figure 11. Impingement Misalignment Causes Fan Rotation

## Appendix A

### III, A, Coherent Stream Impingement (cont.)

#### 6. Ligament Shedding

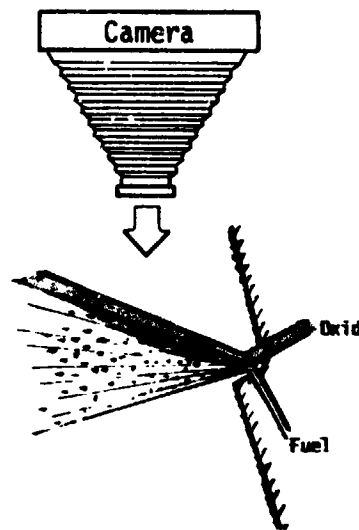
Periodic ligament formation and shedding is another cold flow phenomena which also shows up in hot fire testing. The process of ligament formation and shedding is as follows. The ligaments begin to form downstream of the propellant impingement point where the liquid stream begins to spread into a thin sheet. As these ligaments become increasingly large, surface tension forces are overcome causing the ligament to break off and form droplets. Aerodynamic and inertial forces contribute to this atomization process and further the breakdown of the ligaments into fine droplets.

The periodic ligament shedding is clearly visible in still photographs and in the hot fire movies. They appear as semi-circular waves emitting from the impingement point when viewed as shown in Figure 12. The same ligament shedding frequencies are observed in hot fire testing as in cold flow indicating that they are a consequence of the non-reactive atomization process. The atomization frequency is generally proportional to the injection velocity. The atomization rate is an important factor in determining the first longitudinal stability.

#### B. ATOMIZED SPRAY IMPINGEMENT

Spray impingement to produce intra-element mixing is accomplished by impingement of unlike atomized spray fans produced by like impingement of coherent streams, by solid wall impingement (splash plate elements) or by internally impinged streams with platelet injectors. Prior to the development of the platelet concept the most commonly used atomized spray impingement element was the like-on-like element whose fuel and oxidizer spray fans are radially aligned and canted toward each other.

## Appendix A



ORIGINAL PAGE IS  
OF POOR QUALITY

Injector = Space Shuttle/RCS Unlike Doublet  
Propellant Simulants = Water  
 $\Delta P_o = 21 \text{ psi}$   
 $\Delta P_f = 32 \text{ psi}$   
 $D_o = 0.031 \text{ in.}$   
 $D_f = 0.023 \text{ in.}$

Figure 12. Atomization Process Produces Periodic Ligament Shedding

## Appendix A

### III, 8, Atomized Spray Impingement (cont.)

A multitude of atomized spray impingement platelet elements have been designed and tested at ALRC in recent years. These elements offer certain advantages in terms of improved producibility. Functionally, their spray characteristics are similar to any other impinging spray injector. They produce consistent spray characteristics, predictable atomization efficiency, and consistent mixing characteristics.

The non-reactive impingement mixing characteristics of the atomized spray impingement elements are much the same as the coherent stream elements. Stable orifice flow must be provided to obtain optimum mixing and the Rupe mixing criteria appears to be applicable.

Spray impingement elements offer two major advantages over the coherent stream impingement type of elements: (1) alignment between the oxidizer and fuel orifices is not as critical as with coherent streams since wide spray fans are impinged compared to narrow streams; and (2) the spray resultant momentum angle is not as sensitive to momentum imbalance as with coherent stream impingement.

The principle disadvantages to the spray impingement element is that the pre-atomization enhances RSS. Another disadvantage is they are inherently more difficult to fabricate because of increased number of orifices and compound injection angles. However, this factor can be beneficial for engines that must operate over wide  $P_c/MR$  ranges since it permits operation within the separated RSS regime over the engine entire operating range. Element overlap is used to avoid performance losses due to RSS.

## Appendix A

### IV. REACTIVE STREAM IMPINGEMENT PHENOMENA

Reactive stream impingement can result in Reactive Stream Separation (RSS) which inhibits intra-element momentum mixing. RSS is a consequence of vigorous reaction within the impingement interface which produces combustion gases in sufficient quantities to inhibit liquid stream momentum exchange. The effect of RSS on spray mixing is illustrated in the photographs of Figure 13. Four modes of reactive stream impingement are identified. The first photo in the sequence illustrates the "mix/penetrate" mode which is also observed with non-reactive impingement. The "mix/penetrate" mode is characterized by a uniform spray field with some propellant penetration as evidenced by an oxidizer rich zone opposite the oxidizer stream in the downstream spray. "Penetration" occurs at low injection velocity, (less than 50 ft/sec) low fuel temperatures, (below 70°F) and low chamber pressure (less than 100 psia) and is evidenced by "shot-through" of the fuel and oxidizer. Penetration has been reported in earlier cold flow work and was also observed on this program using propellant simulants as well as reactive streams. Penetration is a consequence of the non-reactive momentum exchange mixing process.

The second photo shows the condition of uniform mixing without evidence of RSS. "Mixing" is observed at moderate injection velocities, (50-100 ft/sec) moderate fuel temperatures, (70-90°F) and moderate chamber pressures (100-200 psia). It is evidenced by a highly uniform spray field which looks similar to a non-reactive spray field. The third photo illustrates the "Mix/Separate" mode which occurs at the onset of RSS. It is evidenced by a slightly non-uniform spray field. The fourth photo shows a condition of highly separated streams (RSS). "Separation" is observed at higher injection velocities (greater than 100 ft/sec), higher fuel temperature, and higher chamber pressures (greater than 200 psia). It is evidenced by highly non-uniform spray fields in which distinct regions of unmixed fuel and oxidizer exist.



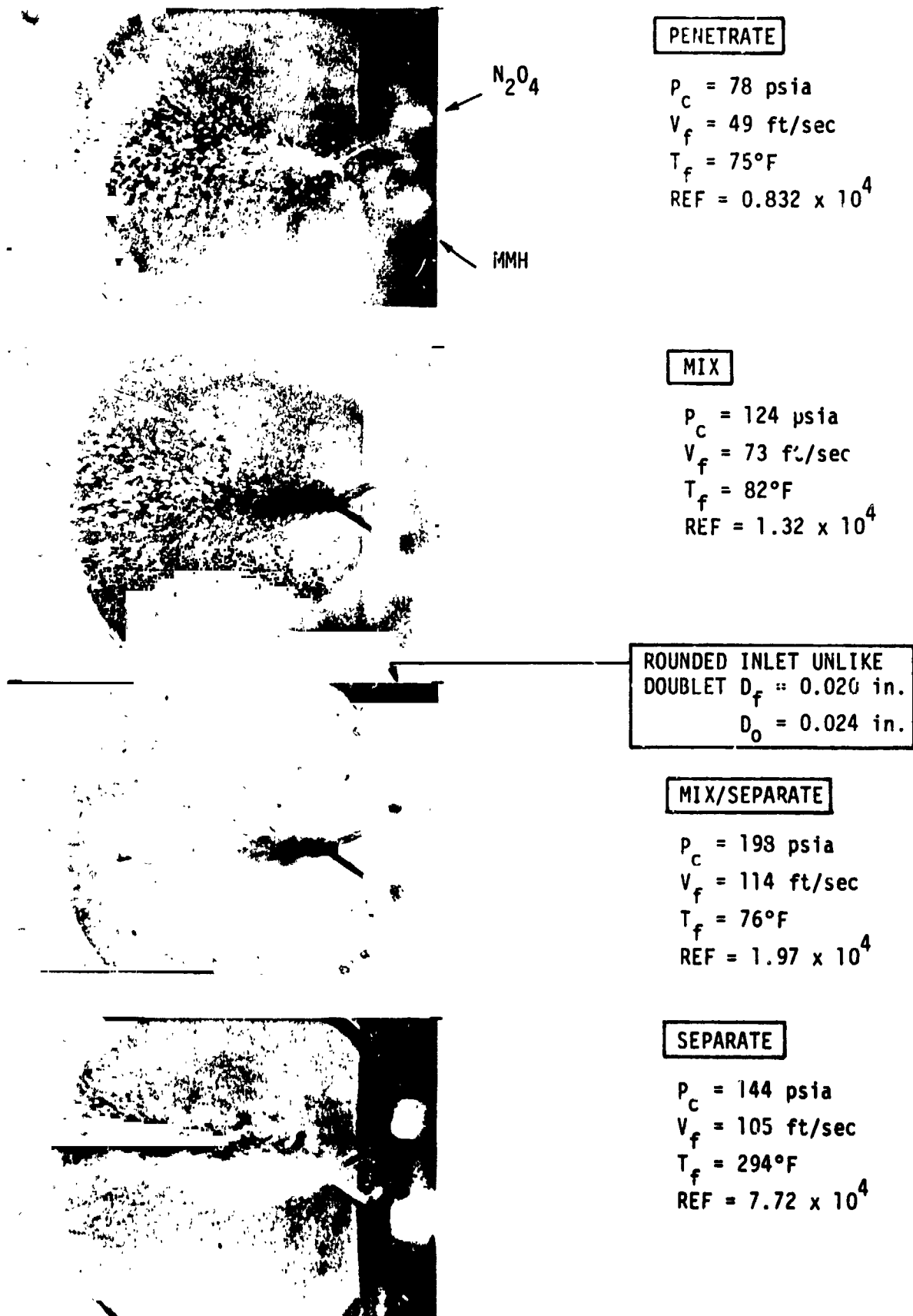


Figure 13. Reactive Stream Impingement Inhibits Intra-Element Mixing

## Appendix A

### IV, Reactive Stream Impingement Phenomena (cont.)

The phenomena of RSS is associated with a vaporization controlled reaction that is controlled by the chamber pressure, fuel injection velocity, interfacial surface area, and fuel temperature. The degree of RSS increases as these parameters are increased. RSS has been characterized for a wide range of amine fuels and a wide range of injectors as listed in Table II.

The RSS characteristics of all of the coherent stream elements (i.e., rounded inlet unlike doublet, triplet, sharp-edged unlike doublet, and Space Shuttle/RCS unlike doublet) were found to be similar and are correlated with the same correlation equation. The similarity in behavior for the triplet and sharp-edged unlike doublet is shown in Figures 14 and 15. The behavior of the Space Shuttle/RCS unlike doublet is illustrated in Figure 16 which shows the element behavior over its whole Pc-MR operating range. The impingement mode and operating condition is indicated next to each photo.

The off-mixture ratio momentum effects on spray mixing are seen to be as strong as the RSS effects with the SS/RCS unlike doublet. It is clearly undesirable to operate at extreme off-MR conditions with unlike doublet elements due to the strong effect on spray distributions. The triplet or pentad coherent elements or atomized spray elements which are less sensitive to momentum effects would be better choices for injectors that must cover wide mixture ratio ranges.

The RSS characteristics of the XDT, the splashplate, and the Space Shuttle/OMS TLOL self-atomizing elements were found to differ from the coherent stream elements in that RSS occurs at lower chamber pressures than for the coherent stream elements. The RSS characteristics of the XDT and the splashplate elements are illustrated in Figures 17 and 18. Increasing chamber pressure and fuel Reynolds Number (REF) promotes RSS. The chamber pressure is a much stronger effect than the fuel velocity (REF) as evidenced

TABLE II

## SUMMARY OF INJECTOR ELEMENTS AND TEST CONDITIONS

INJECTOR ELEMENT	FUEL	$P_c$ (psia)	$V_f$ (ft/sec)	$V_o$ (ft/sec)	$T_f$ (°F)	$T_o$ (°F)	MR
Rounded Inlet Unlike Doublet, $D_f = 0.020$	MMH	80-1000	35-160	30-111	55-300	55-150	1.60-1.70
	A-50	90-1000	50-162	40-114	60-85	55-80	1.60-1.70
	$N_2H_4$	60-300	40-165	34-130	65-160	68-76	1.60-1.70
Small F-O-F Triplet $D_f = 0.020$	MMH	80-210	40-100	30-70	70-300	60-145	1.60-1.70
Large F-O-F Triplet $D_f = 0.029$	MMH	80-195	30-78	32-65	75-300	68-150	1.60-1.70
Small Sharp Edged Unlike Doublet - $D_f = 0.020$	MMH	68-396	35-216	26-150	68-245	68-104	1.60-1.70
	$N_2H_4$	75-392	40-160	34-125	73-173	66-82	1.60-1.70
Large Sharp Edged Unlike Doublet, $D_f = 0.030$	MMH	80-310	34-174	30-110	68-265	66-136	1.60-1.70
	$N_2H_4$	84-410	30-175	30-150	66-80	64-85	1.60-1.70
Space Shuttle/RCS Unlike Doublet, $D_f = 0.023$	MMH	83-247	28-119	25-142	50-137	47-123	1.36-3.15
Space Shuttle/RCS Unlike Doublet, Offset Impinge- ment, $D_f = 0.023$	MMH	114-193	61-106	36-105	75-87	68-80	1.45-3.06
Space Shuttle/OMS TL0L Platelet Injector $D_f = 0.028$	MMH	43-195	29-127	26-112	65-231	62-83	1.44-1.81
	$N_2H_4$	104-397	38-120	40-112	71-155	70-73	1.43-1.96
XDT Platelet, $D_f = 0.021$	MMH	81-194	42-100	32-80	68-291	62-162	1.60-1.70
Splashplate Platelet, $D_f = 0.021$	MMH	81-192	40-104	32-80	71-288	71-154	1.60-1.70

Appendix A

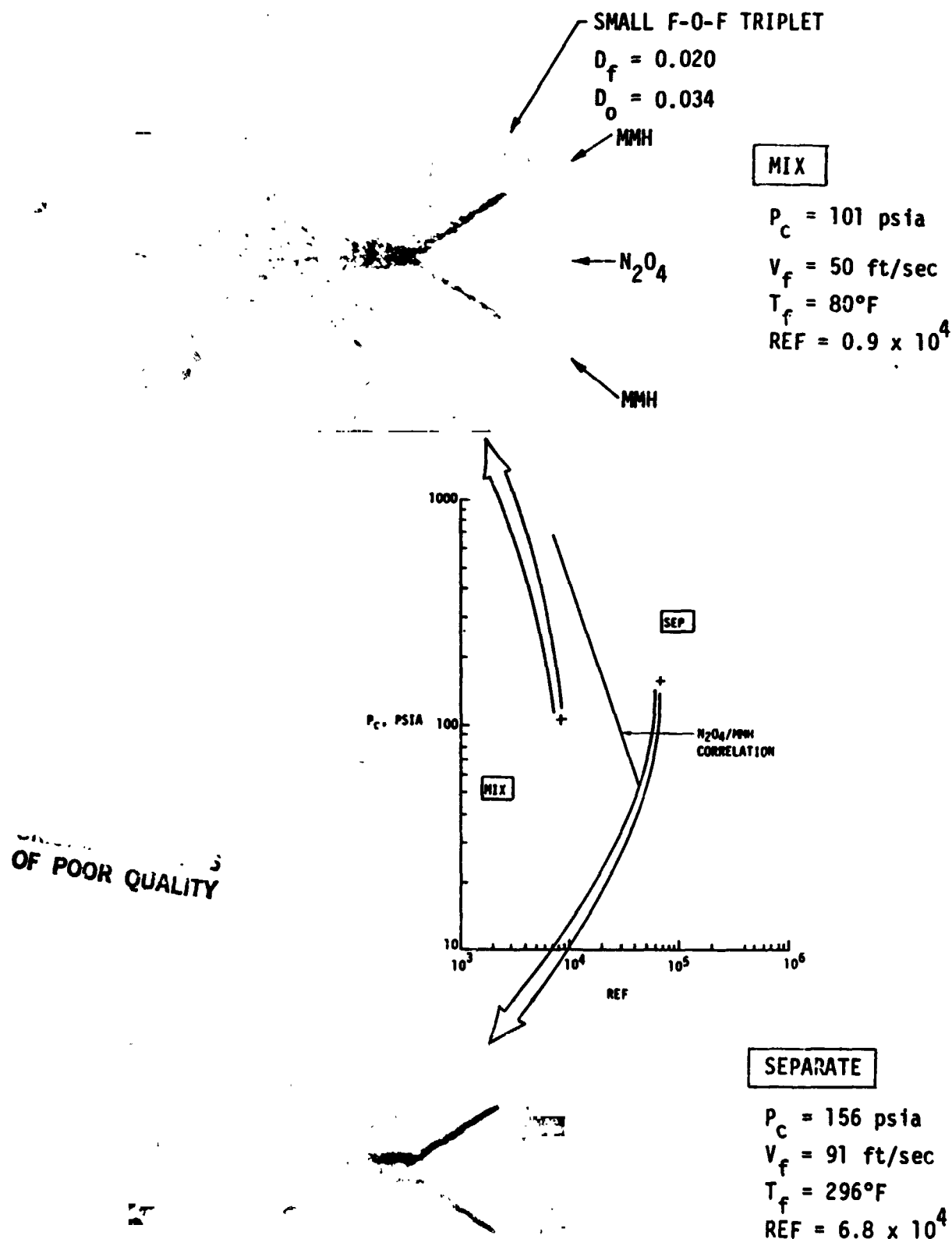


Figure 14. Reactive Stream Impingement with the F-O-F Triplet Element

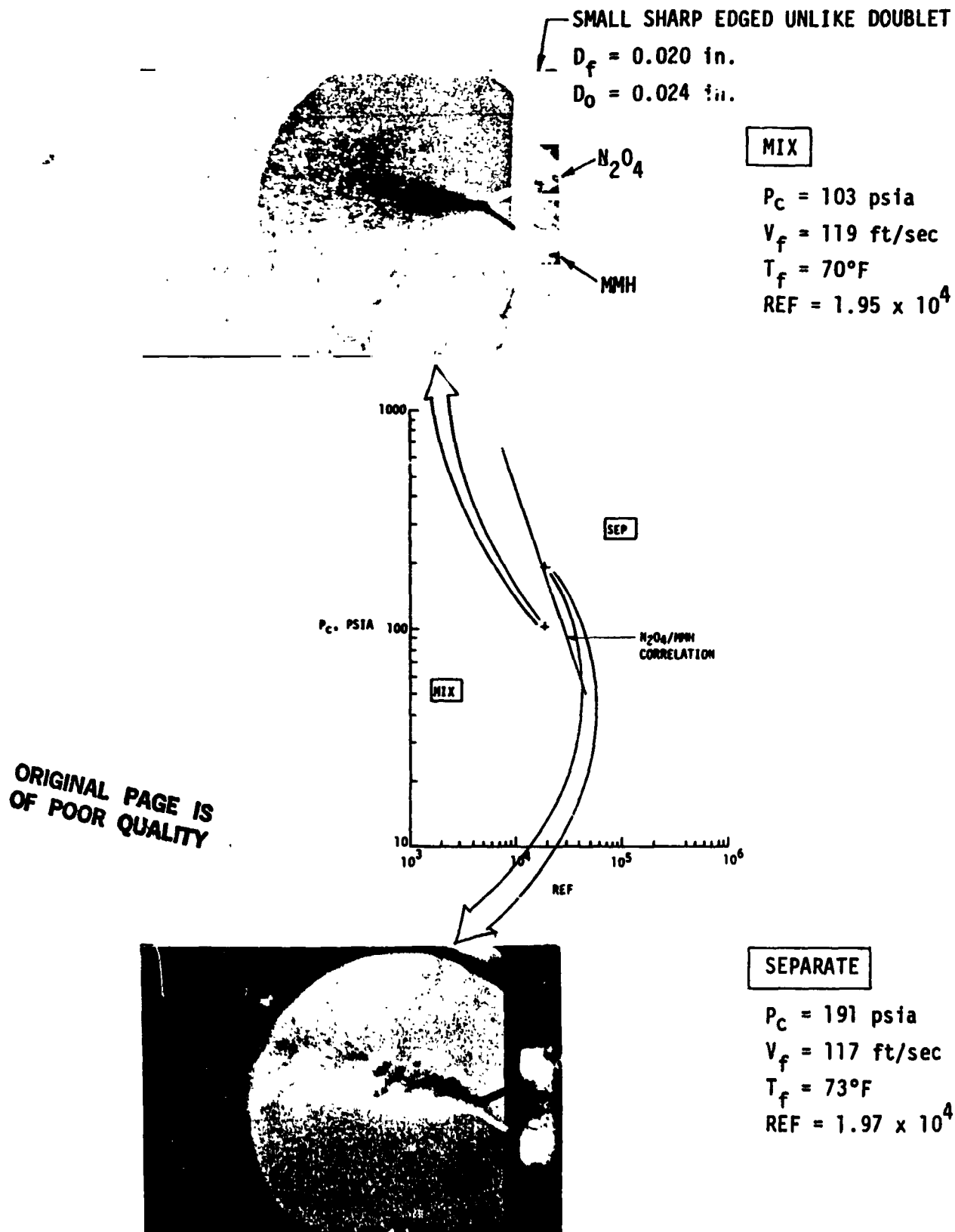


Figure 15. Reactive Stream Impingement with the Sharp Edged Unlike Doublet

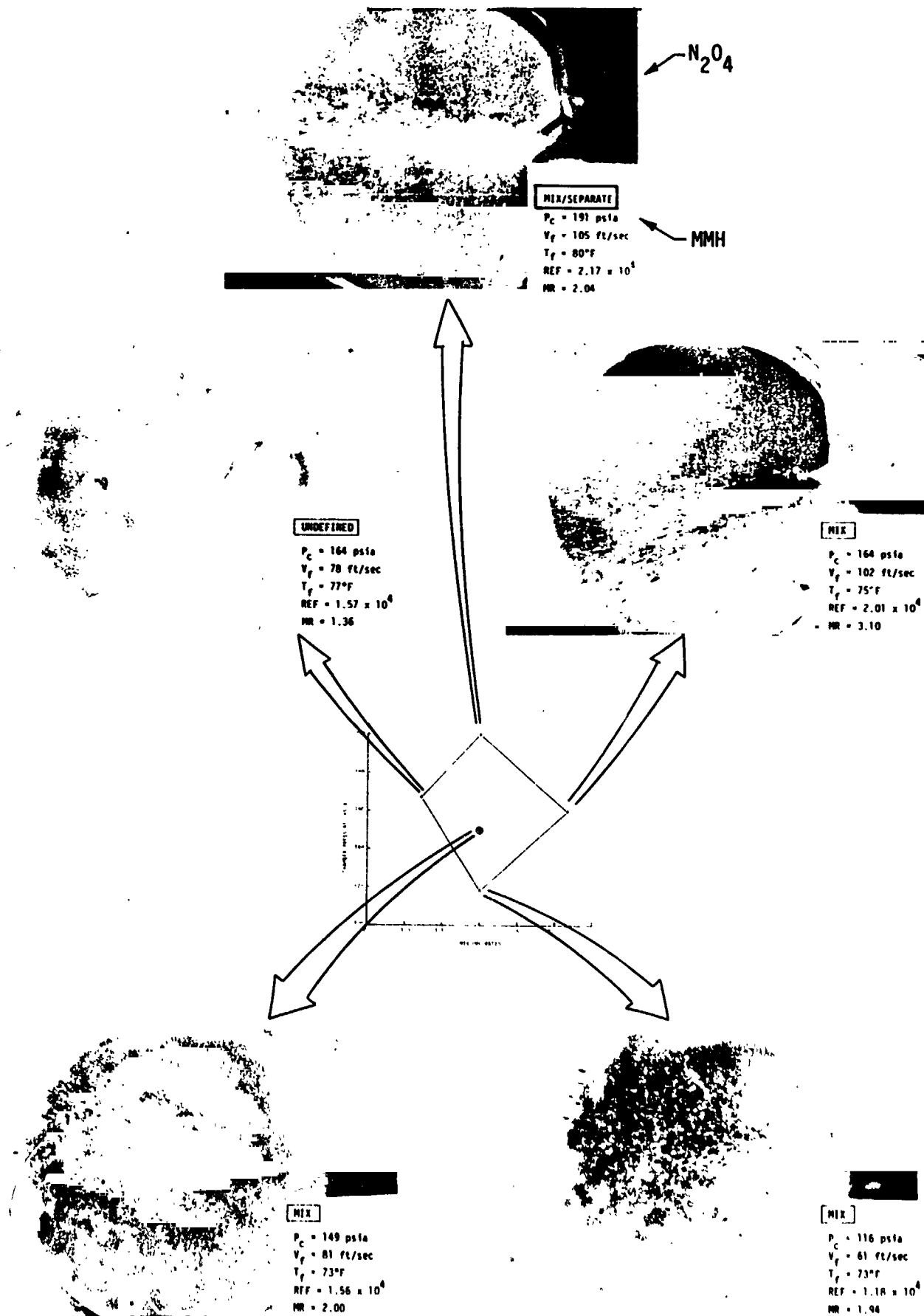
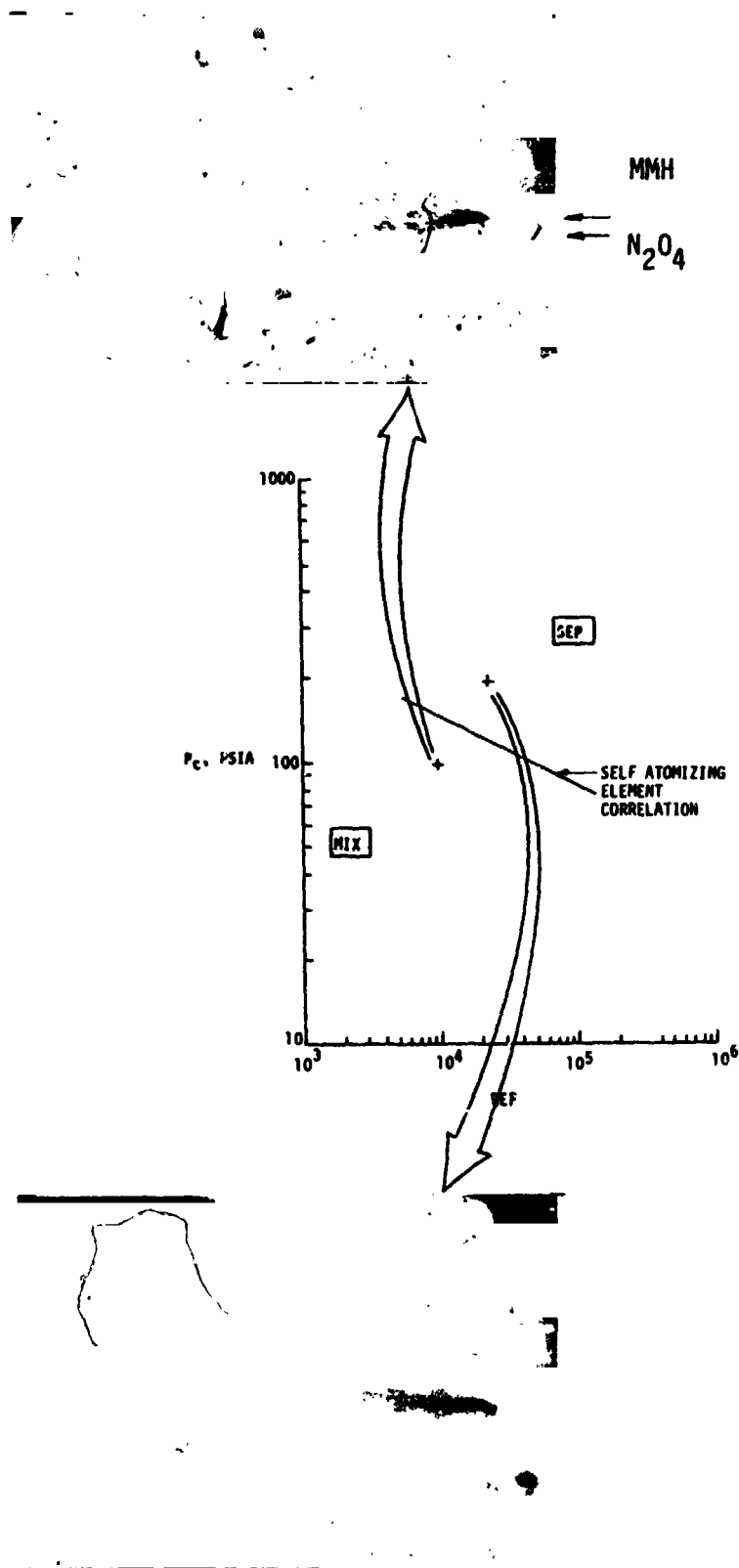


Figure 16. Reactive Stream Impingement with the Space Shuttle/RCS Unlike Doublet



**MIX**

$P_c = 98$  psia  
 $V_f = 53$  ft/sec  
 $T_f = 71^\circ\text{F}$   
 $\text{REF} = 0.913 \times 10^4$

**SEPARATE**

$P_c = 194$  psia  
 $V_f = 100$  ft/sec  
 $T_f = 97^\circ\text{F}$   
 $\text{REF} = 2.18 \times 10^4$

Figure 17. Reactive Stream Impingement with the XDT Platelet Element

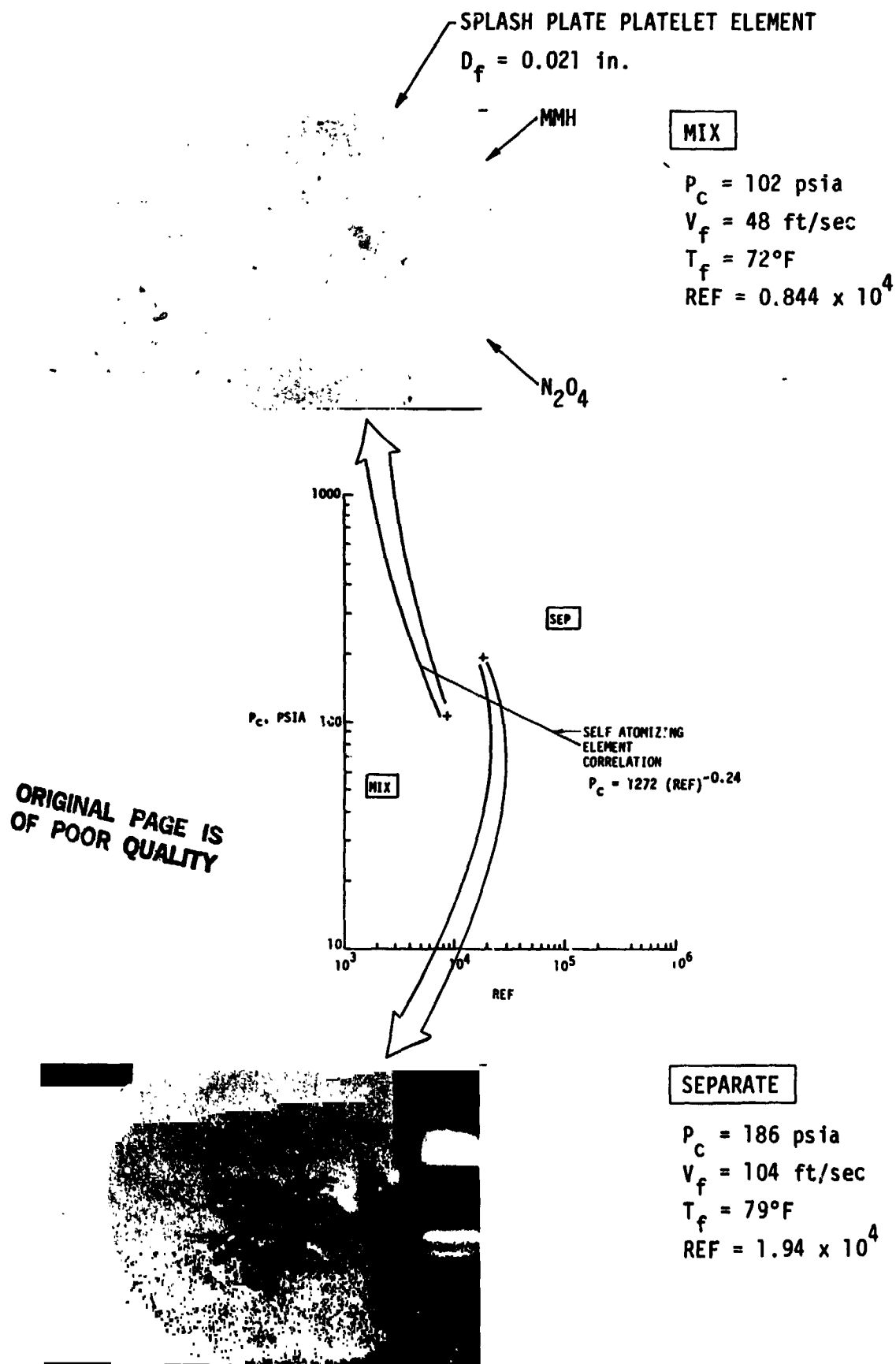


Figure 18. Reactive Stream Impingement with the Splashplate Element



## Appendix A

### IV, Reactive Stream Impingement Phenomena (cont.)

by the small slope of the correlation line. RSS sets in at such low chamber pressure levels ( $\sim 100$  psia) that these elements generally always operate in the separated mode.

The Space Shuttle/OMS TLOL platelet element is an example of an element that operates in a separated mode over its entire operating range as illustrated in Figure 19. The operating conditions are indicated next to each photo. It is evident that this element is insensitive to engine operating mode. Although, it is always separated, the desired engine performance is attained by providing element overlap to take advantage of inter-element mixing. Excellent performance, compatibility and stability are provided by this element since the injector spray mass and mixture ratio distribution remain nearly constant over its whole operating range.

MMH

$N_2O_4$

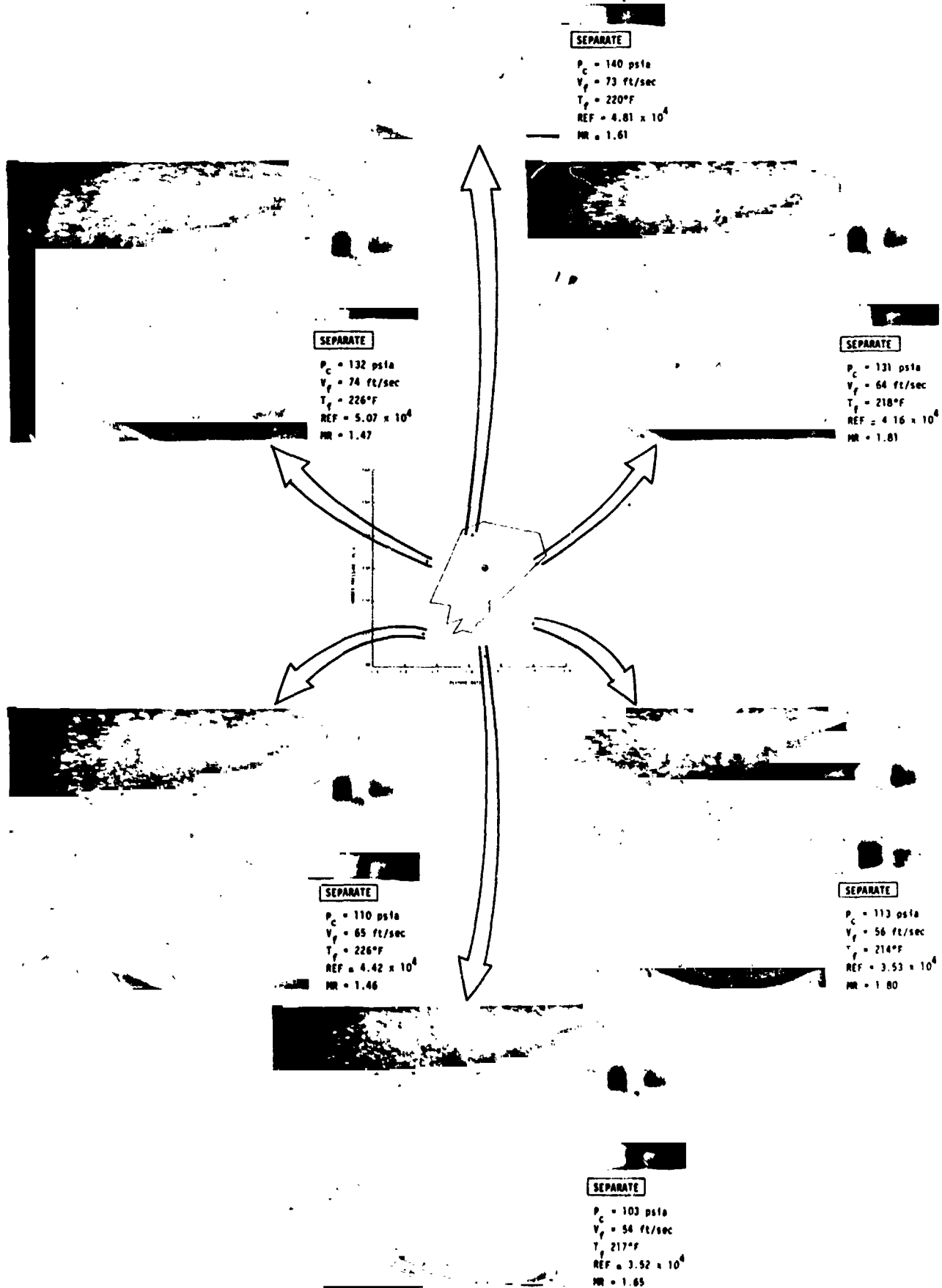


Figure 19. Reactive Stream Impingement with the Space Shuttle/OMS TL0L Platelet Element

## Appendix A

### V. REACTIVE STREAM IMPINGEMENT DATA CORRELATIONS

RSS has been found to correlate best with the chamber pressure and the fuel orifice Reynolds Number. Figure 20 shows the correlation for coherent stream injectors while Figure 21 shows the atomized spray impingement injector correlations. The coherent stream injectors are correlated with the equation;

$$P_c = 4.4 \times 10^8 (\text{REF})^{-1.5} \quad \text{Equation (3)}$$

where:

REF = Fuel Orifice Reynolds Number.

Mixing occurs at chamber pressures less than that specified by Equation (3) and separation occurs at greater chamber pressures. Regimes of RSS with the atomized spray impingement platelet types of injectors are correlated by:

$$P_c = 1272 (\text{REF})^{-0.24} \quad (\text{XDT and splash plate}) \quad \text{Equation (4)}$$

$$P_c = 839 (\text{REF})^{-0.24} \quad (\text{TLOL}). \quad \text{Equation (5)}$$

Again mixing occurs at chamber pressures below this value and separation occurs at pressures greater than this.

# Appendix A

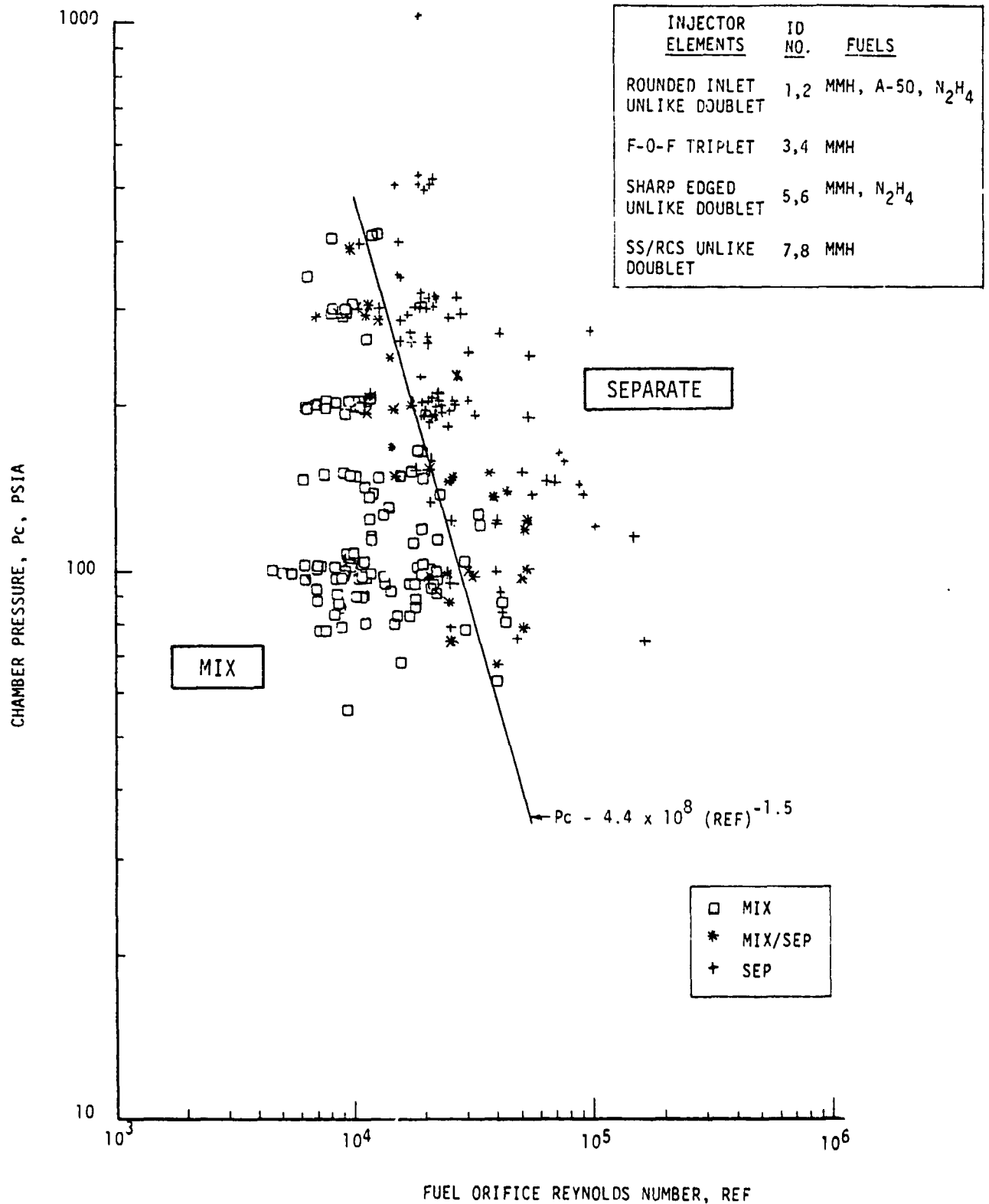


Figure 20. RSS Correlation for Coherent Stream Impingement Injector Elements

## Appendix A

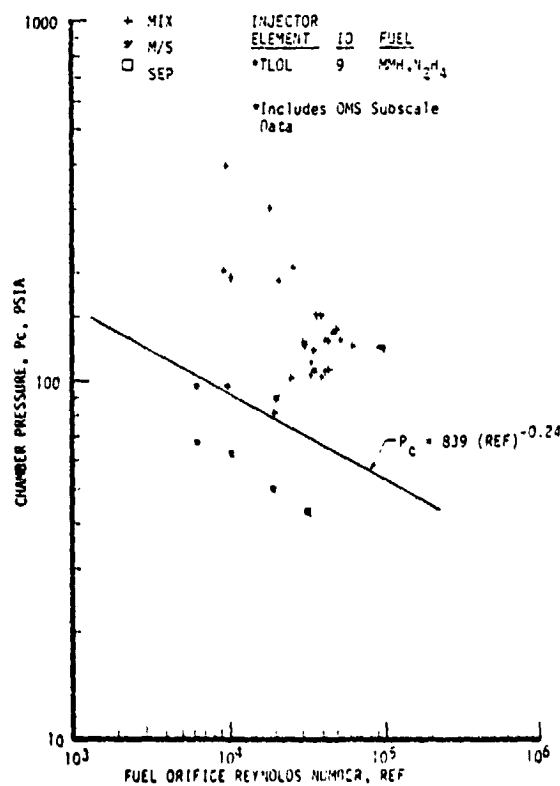
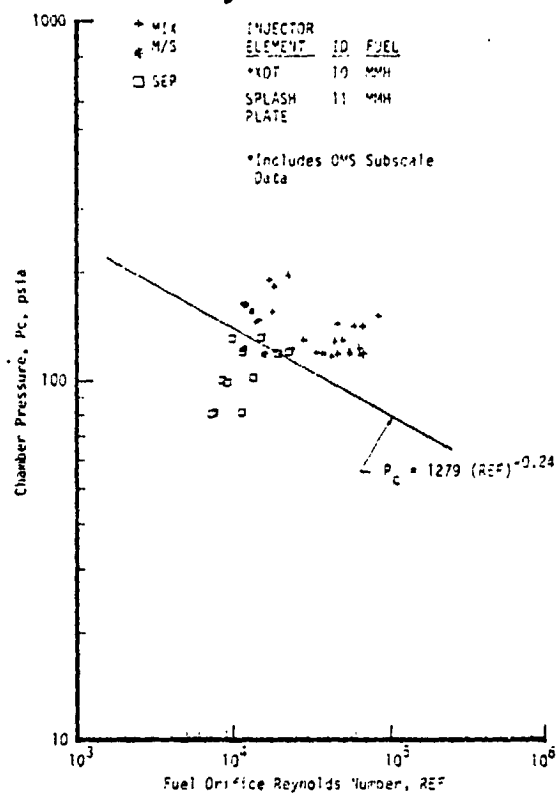


Figure 21 Vaporization Model Correlates RSS for Self-Atomizing Injector Elements

## Appendix A

### VI. REACTIVE STREAM DESIGN CRITERIA

The intent of the design criteria set forth herein is to aid the injector designer in coping with the adverse effects of RSS on engine performance, stability, and compatibility. Since these effects manifest themselves through modifications to the intra- and inter-element mixing, only those factors influencing the mixing processes are dealt with. It is presumed that other factors influencing performance, stability and compatibility have been considered. These other factors include but are not limited to; identification of element size and quantity to provide the required vaporization efficiency; pattern orientation requirements for inter-element mixing and compatibility; chug stability pressure drop requirements.

A prerequisite for designing high performance elements is to provide for hydraulically stable streams or sprays. Therefore, non-reactive impingement criteria are included.

#### A. NON-REACTIVE IMPINGEMENT ELEMENT DESIGN CRITERIA

Criteria 1 Orifice discharge coefficients should be predictable and should not undergo hydraulic flip.

##### Solution

- ° Design sharp edged orifices with  $L/D < 1$  to ensure detached flow.
- ° Design sharp edged orifices with  $L/D > 4$  to ensure attached flow.
- ° Contour orifice inlet

Criteria 2 Stream directional control should be predictable.

## Appendix A

### VI, A, Non-Reactive Impingement Element Design Criteria (cont.)

#### Solution

- ° Design orifice  $L/D > 4$  with contoured inlet.
- ° Design manifold cross velocity for less than  $1/4$  orifice velocity.

#### Criteria 3

Stream impingement should be accurately aligned.

#### Solution

- ° Electrical Discharge Machine (EDM) orifices.

#### Criteria 4

Unlike orifice diameter or spray mismatch should be minimized.

#### Solution

- ° Select element types that minimize unlike orifice diameters (see Table I).
- ° Select non-circular orifices.
- ° Design for equal spray fan width.

#### Criteria 5

Momentum ratios should be selected for optimum mixing.

#### Solution

- ° Use mixing criteria listed in Table I for the particular element of interest.

## Appendix A

### VI, Reactive Stream Design Criteria (cont.)

#### B. REACTIVE IMPINGEMENT ELEMENT DESIGN CRITERIA

Criteria 1      RSS should be avoided to maximize performance.

##### Solution

- ° Select element size and velocity that will permit operation within the mix regimes defined by Equations (3), and (4) and (5).

Criteria 2      ° Transitions from mixed to separated conditions within the engine operating envelope should be avoided.

##### Solution

- ° Select elements that will remain within either the mixed or separated regimes defined by Equations (3) and (4) and (5).

Criteria 3      ° Changes in resultant axial momentum angle within the engine operating envelope should be avoided.

##### Solution

- ° Select elements that are insensitive to momentum imbalance (triplets, pentads, like-on-like).

Criteria 4      ° Inter-element mixing should be maximized.

##### Solution

- ° Orient elements within the pattern to provide spray overlap taking into account the effect of RSS on intra-element mixing.



## Appendix A

### REFERENCES

1. Rupe, J.H., "A Correlation Between the Dynamic Properties of a Pair of Impinging Streams and the Uniformity of Mixture-Ratio Distribution in the Resulting Spray", JPL Progress Rept. No. 20-209, 1956.
2. Rupe, J.H., "An Experimental Correlation of the Nonreactive Properties of Injection Schemes and Combustion Effects in a Liquid Propellant Rocket Engine, Part I. The Application of Nonreactive Spray Properties to Rocket Motor Injector Design", JPL Tech. Rept. 32-255, July 1965.
3. Elverum, G.W. and Morey, T.F., "Criteria for Optimum Mixture Ratio Distributions Using Several Types of Impinging Stream Injector Elements", JPL Memorandum No. 30-5, February 1959.
4. McHale, R.M. and Nurick, W.H., "Noncircular Orifice Holes and Advanced Fabrication Techniques for Liquid Rocket Injectors", Rocketdyne Report R-9271, Contract No. NAS 9-9528, May 1974.
5. Ito, J.I., "A General Model Describing Hydraulic Flip in Sharp Edge Orifices", 7th JANNAF Combustion Meeting, Expanded Abstracts and Slides - Volume I, CPIA Publ. #204, Vol. 1; Feb. 1971.

TABLE B-I

## SUMMARY OF INJECTOR ELEMENTS AND TEST CONDITIONS

INJECTOR ELEMENT	FUEL	$P_c$ (psia)	$V_f$ (ft/sec)	$V_o$ (ft/sec)	$T_f$ (°F)	$T_o$ (°F)	NO. OF TESTS	MR
Rounded Inlet Unlike Doublet, $D_f = 0.020$	MMH	80-1000	35-160	30-111	55-300	55-150	96	1.60-1.70
	A-50	90-1000	50-162	40-114	60-85	55-80	32	1.60-1.70
	$N_2H_4$	60-300	40-165	34-130	65-160	68-76	21	1.60-1.70
Small F-O-F Triplet $D_f = 0.020$	MMH	80-210	40-100	30-70	70-300	60-145	12	1.60-1.70
Large F-O-F Triplet $D_f = 0.029$	MMH	80-195	30-78	32-65	75-300	68-150	11	1.60-1.70
Small Sharp Edged Unlike Doublet - $D_f = 0.020$	MMH	68-396	35-216	26-150	68-245	68-104	24	1.60-1.70
	$N_2H_4$	75-392	40-160	34-125	73-173	66-82	17	1.60-1.70
Large Sharp Edged Unlike Doublet, $D_f = 0.030$	MMH	80-310	34-174	30-110	68-265	66-136	15	1.60-1.70
	$N_2H_4$	84-410	30-175	30-150	66-80	64-85	16	1.60-1.70
Space Shuttle/RCS Unlike Doublet, $D_f = 0.023$	MMH	83-247	28-119	25-142	50-137	47-123	43	1.36-3.15
Space Shuttle/RCS Unlike Doublet, Offset Impinge- ment, $D_f = 0.023$	MMH	114-193	61-106	36-105	75-87	68-80	7	1.45-3.06
Space Shuttle/OMS TL0L Platelet Injector $D_f = 0.028$	MMH	43-195	29-127	26-112	65-231	62-83	19	1.44-1.81
	$N_2H_4$	104-397	38-120	40-112	71-155	70-78	12	1.43-1.96
XDT Platelet, $D_f = 0.021$	MMH	81-194	42-100	32-80	68-291	62-162	16	1.60-1.70
Splashplate Platelet, $D_f = 0.021$	MMH	81-192	40-104	32-80	71-288	71-154	15	1.60-1.70
							356	

## Appendix B

TABLE B-II

### SUMMARY OF INJECTOR ELEMENT TEST RESULTS

List of Symbols  
Description of Headings for Table B-II

$D_f, D_o$	Fuel and oxidizer orifice diameter, in.
DELT I	Impingement point temperature rise, °F
Imp. Angle	Propellant Stream Impingement angle, °
L/D	Orifice length to diameter ratio
MF/MO	Fuel to oxidizer momentum ratio
MR	Oxidizer to fuel mixture ratio
MRVP	Vapor phase mixture ratio
Pc	Chamber pressure, psia
PPF, PPO	Fuel and oxidizer partial pressures, psia
REACT	Reactivity, $Re_f \times XP$
REF, REO	Fuel and oxidizer orifice Reynolds Number based on dia
RELF, RELO	Fuel and oxidizer orifice Reynolds No., based on length
RESID	Propellant stream contact time, sec.
TF	Fuel temperature, °F
TO	Oxidizer temperature, °F
VAVG	Average of fuel and oxidizer injection velocity, ft/sec
VF, VO	Fuel and oxidizer injection velocity, ft/sec
WEF, WEO	Fuel and oxidizer Weber No.
XF, XO	Fuel and oxidizer mole fraction
XP	Product of fuel and oxidizer mole fraction ** 1/2

# Appendix B

TABLE B-II (cont.)

## HYPERGULIC STREAM IMPINGMENT DATA COMPILATION

### INVESTIGATION LAVER

TEST SERIES OC-27-KXX

FUEL TEST TYPE	INJECTOR TYPE	DN (IN)	DF (IN)	L/D	IMP ANGLE (DEG)	PC (PSIA)	VO (FT/S)	VF (FT/S)	TU (F)	TF (F)	MR MF/MD	MODE	REACT (SEC)
MM	101 UNL IAF-DIMPLET	.024	.020	24.	60.	308.	90.5	129.1	88.	87.	1.66	1.239	SEP .442+03
MM	102 UNL IAF-DIMPLET	.024	.020	24.	60.	308.	87.9	132.5	88.	87.	1.57	1.181	SEP .454+03
MM	103 UNL IAF-DIMPLET	.024	.020	24.	60.	309.	89.4	129.9	88.	87.	1.62	1.286	SEP .444+03
MM	104 UNL IAF-DIMPLET	.024	.020	24.	60.	311.	90.3	129.1	88.	87.	1.62	1.301	SEP .438+03
MM	105 UNL IAF-DIMPLET	.024	.020	24.	60.	507.	90.5	125.7	89.	88.	1.70	1.175	SEP .270+03
MM	106 UNL IAF-DIMPLET	.024	.020	24.	60.	1000.	92.0	138.5	89.	88.	1.57	1.181	SEP .51+03
MM	107 UNL IAF-DIMPLET	.024	.020	24.	60.	308.	89.6	124.7	86.	85.	1.70	1.178	SEP .401+03
MM	108 UNL IAF-DIMPLET	.024	.020	24.	60.	263.	86.6	124.6	84.	84.	1.65	1.259	SEP .449+03
MM	109 UNL IAF-DIMPLET	.024	.020	24.	60.	197.	94.6	136.5	84.	84.	1.64	1.240	SEP .65+03
MM	110 UNL IAF-DIMPLET	.024	.020	24.	60.	154.	87.9	129.6	83.	83.	1.60	1.320	SEP .752+03
MM	111 UNL IAF-DIMPLET	.024	.020	24.	60.	100.	92.3	135.5	84.	83.	1.60	1.312	MIX .128+03
MM	112 UNL IAF-DIMPLET	.024	.020	24.	60.	89.	51.1	73.9	76.	76.	1.59	1.108	MIX .759+03
A-50	113 UNL IAF-DIMPLET	.024	.020	24.	60.	101.	91.5	124.0	88.	87.	1.63	1.232	MIX .169+04
A-50	114 UNL IAF-DIMPLET	.024	.020	24.	60.	162.	85.3	117.9	82.	82.	1.66	1.199	MIX .806+03
A-50	115 UNL IAF-DIMPLET	.024	.020	24.	60.	203.	91.0	125.9	81.	78.	1.65	1.203	SEP .624+03
A-50	116 UNL IAF-DIMPLET	.024	.020	24.	60.	269.	83.4	114.4	80.	77.	1.67	1.181	SEP .414+03
A-50	117 UNL IAF-DIMPLET	.024	.020	24.	60.	301.	81.6	85.7	78.	76.	1.64	1.217	SEP .267+03
A-50	118 UNL IAF-DIMPLET	.024	.020	24.	60.	310.	80.7	123.6	81.	81.	1.60	1.276	SEP .428+03
A-50	119 UNL IAF-DIMPLET	.024	.020	24.	60.	510.	85.7	120.4	82.	82.	1.64	1.219	SEP .261+03
A-50	120 UNL IAF-DIMPLET	.024	.020	24.	60.	1003.	87.8	122.8	82.	81.	1.63	1.227	SEP .132+03
A-50	121 UNL IAF-DIMPLET	.024	.020	24.	60.	160.	84.8	125.2	81.	80.	1.62	1.247	MIX .815+03
A-50	122 UNL IAF-DIMPLET	.024	.020	24.	60.	334.	72.8	100.8	81.	80.	1.65	1.200	SEP .310+03
A-50	123 UNL IAF-DIMPLET	.024	.020	24.	60.	314.	75.4	104.6	77.	77.	1.65	1.206	SEP .245+03
MM	124 UNL IAF-DIMPLET	.024	.020	24.	60.	955.	84.6	101.6	82.	82.	1.61	1.293	SEP .942+02
MM	125 UNL IAF-DIMPLET	.024	.020	24.	60.	495.	84.6	130.3	83.	81.	1.60	1.315	SEP .231+03
MM	126 UNL IAF-DIMPLET	.024	.020	24.	60.	296.	86.6	132.1	83.	82.	1.59	1.150	SEP .394+03
MM	127 UNL IAF-DIMPLET	.024	.020	24.	60.	281.	53.7	80.5	84.	81.	1.58	1.172	M/S .251+03
MM	128 UNL IAF-DIMPLET	.024	.020	24.	60.	256.	84.8	126.2	85.	83.	1.58	1.147	SEP .463+03
MM	129 UNL IAF-DIMPLET	.024	.020	24.	60.	191.	91.6	135.5	85.	83.	1.60	1.311	SFP .607+03
MM	130 UNL IAF-DIMPLET	.024	.020	24.	60.	152.	85.9	129.5	85.	82.	1.56	1.184	M/S .784+03
MM	131 UNL IAF-DIMPLET	.024	.020	24.	60.	93.	88.8	133.0	85.	83.	1.57	1.366	MIX .131+04
MM	132 UNL IAF-DIMPLET	.024	.020	24.	60.	116.	91.4	136.4	86.	83.	1.58	1.357	MIX .118+04
MM	133 UNL IAF-DIMPLET	.024	.020	24.	60.	411.	125.8	179.6	83.	83.	1.66	1.218	UNDEF .400+03
MM	134 UNL IAF-DIMPLET	.024	.020	24.	60.	97.	92.8	136.3	77.	197.	1.74	1.216	M/S .103+05
MM	135 UNL IAF-DIMPLET	.024	.020	24.	60.	119.	93.4	139.2	78.	199.	1.72	1.237	M/S .844+04
MM	136 UNL IAF-DIMPLET	.024	.020	24.	60.	150.	92.9	136.5	77.	199.	1.74	1.227	SFP .687+04
MM	137 UNL IAF-DIMPLET	.024	.020	24.	60.	184.	97.7	143.8	76.	199.	1.74	1.218	SFP .570+04
MM	138 UNL IAF-DIMPLET	.024	.020	24.	60.	243.	91.3	148.9	79.	195.	1.60	1.234	SFP .442+04
MM	139 UNL IAF-DIMPLET	.024	.020	24.	60.	103.	35.8	58.4	61.	59.	1.45	1.615	UNDEF .220+03
MM	140 UNL IAF-DIMPLET	.024	.020	24.	60.	81.	97.4	143.0	64.	62.	1.61	1.106	UNDEF .760+03

OF POOR QUALITY

# Appendix B

TABLE B-II (cont.)

## HYPERGOLIC STREAM IMPINGEMENT DATA COMPILATION

### INVESTIGATOR LAWVER

FUEL TEST TYPE	TEST NO.	MODE	PC (PSIA)	VAVG	WEF	NEO	REF	NEU	DELTA (DEG F)	REL	RELO	PPF (PSIA)	PPD (PSIA)	MRVP	XF	XO	XP	RESID
M-M	101	SFP	308	105	43.7	36.0	245+05	651+05	0	59+06	16+07	1.3	23.2	34.8	.0020990	.0020990	.05-08	.44+03
M-M	102	SFP	308	105	46.0	34.0	252+05	632+05	0	60+06	15+07	1.3	23.2	34.8	.0021107	.0021107	.06-08	.45+03
M-M	103	SFP	309	105	44.4	35.2	247+05	633+05	0	59+06	15+07	1.3	23.2	34.8	.0021122	.0021122	.05-08	.44+03
M-M	104	SFP	311	104	44.1	34.6	245+05	635+05	0	59+06	15+07	1.3	23.2	34.8	.0021473	.0021473	.05-08	.44+03
M-M	105	SFP	307	104	48.1	59.6	241+05	655+05	0	58+06	16+07	1.4	23.7	34.8	.0022483	.0022483	.07-08	.27+03
M-M	106	SFP	1000	110	163.5	121.4	265+05	666+05	0	64+06	16+07	1.4	23.7	34.8	.0021094	.0021094	.07-08	.45+03
M-M	107	SFP	308	103	40.5	34.9	231+05	636+05	0	56+06	15+07	1.3	22.1	34.8	.0021319	.0021319	.02-08	.40+03
M-M	108	SFP	263	101	34.2	27.5	211+05	607+05	0	55+06	15+07	1.2	21.1	34.0	.0018579	.0018579	.07-08	.45+03
M-M	109	SFP	197	111	31.1	24.7	253+05	665+05	0	61+06	16+07	1.2	21.1	34.0	.0121789	.0121789	.07-08	.46+03
M-M	110	SFP	156	104	22.4	17.0	238+05	613+05	0	57+06	15+07	1.2	20.5	34.0	.0116654	.0116654	.07-08	.45+03
M-M	111	MIX	100	109	15.5	11.9	249+05	607+05	0	60+06	16+07	1.2	21.1	34.8	.0119139	.0119139	.07-08	.43+04
A-50	112	MIX	49	60	4.7	3.1	112+05	302+05	0	27+06	18+07	2.1	17.3	17.9	.0230361	.0230361	.07-08	.26+03
A-50	113	MIX	101	105	16.1	12.1	211+05	655+05	0	51+06	16+07	2.8	23.2	17.9	.0319658	.0319658	.07-08	.17+04
A-50	114	MIX	162	98	21.8	16.3	186+05	591+05	0	45+06	14+07	2.4	20.0	17.9	.0214929	.0214929	.06-08	.01+03
A-50	115	SFP	203	104	30.9	23.1	193+05	626+05	0	46+06	15+07	2.2	19.5	19.2	.0123346	.0123346	.02-08	.02+03
A-50	116	SFP	268	95	33.6	25.6	174+05	531+05	0	42+06	14+07	2.2	19.0	19.1	.0114765	.0114765	.01-08	.41+03
A-50	117	SFP	301	71	21.2	15.4	129+05	416+05	0	31+06	10+07	2.1	18.1	18.7	.0129751	.0129751	.01-08	.27+03
A-50	118	SFP	310	101	45.7	32.0	194+05	597+05	0	47+06	14+07	2.4	19.5	18.0	.0121621	.0121621	.05-08	.43+03
A-50	119	SFP	510	69	71.4	51.4	190+05	594+05	0	44+06	14+07	2.4	20.0	17.9	.0023380	.0023380	.00-08	.26+03
A-50	120	SFP	1003	101	145.9	107.0	193+05	604+05	0	46+06	15+07	2.4	20.0	18.4	.0022384	.0022384	.01-08	.13+03
A-50	121	MIX	160	103	24.2	17.4	195+05	612+05	0	47+06	15+07	2.3	19.5	18.5	.0118751	.0118751	.00-08	.02+03
A-50	122	SFP	334	83	33.0	24.6	157+05	501+05	0	38+06	12+07	2.3	19.5	18.5	.0193683	.0193683	.03-08	.11+03
A-50	123	SFP	334	86	35.1	25.6	159+05	507+05	0	38+06	12+07	2.2	17.7	17.9	.015683	.015683	.05-08	.29+03
M-M	124	SFP	955	82	83.2	64.0	235+05	682+05	0	44+06	12+07	1.2	20.0	33.9	.0026796	.0026796	.07-08	.48+02
M-M	125	SFP	495	105	70.8	54.0	235+05	618+05	0	56+06	15+07	1.1	20.5	35.6	.0021846	.0021846	.07-08	.23+03
M-M	126	SFP	208	105	83.9	62.5	241+05	618+05	0	58+06	15+07	1.2	20.5	34.8	.0020270	.0020270	.07-08	.40+03
M-M	127	M/S	281	104	15.5	11.4	145+05	316+05	0	35+06	10+06	1.1	21.1	36.4	.0031716	.0031716	.06-08	.25+03
M-M	128	SFP	266	101	34.5	25.4	232+05	599+05	0	56+06	14+07	1.2	21.6	35.6	.0016225	.0016225	.01-08	.46+03
M-M	129	SFP	191	109	29.7	24.5	249+05	607+05	0	60+06	16+07	1.2	21.6	35.6	.0121633	.0121633	.00-08	.07+03
M-M	130	M/S	152	103	21.5	15.8	226+05	606+05	0	57+06	15+07	1.2	21.6	34.4	.0114221	.0114221	.02-08	.28+03
M-M	131	MIX	95	106	14.2	10.5	244+05	627+05	0	59+06	15+07	1.2	21.6	35.6	.0118765	.0118765	.00-08	.13+04
M-M	132	MIX	114	109	17.9	13.4	251+05	609+05	0	60+06	16+07	1.2	22.1	36.4	.0121922	.0121922	.02-08	.11+04
M-M	133	UNDEF	411	146	112.1	90.4	330+05	817+05	0	79+06	21+07	1.2	20.5	34.0	.0012928	.0012928	.07-08	.40+03
M-M	134	M/S	97	109	16.6	11.3	258+05	624+05	0	13+07	15+07	1.7	17.7	2.4	.0116880	.0116880	.18-08	.10+05
M-M	135	M/S	119	111	24.1	14.2	277+05	635+05	0	14+07	15+07	1.7	18.1	2.4	.0222820	.0222820	.19-08	.09+04
M-M	136	SFP	150	109	29.2	17.5	246+05	621+05	0	14+07	15+07	1.7	17.7	2.3	.0121738	.0121738	.19-08	.09+04
M-M	137	SFP	188	115	40.7	24.0	206+05	653+05	0	14+07	16+07	1.7	17.1	2.3	.0120457	.0120457	.18-08	.07+04
M-M	138	SFP	243	115	55.9	28.6	261+05	635+05	0	14+07	15+07	1.2	18.6	2.6	.0175675	.0175675	.19-08	.44+04
M-M	139	UNDEF	103	45	2.4	1.9	810+04	220+05	0	21+06	53+06	.6	12.0	41.2	.0147905	.0147905	.07-08	.22+03
M-M	140	UNDEF	61	115	13.5	9.7	217+05	608+05	0	52+06	15+07	.6	12.9	41.2	.0114484	.0114484	.07-08	.26+03

# Appendix B

TABLE B-II (cont.)

## HYPERGOLIC STREAM IMPINGEMENT DATA COMPILATION

### INVESTIGATOR LAWVER

FUEL TEST TYPE NO.	INJECTOR TYPE	DI (IN)	DF (IN)	L/D	IMP ANGLE (DEG)	PC (PSIA)	VO (FT/S)	VF (FT/S)	TO (F)	TF (F)	MN	MF/HO	MODE	REACT (SEC)
MMH 141	UHL IRE-DOUBLET	.024	.020	24.	60.	81.	90.8	143.2	66.	64.	1.60	1.324	UNDEF	.814+03
MMH 142	UHL IRE-DOUBLET	.024	.020	24.	60.	119.	91.4	136.7	68.	67.	1.59	1.357	MIX	.588+03
MMH 143	UHL IRE-DOUBLET	.024	.020	24.	60.	124.	32.4	54.2	67.	67.	1.42	1.690	UNDEF	.211+03
MMH 144	UHL IRE-DOUBLET	.024	.020	24.	60.	154.	35.9	55.7	67.	67.	1.53	1.453	UNDEF	.181+03
MMH 145	UHL IRE-DOUBLET	.024	.020	24.	60.	152.	84.2	128.4	66.	67.	1.62	1.283	SEP	.432+03
MMH 146	UHL IRE-DOUBLET	.024	.020	24.	60.	190.	90.3	115.5	68.	67.	1.57	1.372	SEP	.366+03
MMH 147	UHL IRE-DOUBLET	.024	.020	24.	60.	258.	84.7	124.2	68.	67.	1.61	1.302	SEP	.246+03
MMH 148	UHL IRE-DOUBLET	.024	.020	24.	60.	102.	37.0	59.8	68.	66.	1.49	1.523	MIX	.304+03
MMH 149	UHL IRE-DOUBLET	.024	.020	24.	60.	99.	89.7	133.6	69.	69.	1.60	1.343	MIX	.740+03
MMH 150	UHL IRE-DOUBLET	.024	.020	24.	60.	247.	90.1	131.9	70.	69.	1.62	1.294	SEP	.246+03
MMH 151	UHL IRE-DOUBLET	.024	.020	24.	60.	454.	95.4	137.8	70.	69.	1.54	1.263	SEP	.158+03
MMH 152	UHL IRE-DOUBLET	.024	.020	24.	60.	958.	101.8	148.3	78.	74.	1.62	1.291	SEP	.109+03
MMH 153	UHL IRE-DOUBLET	.024	.020	24.	60.	98.	29.0	50.3	55.	56.	1.37	1.614	M/P	.170+03
MMH 154	UHL IRE-DOUBLET	.024	.020	24.	60.	100.	24.4	41.9	54.	55.	1.66	1.225	M/P	.133+03
MMH 155	UHL IRE-DOUBLET	.024	.020	24.	60.	102.	36.8	51.4	54.	54.	1.70	1.174	M/P	.156+03
MMH 156	UHL IRE-DOUBLET	.024	.020	24.	60.	107.	49.3	77.1	53.	54.	1.52	1.472	MIX	.220+03
MMH 157	UHL IRE-DOUBLET	.024	.020	24.	60.	102.	53.5	79.2	53.	54.	1.61	1.318	MIX	.237+03
MMH 158	UHL IRE-DOUBLET	.024	.020	24.	60.	101.	24.9	35.6	58.	56.	1.94	.914	M/P	.124+03
MMH 159	UHL IRE-DOUBLET	.024	.020	24.	60.	99.	30.3	43.0	57.	58.	1.68	1.211	M/P	.156+03
MMH 160	UHL IRE-DOUBLET	.024	.020	24.	60.	101.	34.2	56.6	57.	58.	1.65	1.254	M/P	.201+03
MMH 161	UHL IRE-DOUBLET	.024	.020	24.	60.	102.	37.8	58.2	57.	58.	1.54	1.429	M/P	.205+03
MMH 162	UHL IRE-DOUBLET	.024	.020	24.	60.	102.	41.4	50.0	57.	58.	1.82	1.027	M/P	.190+03
MMH 163	UHL IRE-DOUBLET	.024	.020	24.	60.	98.	58.5	85.1	57.	58.	1.63	1.277	MIX	.311+03
MMH 164	UHL IRE-DOUBLET	.024	.020	24.	60.	100.	50.1	72.1	56.	57.	1.65	1.249	MIX	.248+03
MMH 165	UHL IRE-DOUBLET	.024	.020	24.	60.	95.	72.3	106.7	56.	57.	1.61	1.313	MIX	.164+03
MMH 166	UHL IRE-DOUBLET	.024	.020	24.	60.	95.	92.1	134.3	56.	57.	1.63	1.282	MIX	.407+03
MMH 167	UHL IRE-DOUBLET	.024	.020	24.	60.	99.	51.2	74.1	55.	55.	1.63	1.262	MIX	.242+03
MMH 168	UHL IRE-DOUBLET	.024	.020	24.	60.	99.	51.6	74.7	55.	55.	1.63	1.267	MIX	.244+03
MMH 169	UHL IRE-DOUBLET	.024	.020	24.	60.	95.	52.6	75.1	44.	44.	1.66	1.223	UNDEF	.160+03
MMH 170	UHL IRE-DOUBLET	.024	.020	24.	60.	89.	112.4	164.1	44.	44.	1.62	1.281	MIX	.372+03
MMH 171	UHL IRE-DOUBLET	.024	.020	24.	60.	95.	111.0	161.0	44.	44.	1.63	1.265	MIX	.342+03
MMH 172	UHL IRE-DOUBLET	.024	.020	24.	60.	196.	44.8	57.5	44.	44.	1.64	.993	M/P	.593+02
MMH 173	UHL IRE-DOUBLET	.024	.020	24.	60.	194.	44.2	62.7	44.	44.	1.66	1.213	M/P	.640+02
MMH 174	UHL IRE-DOUBLET	.024	.020	24.	60.	201.	53.0	77.5	44.	44.	1.62	1.287	MIX	.779+02
MMH 175	UHL IRE-DOUBLET	.024	.020	24.	60.	192.	71.0	102.9	44.	44.	1.63	1.262	M/P	.168+03
MMH 176	UHL IRE-DOUBLET	.024	.020	24.	60.	97.	52.3	75.7	50.	50.	1.63	1.262	MIX	.203+03
MMH 177	UHL IRE-DOUBLET	.024	.020	24.	60.	97.	52.3	74.4	48.	48.	1.63	1.219	MIX	.184+03
MMH 178	UHL IRE-DOUBLET	.024	.020	24.	60.	97.	50.4	72.8	47.	48.	1.65	1.254	MIX	.178+03
MMH 179	UHL IRE-DOUBLET	.024	.020	24.	60.	97.	52.2	75.0	64.	64.	1.67	1.244	MIX	.369+03
MMH 180	UHL IRE-DOUBLET	.024	.020	24.	60.	202.	49.4	69.6	66.	71.	1.70	1.198	MIX	.193+03

## Appendix B

TABLE B-II (cont.)

## HYPERGOLIC STREAM IMMINGMENT DATA COMPILATION

## INVESTIGATOR LAWVER

FUEL TYPE	TEST NO.	MODE	PC (PSIA)	VAUG	WEF	NEO	REF	RED	DELI (DEG F)	REL	RELO	PPF (PSIA)(PSIA)	PRO	MRVP	XP	XD	XP	RESID
MHM	141	UNOFF	81.	115.	13.6	9.7	221+05	612+05	0.	53+06	15+07	7	13.3	41.2	.0114529.	.0114529.	.53+08	.81+03
MHM	142	MIX	119.	109.	18.3	12.8	218+05	583+05	201.	52+06	14+07	7	14.2	38.7	.0122558.	.0122558.	.55+08	.59+03
MHM	143	UNOFF	129.	41.	3.1	1.7	863+04	206+05	81.	21+06	49+06	7	13.8	37.9	.0138813.	.0138813.	.65+08	.21+03
MHM	144	UNOFF	154.	40.	3.9	2.6	847+04	228+05	78.	21+06	55+06	7	13.8	37.9	.0043088.	.0043088.	.68+08	.18+03
MHM	145	SEP	152.	104.	20.6	15.2	204+05	563+05	182.	49+06	14+07	7	14.2	38.7	.0017771.	.0017771.	.55+08	.41+03
MHM	146	SEP	190.	104.	28.9	20.0	216+05	577+05	198.	52+06	14+07	7	14.2	38.7	.0021417.	.0021417.	.55+08	.37+03
MHM	147	S/P	254.	100.	12.8	23.8	104+05	541+05	328.	47+06	13+07	7	14.2	38.7	.0018273.	.0018273.	.56+08	.25+03
MHM	148	MIX	102.	46.	2.9	1.8	944+04	237+05	114.	23+06	57+06	8	14.2	37.3	.0106627.	.0106627.	.64+08	.30+03
MHM	149	MIX	99.	107.	14.6	10.3	217+05	576+05	161.	52+06	14+07	8	14.2	36.6	.0119176.	.0119176.	.55+08	.74+03
MHM	150	SEP	297.	104.	42.7	31.4	214+05	582+05	678.	51+06	14+07	8	14.8	37.3	.0019809.	.0019809.	.57+08	.25+03
MHM	151	SEP	844.	111.	75.9	57.3	223+05	616+05	940.	54+06	15+07	4	14.4	37.3	.0019785.	.0019785.	.56+08	.16+03
MHM	152	S/P	958.	120.	175.5	134.3	252+05	688+05	1342.	60+06	17+07	9	18.1	38.3	.0018327.	.0018327.	.68+08	.11+03
MHM	153	M/P	98.	34.	2.0	1.0	719+04	173+05	115.	17+06	41+06	5	10.1	34.0	.0132174.	.0132174.	.49+08	.17+03
MHM	154	M/P	100.	34.	1.4	1.0	592+04	174+05	158.	14+06	42+06	5	9.4	37.9	.0115005.	.0115005.	.48+08	.13+03
MHM	155	M/P	102.	42.	2.2	1.7	718+04	218+05	170.	17+06	52+06	5	9.8	39.0	.0066722.	.0066722.	.46+08	.16+03
MHM	156	MIX	107.	60.	5.1	3.1	108+05	291+05	486.	26+06	10+06	5	9.4	37.8	.0036544.	.0036544.	.42+08	.22+03
MHM	157	MIX	102.	63.	5.2	3.5	111+05	316+05	88.	27+06	10+06	5	9.5	37.8	.0032794.	.0032794.	.41+08	.24+03
MHM	158	M/P	101.	31.	1.0	1.0	519+04	175+05	171.	12+06	42+06	6	11.0	39.2	.0137980.	.0137980.	.54+08	.13+03
MHM	159	M/P	99.	35.	1.5	1.1	826+04	183+05	116.	15+06	44+06	6	10.7	38.2	.0133728.	.0133728.	.52+08	.16+03
MHM	160	M/P	101.	46.	2.6	1.9	849+04	236+05	145.	20+06	57+06	6	10.7	38.2	.0144912.	.0144912.	.49+08	.20+03
MHM	161	M/P	102.	44.	2.4	1.4	849+04	228+05	131.	20+06	55+06	6	10.7	38.2	.0145415.	.0145415.	.50+08	.19+03
MHM	162	M/P	102.	46.	2.4	2.1	747+04	249+05	145.	19+06	58+06	6	10.7	38.2	.0129100.	.0129100.	.45+08	.31+03
MHM	163	MIX	98.	69.	5.8	4.1	124+05	352+05	94.	30+06	55+06	6	10.7	38.2	.0134411.	.0134411.	.46+08	.25+03
MHM	164	MIX	100.	54.	4.2	3.0	164+05	506+05	85.	25+06	72+06	5	10.4	38.1	.0122672.	.0122672.	.43+08	.39+03
MHM	165	MIX	95.	86.	8.4	6.0	154+05	434+05	72.	37+06	10+07	5	10.4	38.1	.0117894.	.0117894.	.41+08	.49+03
MHM	166	MIX	95.	104.	13.9	9.8	194+05	552+05	79.	46+06	13+07	5	10.4	38.1	.0133572.	.0133572.	.44+08	.24+03
MHM	167	MIX	99.	80.	4.4	3.1	105+05	306+05	65.	25+06	73+06	5	10.1	39.1	.0133346.	.0133346.	.44+08	.24+03
MHM	168	MIX	99.	60.	4.5	3.2	106+05	307+05	65.	25+06	74+06	4	7.4	42.2	.0031274.	.0031274.	.33+08	.16+03
MHM	169	UNOFF	95.	81.	4.3	3.0	941+04	308+05	75.	23+06	74+06	4	7.4	42.2	.0013595.	.0013595.	.29+08	.37+03
MHM	170	MIX	89.	132.	19.0	13.0	206+05	654+05	102.	49+06	16+07	4	7.4	42.2	.0014737.	.0014737.	.29+08	.34+03
MHM	171	MIX	95.	130.	19.4	13.5	202+05	649+05	104.	48+06	16+07	4	7.4	42.2	.0027065.	.0027065.	.35+08	.59+02
MHM	172	M/P	194.	49.	5.2	4.5	721+04	262+05	76.	19+06	63+06	4	7.4	42.2	.0028724.	.0028724.	.35+08	.64+02
MHM	173	M/P	194.	51.	9.2	4.5	766+04	258+05	67.	19+06	62+06	4	7.4	42.2	.0022351.	.0022351.	.33+08	.78+02
MHM	174	MIX	201.	62.	9.6	6.5	972+04	318+05	71.	23+06	14+06	4	7.4	42.2	.0027430.	.0027430.	.32+08	.11+03
MHM	175	M/S	192.	43.	16.1	11.2	129+05	415+05	116.	31+06	10+07	4	7.4	42.2	.0032118.	.0032118.	.31+08	.20+03
MHM	176	MIX	97.	61.	4.5	3.1	101+05	304+05	83.	24+06	73+06	4	8.6	38.7	.0032265.	.0032265.	.36+08	.18+03
MHM	177	MIX	97.	61.	4.3	3.1	975+04	305+05	82.	23+06	73+06	4	8.2	39.7	.0032265.	.0032265.	.36+08	.18+03
MHM	178	MIX	97.	59.	4.1	2.9	955+04	294+05	69.	23+06	71+06	4	8.0	38.4	.0132631.	.0132631.	.51+08	.39+03
MHM	179	MIX	97.	61.	4.5	3.3	120+05	326+05	64.	29+06	70+06	8	12.9	34.2	.0132631.	.0132631.	.51+08	.39+03
MHM	180	MIX	202.	57.	6.1	6.3	115+05	312+05	110.	28+06	75+06	4	11.5	32.2	.0024881.	.0024881.	.55+08	.19+03

ORIGINAL PAGE IS  
OF POOR QUALITY

TABLE B-II (cont.)

## HYPERGOLIC STREAM IMPINGEMENT DATA COMPILATION

## INVESTIGATOR LANVER

FUEL TYPE	TEST NO.	INJECTOR TYPE	DN (IN)	DF (IN)	L/D	IMP ANGLE (DEG)	PC (PSIA)	VO (FT/S)	VF (FT/S)	TO (F)	TF (F)	MR WF/MO	MODE	REACT (SEC)
MM	181	UNL IAF-DUHHLET	.024	.020	24	60	295	50.4	75.1	67	73	1.60	MIX	.152±03
MM	182	UNL IAF-DUHHLET	.024	.020	24	60	182	108.8	159.2	75	78	1.62	SEP	.651±03
MM	183	UNL IAF-DUHHLET	.024	.020	24	60	198	102.6	150.6	76	77	1.62	SEP	.560±03
MM	184	UNL IAF-DUHHLET	.024	.020	24	60	259	75.2	108.9	71	70	1.57	SEP	.243±03
MM	185	UNL IAF-DUHHLET	.024	.020	24	60	269	68.8	99.8	70	70	1.64	UNDEF	.211±03
MM	186	UNL IAF-DUHHLET	.024	.020	24	60	262	50.4	79.5	69	70	1.51	MIX	.171±03
MM	187	UNL IAF-DUHHLET	.024	.020	24	60	293	48.2	62.5	68	69	1.69	MIX	.116±03
MM	188	UNL IAF-DUHHLET	.024	.020	24	60	300	53.9	80.9	70	70	1.58	M/S	.154±03
MM	189	UNL IAF-DUHHLET	.024	.020	24	60	295	89.7	135.6	73	72	1.57	SEP	.288±03
MM	190	UNL IAF-DUHHLET	.024	.020	24	60	99	50.7	74.5	68	82	1.64	MIX	.535±03
MM	191	UNL IAF-DUHHLET	.024	.020	24	60	98	51.9	77.0	67	93	1.64	MIX	.692±03
MM	192	UNL IAF-DUHHLET	.024	.020	24	60	98	51.8	76.5	71	149	1.69	M/S	.233±04
MM	193	UNL IAF-DUHHLET	.024	.020	24	60	99	51.5	76.4	78	177	1.70	M/S	.410±04
MM	194	UNL IAF-DUHHLET	.024	.020	24	60	79	53.0	74.5	80	200	1.73	M/S	.630±04
MM	195	UNL IAF-DUHHLET	.024	.020	24	60	202	49.9	71.8	82	196	1.77	SEP	.271±04
MM	196	UNL IAF-DUHHLET	.024	.020	24	60	202	49.6	70.9	124	178	1.69	SEP	.324±04
MM	197	UNL IAF-DUHHLET	.024	.020	24	60	202	43.1	67.7	112	89	1.69	MIX	.486±03
A-50	198	UNL IAF-DUHHLET	.024	.020	24	60	92	36.6	51.6	53	60	1.68	M/P	.275±03
A-50	199	UNL IAF-DUHHLET	.024	.020	24	60	94	45.4	66.5	74	85	1.58	UNDEF	.761±03
A-50	200	UNL IAF-DUHHLET	.024	.020	24	60	89	50.3	72.7	65	75	1.60	MIX	.641±03
A-50	201	UNL IAF-DUHHLET	.024	.020	24	60	97	52.6	76.5	68	73	1.59	M	.617±03
A-50	202	UNL IAF-DUHHLET	.024	.020	24	60	81	79.8	114.2	69	74	1.61	M	.114±04
A-50	203	UNL IAF-DUHHLET	.024	.020	24	60	102	90.3	127.2	72	72	1.63	MIX	.100±04
A-50	204	UNL IAF-DUHHLET	.024	.020	24	60	95	111.3	157.2	70	70	1.63	MIX	.125±04
A-50	205	UNL IAF-DUHHLET	.024	.020	24	60	201	41.2	49.7	66	68	1.91	M/P	.172±03
A-50	206	UNL IAF-DUHHLET	.024	.020	24	60	199	51.5	70.6	77	69	1.67	MIX	.207±03
A-50	207	UNL IAF-DUHHLET	.024	.020	24	60	193	114.1	162.0	80	81	1.61	SEP	.884±03
A-50	208	UNL IAF-DUHHLET	.024	.020	24	60	295	44.9	64.6	70	74	1.60	MIX	.174±03
A-50	209	UNL IAF-DUHHLET	.024	.020	24	60	291	43.6	64.1	63	63	1.57	MIX	.133±03
A-50	21	UNL IAF-DUHHLET	.024	.020	24	60	293	42.1	60.0	61	64	1.62	MIX	.123±03
A-50	211	UNL IAF-DUHHLET	.024	.020	24	60	290	42.8	67.5	62	88	1.47	MIX	.154±03
A-50	212	UNL IAF-DUHHLET	.024	.020	24	60	290	51.7	76.5	78	84	1.61	M/S	.291±03
A-50	213	UNL IAF-DUHHLET	.024	.020	24	60	289	74.2	106.3	78	79	1.60	SEP	.355±03
A-50	214	UNL IAF-DUHHLET	.024	.020	24	60	293	90.8	130.7	75	77	1.60	SEP	.410±03
A-50	215	UNL IAF-DUHHLET	.024	.020	24	60	292	112.8	163.2	71	75	1.59	SEP	.470±03
A-50	216	UNL IAF-DUHHLET	.024	.020	24	60	489	72.3	104.2	66	70	1.60	SEP	.157±03
A-50	217	UNL IAF-DUHHLET	.024	.020	24	60	491	92.6	133.4	68	68	1.60	SEP	.193±03
MM	218	XDT1	.024	.021	0	0	135	44.0	56.8	65	70	1.67	MIX	.238±03
MM	219	XDT1	.024	.021	0	0	124	50.3	63.5	72	73	1.70	MIX	.341±03
MM	220	XDT1	.024	.021	0	0	98	39.9	52.6	69	71	1.63	MIX	.327±03



TABLE B-II (cont.)

## HYPERGOLIC STREAM IMPINGEMENT DATA COMPILATION

## INVESTIGATOR LAWVER

FUEL TYPE	TEST NO.	MODE	PC (PSIA)	WAVG	WEP	WEO	PEF	RED	DELT (DEG F)	RELF	RELO	PPI (PSIA)	PPO	MRVP	XF	XO	XP	REBID
MM	181	MIX	295.	60.	13.6	9.6	126+05	330+05	128.	30+06	77+06	.9	13.8	30.8	.0034897.		57-08	15+03
MM	182	SFP	182.	124.	38.7	28.7	280+05	723+05	129.	.67+06	.17+07	1.1	16.9	32.0	.0110102.		59-08	65+03
MM	183	SFP	194.	121.	37.9	27.9	263+05	686+05	129.	.63+06	.16+07	1.0	17.3	33.7	.0111663.		62-08	58+03
MM	184	SFP	259.	84.	25.4	17.6	178+05	489+05	141.	.43+06	.11+07	.8	15.2	37.0	.0013770.		61-08	24+03
MM	185	MIX	269.	81.	22.2	16.6	163+05	444+05	141.	.39+06	.11+07	.8	14.8	36.0	.0015223.		59-08	21+03
MM	186	MIX	262.	62.	13.7	6.6	150+05	324+05	101.	.31+06	.78+06	.8	14.5	35.4	.004722.		61-08	17+03
MM	187	MIX	293.	51.	9.5	7.4	101+05	242+05	95.	.24+06	.68+06	.8	14.2	35.9	.0040298.		61-08	12+03
MM	188	M/S	100.	64.	16.3	11.3	132+05	348+05	108.	.32+06	.84+06	.8	14.8	36.0	.0033321.		62-08	15+03
MM	189	SFP	295.	104.	45.0	31.5	226+05	589+05	140.	.54+06	.14+07	.9	16.0	36.4	.0019571.		61-08	29+03
MM	190	MIX	99.	60.	4.6	3.2	134+05	317+05	61.	.33+06	.76+06	1.2	12.9	22.6	.0134107.		50-08	54+03
MM	191	MIX	94.	61.	5.0	3.3	154+05	321+05	49.	.37+06	.77+06	1.6	12.3	26.4	.0232498.		39-08	59+03
MM	192	M/S	94.	61.	5.4	3.4	220+05	336+05	40.	.55+06	.81+06	6.5	15.2	5.3	.0733618.		20-08	23+04
MM	193	M/S	99.	61.	5.4	3.6	275+05	344+05	27.	.66+06	.84+06	12.0	18.1	3.6	.1234448.		21-08	1+04
MM	194	M/S	99.	62.	6.4	3.8	275+05	363+05	18.	.79+06	.87+06	19.1	19.0	2.4	.1933715.		22-08	03+04
MM	195	SFP	202.	58.	10.8	7.0	292+05	346+05	54.	.70+06	.83+06	17.6	20.0	2.8	.0925358.		23-08	21+04
MM	196	SFP	202.	58.	10.2	6.8	257+05	437+05	68.	.62+06	.10+07	12.2	52.9	9.5	.0826073.		11-07	32+04
MM	197	MIX	202.	56.	7.9	6.0	131+05	408+05	115.	.31+06	.98+06	1.4	40.5	56.0	.0125927.		19-07	49+03
A-50	198	M/P	52.	42.	2.3	1.5	695+04	216+05	111.	.17+06	.52+06	2.1	9.4	15.1	.023786.		30-08	28+03
A-50	199	U/NFF	94.	54.	4.0	2.6	108+05	310+05	89.	.26+06	.72+06	2.1	14.5	13.8	.034363.		46-08	24+03
A-50	200	MIX	89.	59.	4.5	2.1	119+05	316+05	109.	.26+06	.76+06	2.1	13.2	14.2	.023722.		37-08	24+03
A-50	201	MIX	97.	62.	5.4	3.1	113+05	336+05	143.	.27+06	.81+06	2.0	14.2	15.8	.024571.		42-08	02+03
A-50	202	MIX	91.	93.	10.1	6.7	170+05	512+05	145.	.41+06	.12+07	2.0	14.5	15.6	.033521.		41-08	11+04
A-50	203	MIX	102.	104.	15.8	10.9	186+05	589+05	149.	.45+06	.14+07	1.9	15.6	17.6	.025277.		47-08	10+04
A-50	204	MIX	95.	129.	22.4	15.3	227+05	719+05	159.	.54+06	.17+07	1.9	14.8	17.5	.025235.		42-08	12+04
A-50	205	M/P	201.	44.	4.7	4.0	767+04	260+05	172.	.17+06	.62+06	1.8	13.5	16.9	.014752.		45-08	17+03
A-50	206	MIX	199.	59.	9.5	7.1	101+05	347+05	143.	.24+06	.83+06	1.8	17.7	21.2	.014886.		65-08	29+03
A-50	207	SFP	193.	132.	48.4	34.4	254+05	741+05	202.	.61+06	.19+07	2.4	19.0	17.5	.015149.		53-08	08+03
A-50	208	MIX	205.	52.	11.8	7.7	260+05	490+05	202.	.23+06	.70+06	2.0	14.8	16.1	.014598.		76-08	18+03
A-50	209	MIX	201.	52.	11.4	6.9	481+04	271+05	202.	.21+06	.65+06	1.5	12.6	18.0	.014607.		43-08	13+03
A-50	210	MIX	203.	44.	10.1	6.5	430+04	259+05	202.	.20+06	.62+06	1.6	12.0	16.7	.014857.		39-08	12+03
A-50	211	MIX	200.	51.	12.6	8.7	460+04	255+05	277.	.25+06	.64+06	1.8	12.3	15.5	.014549.		38-08	15+03
A-50	212	M/S	200.	62.	19.4	11.3	123+05	363+05	391.	.30+06	.87+06	2.6	18.1	15.9	.014691.		53-08	29+03
A-50	213	SEP	209.	87.	31.4	21.3	164+05	496+05	282.	.39+06	.12+07	2.3	17.3	16.9	.014850.		52-08	35+03
A-50	214	SEP	203.	106.	48.1	32.3	190+05	604+05	332.	.48+06	.14+07	2.2	16.9	17.1	.014849.		49-08	41+03
A-50	215	SEP	202.	132.	74.6	48.6	244+05	733+05	378.	.59+06	.18+07	2.1	15.2	16.8	.015081.		43-08	47+03
A-50	216	SFP	489.	85.	50.7	32.9	150+05	462+05	893.	.36+06	.11+07	1.9	14.2	16.8	.004720.		43-08	16+03
A-50	217	SFP	491.	108.	83.5	54.4	190+05	592+05	762.	.46+06	.14+07	1.8	14.2	17.6	.004841.		42-08	19+03
MM	218	MIX	115.	42.	3.8	3.3	276+04	274+05	214.	.98+03	.28+04	.8	13.2	32.6	.014698.		90-10	24+03
MM	219	MIX	124.	55.	4.4	4.1	112+05	328+05	209.	.11+08	.33+04	.9	15.6	34.4	.014973.		99-10	34+03
MM	220	MIX	98.	45.	2.4	2.0	913+04	256+05	183.	.91+03	.26+04	.8	14.5	34.2	.014863.		10-09	33+03

## Appendix B

TABLE B-II (cont.)

## HYPERGOLIC STREAM IMPINGMENT DATA COMPILATION

## INVESTIGATOR LANVER

FUEL TEST TYPE NO.	INJECTOR TYPE	ON OF (IN)	L/D	IMP ANGLE (DEG)	PC (PSIA)	VO (FT/S)	VF (FT/S)	TO (F)	TF (F)	HR WF/MD	MODE	REACT (SEC)
MM 221	XOTI	.024 .021	0.	0.	81.	32.6	42.6	62.	68.	1.66 1.024	MIX	.271+03
MM 222	XOTI	.024 .021	0.	0.	146.	59.7	76.1	76.	75.	1.69 .986	SEP	.379+03
MM 223	XOTI	.024 .021	0.	0.	194.	79.1	100.7	74.	97.	1.71 .918	SEP	.651+03
MM 224	XOTI	.024 .021	0.	0.	122.	50.6	63.6	77.	141.	1.77 .930	MIX	.151+04
MM 225	XOTI	.024 .021	0.	0.	123.	51.3	64.4	80.	164.	1.80 .909	MIX	.236+04
MM 226	XOTI	.024 .021	0.	0.	122.	51.2	66.0	93.	229.	1.82 .925	SEP	.803+04
MM 227	XOTI	.024 .021	0.	0.	122.	51.9	66.7	116.	242.	1.81 .929	SEP	.125+05
MM 228	XOTI	.024 .021	0.	0.	144.	61.3	78.7	127.	249.	1.80 .928	SEP	.158+05
MM 229	XOTI	.024 .021	0.	0.	119.	53.0	71.1	109.	245.	1.75 1.001	SEP	.133+05
MM 230	XOTI	.024 .021	0.	0.	122.	56.1	70.5	120.	268.	1.75 1.011	SEP	.200+05
MM 231	XOTI	.024 .021	0.	0.	146.	62.2	83.5	136.	280.	1.76 .999	SEP	.273+05
MM 232	XOTI	.024 .021	0.	0.	145.	63.7	86.0	162.	291.	1.72 1.022	SEP	.420+05
MM 233	XOTI	.024 .021	0.	0.	124.	53.3	73.3	153.	285.	1.69 1.080	SEP	.357+05
MM 234	SPLASH PLATE	.024 .021	0.	00.	123.	48.9	62.7	13.	70.	1.68 .996	M/S	.371+03
MM 235	SPLASH PLATE	.024 .021	0.	00.	102.	37.8	48.2	71.	72.	1.69 .981	MIX	.303+03
MM 236	SPLASH PLATE	.024 .021	0.	00.	81.	31.8	40.8	74.	76.	1.68 .997	M/P	.371+03
MM 237	SPLASH PLATE	.024 .021	0.	00.	144.	59.8	76.8	70.	82.	1.68 .999	SEP	.472+03
MM 238	SPLASH PLATE	.024 .021	0.	00.	160.	63.1	104.2	74.	79.	1.65 1.027	SEP	.470+03
MM 239	SPLASH PLATE	.024 .021	0.	00.	164.	53.2	70.1	74.	74.	1.66 1.052	M/S	.300+03
MM 240	SPLASH PLATE	.024 .021	0.	00.	160.	55.5	71.9	77.	79.	1.66 1.018	M/S	.368+03
MM 241	SPLASH PLATE	.024 .021	0.	00.	160.	53.4	66.4	78.	71.	1.67 1.001	M/S	.281+03
MM 242	SPLASH PLATE	.024 .021	0.	00.	192.	74.0	103.2	78.	75.	1.64 1.038	SEP	.406+03
MM 243	SPLASH PLATE	.024 .021	0.	00.	123.	44.9	66.3	79.	170.	1.72 1.015	SEP	.269+04
MM 244	SPLASH PLATE	.024 .021	0.	00.	117.	51.6	71.5	85.	239.	1.72 1.054	SEP	.938+04
MM 245	SPLASH PLATE	.024 .021	0.	00.	119.	52.4	73.1	136.	286.	1.70 1.009	SEP	.322+05
MM 246	SPLASH PLATE	.024 .021	0.	00.	139.	61.1	88.6	132.	283.	1.60 1.086	S/P	.302+05
MM 247	SPLASH PLATE	.024 .021	0.	00.	137.	64.7	89.0	153.	280.	1.69 1.058	SEP	.406+05
MM 248	SPLASH PLATE	.024 .021	0.	00.	147.	61.4	84.8	154.	287.	1.69 1.068	SEP	.360+05
MM 249	SPLASH PLATE	.024 .021	0.	00.	124.	48.1	51.4	73.	75.	2.15 2.818	MIX	.802+03
MM 250	TRIPLT	.050 .029	4.	32.	125.	49.7	48.8	70.	75.	2.37 2.332	MIX	.747+03
MM 251	TRIPLT	.050 .029	4.	32.	99.	38.5	38.6	68.	78.	2.33 2.424	MIX	.705+03
MM 252	TRIPLT	.050 .029	4.	32.	80.	31.7	30.6	72.	78.	2.41 2.259	MIX	.810+03
MM 253	TRIPLT	.050 .029	4.	32.	146.	54.1	63.4	72.	70.	2.13 2.879	MIX	.875+03
MM 254	TRIPLT	.050 .029	4.	32.	140.	70.6	71.8	71.	69.	2.28 2.503	SEP	.665+03
MM 255	TRIPLT	.050 .029	4.	32.	116.	52.1	51.6	77.	178.	2.23 2.789	MIX	.762+04
MM 256	TRIPLT	.050 .029	4.	32.	116.	53.8	61.5	76.	244.	2.27 2.828	M/S	.220+05
MM 257	TRIPLT	.050 .029	4.	32.	116.	50.7	71.6	100.	312.	1.90 4.039	SEP	.144+06
MM 258	TRIPLT	.050 .029	4.	32.	131.	65.3	74.6	120.	300.	2.31 2.796	SEP	.826+05
MM 259	TRIPLT	.050 .029	4.	32.	131.	65.4	71.2	153.	301.	2.30 2.697	SEP	.108+06
MM 260	TRIPLT	.050 .029	4.	32.	126.	50.4	67.5	59.	71.	1.76 4.279	M/P	.548+03
MM 275	SMALL TRIPLT	.314 .020	0.	32.								

TABLE B-II (cont.)

## HYPERGOLIC STREAM IMPINGEMENT DATA COMPILATION

## INVESTIGATOR LAHWER

FUEL TYPE	TEST NO.	MODE	PC (PSIA)	VAVG	WEF	WEO	REF	HEU	DELTA (DEG F)	REL F	RELO	PPF (PSIA)(PSTIA)	MRVP	XF	NO	XP	RESID
MMH	221	MTX	81.	34.	1.3	1.1	718+05	202+05	145.	72+03	20+04	8	12.3	32.7	.01	4913.	98-10
MMH	222	SFP	148.	66.	7.5	7.1	137+05	399+05	229.	14+08	40+04	1.0	17.3	35.6	.01	4997.	10-09
MMH	223	SFP	188.	87.	17.4	10.5	218+05	538+05	221.	22+08	54+04	1.8	18.6	21.2	.01	4977.	83-10
MMH	224	MTX	122.	55.	4.9	4.2	190+05	340+05	158.	19+04	34+04	5.3	17.7	7.5	.04	4954.	45-10
MMH	225	MTX	123.	54.	5.2	4.4	224+05	351+05	137.	22+08	35+04	8.6	19.0	5.0	.07	4964.	37-10
MMH	226	SFP	122.	54.	6.2	4.7	345+05	380+05	82.	34+08	38+04	30.9	26.2	2.1	.25	5008.	46-10
MMH	227	SFP	122.	57.	6.5	5.5	377+05	430+05	82.	38+04	44+04	37.0	44.4	2.9	.30	5031.	68-10
MMH	228	SFP	140.	68.	10.9	9.7	464+05	548+05	82.	46+04	55+04	42.3	56.5	3.2	.29	5072.	78-10
MMH	229	SFP	119.	60.	7.3	5.4	409+05	432+05	73.	41+04	43+04	39.3	37.8	2.4	.33	4716.	60-10
MMH	230	SFP	122.	59.	7.8	5.7	467+05	448+05	42.	47+04	45+04	56.8	48.2	2.1	.47	4972.	76-10
MMH	231	SFP	146.	70.	13.4	10.8	504+05	586+05	46.	59+04	59+04	65.9	68.5	2.6	.45	5062.	91-10
MMH	232	SFP	145.	72.	14.5	13.7	544+05	704+05	40.	65+04	70+04	74.7	116.0	3.7	.52	4993.	14-09
MMH	233	SFP	124.	61.	8.9	7.6	538+05	558+05	30.	54+04	56+04	69.7	97.1	3.4	.56	5031.	13-09
MMH	234	MTX	123.	58.	4.2	3.9	114+05	321+05	195.	11+04	32+04	1.0	16.4	32.3	.01	5049.	10-09
MMH	235	MTX	102.	42.	2.1	1.9	844+04	248+05	196.	84+03	25+04	9	19.2	34.6	.01	5412.	11-09
MMH	237	M/P	81.	35.	1.2	1.1	780+04	210+05	178.	74+03	21+04	1.0	16.5	33.0	.01	5119.	13-09
MMH	238	SFP	140.	66.	7.5	7.6	147+05	404+05	178.	15+04	40+04	1.2	18.1	31.0	.01	4853.	10-09
MMH	239	SFP	186.	89.	17.8	10.3	144+05	545+05	178.	14+04	55+04	1.1	18.6	34.1	.01	4653.	91-10
MMH	240	M/S	100.	60.	7.0	6.2	125+05	351+05	189.	12+04	35+04	9	16.5	35.0	.01	6128.	10-09
MMH	241	M/S	100.	62.	7.3	6.8	134+05	373+05	182.	13+04	37+04	1.1	17.7	32.6	.01	5785.	10-09
MMH	242	M/S	100.	59.	6.8	6.4	119+05	361+05	189.	12+04	36+04	8	18.1	42.1	.01	6250.	12-09
MMH	243	SFP	192.	88.	17.9	10.2	146+05	534+05	234.	19+04	53+04	1.0	18.1	37.2	.01	4857.	92-10
MMH	244	SFP	123.	56.	5.0	4.2	240+05	319+05	113.	24+04	34+04	10.7	18.6	4.2	.08	5008.	35-10
MMH	245	SFP	117.	59.	7.2	4.4	397+05	368+05	63.	40+04	36+04	35.1	21.6	1.6	.30	4639.	44-10
MMH	246	S/P	110.	60.	8.5	6.3	568+05	494+05	29.	55+04	49+04	72.0	68.9	2.4	.60	4411.	10-09
MMH	247	SFP	150.	73.	14.5	10.3	642+05	741+05	44.	64+04	54+04	68.2	67.8	2.3	.49	4667.	85-10
MMH	248	SFP	137.	74.	14.6	12.4	685+05	877+05	43.	66+04	68+04	72.0	97.1	3.3	.53	4584.	12-09
MMH	249	SFP	107.	70.	14.1	12.0	629+05	868+05	44.	63+04	65+04	71.2	99.1	3.4	.48	5180.	13-09
MMH	250	M/S	120.	64.	17.1	6.1	131+05	652+05	44.	50+05	28+06	1.0	16.0	33.2	.01	5126.	39-08
MMH	251	M/S	125.	62.	14.7	8.3	123+05	602+05	44.	49+05	26+06	1.0	14.8	30.8	.01	4944.	34-08
MMH	252	MTX	99.	56.	7.3	3.9	160+05	507+05	44.	40+05	37+04	1.1	14.2	27.2	.01	5020.	37-08
MMH	253	MTX	80.	40.	3.7	2.2	795+04	427+05	44.	32+04	37+04	1.1	15.6	29.8	.01	4990.	45-08
MMH	254	MTX	140.	80.	28.9	13.3	162+05	762+05	44.	65+05	31+06	1.0	15.6	31.5	.01	4789.	11-07
MMH	255	SFP	190.	101.	57.2	30.7	186+05	103+06	44.	75+05	31+06	8	15.2	38.3	.00	4926.	11-07
MMH	256	MTX	119.	79.	23.3	9.0	368+05	727+05	44.	12+06	24+04	12.7	17.7	3.4	.10	4433.	10-08
MMH	257	M/S	116.	75.	29.4	9.3	494+05	741+05	44.	20+06	30+06	38.5	17.3	1.2	.33	4207.	17-08
MMH	258	SFP	113.	91.	54.0	14.7	540+05	113+06	44.	37+06	45+06	100.6	74.1	1.9	.69	3884.	12-07
MMH	259	SFP	131.	91.	56.6	14.8	646+05	116+06	44.	34+06	46+06	65.8	48.2	1.5	.65	4082.	89-08
MMH	260	SFP	137.	84.	54.2	25.4	810+05	139+06	44.	33+06	46+06	67.0	97.1	2.8	.64	4463.	15-07
MMH	275	M/P	120.	81.	18.9	5.5	111+05	424+05	44.	45+05	37+06	8	11.4	27.3	.01	5204.	10-08

ORIGINAL PAGE IS  
OF POOR QUALITY

TABLE B-II (cont.)

## HYPERBOLIC STREAM IMPINGEMENT DATA COMPILATION

FUEL TEST TYPE NO.	INJECTOR TYPE	DN (IN)	DF (IN)	L/D	IMP ANGLE (DEG)	PC (PSIA)	VU (FT/S)	VF (FT/S)	TD (F)	TF (F)	HN	HF/HO	MODE	REACT (SEC)
MMH 276	SMALL TRIPLETT	.034	.020	4	32	129	47.0	65.9	78	77	1.66	4.760	MIX	.769+03
MMH 277	SMALL TRIPLETT	.034	.020	4	32	101	36.1	50.0	71	80	1.67	4.082	MIX	.736+03
MMH 278	SMALL TRIPLETT	.034	.020	4	32	81	30.5	38.7	71	77	1.84	3.887	MIX	.659+03
MMH 279	SMALL TRIPLETT	.034	.020	4	32	157	54.1	71.5	71	75	1.63	4.960	M/S	.650+03
MMH 280	SMALL TRIPLETT	.034	.020	4	32	210	72.2	102.7	72	73	1.64	4.896	SEP	.621+03
MMH 281	SMALL TRIPLETT	.034	.020	4	32	129	48.4	71.5	80	150	1.64	5.079	MIX	.377+04
MMH 282	SMALL TRIPLETT	.034	.020	4	32	129	48.8	74.5	85	226	1.66	5.163	M/S	.143+05
MMH 283	SMALL TRIPLETT	.034	.020	4	32	132	47.3	73.1	85	250	1.68	5.188	M/S	.191+05
MMH 284	SMALL TRIPLETT	.034	.020	4	32	130	49.3	76.0	130	287	1.66	5.211	SEP	.540+05
MMH 285	SMALL TRIPLETT	.034	.020	4	32	156	58.6	90.9	131	206	1.67	5.232	SEP	.613+05
MMH 286	SMALL TRIPLETT	.034	.020	4	32	150	61.3	95.0	145	297	1.66	5.280	SEP	.783+05
MMH 287	UNL IRE-DUINLET	.024	.020	24	60	124	49.2	72.5	72	72	1.63	1.309	MIX	.458+03
MMH 288	UNL IRE-DUINLET	.024	.020	24	60	94	39.3	57.6	73	72	1.62	1.299	M/P	.368+03
MMH 289	UNL IRE-DUINLET	.024	.020	24	60	78	33.5	50.1	75	76	1.54	1.439	M/P	.456+03
MMH 290	UNL IRE-DUINLET	.024	.020	24	60	78	33.2	48.6	74	75	1.62	1.294	M/P	.426+03
MMH 291	UNL IRE-DUINLET	.024	.020	24	60	147	54.9	84.1	75	75	1.66	1.241	MIX	.398+03
MMH 292	UNL IRE-DUINLET	.024	.020	24	60	144	78.9	113.9	76	76	1.65	1.265	M/S	.414+03
MMH 293	UNL IRE-DUINLET	.024	.020	24	60	123	50.7	76.7	75	185	1.68	1.293	SEP	.363+04
MMH 294	UNL IRE-DUINLET	.024	.020	24	60	123	51.0	76.5	80	249	1.74	1.282	SEP	.102+05
MMH 295	UNL IRE-DUINLET	.024	.020	24	60	121	51.0	82.4	116	240	1.65	1.160	SEP	.144+05
MMH 296	UNL IRE-DUINLET	.024	.020	24	60	145	64.5	99.4	131	290	1.71	1.296	SEP	.332+05
MMH 297	UNL IRE-DUINLET	.024	.020	24	60	144	66.6	104.6	142	294	1.65	1.371	SEP	.463+05

TABLE B-II (cont.)

## HYPERGOLIC STREAM IMPINGEMENT DATA COMPILATION

## INVESTIGATOR LAWVER

FUEL TYPE	TEST NO.	MODE	PC (PSIA)	WAVG	WEF	WED	REF	REQ	DELTA (DEG F)	RELU RELU	PPF (PSIA/PSIA)	MRVP	XP	RESD
MM	276	WIX	120.	79.	18.7	5.4	115+05	445+05	44.	18+06	1.0	18.1	15.2	17+03
MM	277	WIX	101.	60.	8.6	2.4	900+04	328+05	44.	13+06	1.1	15.2	27.6	15+08
MM	278	WIX	81.	47.	4.1	1.4	650+04	277+05	44.	11+06	1.0	15.2	29.8	17+08
MM	279	WIX	157.	93.	31.5	8.4	133+05	492+05	44.	20+06	1.0	15.2	31.6	13+08
MM	280	SEP	210.	121.	73.7	20.2	173+05	660+05	44.	26+06	1.0	15.2	31.6	12+08
MM	281	WIX	120.	84.	25.1	5.6	216+05	463+05	44.	19+06	1.0	15.2	31.6	12+08
MM	282	M/S	120.	86.	31.7	6.0	364+05	482+05	44.	19+06	1.0	15.2	31.6	12+08
MM	283	M/S	132.	64.	13.0	5.8	433+05	467+05	44.	19+06	1.0	15.2	31.6	12+08
MM	284	SEP	150.	105.	67.4	13.9	280+05	751+05	44.	30+06	1.0	15.2	31.6	12+08
MM	285	SEP	150.	110.	70.8	16.1	313+05	855+05	44.	34+06	1.0	15.2	31.6	12+08
MM	286	WIX	120.	58.	5.5	3.4	132+05	121+05	44.	12+06	1.0	15.2	31.6	12+08
MM	287	WIX	94.	46.	2.7	2.0	900+04	258+05	44.	12+06	1.0	15.2	31.6	12+08
MM	288	M/S	74.	39.	1.6	1.1	860+04	219+05	44.	12+06	1.0	15.2	31.6	12+08
MM	289	W/P	74.	39.	1.5	1.1	860+04	219+05	44.	12+06	1.0	15.2	31.6	12+08
MM	290	W/P	147.	147.	6.7	6.4	1.4+05	527+05	44.	12+06	1.0	15.2	31.6	12+08
MM	291	WIX	198.	42.	21.5	16.5	197+05	527+05	44.	12+06	1.0	15.2	31.6	12+08
MM	292	M/S	123.	60.	7.4	4.2	201+05	337+05	44.	12+06	1.0	15.2	31.6	12+08
MM	293	SEP	123.	61.	8.8	4.4	441+05	349+05	44.	12+06	1.0	15.2	31.6	12+08
MM	294	SEP	121.	40.	9.4	5.7	478+05	487+05	44.	12+06	1.0	15.2	31.6	12+08
MM	295	SEP	121.	40.	9.4	5.7	478+05	487+05	44.	12+06	1.0	15.2	31.6	12+08
MM	296	SEP	145.	77.	18.4	11.2	718+05	590+05	44.	12+06	1.0	15.2	31.6	12+08
MM	297	SEP	145.	77.	18.4	11.2	718+05	590+05	44.	12+06	1.0	15.2	31.6	12+08
MM	298	SEP	145.	77.	18.4	11.2	718+05	590+05	44.	12+06	1.0	15.2	31.6	12+08
MM	299	SEP	145.	77.	18.4	11.2	718+05	590+05	44.	12+06	1.0	15.2	31.6	12+08
MM	300	SEP	145.	77.	18.4	11.2	718+05	590+05	44.	12+06	1.0	15.2	31.6	12+08
MM	301	SEP	145.	77.	18.4	11.2	718+05	590+05	44.	12+06	1.0	15.2	31.6	12+08
MM	302	SEP	145.	77.	18.4	11.2	718+05	590+05	44.	12+06	1.0	15.2	31.6	12+08
MM	303	SEP	145.	77.	18.4	11.2	718+05	590+05	44.	12+06	1.0	15.2	31.6	12+08
MM	304	SEP	145.	77.	18.4	11.2	718+05	590+05	44.	12+06	1.0	15.2	31.6	12+08
MM	305	SEP	145.	77.	18.4	11.2	718+05	590+05	44.	12+06	1.0	15.2	31.6	12+08
MM	306	SEP	145.	77.	18.4	11.2	718+05	590+05	44.	12+06	1.0	15.2	31.6	12+08
MM	307	SEP	145.	77.	18.4	11.2	718+05	590+05	44.	12+06	1.0	15.2	31.6	12+08
MM	308	SEP	145.	77.	18.4	11.2	718+05	590+05	44.	12+06	1.0	15.2	31.6	12+08
MM	309	SEP	145.	77.	18.4	11.2	718+05	590+05	44.	12+06	1.0	15.2	31.6	12+08
MM	310	SEP	145.	77.	18.4	11.2	718+05	590+05	44.	12+06	1.0	15.2	31.6	12+08
MM	311	SEP	145.	77.	18.4	11.2	718+05	590+05	44.	12+06	1.0	15.2	31.6	12+08
MM	312	SEP	145.	77.	18.4	11.2	718+05	590+05	44.	12+06	1.0	15.2	31.6	12+08
MM	313	SEP	145.	77.	18.4	11.2	718+05	590+05	44.	12+06	1.0	15.2	31.6	12+08
MM	314	SEP	145.	77.	18.4	11.2	718+05	590+05	44.	12+06	1.0	15.2	31.6	12+08
MM	315	SEP	145.	77.	18.4	11.2	718+05	590+05	44.	12+06	1.0	15.2	31.6	12+08
MM	316	SEP	145.	77.	18.4	11.2	718+05	590+05	44.	12+06	1.0	15.2	31.6	12+08
MM	317	SEP	145.	77.	18.4	11.2	718+05	590+05	44.	12+06	1.0	15.2	31.6	12+08
MM	318	SEP	145.	77.	18.4	11.2	718+05	590+05	44.	12+06	1.0	15.2	31.6	12+08
MM	319	SEP	145.	77.	18.4	11.2	718+05	590+05	44.	12+06	1.0	15.2	31.6	12+08
MM	320	SEP	145.	77.	18.4	11.2	718+05	590+05	44.	12+06	1.0	15.2	31.6	12+08
MM	321	SEP	145.	77.	18.4	11.2	718+05	590+05	44.	12+06	1.0	15.2	31.6	12+08
MM	322	SEP	145.	77.	18.4	11.2	718+05	590+05	44.	12+06	1.0	15.2	31.6	12+08
MM	323	SEP	145.	77.	18.4	11.2	718+05	590+05	44.	12+06	1.0	15.2	31.6	12+08
MM	324	SEP	145.	77.	18.4	11.2	718+05	590+05	44.	12+06	1.0	15.2	31.6	12+08
MM	325	SEP	145.	77.	18.4	11.2	718+05	590+05	44.	12+06	1.0	15.2	31.6	12+08
MM	326	SEP	145.	77.	18.4	11.2	718+05	590+05	44.	12+06	1.0	15.2	31.6	12+08
MM	327	SEP	145.	77.	18.4	11.2	718+05	590+05	44.	12+06	1.0	15.2	31.6	12+08
MM	328	SEP	145.	77.	18.4	11.2	718+05	590+05	44.	12+06	1.0	15.2	31.6	12+08
MM	329	SEP	145.	77.	18.4	11.2	718+05	590+05	44.	12+06	1.0	15.2	31.6	12+08
MM	330	SEP	145.	77.	18.4	11.2	718+05	590+05	44.	12+06	1.0	15.2	31.6	12+08
MM	331	SEP	145.	77.	18.4	11.2	718+05	590+05	44.	12+06	1.0	15.2	31.6	12+08
MM	332	SEP	145.	77.	18.4	11.2	718+05	590+05	44.	12+06	1.0	15.2	31.6	12+08
MM	333	SEP	145.	77.	18.4	11.2	718+05	590+05	44.	12+06	1.0	15.2	31.6	12+08
MM	334	SEP	145.	77.	18.4	11.2	718+05	590+05	44.	12+06	1.0	15.2	31.6	12+08
MM	335	SEP	145.	77.	18.4	11.2	718+05	590+05	44.	12+06	1.0	15.2	31.6	12+08
MM	336	SEP	145.	77.	18.4	11.2	718+05	590+05	44.	12+06	1.0	15.2	31.6	12+08
MM	337	SEP	145.	77.	18.4	11.2	718+05	590+05	44.	12+06	1.0	15.2	31.6	12+08
MM	338	SEP	145.	77.	18.4	11.2	718+05	590+05	44.	12+06	1.0	15.2	31.6	12+08
MM	339	SEP	145.	77.	18.4	11.2	718+05	590+05	44.	12+06	1.0	15.2	31.6	12+08
MM	340	SEP	145.	77.	18.4	11.2	718+05	590+05	44.	12+06	1.0	15.2	31.6	12+08
MM	341	SEP	145.	77.	18.4	11.2	718+05	590+05	44.	12+06	1.0	15.2	31.6	12+08
MM	342	SEP	145.	77.	18.4	11.2	718+05	590+05	44.	12+06	1.0	15.2	31.6	12+08
MM	343	SEP	145.	77.	18.4	11.2	718+05	590+05	44.	12+06	1.0	15.2	31.6	12+08
MM	344	SEP	145.	77.	18.4	11.2	718+05	590+05	44.	12+06	1.0	15.2	31.6	12+08
MM	345	SEP	145.	77.	18.4	11.2	718+05	590+05	44.	12+06	1.0	15.2	31.6	12+08
MM	346	SEP	145.	77.	18.4	11.2	718+05	590+05	44.	12+06	1.0	15.2	31.6	12+08
MM	347	SEP	145.	77.	18.4	11.2	718+05	590+05	44.	12+06	1.0	15.2	31.6	12+08
MM	348	SEP	145.	77.	18.4	11.2	718+05	590+05	44.	12+06	1.0	15.2	31.6	12+08
MM	349	SEP	145.	77.	18.4	11.2	718+05	590+05	44.	12+06	1.0	15.2	31.6	12+08
MM	350	SEP	145.	77.	18.4	11.2	718+05	590+05	44.	12+06	1.0	15.2	31.6	12+08
MM	351	SEP	145.	77.	18.4	11.2	718+05	590+05	44.	12+06	1.0	15.2	31.6	12+08
MM	352	SEP	145.	77.	18.4	11.2	718+05	590+05	44.	12+06	1.0	15.2	31.6	12+08
MM	353	SEP	145.	77.	18.4	11.2	718+05	590+05	44.	12+06	1.0	15.2	31.6	12+08
MM	354	SEP	145.	77.	18.4	11.2	718+05	590+05	44.	12+06	1.0	15.2	31.6	12+08
MM	355	SEP	145.	77.	18.4	11.2	718+05	590+05	44.	12+06	1.0	15.2	31.6	12+08
MM	356	SEP	145.	77.	18.4	11.2	718+05	590+05	44.	12+06	1.0	15.2	31.6	12+08
MM	357	SEP	145.	77.	18.4	11.2	718+05	590+05	44.	12+06	1.0	15.2	31.6	12+08
MM	358	SEP	145.	77.	18.4	11.2	718+05	590+05	44.	12+06	1.0	15.2	31.6	12+08
MM	359	SEP	145.	77.	18.4	11.2	718+05	590+05	44.	12+06	1.0	15.2	31.6	12+08
MM	360	SEP	145.	77.	18.4	11.2	718+05	590+05	44.	12+06	1.0	15.2	31.6	12+08
MM	361	SEP	145.	77.	18.4	11.2	718+05	590+05	44.	12+06	1.0	15.2	31.6	12+08
MM	362	SEP	145.	77.	18.4	11.2	718+05	590+05	44.	12+06	1.0	15.2	31.6	12+08
MM	363	SEP	145.	77.	18.4	11.2	718+05	590+05	44.	12+06	1.0	15.2	31.6	12+08
MM	364	SEP	145.	77.	18.4	11.2	718+05	590+05	44.	12+06	1.0	15.2	31.6	12+08
MM	365	SEP	145.	77.	18.4	11.2	718+05	590+05	44.	12+06	1.0	15.2	31.6	12+08
MM	366	SEP												

TABLE B-II (cont.)

## HYPERGOLIC STREAM IMPINGMENT DATA COMPILATION

INVESTIGATOR SCHNEIDER

TEST SERIES 0002-673-XXX

FUEL TEST TYPE NO.	INJECTOR TYPE	MUNE	DU	OF	L/D	ANGLE (DEG)	PC (PSIA)	REF	VO (FT/S)	VF (FT/S)	TU (F)	TF (F)	HR	M/HNO	MEF	MHVP	PPU (PSIA)	PPF (PSIA)
101	MUNOT	UNDEF	.032	.023	12	78	215	.171x05	80.1	113.5	47	48	2.20	.044	25.5	38.7	8.0	14
102	MUNOT	UNDEF	.032	.023	12	74	180	.142x05	88.2	94.9	46	50	2.90	.371	15.0	37.1	6.2	14
103	MUNOT	UNDEF	.032	.023	12	74	139	.129x05	48.4	76.3	77	59	1.94	.613	7.6	59.2	17.7	6
104	MUNOT	UNDEF	.032	.023	12	74	139	.122x05	47.9	75.2	97	55	1.91	.622	7.3	102.6	20.7	5
105	MUNOT	UNDEF	.032	.023	12	74	140	.129x05	47.8	74.1	77	62	1.98	.762	7.2	55.2	17.7	6
106	MUNOT	UNDEF	.032	.023	12	74	83	.023x04	29.6	45.4	60	60	2.00	.766	1.6	52.6	19.0	7
107	MUNOT	UNDEF	.032	.023	12	74	110	.111x05	38.8	59.3	80	69	2.01	.700	3.7	47.1	19.0	8
108	MUNOT	UNDEF	.032	.023	12	74	144	.147x05	84.3	46.2	80	71	2.01	.761	16.9	43.9	19.0	8
109	MUNOT	UNDEF	.032	.023	12	74	223	.230x05	80.1	118.9	82	73	2.07	.717	30.4	43.3	20.0	9
110	MUNOT	UNDEF	.032	.023	12	74	171	.124x05	38.8	69.9	72	64	1.71	1.054	7.9	47.0	15.0	7
111	MUNOT	UNDEF	.032	.023	12	74	94	.785x04	26.5	48.1	72	84	1.99	.778	1.7	47.0	15.0	7
112	MUNOT	UNDEF	.032	.023	12	74	143	.198x05	91.2	93.1	74	84	3.04	.336	16.1	29.8	16.1	10.2
113	MUNOT	MIX	.032	.023	12	78	149	.156x05	51.9	80.6	69	73	2.00	.777	9.3	32.0	14.2	9
114	MUNOT	MIX	.032	.023	12	74	116	.118x05	34.2	61.1	71	75	1.94	.624	4.1	33.5	15.2	9
115	MUNOT	M/S	.032	.023	12	74	140	.217x05	64.2	105.3	74	80	2.04	.746	20.5	29.7	16.5	11.1
116	MUNOT	M/S	.032	.023	12	74	227	.271x05	87.4	130.6	80	81	2.07	.722	37.5	33.1	19.0	11.1
117	MUNOT	UNDEF	.032	.023	12	74	259	.164x05	41.2	81.1	73	81	1.56	1.246	16.5	28.3	16.0	11.1
118	MUNOT	SEP	.032	.023	12	74	164	.157x05	34.1	76.2	84	77	1.36	1.665	9.6	26.0	14.2	11.0
119	MUNOT	MIX	.032	.023	12	74	164	.201x05	102.6	102.6	80	75	3.10	.321	10.4	38.8	19.0	11.0
120	MUNOT	MIX	.032	.023	12	74	90	.047x04	26.7	33.1	71	74	2.50	.496	4	32.5	15.2	9
121	MUNOT	MIX	.032	.023	12	74	91	.054x04	25.5	34.4	70	89	2.08	.724	1.3	22.0	14.0	11.4
122	MUNOT	MIX	.032	.023	12	74	91	.103x05	25.0	39.9	71	104	1.98	.808	1.5	13.5	15.2	2.4
123	MUNOT	M/S	.032	.023	12	74	140	.258x05	50.4	61.0	74	137	2.00	.804	10.4	7.0	16.5	4.9
124	MUNOT	M/S	.032	.023	12	74	243	.162x05	34.8	47.6	75	130	2.37	.570	5.7	8.8	16.9	4.2
125	MUNOT	MIX	.032	.023	12	74	240	.754x04	22.3	24.4	71	112	2.50	.568	2.0	12.4	15.2	2.6
126	MUNOT	MIX	.032	.023	12	74	241	.174x05	50.6	52.6	71	130	3.04	.336	7.0	8.0	15.2	4.2
127	MUNOT	M/S	.032	.023	12	74	80	.222x05	44.1	70.9	72	135	2.00	.804	4.4	7.5	15.0	4.7
128	MUNOT	M/S	.032	.023	12	74	80	.448x05	141.6	142.9	98	145	3.14	.321	19.0	10.6	29.4	5.9
129	MUNOT	MIX	.032	.023	12	74	240	.544x04	22.6	23.2	73	107	3.10	.329	1.4	14.5	16.0	2.4
130	MUNOT	UNDEF	.032	.023	12	74	87	.112x05	25.9	35.5	68	121	2.10	.727	1.4	8.4	13.5	3.4
131	MUNOT	MIX	.032	.023	12	74	90	.109x05	26.0	36.0	84	122	2.20	.664	1.4	8.3	12.9	3.5
132	MUNOT	UNDEF	.032	.023	12	74	163	.354x05	110.2	109.0	112	140	3.15	.314	20.9	16.5	40.5	5.1
133	MUNOT	MIX	.032	.023	12	74	164	.341x05	110.1	109.5	112	134	3.12	.319	20.9	16.4	40.5	5.1
134	MUNOT	UNDEF	.032	.023	12	74	153	.35x05	52.9	115.1	108	131	1.43	1.520	21.4	17.4	37.0	4.3
135	MUNOT	SEP	.032	.023	12	74	192	.325x05	71.0	109.0	117	127	2.01	.761	24.2	23.5	45.4	3.9
136	MUNOT	M/S	.032	.023	12	74	140	.258x05	53.8	66.2	114	124	1.92	.835	11.3	23.7	45.5	3.6
137	MUNOT	MIX	.032	.023	12	74	113	.178x05	41.4	66.4	67	113	1.99	.805	5.1	11.2	13.6	2.7
138	MUNOT	MIX	.032	.023	12	74	80	.147x05	34.2	52.2	122	120	2.00	.762	2.3	30.8	51.0	3.3
139	MUNOT	MIX	.032	.023	12	74	162	.332x05	106.9	110.4	123	129	3.02	.336	20.8	25.4	11.0	4.1
140	MUNOT	MIX	.032	.023	12	74	245	.622x04	23.1	30.0	76	116	2.40	.541	6.3	20.1	26.1	2.9

TABLE B-II (cont.)

## HYPERGOLIC STREAM IMPINGEMENT DATA COMPILATION

INVESTIGATOR SCHNEIDLER

FUEL TEST TYPE NO.	INJECTION TIME	MODE	DU (IN)	UF (IN)	L/D	IMP ANGLE (DEG)	PC (PSIA)	REF	VU (FT/S)	VF (FT/S)	TU (F)	TF (F)	MR	MF/MU	MEF	MRVP	PPU (PSIA)	PPF
4M 141	MOROT	MIX	.032	.023	12	74	9	.410+05	17.2	140.4	62	127	1.97	.818	18.2	11.0	20.0	3.9
4M 142	MOROT	MIX	.032	.023	12	74	9	.085+04	23.9	32.8	80	114	2.30	.596	2.7	14.7	19.0	2.7
4M 143	MOROT	UNDEF	.032	.023	12	74	121	.211+05	80.6	46.4	74	87	2.22	.033	11.0	25.4	10.5	1.3
4M 144	MOROT	UNDEF	.032	.023	12	74	140	.170+05	53.1	61.2	70	82	2.04	.750	4.5	25.0	14.5	1.2
4M 145	MOROT	UNDEF	.032	.023	12	74	140	.165+05	53.1	79.5	71	81	2.09	.713	9.1	26.9	15.2	1.1
4M 146	MOROT	UNDEF	.032	.023	12	74	114	.124+05	41.5	60.6	69	79	2.13	.687	4.1	27.1	14.5	1.1
4M 147	MOROT	UNDEF	.032	.023	12	74	193	.200+05	67.5	102.7	69	77	2.04	.704	19.0	20.5	14.5	1.0
4M 148	MOROT	UNDEF	.032	.023	12	74	104	.152+05	35.0	76.5	68	78	1.45	1.452	4.2	20.7	14.2	1.0
4M 149	MOROT	UNDEF	.032	.023	12	74	150	.209+05	104.5	105.9	72	75	3.00	.331	10.8	32.4	15.0	1.0
4M 150	MOROT	UNDEF	.024	.020	5	50	113	.118+05	49.4	69.4	67	74	1.70	.027	4.2	29.9	13.6	1.0
4M 151	MOROT	UNDEF	.024	.020	5	50	109	.327+05	44.4	64.9	72	219	1.00	.408	5.3	1.5	15.8	20.7
4M 152	MOROT	UNDEF	.024	.020	5	50	101	.307+05	45.9	70.6	63	252	1.65	.078	5.9	1.2	20.5	44.6
4M 153	MOROT	MIX	.024	.020	5	50	84	.397+05	144.2	210.3	73	83	1.65	.078	26.9	27.0	10.5	1.2
4M 154	MOROT	MIX	.024	.020	5	50	84	.251+05	100.7	147.9	72	74	1.62	.407	10.0	33.4	15.0	1.0
4M 155	MOROT	MIX	.024	.020	5	50	83	.152+05	54.4	109.2	72	73	1.57	.905	5.0	34.4	15.0	1.0
4M 156	MOROT	MIX	.024	.020	5	50	103	.115+05	41.7	119.2	70	70	1.63	.025	12.1	30.0	14.0	1.0
4M 157	MOROT	MIX	.024	.020	5	50	114	.119+05	49.0	68.7	72	70	1.70	.025	4.5	31.5	15.0	1.0
4M 158	MOROT	MIX	.024	.020	5	50	144	.150+05	64.0	41.4	73	70	1.00	.001	10.4	34.9	10.4	1.0
4M 159	MOROT	MIX	.024	.020	5	50	191	.197+05	42.0	117.4	74	73	1.00	.002	21.4	30.1	10.5	1.0
4M 160	MOROT	MIX	.024	.020	5	50	291	.112+05	48.4	65.3	76	75	1.70	.700	10.4	35.0	17.5	1.0
4M 161	MOROT	MIX	.024	.020	5	50	390	.155+05	64.6	92.4	74	73	1.60	.002	28.1	30.1	10.5	1.0
4M 162	MOROT	MIX	.024	.020	5	50	141	.014+04	20.1	34.6	79	79	1.79	.741	1.1	34.1	10.5	1.0
4M 163	MOROT	MIX	.024	.020	5	50	300	.964+04	42.1	50.4	74	71	1.71	.011	10.9	30.5	10.5	1.0
4M 164	MOROT	MIX	.024	.020	5	50	344	.043+04	29.7	37.5	76	75	1.80	.071	4.0	35.0	17.5	1.0
4M 165	MOROT	MIX	.024	.020	5	50	255	.157+05	64.0	97.4	64	68	1.00	.043	22.5	37.5	14.2	1.0
4M 166	MOROT	MIX	.024	.020	5	50	190	.144+05	64.5	92.4	64	68	1.00	.063	13.0	30.0	14.5	1.0
4M 167	MOROT	MIX	.024	.020	5	50	200	.203+05	104.2	150.7	71	78	1.65	.077	30.1	29.1	15.2	1.1
4M 168	MOROT	MIX	.024	.020	5	50	193	.923+04	40.4	54.3	73	74	1.79	.702	4.7	34.2	10.0	1.0
4M 169	MOROT	MIX	.024	.020	5	50	197	.103+05	42.0	62.1	72	71	1.04	.083	4.0	30.7	15.0	1.0
4M 170	MOROT	MIX	.024	.020	5	50	410	.412+05	60.4	95.6	73	213	1.04	.900	4.0	1.7	10.0	24.2
4M 171	MOROT	MIX	.024	.020	5	50	190	.305+05	45.4	70.0	77	207	1.07	.920	5.2	2.0	17.7	21.9
4M 172	MOROT	MIX	.024	.020	5	50	100	.391+05	45.5	71.8	87	244	1.07	.945	5.9	1.5	22.0	30.5
4M 173	MOROT	MIX	.024	.020	5	50	151	.381+05	44.0	69.0	104	253	1.08	.921	8.3	2.1	33.9	40.1
4M 174	MOROT	MIX	.036	.030	5	50	131	.224+05	54.0	81.3	63	43	1.72	.001	11.0	34.0	20.5	1.2
4M 175	MOROT	MIX	.036	.030	5	50	133	.209+05	59.0	60.7	67	76	1.72	.745	10.7	44.4	22.0	1.0
4M 176	MOROT	MIX	.036	.030	5	50	145	.200+05	57.5	74.5	60	70	1.71	.809	14.7	37.7	14.0	1.0
4M 177	MOROT	MIX	.036	.030	5	50	319	.145+05	57.1	70.1	71	75	1.79	.744	22.4	31.6	15.2	1.0
4M 178	MOROT	MIX	.036	.030	5	50	149	.960+04	27.1	40.1	60	68	1.61	.920	3.0	35.0	15.5	1.0
4M 179	MOROT	MIX	.036	.030	5	50	190	.107+05	20.5	41.8	76	75	1.62	.904	4.3	35.0	17.5	1.0
4M 180	MOROT	MIX	.036	.030	5	50	299	.024+04	27.4	30.2	72	68	1.90	.057	4.3	40.0	15.0	1.0

# Appendix B

TABLE B-II (cont.)

## HYPERGOLIC STREAM IMPINGEMENT DATA COMPILATION

INVESTIGATOR SCHNEIDER

FUEL TEST NO.	INJECTOR TYPE	MODE	DU (in)	DF (in)	L/D	IMP ANGLE (DEG)	PC (PSIA)	KEP (FT/S)	VO (FT/S)	VF (FT/S)	TU (F)	TF (F)	MH	MF/HU	NEP	MRVP	PPU (PSIA)	PPF (PSIA)
181	UNLINE UNIM SE	MIX	.036	.036	5	50	299	.921+04	27.2	37.9	69	69	1.71	.614	5.3	30.0	14.3	0
182	UNLINE UNIM SE	MIX	.036	.036	5	50	81	.924+04	24.8	34.4	67	68	1.72	.605	1.2	30.5	14.3	0
183	UNLINE UNIM SE	SLO	.036	.036	5	50	79	.953+05	66.6	90.6	81	77	1.63	.690	9.3	37.0	19.5	1.0
184	UNLINE UNIM SE	SEP	.036	.036	5	50	195	.194+05	52.5	76.0	70	77	1.65	.677	14.1	29.1	14.0	1.0
185	UNLINE UNIM SF	SEP	.036	.036	5	50	75	.980+05	42.1	60.7	70	225	1.66	.453	5.5	1.3	14.0	20.4
186	UNLINE UNIM SE	SEP	.036	.036	5	50	74	.161+06	104.7	173.7	130	265	1.63	.671	40.5	2.7	60.0	54.5
187	UNLINE UNIM SE	SLO	.036	.036	5	50	98	.319+05	30.3	44.1	114	223	1.72	.650	3.2	3.9	47.3	20.4
188	UNLINE UNIM SE	M/S	.036	.036	5	50	115	.146+06	110.5	172.0	130	250	1.62	.496	60.1	3.0	46.3	43.1
189	UNLINE UNIM SE	SEP	.036	.036	5	50	150	.374+05	29.8	46.0	124	243	1.65	.435	5.5	3.4	52.9	37.8
190	UNLINE UNIM SE	M/S	.036	.036	5	50	87	.280+05	74.7	80.0	65	75	1.68	.693	7.7	27.0	13.2	1.0
191	UNLINE UNIM CORE	UNDEF	.036	.036	1	32	87	.101+05	38.1	44.1	83	70	1.62	.714	2.2	40.9	20.5	0
192	UNLINE UNIM CORE	M/S	.036	.036	1	32	97	.970+04	37.8	43.4	64	68	1.66	.691	2.1	34.2	12.9	0
193	UNLINE UNIM CORE	M/S	.036	.036	1	32	63	.302+05	39.2	45.0	74	67	1.61	.728	1.5	44.5	16.5	1.7
194	UNLINE UNIM CORE	M/S	.036	.036	1	32	97	.930+04	25.6	24.8	71	65	1.56	.683	.9	43.9	15.2	1.7
195	UNLINE UNIM CORE	M/S	.036	.036	1	32	68	.935+04	25.9	24.1	64	65	1.59	.683	.7	42.0	14.5	1.7
196	UNLINE UNIM CORE	M/S	.036	.036	1	32	43	.923+05	112.2	127.0	76	81	1.67	.681	2.3	30.9	17.3	1.1
197	UNLINE UNIM CORE	M/S	.036	.036	1	32	43	.923+05	74.4	60.3	62	73	1.65	.703	7.7	27.0	12.3	1.9
198	UNLINE UNIM CORE	M/S	.036	.036	1	32	50	.198+05	74.4	64.9	72	72	1.66	.688	4.2	35.5	15.0	1.9
199	UNLINE UNIM CORE	M/S	.036	.036	1	32	195	.103+05	39.0	44.3	70	72	1.67	.681	4.5	33.7	14.0	0
200	UNLINE UNIM CORE	UNDEF	.036	.036	1	32	130	.990+05	50.9	73.9	71	221	1.44	1.007	10.9	1.4	15.2	27.5
201	UNLINE UNIM CORE	UNDEF	.036	.036	1	32	140	.216+5	56.7	73.2	71	231	1.63	.793	11.6	1.2	13.2	31.7
202	UNLINE UNIM CORE	SEP	.036	.036	1	32	132	.507+05	52.0	74.2	71	226	1.47	.971	11.3	1.3	15.2	24.0
203	UNLINE UNIM CORE	SEP	.036	.036	1	32	140	.981+05	56.4	72.9	75	220	1.61	.602	11.4	1.0	16.9	27.1
204	UNLINE UNIM CORE	SEP	.036	.036	1	32	131	.916+05	55.4	61.8	71	216	1.61	.636	6.1	1.5	15.2	26.3
205	UNLINE UNIM CORE	SEP	.036	.036	1	32	121	.309+05	39.9	57.0	69	215	1.84	1.004	6.1	1.5	14.5	25.0
206	UNLINE UNIM CORE	SEP	.036	.036	1	32	113	.353+05	46.0	54.5	69	214	1.80	.942	5.3	1.5	14.5	24.0
207	UNLINE UNIM CORE	SEP	.036	.036	1	32	103	.352+05	43.6	54.3	69	217	1.65	.766	4.6	1.4	14.5	23.8
208	UNLINE UNIM CORE	SEP	.036	.036	1	32	119	.442+05	45.0	64.7	71	226	1.66	.984	7.1	1.3	15.2	24.0
209	UNLINE UNIM CORE	SEP	.036	.036	1	32	204	.140+05	79.2	78.1	75	77	1.76	.429	5.4	163.7	17.3	1.3
210	UNLINE UNIM CORE	SEP	.036	.036	1	32	202	.940+04	39.8	38.7	76	80	1.69	.576	1.6	163.0	16.1	1.3
211	UNLINE UNIM CORE	SEP	.036	.036	1	32	397	.993+04	41.5	41.3	75	79	1.66	.599	4.0	150.5	16.1	1.3
212	UNLINE UNIM CORE	SEP	.036	.036	1	32	301	.195+05	80.1	81.9	76	76	1.61	.635	12.1	163.7	17.3	1.3
213	UNLINE UNIM CORE	SEP	.036	.036	1	32	110	.350+05	87.0	90.6	70	150	1.65	.631	6.3	19.2	14.0	2.5
214	UNLINE UNIM CORE	SEP	.036	.036	1	32	104	.990+05	81.6	87.6	75	143	1.62	.603	6.1	11.3	16.9	5.2
215	UNLINE UNIM CORE	SEP	.036	.036	1	32	106	.355+05	94.9	90.2	76	153	1.60	.628	6.2	20.7	17.3	2.7
216	UNLINE UNIM CORE	SEP	.036	.036	1	32	104	.914+05	86.7	103.9	76	155	1.43	.638	8.3	19.9	17.3	2.9
217	UNLINE UNIM CORE	SEP	.036	.036	1	32	120	.914+05	102.9	105.3	75	155	1.79	.535	10.0	19.4	16.9	2.9
218	UNLINE UNIM CORE	SEP	.036	.036	1	32	137	.963+05	112.1	118.5	75	152	1.62	.652	13.5	20.7	16.9	2.7
219	UNLINE UNIM CORE	SEP	.036	.036	1	32	124	.963+05	101.5	120.1	75	149	1.43	.636	13.0	22.2	16.9	2.5
220	UNLINE UNIM CORE	SEP	.036	.036	1	32	124	.961+05	101.5	120.1	75	149	1.43	.636	13.0	22.2	16.9	2.5



TABLE B-II (cont.)

HYPERGEOMETRIC STREAM IMPINGEMENT DATA (CONTINUATION)																	
INVESTIGATOR SCHNEFJURM																	
FUEL TEST TYPE NO.	INJECTION TYPE	MODE	NO (10)	PF (10)	L/D ANGLE (DEG)	PC (PSIA)	KEP	VI (FT/SEC)	VE (FT/SEC)	TU (FT)	TF (FT)	MM (FT/MI)	MEP	MHVP	MPU (PSIA)	MPT	
42-4 121	VALVE	SE	024	020	5	70	203005	124.6	157.0	77	70	1.05	757	0.0	175.5	17.1	5
42-4 122	VALVE	SE	024	020	5	70	257005	124.5	157.7	80	74	1.04	764	7.0	196.2	19.0	5
42-4 123	VALVE	SE	024	020	5	70	101005	90.0	61.5	76	74	1.50	910	1.7	160.5	17.5	5
42-4 124	VALVE	SE	024	020	5	200	118005	90.0	104.5	76	74	1.81	500	9.9	180.2	17.5	5
42-4 125	VALVE	SE	024	020	5	197	051004	34.0	34.0	76	73	1.76	665	1.3	184.9	17.5	5
42-4 126	VALVE	SE	024	020	5	200	113005	55.0	60.6	74	77	1.63	776	4.2	175.0	16.1	5
42-4 127	VALVE	SE	024	020	5	200	110004	47.5	47.5	72	77	1.84	604	2.2	171.2	17.1	5
42-4 128	VALVE	SE	024	020	5	200	253005	124.1	157.5	82	71	1.04	761	29.9	223.4	20.0	5
42-4 129	VALVE	SE	024	020	5	200	107005	54.0	55.2	79	77	1.66	747	5.1	176.7	16.0	5
42-4 130	VALVE	SE	024	020	5	200	121005	47.0	102.0	80	70	1.67	717	12.9	180.0	19.0	5
42-4 131	VALVE	SE	024	020	5	200	210005	100.5	133.4	77	72	1.64	765	15.4	194.1	17.1	5
42-4 132	VALVE	SE	024	020	5	200	130005	50.5	61.2	73	77	1.63	779	6.9	156.2	16.0	5
42-4 133	VALVE	SE	024	020	5	200	134005	67.1	62.4	68	72	1.68	715	11.5	157.7	14.2	5
42-4 134	VALVE	SE	024	020	5	200	300005	85.7	111.4	66	151	1.64	604	15.2	17.5	13.5	5
42-4 135	VALVE	SE	024	020	5	190	253005	65.5	75.7	60	154	1.67	767	6.0	22.1	19.0	5
42-4 136	VALVE	SE	024	020	5	200	412005	130.5	141.1	79	159	1.62	610	9.3	19.5	19.0	5
42-4 137	VALVE	SE	024	020	5	200	703005	211.7	317.9	74	173	1.59	1125	140.7	13.2	16.5	4.2
42-4 138	VALVE	SE	036	030	5	107	050004	32.5	37.5	76	72	1.90	571	1.2	169.9	17.5	5
42-4 139	VALVE	SE	036	030	5	150	017004	27.2	37.0	73	74	1.53	770	1.3	160.0	16.0	5
42-4 140	VALVE	SE	036	030	5	200	173004	30.2	31.0	71	75	1.60	560	1.2	155.9	15.2	5
42-4 141	VALVE	SE	036	030	5	200	110005	40.6	47.4	69	74	1.77	662	3.0	152.7	14.5	5
42-4 142	VALVE	SE	036	030	5	200	227005	75.6	41.0	69	75	1.73	693	11.0	146.9	14.5	5
42-4 143	VALVE	SE	036	030	5	200	094004	25.7	37.0	64	69	1.35	1100	1.0	157.0	16.9	5
42-4 144	VALVE	SE	036	030	5	200	057004	24.0	35.0	72	71	1.44	990	7	177.5	15.0	5
42-4 145	VALVE	SE	036	030	5	200	253005	60.1	133.1	70	747	1.72	606	6.4	180.2	16.1	5
42-4 146	VALVE	SE	036	030	5	200	412005	147.1	175.4	74	71	1.73	689	16.3	146.4	16.5	5
42-4 147	VALVE	SE	036	030	5	200	127005	41.4	50.5	66	72	1.64	771	7.1	157.7	14.2	5
42-4 148	VALVE	SE	036	030	5	200	121005	43.0	50.4	70	72	1.74	674	6.0	190.5	16.1	5
42-4 149	VALVE	SE	036	030	5	200	023004	27.0	37.5	67	80	1.62	764	3.2	184.0	16.0	5
42-4 150	VALVE	SE	036	030	5	200	271005	60.0	101.5	65	80	1.71	702	22.0	192.2	21.0	5
42-4 151	VALVE	SE	036	030	5	200	182005	50.1	71.1	76	78	1.69	723	4.7	163.7	17.5	5
42-4 152	VALVE	SE	036	030	5	200	095004	35.0	47.0	73	81	1.65	606	2.0	159.1	16.0	5
42-4 153	VALVE	SE	036	030	5	200	412005	147.1	175.4	70	72	1.73	682	49.3	164.0	14.0	5
42-4 154	VALVE	SE	036	030	5	200	157005	63.5	67.2	76	73	1.57	611	2.4	184.9	17.5	5
42-4 155	VALVE	SE	036	030	5	200	157005	63.5	67.2	76	73	1.57	611	2.4	184.9	17.5	5
42-4 156	VALVE	SE	036	030	5	200	212005	42.0	105.9	75	75	1.61	773	2.5	171.0	16.9	5
42-4 157	VALVE	SE	036	030	5	200	111005	43.5	50.4	74	84	1.55	636	1.0	124.9	16.5	5
42-4 158	VALVE	SE	036	030	5	200	095004	32.9	41.1	73	65	1.47	933	1.0	117.2	16.0	5
42-4 159	VALVE	SE	036	030	5	200	111005	40.0	57.9	73	42	1.60	760	1.3	132.0	16.0	5
42-4 160	VALVE	SE	036	030	5	200	182005	40.0	105.0	73	65	1.64	742	4.0	216.9	16.0	5

HYPERBOLIC SINEM IMPINGMENT DATA CUMULATION

INVESTIGATUR SCHNEIDER

ORIGINAL PAGE IS  
OF POOR QUALITY